UNIVERSITY OF NAPLES FEDERICO II

Department of Structures

for Engineering and Architecture

Ph.D. Programme in Construction Engineering
XXVII Cycle

LOSANNO DANIELE

Ph.D. Thesis

OPTIMIZATION OF SUPPLEMENTAL DAMPING IN CIVIL ENGINEERING STRUCTURES

TUTOR: PROF. ING. GIORGIO SERINO

2015

"Homo quisque faber ipse fortunae suae"

Sallustio, Epistulae ad Caesarem senem de re pubblica, De rep., 1, 1, 2

Acknowledgements

This PhD program gave me the chance to deeply improve myself, not only from the academic point of view but also as a human kind. I finally realized that knowledge is endless and intelligent people never stop pursuing education to become wiser, being always aware that what they know is never enough. This awareness made me striving for better understanding of my favourite topics, i.e. structural dynamics and earthquake engineering.

First of all, I would like to express my deepest gratitude to Prof. Giorgio Serino. I am very grateful to him for his encouragement and his great confidence in me: it is due to his interest and guidance that I was able to develop my research program, to better appreciate teaching activity and provide support to students who needed. I also thank him for giving me the possibility to attend, during the PhD program, a second level Master in Emerging Technologies for Construction and to spend a period at University of California Berkeley as visiting scholar. My experience in Berkeley was amazing, broadening my mind and making me really appreciate meritocracy. There I also went to know great people like Prof. F.C. Filippou.

Special thanks go to Eng. Mariacristina Spizzuoco for giving me support and advices during all my staying here.

Furthermore, I would like to acknowledge all the people I worked with during these years, past and present colleagues at the Department of Structures for Engineering and Architecture at the University of Naples Federico II, in particular my officemates.

Special tanks are expressed to my good friends and all people who believed in me and gave me their encouragement to go on and do my best.

Special thanks are due to my great family for their constant love and deep consideration. Finally, I would like to thank Paola for her love, care and motivation, and for sharing my successes and disappointments. Without their full support and encouragement, this thesis would not have been accomplished.

Daniele Losanno

ABSRACT

In the last decades the number of applications in civil engineering of special anti-seismic devices such as isolators and supplemental damping systems has been continuously growing thanks to their capability to provide higher safety levels to both new mission critical and existing structures. Passive control systems still appear very attractive with respect to active or semi-active control systems thanks to their capability to work without any external power source.

The design of such systems, i.e. supplemental damping systems or seismic isolation ones, usually involves a trial and error process for the achievement of a satisfactory performance of the structural system. To improve competitiveness and effectiveness of passive control systems, their design should be tuned to an optimal value corresponding to a target performance.

Aim of the thesis is the investigation of the effects of supplemental damping on the definition of its optimal value in typical passively controlled civil engineering structures, such as damper braced frames or isolated bridges.

In case of supplemental damping systems, these are usually inserted in a bracing configuration into new or existing structures, thus being activated by interstory drifts. Structural dynamics of the damping-braced frame may be strongly affected not only in terms of damping but also eigenvalues and eigenvectors. In addition to this, the effect of the brace stiffness in energy dissipation mechanism of supplemental dampers is still not fully addressed in most design and optimization procedures. Even if it is well known that stiffer braces improve damping capacity, the exact value of the brace stiffness is usually neglected, while in practice brace dimensions have to be limited for functional or aesthetic requirements. This thesis properly addresses the effects of the frame to brace relative stiffness parameter on the dynamic behavior and the optimization procedure of single story and multistory frames.

In case of seismic isolation, large displacements are usually introduced at the level of the system and supplemental damping is needed for their mitigation. Also in this case an optimal damping level of the isolation system may be defined, since very high damping is not beneficial.

Chapter 1 introduces the concept of passive control against earthquake induced vibrations. An overview of most commonly adopted supplemental damping and seismic isolation systems with their characteristics is provided.

Chapter 2 is devoted to modeling of damping systems. Concepts of equivalent damping and stiffness are introduced, due to their common use in simplified nonlinear analysis methods. Different kinds of hysteresis, viscous and viscoelastic models are described and mathematical laws for representation of corresponding behavior are suggested. In addition to this, a specific section is devoted to show the effects of the damper supporting brace stiffness on the brace-damper assembly force-displacement behavior. In the final section, elastomeric and friction isolators' behavior is presented.

Chapter 3 deals with the general problem of designing supplemental damping systems. After showing effects of damping on structural dynamics of a simple system, general considerations for structures with passive energy dissipation systems are provided. Difference between traditional and supplementally damped structures are highlighted. In a following section, code provisions for supplementally damped structures are provided. Due to deficient European seismic regulations for this kind of structures, American FEMA provisions represent the most acknowledged references. According to those, the different analysis methods and mechanical models, with their applicability and their approximations, together with the definition of equivalent damping are illustrated in detail. A hint to yielding frames with supplemental damping systems is also provided.

Chapter 4 deals with an optimal design problem for a simple linear-elastic frame equipped with dissipative braces (steel diagonal brace in series with a dissipative viscous or friction device). Aim of the chapter is the definition of the optimal device parameter (the viscous damping coefficient or the yielding force) able to provide the minimum frame displacement or base shear. An analytical approach is suggested for determining the theoretical optimal value of the viscous damping or the yielding force parameter, able to minimize the maximum displacements, clearly accounting for the influence of the supporting brace stiffness. Properly defined design spectra are provided in the first part of the chapter.

It is proved that extremely varying damping coefficients are able to vary the dynamic properties (frequency and mode shapes) of the structure between two limit cases, namely those

corresponding to the bare frame (zero value of the damping parameter) and the elastically braced frame (theoretically infinite value of the damping parameter).

The proposed analytical method is validated by means of numerical analyses carried out on a simple frame subjected to seven spectrum-compatible earthquake records, according to the Italian Code for Constructions. Therefore, an effective design method is delivered: proposed optimal values can be assumed as a starting point of the optimization operative procedure; then, an iterative analysis is needed in seismic perspective in order to determine the effective optimal values of the design parameters for the minimization of the desired response.

Chapter 5 represents a further development of the work presented in Chapter 4 in the case of a multi degree of freedom system. In the first part of the work, a theoretical study in frequency domain has been developed in order to detect the dynamic behavior of a MDOFs frame equipped with viscous dissipative braces. Each brace mounted in series with a damper is modeled by a Maxwell element having a complex stiffness acting in parallel with the stiffness of the bare frame. The proposed approach allows to take into account the effect of the brace stiffness on the optimal value of the viscous damping coefficient and the effectiveness of the supplemental damping system. With the aim of defining an optimal damping parameter, assumed as the one able to yield the minimum resonance peak in the overall range of frequencies, a numerical solution for different MDOFs systems is provided.

In the second part of the work, a wide numerical investigation is carried out on different 3 DOFs frames under different recorded earthquakes, assumed to be subjected to a retrofit intervention by means of viscous dissipative braces. The analysis is devoted to prove the combined effect of the brace-damper stiffness on the dynamic behavior of the frame structures, and to validate the optimization procedure. Time history analysis demonstrate the effectiveness of the theoretically obtained design parameter.

Chapter 6 presents the definition of optimal design parameters characterizing the isolation system of a bridge, both in case of elastomeric and sliding bearings, having viscoelastic or rigid-plastic behavior, respectively, installed between the piers and the deck. In this case the isolation period is usually defined a priori, than objective of the design becomes the definition of the optimum damping level of the system.

Using frequency response analysis, a simple procedure is proposed to determine the optimal value of the viscous coefficient or the yield displacement of the isolators. The adequacy of the

proposed procedure is finally verified through time-history analyses performed on a practical case under natural earthquakes.

Chapter 7 depicts the main conclusion of the work, with an insight to future developments.

Keywords: *optimal damping; optimal design; damper brace assembly; seismic isolation damping*.

LIST OF CONTENTS

LIST OF FIGURES

LIST OF TABLES

Chapter 1

1. INTRODUCTION TO PASSIVE CONTROL SYSTEMS

1.1 Introduction

The basic principle of conventional earthquake-resistant design is to ensure an acceptable safety level while avoiding catastrophic failures and loss of life. When a structure does not collapse during a major earthquake, and the occupants can evacuate safely, it is considered that this structure has fulfilled its function even though it may never be functional again. Generally, designing for the so called "life-safety" performance level is considered adequate for ordinary structures and has been the basis for modern seismic provisions up to this day (Christopoulos and Filiatrault 2006).

This approach may not be acceptable for new strategic structures, such as those important for management of the seismic emergency. Also existing structures often suffer from lack of capacity design concepts that makes conventional retrofit techniques unsatisfactory.

In these cases passive control strategies may play a very important role to achieve the desired level of performance.

For mission critical structures, however, higher performance levels can be expected, while keeping economic factors in mind. For example, avoiding collapse is not sufficient for facilities such as hospitals, police stations, communication centers and many other structures that must

remain functional immediately after an earthquake. Over the last 40 years, a large amount of research has been devoted into developing innovative earthquake resistant systems in order to raise the seismic performance level of structures, while keeping construction costs reasonable. Most of these systems are intended to dissipate the seismic energy introduced into the structure during an earthquake by supplemental damping mechanisms and/or to isolate the main structural elements from receiving this energy through isolation systems.

A part from new designed civil structures, an important problem is also related to safety level of existing ones. In order to prevent collapse during severe earthquake shaking, existing structures may need to develop high level of interstory drifts in order to dissipate a sufficient amount of energy to prevent collapse. However, interstory drifts of this magnitude will generally result in severe damage to a building's non-structural components. In addition to this, older civil structures, due to absence of capacity design criteria and lack of technical details in critical regions, cannot be cyclically deformed into inelastic range without risk of collapse. Conventional upgrading schemes for building and bridges generally involve strengthening and stiffening effects, thus attracting greater seismic forces involving expensive foundation work, column strengthening and so on. At the same time, innovative techniques for ductility improvement (i.e. FRP column confinement), may not be sufficient for providing the needed plastic deformation capacity.

As a response to the shortcomings of conventional seismic design (i.e. strength reduction factor R), a number of innovative approaches have been developed with the aim of reducing the energy adsorbed by the structure, and in particular the dissipation of energy due to structural damage.

Supplemental damping systems use special devices that are often referred to as "mechanical dampers". This supplemental mechanical energy dissipation, activated trough movements of the main structural system, reduces the overall dynamic response of the structure during a major earthquake. Furthermore, the main elements of the structure are protected by diverting the seismic energy to these mechanical devices that can be inspected and even replaced following an earthquake. Ideally, if all the seismic energy adsorbed by the mechanical dampers, the main structure will not sustain any damage.

Seismic isolation systems involve the installation of isolators beneath the supporting points of a structure. For buildings, the isolators are usually located between the superstructure and the foundations while for bridges they are introduced between the deck and the piers. The isolators, designed to have a much lower lateral stiffness than the superstructure they protect, separate

the main structure from structural elements connected to the ground. From an energy point of view, a seismic isolation system limits the transfer of seismic energy to the superstructure. Ideally, if no seismic energy is transmitted to the superstructure, it remains literally unaffected by a seismic attack. Conversely, the isolators must be capable of undergoing the movements imposed by ground shaking, while maintaining their ability to carry gravity loads from the superstructure to the ground. In order to reduce isolators' deformations, supplemental damping systems can also be provided.

1.2   Passive control systems: general basis

Innovative protection strategies against earthquake have been rapidly adopted in the last decades. A classification of the most common control systems includes four groups, identified as (i) passive, (ii) active, (iii) hybrid, and (iv) semi-active control systems, in compliance with the basic principles behind the control strategies (Di Sarno and Elnashai 2005). Relevant assumptions and specific mechanisms characterizing each category are summarized hereafter.

Active control systems (ii) possess external sources powering control actuator(s) that apply forces to the structure in a predefined manner. These forces can be used both to add and dissipate energy in the structure. In an active feedback control system, the signals sent to the control actuators depend upon the dynamic response of the system that is measured through physical sensors, i.e., optical, mechanical, electrical or chemical sensors.

Unlike devices for active control, passive control systems (i) do not require any external power source; the vibration causes them to impart forces which protect the structure.

Hybrid systems (iii) combine both active and passive control approaches. To maximize the system efficiency, it is common practice to employ active devices that may redress drawbacks exhibited by certain passive dampers, and vice versa.

Similar in principle to active control, semi-active control systems (iv) require lower external energy sources. Typically, they do not add energy to the structural system. Therefore, bounded-input as well as bounded-output stability is guaranteed. Semi-active control devices are often viewed as controllable or smart passive devices.

Passive control systems can be mainly classified in

1)   base isolation,

2)   supplemental damping systems

whose different working principles will be described in following paragraphs.

Also tuned/liquid mass dampers have to be mentioned among this category, but are not the object of the present thesis.

A passive control system, whether an energy dissipation system or a dynamic vibration adsorber, or even a seismic isolation system, develops motion control forces at the points of attachment of the system. The power needed to generate these forces is provided by the motion of the points of attachment during dynamic excitation (Figure 1.1). The relative motion of these points of attachment determines the amplitude and direction of the control forces.
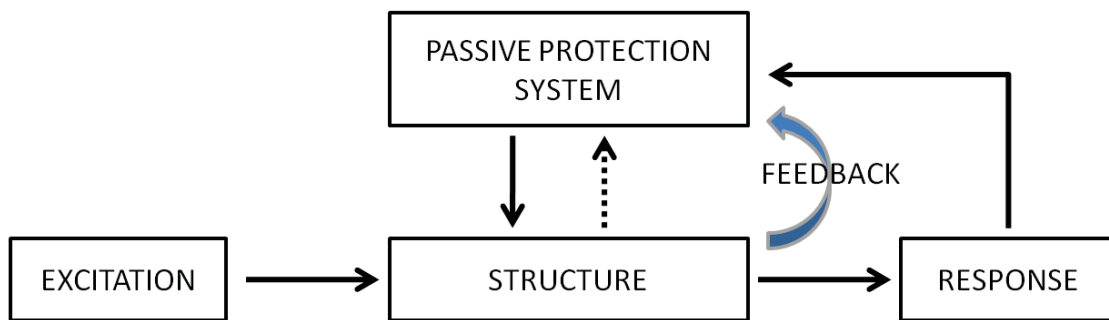
Figure 1.1Passive control system working principle.

The effectiveness of passive protection systems is based on the reduction of elements seismic demand, enhancing structural ability to dissipate energy and allowing the structure to remain elastic without suffering significant damage during strong earthquakes, contrary to what happens in the conventional design that aims to increase the energy dissipation capacity accepting the presence of damage and the formation of plastic hinges within the elements. Passive control systems allow the reduction of the structural response to seismic input providing additional energy dissipation capacities or modifying dynamic structural properties.

The effectiveness of seismically isolated structures or structures with supplemental damping has been recently codified in international seismic regulations and recommendations. In Europe, regulations for base isolated systems have been suggested. It is recognized that passive energy dissipation devices can absorb a portion of the earthquake-induced energy in structures and reduce the demand on primary structural members such as beams, columns, beam–column joints, and walls; thus, structural safety may be guaranteed.

Seismic isolation and supplemental damping systems are viable retrofitting strategies to enhance earthquake performance in building structures and/or whenever owners can afford the costs of design, fabrication, and installation of these special devices. These costs are offset by the reduced need for stiffening and strengthening.

1.2.1   Base Isolation

Base isolation is a viable strategy for retrofitting steel and composite buildings because of its (i) functionality; (ii) contents protection; (iii) investment protection and (iv) construction economy. Composite structures are generally used for buildings in commercial and financial areas which contain sensitive and valuable equipment vital for business and emergency use; their disruption after an earthquake can have a devastating socioeconomic impact. Fixed-base buildings may, in fact, undergo large storey drifts (flexible structures) or high floor accelerations (rigid structures) causing structural and/or non-structural damage. In these cases, retrofitting via seismic isolation is a cost-effective option; drifts and accelerations may be reduced by a factor of 2÷6 (Figure 1.2, Figure 1.3). Buildings retrofitted with seismic isolation systems consist of three distinct parts: the structure above the isolation system, the isolation system itself and the foundation and other structural elements below the isolation system. Each should be properly assessed and detailed to ensure the effectiveness of this rehabilitation strategy. Transient design situations such as lifting the superstructure, cutting structural elements, placing the isolators and giving back the load to the columns, should be adequately checked at the design stage. Isolators are generally located in sub-basements, at the top of basement columns, or at the bottom or top of first-storey columns. Therefore, the working site is limited to garages or warehouses with no interruption of activities within the building and no damage to finishes and equipment. From a mechanical viewpoint, the use of isolation devices in seismic applications, particularly for retrofitting, relies upon three fundamental mechanical properties: (i) horizontal flexibility to increase structural period and reduce the transfer of seismic energy to the superstructure (except for very soft sites); (ii) energy dissipation (damping) to reduce displacements; and (iii) sufficient stiffness at small displacements to provide adequate rigidity for service level environmental loads. Isolators should exhibit significant energy dissipation capacity and/or recentering capability. This target can be achieved either by choosing devices with intrinsic dissipative and re-centring capacities or by providing ad hoc additional elements.
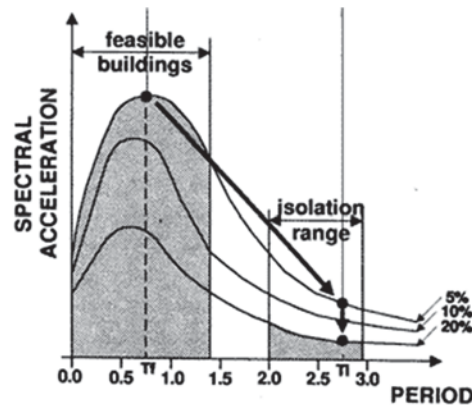
Figure 1.2Response spectrum acceleration highlighting range periods characteristics of conventional and isolated buildings.
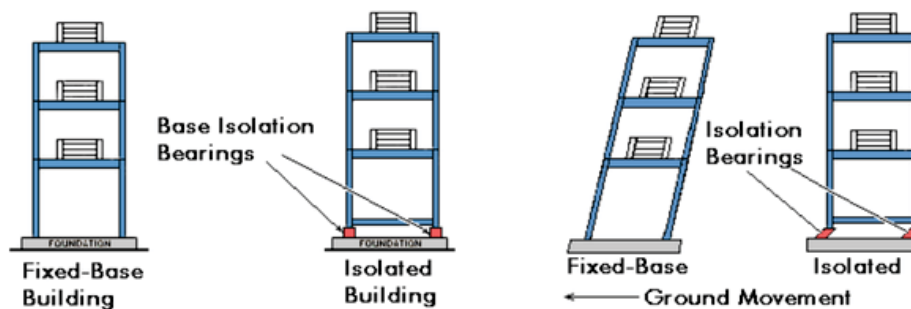
Figure 1.3Fixed base and isolated buildings deformations.

1.2.2 Supplemental damping

Design and retrofit of steel and composite buildings may also be performed by employing dampers. Recently, their use has been allowed by US design and assessment guidance documents which also provide comprehensive design rules. These devices, like base isolation, reduce the demand on the structure by enhancing global damping; this limits damage to structural and/or non-structural components.

Dampers may be grouped as a function of their mechanical response as follows:

- *Displacement-dependent dampers*: force–displacement response characteristics depend primarily on the relative displacements. They include hysteretic (metallic), friction based, and SMA dampers.

- *Velocity-dependent dampers*: force-displacement response characteristics depend primarily on the relative velocity or the frequency of the motion. They include primarily viscous dampers. Viscoelastic devices are displacement and velocity dependent; they exhibit an elastic stiffness along with a viscous component.

All devices possess a similar feature, i.e. they convert external kinetic energy into heat; however, the latter may be performed in different ways. Dampers may assume different

configurations with respect to the structural system that resists lateral forces (Figure 1.4). They can be placed either externally or share common elements with the structural systems. These layouts point to a fundamental difference between structures with dampers and base isolation: the latter forms a series system (structure and isolators) while the former is a parallel system (structure and dampers). Isolators dissipate the input energy before it is transferred to the superstructure. By contrast, dampers receive and dissipate seismic energy in combination with the lateral force-resisting structure. The amount of dissipation depends upon the dynamic characteristics of both components. As a result, the damping should be tuned for optimum performance of the overall system; this is usually a cumbersome iterative design procedure.

A large number of passive control systems has been developed and installed in structures for performance enhancement under earthquake loads (Figure 1.5). These devices provide additional damping to the structure, thus increasing dissipated energy. With respect to the case of base isolation systems, energy dissipators do not have to carry the structural weight, thus allowing easier, smaller and cheaper elements. Furthermore their eventual substitution after a strong earthquake requires a less invasive intervention since their location is not at the interface between the bottom of the structure and foundation system. They are generally located in steel braces connecting two adjacent floors or between wall infills and beams since their correct operating needs relative displacements. The components and connections transferring forces between energy dissipation devices shall be designed to remain linearly elastic.

The employment of energy dissipation devices provides a reduction of bending moment and shear forces acting in columns next to braces. The drawback is that dissipative braces also generate an increasing of the axial force and sometimes of the base shear, thus requiring a local strengthening to the foundation system.

Energy dissipation systems may be considered in a somewhat broader context than isolation systems. For taller buildings (where isolation systems may not be feasible) energy dissipation systems can be considered as a valid design strategy; moreover they could be useful for control of building response due to small earthquakes, wind or mechanical loads.
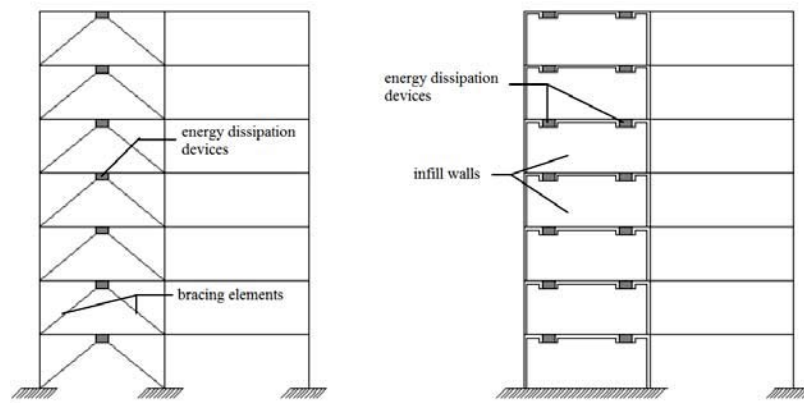
Figure 1.4 Typical configurations for insertion of dissipative devices into frames.

Figure 1.5 Applications of dampers in new or existing frames: (a) viscous fluid devices and (b) buckling restrained braces.

1.3   Energy balance equation

The energy concept has been profitable used in the past for the analysis and design of traditional constructions and, more recently, has also been applied to gain deeper insight into the behaviour of passively controlled structures.

 Let us consider a simple SDOF structural system (Figure 1.6) of mass m subjected to a seismic input at its base represented by a given ground acceleration $\ddot{x}_g(t)$ (Serino and Occhiuzzi 1994). The system is provided with a dashpot of the linear viscous type, with a velocity proportionally constant equal to C_d. Denoting with x the displacement of the mass m relative to the base and with $f_R(x, \dot{x}, t, ...)$ the total restoring force acting in the columns, not necessarily elastic nor linear, the equation of motion is given by:

18

$$m\ddot{x}(t) + C_d\dot{x}(t) + f_R(x, \dot{x}, t, \dots) = -m\ddot{x}_g(t) \tag{1.1}$$

The viscous damping force $C_d\dot{x}(t)$ accounts for all inherent velocity dependent energy dissipating mechanisms in the structure other than the inelastic hysteretic energy dissipated by the structural members. Note that these damping mechanisms are usually not velocity dependent, but are expressed in this way for mathematical convenience.
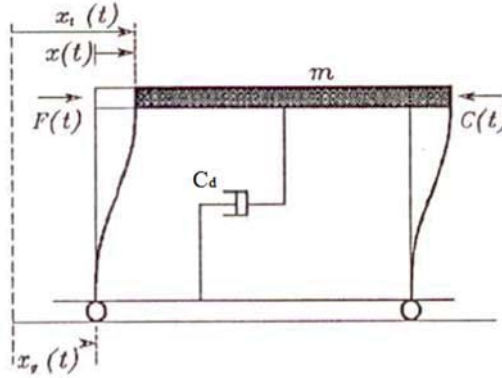
Figure 1.6 Structural scheme for energy balance equation.

Given $x_t(t) = x(t) + x_g(t)$ and multiplying both sides of eq.1.1 by $dx = \dot{x}(t)dt$ and integrating between the starting time of the excitation $t = 0$, when the system is supposed to be at rest $(x(0) = \dot{x}(0) = 0)$, and the generic time $\bar{t}$ we obtain:

$$\int_0^{\bar{t}} m\ddot{x}_t(t)\, dx + \int_0^{\bar{t}} C_d\dot{x}(t)dx + \int_0^{\bar{t}} F_R(x, \dot{x}, t, \dots)dx = 0$$

where $x_t(t) = x(t) + x_g(t)$ denotes the absolute displacement of mass m with respect to a fixed reference system. The first term on the left hand side can be written in the form

$$\int_0^{\bar{t}} m\ddot{x}_t(t)\, dx = \int_0^{\bar{t}} m\ddot{x}_t(t)\, dx_t - \int_0^{\bar{t}} m\ddot{x}_t(t)\, dx_g = \frac{1}{2}m\dot{x}_t^2(\bar{t}) - \int_0^{\bar{t}} m\ddot{x}_t(t)\, dx_g$$

i.e., as the sum of the absolute kinetic energy and the work done by the total input force acting at the base of the structure, which corresponds to the seismic input energy. Substituting the latter in the previous equation the energy balance equation at time $\bar{t}$ is obtained:

$$E_K(\bar{t}) + E_D(\bar{t}) + E_R(\bar{t}) = E_I^e(\bar{t})$$

where:

$E_K(\bar{t}) = \frac{1}{2}m\dot{x}_t^2(\bar{t})$, is the absolute kinetic energy;

$E_D(\bar{t}) = \int_0^{\bar{t}} C_d\dot{x}(t)dx$, is the equivalent viscous damping dissipated energy;

$E_R(\bar{t}) = E_H(\bar{t}) + E_S(\bar{t}) = \int_0^{\bar{t}} F_R(x, \dot{x}, t, \dots)dx$, is the restoring force adsorbed energy;

19

$E_I^e(\bar{t}) = \int_0^{\bar{t}} m\ddot{x}_t(t)\, dx_g$, is the seismic input energy, having a true physical meaning as it is defined as the total base shear integrated over the ground displacement.

It is worthy to point out that in defining the energy quantities, we called "dissipated" an irrecoverable energy quota, e.g. transformed into heat or lost in material plastic deformation, while we called "adsorbed" an energy quantity corresponding to the area below a generic force-displacement curve, which thus may be totally or partially recovered. With this in mind, the restoring force adsorbed energy can be split into two quantities: the irrecoverable hysteretic energy $E_H(\bar{t})$ and the elastic stored energy $E_S(\bar{t})$, which is completely recoverable.

$$E_K(\bar{t}) + E_D(\bar{t}) + E_H(\bar{t}) + E_S(\bar{t}) = E_I^e(\bar{t}) \qquad (1.2)$$

The energy balance equation given in (1.2) provides a very useful tool to understand how a control system operates. Introducing a supplemental damping system (both viscous and hysteretic type), the global dissipated energy quotas $E_D(\bar{t})$ increase so that, for a given input energy, absolute kinetic energy and elastic stored energy decrease and thus structural response is reduced.

In case of base isolation, the input energy $E_I^e(\bar{t})$ reaching the superstructure is significantly reduced and energy dissipation is concentrated in the isolation system.

It is very important to understand that for design purposes, the most desirable response of a structure equipped with a passive energy dissipating system is not necessarily associated with maximum energy dissipated by dampers. This can be seen by defining the vibrational energy $E_{vb}(\bar{t})$, which corresponds to the portion of the input energy at time $\bar{t}$ that has not been dissipated by viscous damping or by supplemental damping system and that can potentially cause damage to the structure (Christopoulos and Filiatrault 2006). The main structure is therefore best protected when $E_{vb}(\bar{t})$ is minimized at all times.

It can be seen that the vibrational energy is equal to the sum of the kinetic energy and adsorbed energy flowing in the system at time $\bar{t}$:

$$E_{vb}(\bar{t}) = E_K(\bar{t}) + E_R(\bar{t})$$

From eq. (1.2), the vibrational energy is also equal to the difference between the seismic input energy and the supplementally dissipated energy:

$$E_{vb}(\bar{t}) = E_I^e(\bar{t}) - E_D(\bar{t}) \qquad (1.3)$$

Therefore, the design strategy resides in minimizing the difference between the seismic input energy and the energy dissipated by the dampers. This goal can be achieved by:

- Seismic isolation, mainly reducing input energy but also providing additional damping to reduce structure's displacements to acceptable values;
- Supplemental damping systems, mainly increasing dissipated energy (Figure 1.7).

Equation (1.3) clearly shows that maximizing the energy dissipated by the supplemental dampers does not necessarily lead to a minimum vibrational energy, since the amount of input energy can also increase significantly. This result leads also to the conclusion that for design purposes, the optimum properties of the selected passive energy dissipating system depend on both the properties of the ground motion and of the structural system.

The means by which energy is dissipated is either yielding of mild steel, sliding friction, motion of a piston or a plate within a viscous fluid, orificing of fluid, or viscoelastic action in polymeric materials. In addition to increasing the energy dissipation capacity per unit drift of a structure, some energy dissipation systems also increase strength and stiffness. Such systems include the following types of energy dissipation devices: metallic yielding, friction and viscoelastic. Energy dissipation systems utilizing fluid viscous dampers will not generally increase the strength or stiffness of a structure unless the excitation frequency is high.

| (a) | (b) |
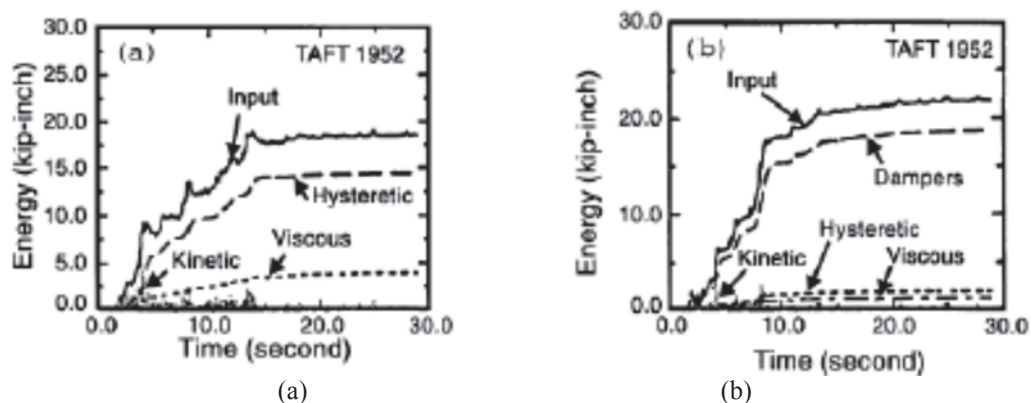
Figure 1.7 Energy plot for a structure (a) w/o dampers (b)with dampers (Lobo et al., 1993).

1.4   Supplemental damping systems

The primary reason for introducing energy dissipation devices into a building frame is to reduce the displacements and damage in the frame. Displacement reduction is achieved by adding either stiffness and/or energy dissipation (generally termed damping) to the building frame. Metallic-yielding, friction and viscoelastic energy dissipation devices typically introduce both stiffness and damping; viscous dampers will generally only increase the damping in a building frame. Figure 1.8 simply illustrates the impact of different types of dampers on the force-

displacement response of a building. The addition of viscous dampers does not change the force-displacement relation; that is, the "with viscous EDS" curve is essentially identical to the "without EDS" curve in Figure 1.8.
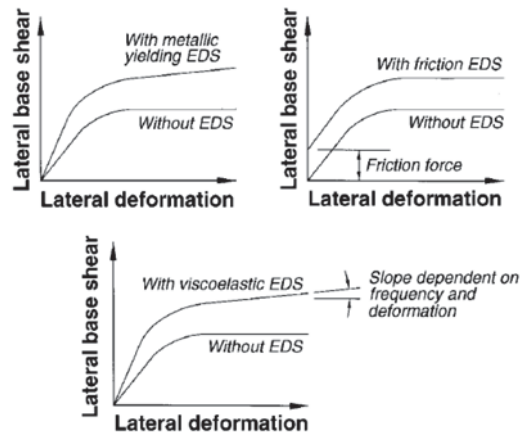
Figure 1.8 Effects of energy dissipation on the force-displacement response of a building (FEMA 274).

The degree to which a certain device is able to limit damaging deformations in structural components depends on the inherent properties of the basic structure, the properties of the device and its connecting elements, the characteristics of the ground motion, and the limit state being investigated. Given the large variations in each of these parameters, it is usually necessary to perform an extensive suite of nonlinear response-history analyses to determine which particular passive energy dissipation system is best suited for a given case.

Figure 1.9 summarizes the main properties of most acknowledged damping systems:

	Viscous Fluid Damper	Viscoelastic Solid Damper	Metallic Damper	Friction Damper
Basic Construction				
Idealized Hysteretic Behavior				
Idealized Physical Model			Idealized Model Not Available	
Advantages	- Activated at low displacements - Minimal restoring force - For linear damper, modeling of damper is simplified. - Properties largely frequency and temperature-independent - Proven record of performance in military applications	- Activated at low displacements - Provides restoring force - Linear behavior, therefore simplified modeling of damper	- Stable hysteretic behavior - Long-term reliability - Insensitivity to ambient temperature - Materials and behavior familiar to practicing engineers	- Large energy dissipation per cycle - Insensitivity to ambient temperature
Disadvantages	- Possible fluid seal leakage (reliability concern)	- Limited deformation capacity - Properties are frequency and temperature-dependent - Possible debonding and tearing of VE material (reliability concern)	- Device damaged after earthquake; may require replacement - Nonlinear behavior; may require nonlinear analysis	- Sliding interface conditions may change with time (reliability concern) - Strongly nonlinear behavior; may excite higher modes and require nonlinear analysis - Permanent displacements if no restoring force mechanism provided
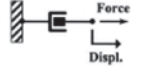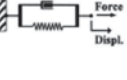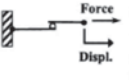
Figure 1.9 Summary of construction, hysteretic behavior, physical models, advantages, and disadvantages of passive energy dissipation devices for seismic protection applications.

1.4.1 Displacement-dependent devices

Displacement-dependent devices, also known as rate-independent, may exhibit either rigid-plastic (friction devices), bilinear (metallic yielding devices), or trilinear hysteresis. The response of displacement-dependent devices should be independent of velocity and/or frequency of excitation, thus they are also called rate-independent. The force-displacement response of a displacement-dependent device is primarily a function of the relative displacement between each end of the device. Figure 1.10 shows force-displacement relations for displacement-dependent devices.
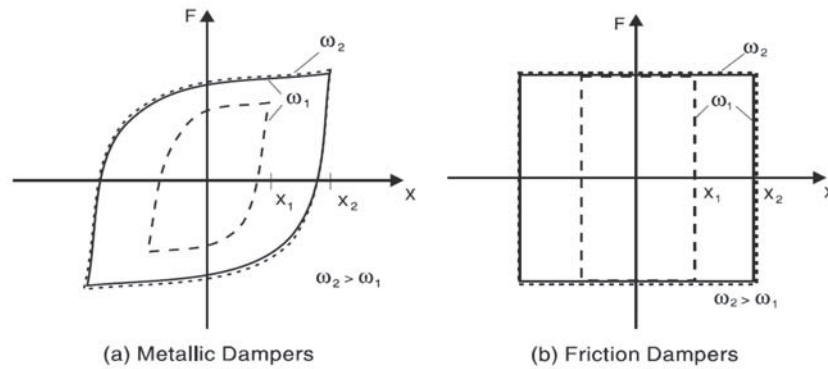
Figure 1.10 Idealized force-displacement response of hysteretic devices (FEMA 273).

1.4.1.1 Metallic yield dampers

Hysteretic dampers are metal devices that can dissipate energy from an earthquake through inelastic deformation of metals. These dampers may yield either in bending, torsion and/or axially (mild steel) or shear (mild steel or lead): as a result they will be damaged after an earthquake and may need to be replaced (Figure 1.11).
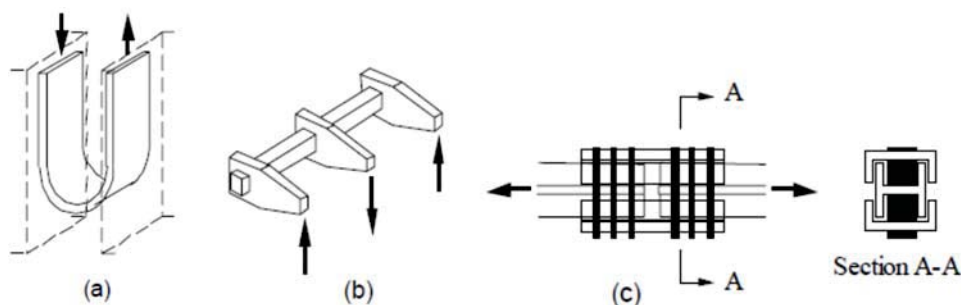
Figure 1.11 Metallic dampers: a) U-steel; b) torsional-beam; c) flexural-beam (Kelly et al., 1972).

Some particularly desirable features of these devices are their stable hysteretic behavior, low-cycle fatigue property, long term reliability, and relative insensitivity to environmental temperature. Hence, numerous analytical and experimental investigations have been conducted to determine these characteristics of individual devices. After gaining confidence in their performance based primarily on experimental evidence, implementation of metallic devices in full-scale structures has taken place. The earliest implementations of metallic dampers in structural systems occurred in New Zealand and Japan (Aiken and Kelly 1992).

Two major types of metallic dampers are buckling-restrained brace dampers (BRBs) and added damping and stiffness dampers (ADAS), yielding axially and flexurally, respectively.

1.4.1.1.1 ADAS dampers

ADAS (added damping and stiffness) dampers consist of a series of steel plates wherein the bottom of the plates are attached to the top of a chevron bracing arrangement and the top of the plates are attached to the floor level above the bracing (Figure 1.12). As the floor level above deforms laterally with respect to the chevron bracing, the steel plates are subjected to a shear force. The shear forces induce bending moments over the height of the plates, with bending occurring about the weak axis of the plate cross section. The geometrical configuration of the plates is such that the bending moments produce a uniform flexural stress distribution over the height of the plates. Thus, inelastic action occurs uniformly over the full height of the plates. For example, in the case where the plates are fixed-pinned, the geometry is triangular (Figure 1.13 (a)). In the case where the plates are fixed-fixed, the geometry is an hourglass shape (Figure 1.13 (b)). To ensure that the relative deformation of the ADAS device is approximately equal to that of the story in which is installed, the chevron bracing must be very stiff.

Pioneering applications of ADAS were made in New Zealand and Japan; recently they have also been used for seismic rehabilitation of steel and composite structures. Chevron braces are usually combined with ADAS devices (Figure 1.12); ADAS dampers, located between the end of cross braces and beam mid-span, are activated by storey drifts. These dampers should be designed in such a way that at their yielding, axial loads in the braces are lower than buckling load. The design is therefore uneconomical because the tensile plastic capacity of diagonals is not fully exploited. The performance of these dampers depends upon the elastic stiffness and yield force of the damper and the elastic stiffness of the structure to which it is applied. To achieve maximum effectiveness the device should have high stiffness. In practical applications (damping of the device varying between 10 and 15%), it is difficult to separate the effects of added stiffness from the effects of added damping on response; both tend to reduce the displacement response. The higher the device-to-structure stiffness is, the higher the damping will be. As a consequence, hysteretic dampers do not simply add damping, but modify significantly all dynamic characteristics of the structure. Typically, they reduce the fundamental period, thus increasing the base shear. However, these systems are particularly attractive for retrofitting of steel buildings that are vulnerable to resonant response with the ground.
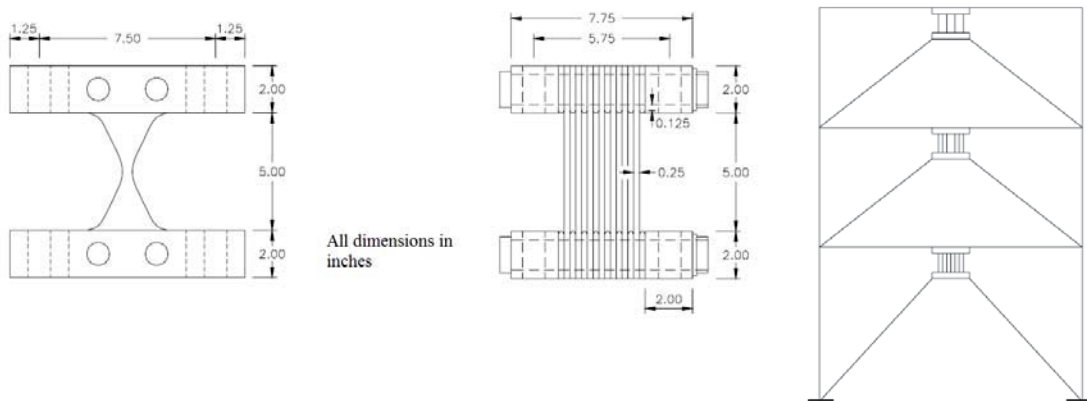
Figure 1.12 ADAS device model.

(a)
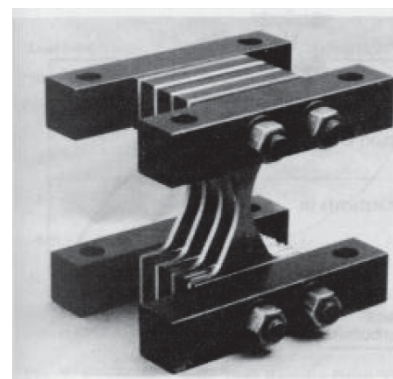
(b)

Figure 1.13 (a) TADAS device and (b) ADAS device.

1.4.1.1.2. BRB dampers

A variation of the devices described above but operating on the same metallic yielding principle is the tension/compression yielding brace, also called the unbonded brace (Clark et al 1999; Wada et al 1999), which has found applications in Japan and the USA. As shown in Figure 1.14(a), an unbonded brace is a bracing member consisting of a core steel plate encased in a concrete-filled steel tube. A special coating is provided between the core plate and concrete in order to reduce friction. The core steel plate provides stable energy dissipation by yielding under reversed axial loading, while the surrounding concrete-filled steel tube resists compression buckling. Experimental and analytical work on hysteretic dampers has been carried out in Europe during the last decade; several new configurations and devices have been proposed.

Under compressive loads, the damper behavior is essentially identical to its behavior in tension (Figure 1.14(b)). Since buckling is prevented, significant energy dissipation can occur over a cycle of motion.

In many cases, BRB dampers are installed within a chevron bracing arrangement. In this case, under lateral load, one damper is in compression and the other is in tension, and hence zero vertical load is applied at the intersection point between the dampers and the beam above. In this regard, the dampers may be considered as superior to a conventional chevron bracing arrangement where the compression member is expected to buckle elastically, leaving a potentially large unbalanced vertical force component in the tension member that is, in turn, applied to the beam above.

During the initial elastic response of the BRB damper, the device provides stiffness only. As the BRB damper yields, the stiffness reduces and energy dissipation occurs due to inelastic hysteretic response.

(a)

(b)
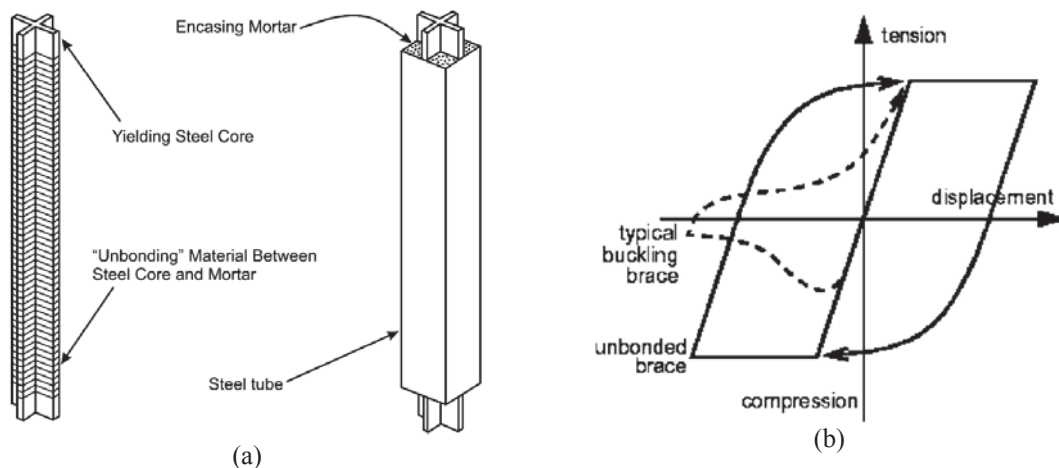
Figure 1.14 (a) Unbounded brace and (b) corresponding axial force-displacement behavior.

Figure 1.15 BRB attached to conventional steel brace.

A cheaper configuration for inserting BRB devices (Figure 1.15), is to attach them at the edge of an elastic-designed steel brace, so limiting the dimension of the device.

Note that, in present seismic design documents (BSSC 2004; ASCE 2005), buckling-restrained braces are regarded as being part of a bracing system, rather than as part of a damping system. A response modification factor (R), which accounts for the hysteretic energy dissipation capacity of the BRB, is assigned to structures that incorporate BRB devices and the design process is similar to that used for other conventional bracing systems. Specifically, R values of 7 and 8 are used for BRB frames with non-moment resisting beam-column connections and moment resisting beam-column connections, respectively. Proponents of the BRB system have encouraged the classification as a bracing system so as to foster more rapid implementation.

1.4.1.1.3. Shear link dampers

A more recent application of metallic damper is represented by shear link devices, designed to yield in shear to limit the maximum force due to lateral loads transmitted to primary structural members (Figure 1.16(a)). They are usually attached to diagonal or chevron brace, activated by interstory drift.

A particular shear link device (Bozzo shear link) is shown in Figure 1.16 (Hurtado and Bozzo 2008).

| (a) | (b) |
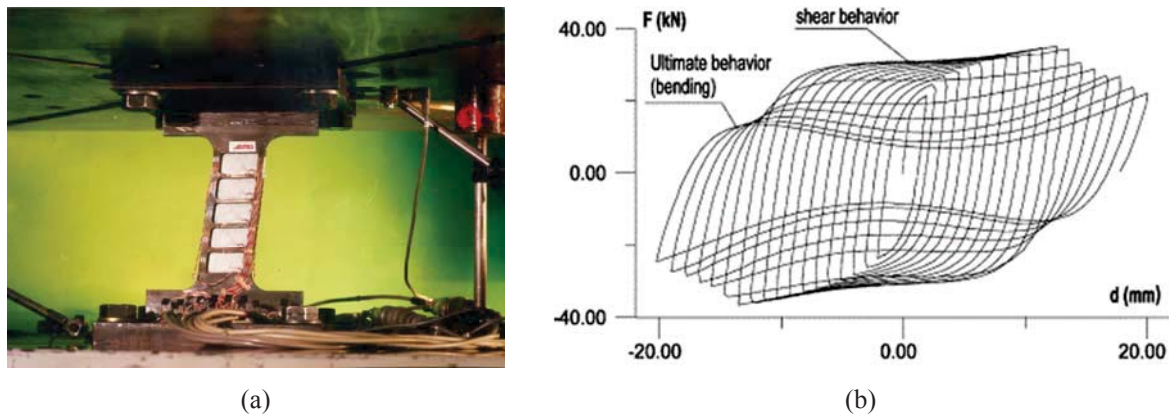
Figure 1.16 (a) Shear link energy dissipation device and (b) corresponding shear force-displacement behavior.

It essentially consists in a metallic plate to yield in shear. The main shape is obtained from a rectangular hot laminated element in structural steel, which is made thinner by a milling process. In this way, without any welded part, it is possible to obtain some thinner "windows" that under shear stress can yield in a stable manner (Figure 1.16(b)), thanks to transverse and longitudinal stiffeners.

Moreover, thanks to small transversal dimensions of the milled areas, uniform energy dissipation is ensured for very low values of shear stresses, since the device requires low shear forces to yield. Consequently, it has the advantage of starting to dissipate energy at very small deformations with the potential of reducing inter-storey drifts for buildings, thus providing an important benefit for non–structural elements.

Shear link energy dissipation device must be designed so that yielding is reached before buckling in supporting braces.

1.4.1.2. Friction dampers

These dampers rely upon the mechanism of friction between two solid bodies sliding relative to one another. Friction is an excellent mechanism of energy dissipation; it has been used extensively and successfully in automotive breaks to dissipate kinetic energy.

Various materials are used for the sliding surface such as brake pad material on steel, steel on steel, steel on brass in slip-bolted connections, graphite-impregnated bronze on stainless steel and other metal alloys. The choice of the base metal for friction dampers is crucial; poor corrosion resistance can often reduce the coefficient of friction assumed in the design for the intended life of the device. Low-carbon alloy steels corrode and their interface properties vary with time, while brass and bronze promote additional corrosion when in contact with low

carbon. By contrast, stainless steels do not appear to suffer additional corrosion when in contact with brass or steel; therefore, they are suitable for such devices. Generally, friction devices offer good seismic performance and their response is independent of loading amplitude, frequency and number of cycles. They combine high energy-dissipation potential and relatively low cost, and are easy to install and maintain. In designing friction-based dampers it is essential to minimize stick-slip phenomena, thus avoiding high frequency excitation. The ratio of initial slip load to storey yielding shear and ratio of bracing-to-storey stiffness also significantly affect the performance of the device. Friction devices usually produce a stable rectangular hysteresis, although some are configured to produce self-centring force and provide nonrectangular hysteresis shapes with load proportional to displacement. The Coulomb model is a macroscopic hysteretic model for friction-based dampers with a constant coefficient of friction.

Friction dampers have been commonly placed within diagonal braces, as with yielding metal dampers, but can also be placed horizontally between the top of a wall and the beam above. These devices initially possess finite stiffness because they are mounted on braces; therefore, their behaviour is similar to hysteretic damping.

A typical friction damper (Palle friction damper) is shown in Figure 1.17: it can be installed at the crossing of two braces where tension in one brace forces the joint to slip, thus activating four links which in turn force the joint in the other brace to slip (Pall and Marsh 1982; Pall and Pall 1993). This device is fixed under wind and moderate earthquakes but slips under intense ground motions, thus protecting primary structural members from yielding.
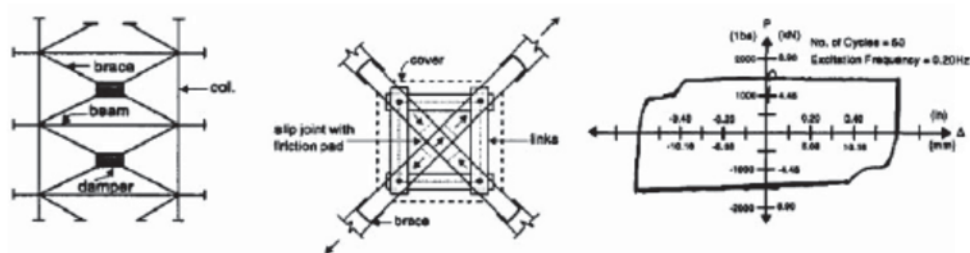
Figure 1.17 Palle friction device: frame location (left), device layout (middle) and hysteretic loop (right).

Sliding connections contribute to elevate friction and hence, energy dissipation.

The device can be calibrated via the tightening force applied to the bolts. Diagonal braces using the Pall system possess enhanced dissipative capacity -the energy dissipation is roughly two-fold- with regard to ordinary cross-bracings.

During cyclic loading, the mechanism enforces slippage in both tensile and compressive directions. Generally, friction devices generate rectangular hysteresis curves. This force system

causes the rectangular damper to deform into a parallelogram, dissipating energy at the bolted joints through sliding friction. In recent years, there have been a number of structural applications of friction dampers aimed at providing enhanced seismic protection of new and retrofitted structures. This activity in North America is primarily associated with the use of Pall friction devices in Canada and the USA; and slotted-bolted connection in the USA (Grigorian et al 1993).

Recently, novel friction dampers have been tested experimentally and many have been installed in new and existing buildings around the world. Two examples of devices for braced connections are provided in Figure 1.18; they are a slotted bolted connection energy dissipator and a novel device for inverted V-braced connections, respectively. Slotted bolted connections are becoming very popular for braced connections because they require only a slight modification of standard construction practice, and are thus easy to construct and implement. They also make use of materials widely available on the market, and are a cost-effective mean of retrofitting existing steel and composite framed buildings. These connections are designed to dissipate energy through friction between the steel surfaces along the brace in tension and compression loading cycles; alternatively, brass in contact with steel may be used. Experimental tests have shown that the behaviour of connections with brass on steel is more uniform; moreover, they are simpler to model analytically than those using steel on steel, and their performance in braced systems is very satisfactory. It has slotted holes in the main connection plate which are parallel to the line of loading. The main plate is sandwiched between two outer members. A friction lining pad is placed between each outer member and the main plate. The lining pad moves with the outer member. Two bolts are used to clamp together the plates and lining pads. Upon tightening the bolts, frictions develop between the contact surfaces of lining pads and slotted plate.

When either tensile or compressive forces are applied to the connection and the friction is exceeded, the slotted plane slips relative to the lining pads and energy is dissipated. The effectiveness of the novel damper for inverted V-braced connections (Figure 1.18) has been assessed experimentally and numerically. The damper consists of three steel plates, i.e. one central (vertical), two on the side (horizontally) and two circular friction pad discs sandwiched between the steel plates. The central plate is used for the connection with the mid-span of the floor beam in the frame. This connection is pinned and thus increases the relative rotation between the central and the side plates; as a result, energy dissipation is enhanced.
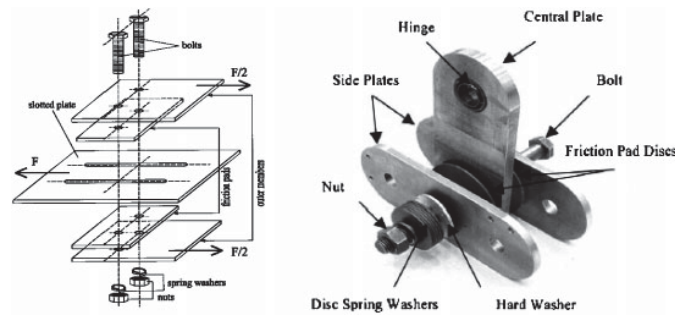
Figure 1.18 Novel friction dampers for braced connections: slotted bolted connection (left) and inverted V-braced connection (right).

Experimental testing (e.g., see Pall and Marsh 1982) has shown that a reasonable model for defining the behavior of friction dampers is given by the idealized Coulomb model of friction:

$$P = \mu N \, \mathrm{sgn}(\dot{u})$$

where $\mu =$ coefficient of dynamic friction, and $N =$ normal force at the sliding interface. Within the context of a friction damper, the idealized Coulomb model assumes that the clamping (or normal) force and the coefficient of friction are maintained at constant values over extended durations of time. This can be difficult to achieve in practice and thus the damper friction force may change with time. The potential variability in the friction force could be accounted for in design in a manner similar to the way that variability in other structural parameters might be considered. The idealized hysteretic response of a friction damper for cyclic loading reveals that the force output is bounded and has the same value for each direction of sliding. The hysteresis loops are rectangular, indicating that significant energy can be dissipated per cycle of motion. However, the rectangular shape of the hysteresis loops indicates that the cyclic behavior of friction dampers is strongly nonlinear. The deformations of the structural framing are largely restricted until the friction force is overcome; thus, the dampers add initial stiffness to the structural system. Note that, if a restoring force mechanism is not provided within the friction damper system, permanent deformation of the structure may exist after an earthquake.

The Sumitomo Device was designed and developed by Sumitomo Metal Industries, Ltd., Japan, originally as a shock absorber in a railway rolling stock. It is a cylindrical device with friction pads that slide directly on the inner surface of the steel casing of the device (Figure 1.19). The friction device might be attached to the underside of the floor beams and connected to chevron brace assemblages. The Sumitomo dampers exhibited outstanding behavior: their hysteretic behavior is extremely regular and repeatable. The devices show almost no variation in slip load

during earthquake motion; their force-displacement response is known to be quite independent of loading frequency, amplitude, number of loading cycles, and temperature.
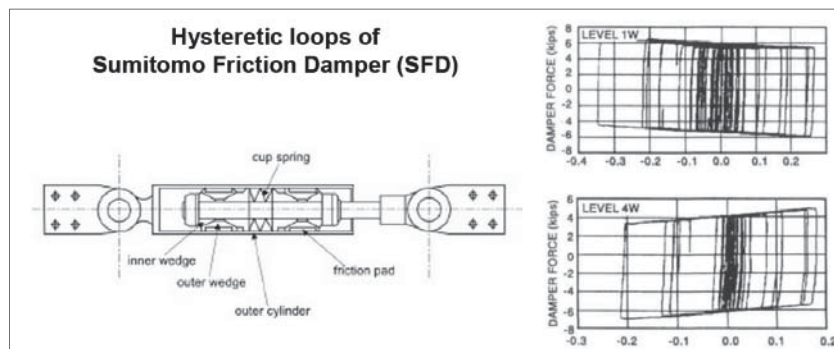
Figure 1.19 Sumitomo friction device.

Friction devices are insensitive to temperature variation. Among their disadvantages it is important to highlight that the interface condition could change with time; moreover the friction coefficient, during the displacement, is a function of velocity, axial force and contact surface's conditions. Consequently it is difficult to ensure a friction coefficient independent by time and by device's status. A further disadvantage is that if restoring forces are not provided, a structure equipped with friction dampers may present permanent displacements after a strong ground motion.

1.4.2. Velocity-dependent devices

Velocity-dependent devices response depends on the relative velocity between each end of the damper; they are also known as rate-dependent devices and include solid/fluid visco-elastic devices, and fluid viscous devices, that respectively consist in dampers operating by deformation of visco-elastic materials and dampers operating by forcing a fluid through an orifice. In Figure 1.20 typical behaviour of these devices is depicted.
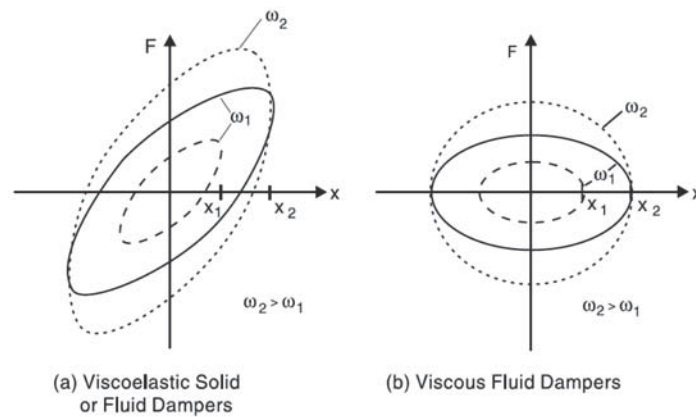
Figure 1.20 Idealized force-displacement loops of velocity-dependent energy dissipation devices (from FEMA 273).

Typically these devices exhibit stiffness and damping coefficients which are frequency dependent. Moreover, damping force in these devices is proportional to velocity, that is, the behaviour is viscous. Accordingly, they are classified as viscoelastic systems. A purely viscous device is a special case of a viscoelastic device with zero stiffness and frequency independent properties.

1.4.2.1. Viscous dampers

The viscous fluid (VF) devices, developed recently, include viscous walls and VF dampers. The viscous wall, developed by Sumitomo Construction Company, consists of a plate moving in a thin steel case filled with highly VF (Figure 1.21).
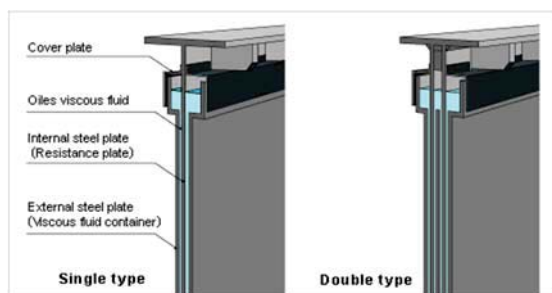
Figure 1.21 Oiles viscous wall damper.

The VF damper, widely used in the military and aerospace industry for many years, has recently been adapted for structural applications in civil engineering.

A VF damper generally consists of a piston within a damper housing filled with a compound of silicone or similar type of oil; the piston may contain a number of small orifices through which

34

the fluid may pass from one side of the piston to the other (Figure 1.22). Thus, VF dampers dissipate energy through the movement of a piston in a highly VF based on the concept of fluid orificing. Viscous fluid dampers have in recent years been incorporated into a large number of civil engineering structures. In several applications, they were used in combination with seismic isolation systems.
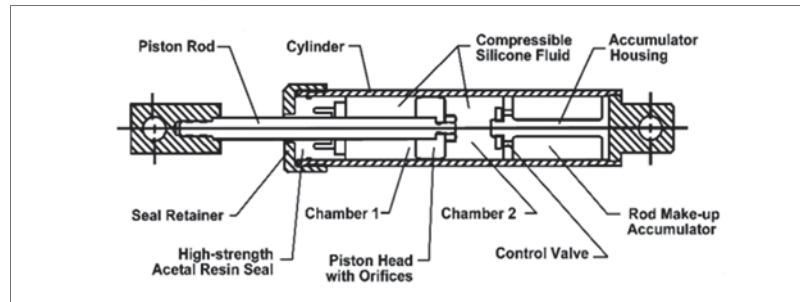
Figure 1.22 Viscous fluid damper.

As the damper piston rod and piston head are stroked, fluid is forced to flow through orifices either around or through the piston head. The resulting differential in pressure across the piston head (very high pressure on the upstream side and very low pressure on the downstream side) can produce very large forces that resist the relative motion of the damper. The fluid flows at high velocities, resulting in the development of friction between fluid particles and the piston head. The friction forces give rise to energy dissipation in the form of heat. The associated temperature increase can be significant, particularly when the damper is subjected to long-duration or large-amplitude motions. Mechanisms are available to compensate for the temperature rise such that the influence on the damper behavior is relatively minor (Soong and Dargush 1997). However, the increase in temperature may be of concern due to the potential for heat-induced damage to the damper seals. In this case, the temperature rise can be reduced by reducing the pressure differential across the piston head (e.g., by employing a damper with a larger piston head). During seismic events the oil starts to move and its temperature increases, thus causing a decrease of its viscosity and capability of dissipating energy. If time duration of an earthquake is relatively short, temperature increase may not be significant.

Interestingly, although the damper is called a viscous fluid damper, the fluid typically has a relatively low viscosity (e.g., silicone oil with a kinematic viscosity on the order of 0.001 m^2/s at 20°C). The term viscous fluid damper is associated with the macroscopic behavior of the damper which is essentially the same as that of an ideal linear or nonlinear viscous dashpot (i.e., the resisting force is directly related to the velocity). Note that the fluid damper shown in Figure

1.22 includes a double-ended piston rod (Constantinou and Symans 1993) (i.e., the piston rod projects outward from both sides of the piston head and exits the damper at both ends of the main cylinder). Such configurations are useful for minimizing the development of restoring forces (stiffness) due to fluid compression. Moreover, these viscous dampers exhibit stiffening characteristics at higher frequencies of deformation; thus, they are used to damp higher mode effects. As an alternative to viscous fluid dampers, viscoelastic fluid dampers, which are intentionally designed to provide stiffness in addition to damping, have recently become available for structural applications. These dampers provide damping forces via fluid orificing and restoring forces via compression of an elastomer. Thus, more accurately, the dampers may be referred to as viscoelastic fluid/solid dampers.

Viscous dampers have low resistance to deformation when loads are applied slowly, but resistance increases as the applied deformation rate increases. When they are installed in buildings, usually in bracings, input energy due to earthquake loading is transformed by friction into heat. Viscous dampers have been used to control the vibrations of new buildings and to retrofit either RC or steel frames, especially in Japan and in US.

1.4.2.2. Viscoelastic dampers

These devices are based on viscoelastic materials (VE), such as copolymers or glassy substances, with high energy dissipation due to shear deformations. Viscoelastic materials have linear response over a wide range of strains at constant temperature. At large strains, e.g. 300–500%, the energy dissipation produces self-heating, affecting the mechanical properties of the material, which then becomes highly nonlinear. Typical viscoelastic dampers are shown in Figure 1.23: they consist of viscoelastic layers bounded with steel plates. Mounted in the structure, shear deformation and hence, energy dissipation, take place when structural vibration induces relative motion between outer steel flanges and centre plates.

The device is mounted in the structure so that relative floor displacement causes shear deformation of the device. The mechanical properties of VE materials depend on temperature, frequency and strain amplitude.

The expected frequencies of the device motion can be approximated with sufficient accuracy to establish the proper frequency property for a specific application (Shen and Soong 1995). The device temperature will increase from the initial ambient temperature of the device as the dissipated energy is converted to heat. This range of expected temperature for which the device operates must be included in the design for a specific application.

The main VE material properties used in the designing VE devices are the storage modulus, G', which provides the "elastic" shear stiffness of the material, and the shear loss modulus, G'', which represents the velocity-dependent or viscous stiffness of the material (Fu and Kasai 1998). The material stress-strain relationship can be expressed as

$$\tau(t) = G'\gamma(t) \pm G''\dot{\gamma}(t)/\omega$$

where $\tau(t)$ is the shear stress as a function of time; $\gamma(t)$ is the shear strain as a function of time; $\dot{\gamma}(t)$ is the shear strain rate of change (shear velocity) as a function of time; and ω is the circular cyclic frequency in radians per sec.
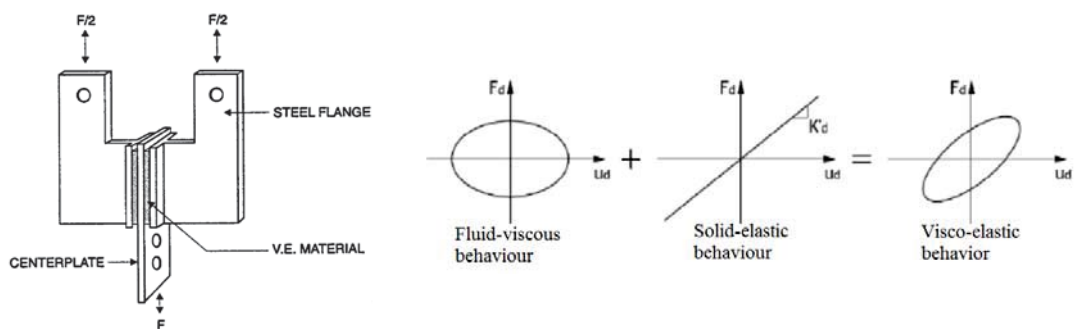
Figure 1.23 Visco-elastic damper and mechanical behavior.

Figure 1.24 shows dependence of VE-behavior on cyclic amplitude and frequency, or rate dependence.
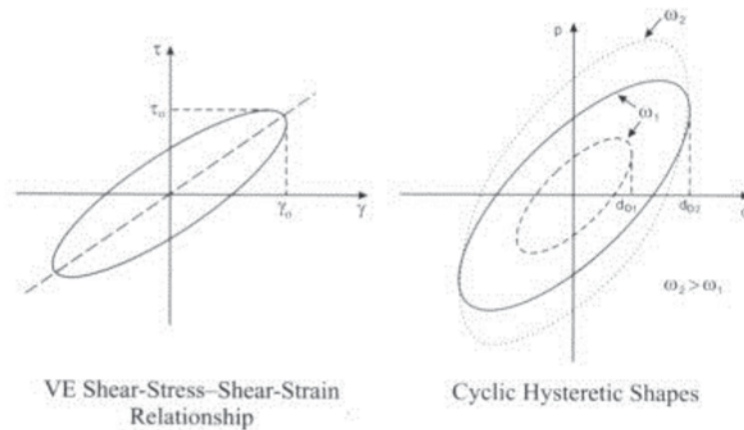
Figure 1.24 Typical hysteretic shapes of VE solid device.

Several analytical expressions are provided in the literature for G' and shear loss G''. In general, the storage and loss moduli are dependent on frequency of motion, strain amplitude, and temperature. At a given frequency and shear strain amplitude, the storage and loss moduli have similar values that increase with an increase in the frequency of motion. Thus, at low frequencies, viscoelastic dampers exhibit low stiffness and energy dissipation capacity.

Conversely, at high frequencies, stiffness and energy dissipation capacity are increased. Note that increases in temperature, due to cycling of the damper, can significantly reduce the storage and loss moduli, resulting in reduced stiffness and energy dissipation capacity (Figure 1.26(a)). A simplified bounding analysis can be employed wherein lower and upper bound temperatures are used to predict maximum forces and displacements, respectively.

Viscoelastic materials do not gain plastic deformations and, at the same time, provide stable behavior with dissipative capacity for small values of deformations. Main drawbacks are limited maximum strain and potential debonding failure.

It has been observed that the variations in $G'(\omega)$ and $G''(\omega)$ fall into straight lines on a log-log plot with respect to cyclic frequency (Figure 1.25). Thus, at a given temperature, only two tests at different frequencies are needed to define this log-log plot straight-line relationship.
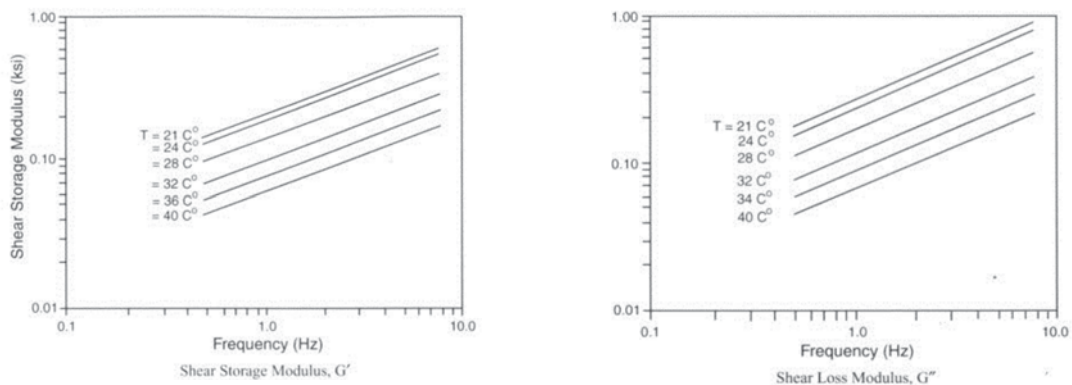
Figure 1.25 Dependence of shear moduli on temperature and frequency.

Experimental data have shown that, although $G'(\omega)$ and $G''(\omega)$ are functions of excitation frequency, their ratio, i.e. the loss factor $\eta = \dfrac{G''}{G'}$, usually varies between 0.8 and 1.40 (Figure 1.26(b)). For practical applications it is independent of strain and temperature and is also often used as a measure of energy dissipation capacity of the viscoelastic material.

Temp. ($^\circ$C)	Freq. (Hz)	Strain (%)	G′ (psi)	G″ (psi)	η
24	1.0	5	142	170	1.20
24	1.0	20	139	167	1.20
24	3.0	5	272	324	1.19
24	3.0	20	256	306	1.20
36	1.0	5	59	67	1.13
36	1.0	20	58	65	1.12
36	3.0	5	108	119	1.10
36	3.0	20	103	112	1.09
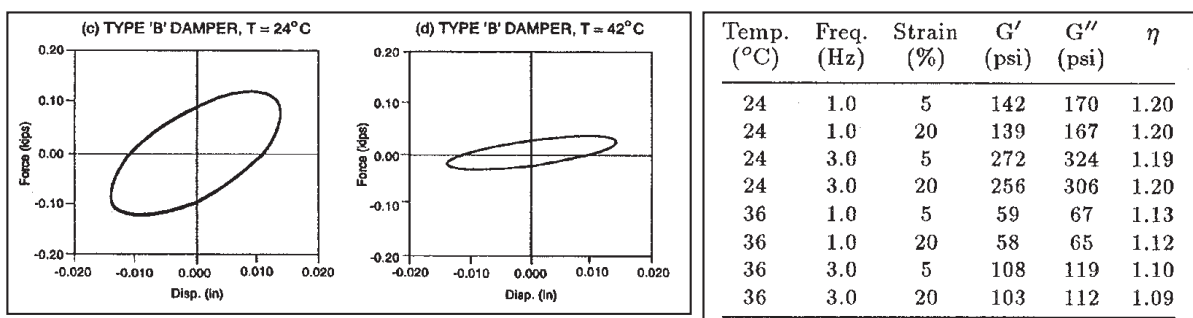
Figure 1.26 (a) Hysteretic cycles for different temperatures; (b) Values of G', G'' and η for several values of temperature, frequency and strain amplitude.

VE dampers are among the first energy dissipation devices employed in order to control vibration induced by the wind action in high-rise buildings, such as it was the case of World Trade Center of New York in 1969.

1.4.3. Other dampers

This classification (other) includes all devices that cannot be classified as either displacement or velocity-dependent. Examples of "other" devices include shape-memory alloys (SMA), friction-spring assemblies and pressurized fluid- viscous dampers with recentering capability. Figure 1.27 presents force-displacement relations for these devices, which dissipate energy while providing recentering capability, and resist motion with a nearly constant force.
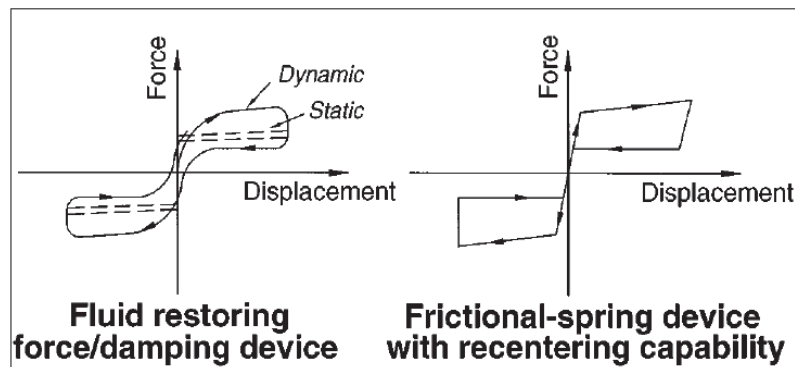
Figure 1.27 Idealized force-displacement loops of energy dissipation devices with recentering capability (from FEMA 273).

Shape memory alloys are metal alloys which can sustain large strains (up to 10%) with no residual deformation after unloading (super-elasticity). This property is due to reversible solid-to-solid phase transformations (austenite to martensite), which can be either thermal or stress induced. The chemical instability of the martensite which switches to austenite at low stresses generates stable hysteretic loops, thus giving rise to adequate energy dissipation capacity (Duerig et al 1990). It suffices here to say that these special metal alloys exhibit advantageous re-centring properties and high low-cyclic fatigue resistance; therefore, SMAs are particularly attractive for applications in seismic design and redesign. Recently, they have been implemented in several dissipative devices for earthquake protection, especially diagonal braces and base-isolation systems. These devices combine re-centring and dissipative properties, as displayed in Figure 1.27.

39

1.5 Seismic isolation systems

Base isolation represents an effective way to reduce seismic stresses in buildings by inserting an horizontally flexible and dissipative interface at the base of the building, between foundation system and superstructure. The structure rests on special isolation devices which allow significant relative displacements and provide sufficient energy dissipation capability to limit them.

The presence of these elements leads to the decoupling of the building from the soil movement, making the building more flexible and thus producing a lengthening of the structural period of vibration. Added damping is an inherent property of most isolators, but may also be provided by supplemental energy dissipation devices installed across the isolation interface. In this way the response spectrum acceleration coordinate is brought down, as Figure 1.2 depicts.

Seismic isolators are mainly divided into elastomeric (Figure 1.28(a)) and friction isolators (Figure 1.28(b)), according to the type of energy dissipation mechanism.

(a)   (b)

Figure 1.28 (a) LDRB-LC and (b) FPS isolators (courtesy of FIP Industriale).

1.5.1 Elastomeric isolators

Elastomeric isolators are usually made of layers of rubber separated by steel shims, which constrain lateral deformation of the rubber under vertical loads. Laminated rubber bearings can withstand large gravity loads, while providing only a fraction of the lateral stiffness of the superstructure they support. As shown in Figure 1.28(a), a typical laminated-rubber bearing is composed of elastomeric tuber layers alternating with steel plates solidly joined together under high pressure and temperature through a process called vulcanization. The vertical stiffness of the bearing is greatly enhanced by the presence of the steel plates.

40

Elastomers manufactured with special fillers ensure elevated hysteretic energy dissipation. Elastomeric devices are high-damping rubber bearings (HDRBs), low-damping rubber bearings (LDRBs) or low-damping rubber bearings with a lead core (LDRB-LC). These devices have been used worldwide in new and existing structures because of their high efficiency.

Increasing damping in rubber allows to reduce the relative displacement between the structure and everything else connected with it.

HDLRBs and LDLRBs respectively provide a damping ratio around 10-15% in the first case, and 5% in the second. More recently, high damping rubbers have been suggested for laminated rubber bearings, reaching values of equivalent viscous damping of approximately 20% at shear strains of 300%. Using lead core in conjunction with low damping rubber also provides relatively high level of damping. Lead has not only very good fatigue resistance properties but is also commonly available since it is used in batteries at a purity level of more than 99.9%.

1.5.2 Friction isolators

An alternative type of isolation device is given by friction isolation devices. In this case the structure is supported by sliding seals which frictional forces oppose to the structural movement dissipating energy. The main parameter in this type of isolation system is the coefficient of friction relative to the contact surfaces and its main advantage is the cost and the absence of limitation to the allowable vertical load to be transmitted. They have two main disadvantages: friction is usually difficult to quantify (usually in the range 4÷12 %, mainly depending on velocity, pressure and surface conditions) and permanent offset between the sliding parts may occur after an earthquake, especially in non re-centring systems.

Sliding devices are usually flat assemblies, such as sliding poly-tetrafluoroethylene (PTFE), or, more commonly, have a curved surface, i.e. a friction–pendulum system (FPS). The latter overcomes the above disadvantages by employing a curved rather than a flat surface. One example of frictional isolation system is the friction pendulum (FPS), depicted in Figure 1.29.
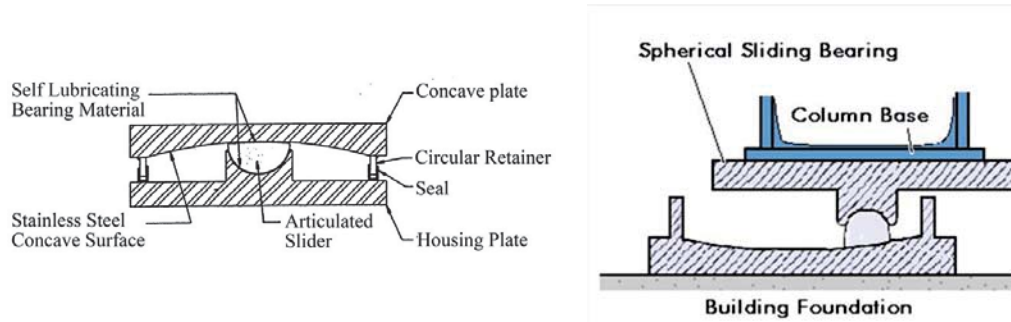
Figure 1.29 Friction pendulum system.

This system consists of two sliding plates characterized by curved surfaces covered with a layer of stainless steel; between them there is an articulated slider that can move on the curved surfaces. The side of the slider in contact with the spherical surfaces is coated with a low friction material. Friction pendulum bearings use characteristics of a pendulum to lengthen the natural period of the isolated structure so that to reduce earthquake forces. The curved shape of FPS surfaces should enable the structure to return to its initial position after the action of an earthquake, using the weight of the structure itself.

The choice of isolators should comply with specific acceptance criteria. In particular, it should remain stable for design displacements and provide increasing resistance with increasing displacement (no degradation) under repeated cyclic load.

REFERENCES

Aiken ID, Kelly JM (1992) Comparative study of four passive energy dissipation systems. Bull NZ Nat Soc Earthq Engng 25:175–92.

ASCE (2005) Minimum design loads for buildings and other structures.

BSSC (2004) Building Seismic Safety Council. FEMA 450 - NEPHR Recommended Provisions For Seismic Regulations For New Buildings and Other Structures, U.S.A.

Christopoulos C, Filiatrault A (2006) Principles of Passive Supplemental Damping and Seismic Isolation. IUSS Press 133:1192.

Clark PW, Aiken ID, Tajirian F, et al (1999) Design procedures for buildings incorporating hysteretic damping devices. Int. Post-SmiRT Conf. Semin. Seism. Isol. Passiv. Energy Dissipation Act. Control Vib. Struct.

Constantinou MC, Symans M (1993) Experimental study of seismic response of buildings with supplemental fluid dampers. J Struct Des Tall Build 2:93–132.

Di Sarno L, Elnashai AS (2005) Innovative strategies for seismic retrofitting of steel and composite structures. Prog Struct Eng Mater 7:115–135. doi: 10.1002/pse.195

Duerig TW, Melton KN, Stockel D, C.M. W (1990) Engineering aspects of shape memory alloys. London, UK

Fu Y, Kasai K (1998) Comparative Study of Frames Using Viscoelastic and Viscous Dampers. J Struct Eng 124:513–522. doi: 10.1061/(ASCE)0733-9445(1998)124:5(513)

Grigorian CE, Yang TS, Popov EP (1993) Slotted bolted connection energy dissipators. Earthq Spectra 9:491–504.

Hurtado F, Bozzo LM (2008) Numerical and experimental analysis of a shear link energy dissipator for seismic protection of buildings. 14th World Conf. Earthq. E ngineering

Pall AS, Marsh C (1982) Response of friction damped braced frames. ASCE, J Struct Div 1208:1313–23.

Pall AS, Pall R (1993) Friction-dampers used for seismic control of new and existing building in Canada. ATC 17-1 Semin. Isol. Energy Dissipation Act. Control. pp 675–686

Serino G, Occhiuzzi A (1994) The energy approach in active/hybrid vibration control. First World Conf. Struct. Control

Shen KL, Soong TT (1995) Modeling of viscoelastic dampers for structural applications. J Eng Mech 121:694–701.

Soong TT, Dargush GF (1997) Passive Energy Dissipation Systems in Structural Engineering. 368.

Wada A, Y.H. H, M. I (1999) Passive damping technology for buildings in Japan. Prog Struct Engng Mater 2:1–15.

Chapter 2

2. MODELING OF DAMPING SYSTEMS

2.1 Introduction

This chapter describes mechanical properties and mathematical modeling of dampers, not only supplemental damping systems but also seismic isolators, making some general comments on their structural applicability. The concept of replacing the complicated and often nonlinear behaviour of dampers and isolators by equivalent linear stiffness and damping characteristics has enormous benefits for the preliminary analysis and design of passively controlled structures. As noted above, the force-displacement relation for selected types of devices may be dependent on environmental conditions (e.g., wind, aging, and operating temperature), excitation frequency, sustained deformations and bilateral deformations. Such dependence should be accounted for and could be investigated by analysis of the mathematical model with limiting values assigned to the properties of the devices.

2.2 Effective damping and stiffness

Although damping in actual structures is due to several energy-dissipating mechanisms acting simultaneously (friction, hysteresis, etc.), a mathematically convenient approach is to idealize them by equivalent viscous damping.

Damping in actual structures is usually represented by equivalent viscous damping. It is the simplest form of damping to use since the governing differential equation of motion is linear and hence amenable to analytical solution. The advantage of using a linear equation of motion usually outweighs whatever compromises are necessary in the viscous damping approximation. In this section we determine the damping coefficient for viscous damping so that it is equivalent in some sense to the combined effect of all damping mechanisms present in the actual structure. The simplest definition of equivalent viscous damping is based on the measured response of a system to harmonic force at exciting frequency $\bar{\omega}$ equal to the natural frequency ω of the system. The damping ratio ζ_{eq} is calculated through the dynamic amplification factor. This is the equivalent viscous damping since it accounts for all the energy-dissipating mechanisms that existed in the experiments.

Another definition of equivalent viscous damping is that it is the amount of damping that provides the same bandwidth in the frequency-response curve as obtained experimentally for an actual system, (i.e. the halphpower bandwidth method). The damping ratio ζ_{eq} can also be calculated in free vibration by means of the logarithmic decay.

If the system's resisting force is measured during vibration, an effective method for defining equivalent viscous damping is to equate the energy dissipated in a vibration cycle of the actual structure and an equivalent viscous system. For an actual structure the force-displacement relation obtained from an experiment under cyclic loading with displacement amplitude u_o is determined; such a relation of arbitrary shape is shown schematically in Figure 2.1. The energy dissipated in the actual structure is given by the area E_D enclosed by the hysteresis loop. Equating this to the energy dissipated by viscous damping at the same amplitude leads to

$$\zeta_{eq} = \frac{1}{4\pi} \frac{1}{\bar{\omega}/\omega} \frac{E_D}{E_S} \tag{2.1}$$
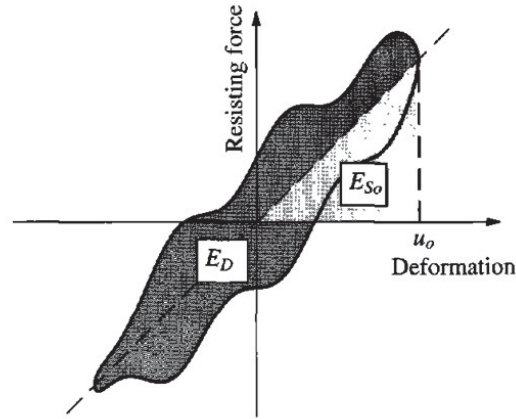
Figure 2.1 Energy dissipated in a cycle of harmonic vibration determined from experiment (Chopra 2011).

where the strain energy, $E_S = \dfrac{1}{2} k_{eff} u_0^2$, is calculated from the secant stiffness determined by experiment at maximum displacement.

Secant stiffness can be determined as follows:

$$k_{eff} = \frac{\left|F^+\right| + \left|F^-\right|}{\left|u_0^+\right| + \left|u_0^-\right|}$$

where $\left|u_0^+\right|$ and $\left|u_0^-\right|$ are maximum positive and negative displacements, respectively, $\left|F^+\right|$ and $\left|F^-\right|$ the corresponding restoring force.

If the experiment leading to the force-deformation curve of Figure 2.1 and hence E_D is conducted at $\bar{\omega} = \omega$ where the response of the system is most sensitive to damping, eq. (2.1) specializes to

$$\zeta_{eq} = \frac{1}{4\pi} \frac{E_D}{E_S}$$

The damping ratio ζ_{eq} determined from a test at $\bar{\omega} = \omega$ would not be correct at any other exciting frequency, but it would be a satisfactory approximation.

The energy dissipated in inelastic deformations of the structure can also be modeled by equivalent viscous damping. This idealization is generally not satisfactory, however, for the large inelastic deformations of structures expected during strong earthquakes. Inelastic deformations and associated energy dissipation should be accounted by nonlinear force-deformation relations.

Experiments on structural metals indicate that the energy dissipated internally in cyclic straining of the material is essentially independent of the cyclic frequency. Similarly, forced vibration tests on structures indicate that the equivalent viscous damping ratio is roughly the same for all natural modes and frequencies. Thus we refer to this type of damping as rate-independent linear damping. Other terms used for this mechanism of internal damping are structural damping, solid damping, and hysteretic damping.

2.3 Displacement dependent dampers

Metallic yielding and friction devices dissipate energy through yielding of metallic materials or through sliding contact friction between adjoining surfaces, respectively. Both devices can be considered hysteretic since their energy dissipation is not sensitive to the relative velocity. Thus they can be modeled with force-displacement hysteretic relationships that are well known to structural engineers.

These energy dissipation devices could be small relative to the structural framing member sizes. If this is true, then when the structural members begin to yield, their energy dissipation can far exceed the device energy dissipation. In other words, hysteretic dampers can be extremely effective and can be evaluated as equivalent viscous damping until the structure yields.

Some typical models that have been used to represent the nonlinear force-displacement relationships are the simple elastoplastic model, the bilinear model, and the Bouc-Wen model which are illustrated in Figure 2.2 and discussed below. The cyclic hysteretic characteristics of these models is based on their skeleton curve, which is the name given to the monotonic force-deflection curve obtained by increasing the force acting on the structure from 0 to the desired force or displacement.

and discussed below. The cyclic hysteretic characteristics of these models is based on their skeleton curve, which is the name given to the monotonic force-deflection curve obtained by increasing the force acting on the structure from 0 to the desired force or displacement.
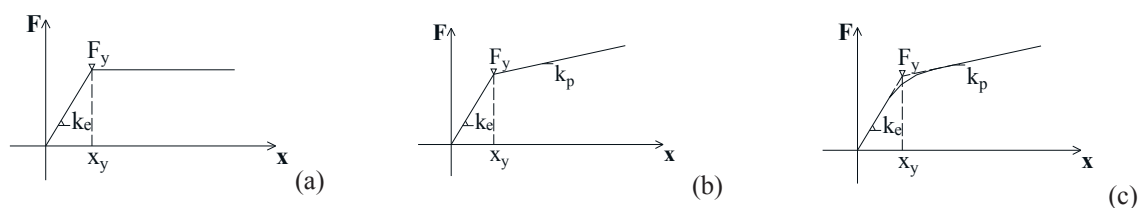
Figure 2.2 Hysteretic force-displacement models: elastoplastic (a), bilinear (b), Bouc-Wen (c).

Rheological models and corresponding hysteresis cycles of elastoplastic and bilinear force-displacement relationships are shown in Figure 2.3:
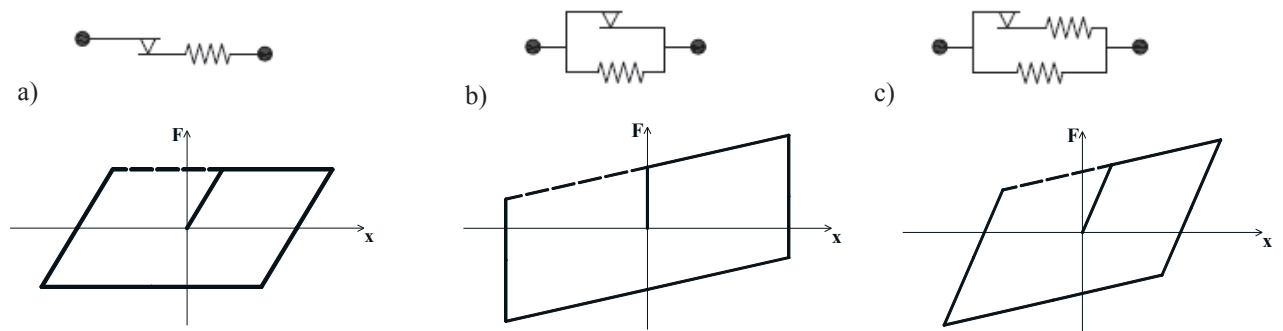
Figure 2.3 Rheological models and hysteresis loops: (a) elastoplastic (b) rigid – plastic with hardening (c) elastic – plastic with hardening (bilinear).

Friction behavior can be modeled with an elastoplastic behavior with infinite elastic stiffness (Figure 2.4). This means that at the initial state, the device provides a significant contribution to the global stiffness of the structure.
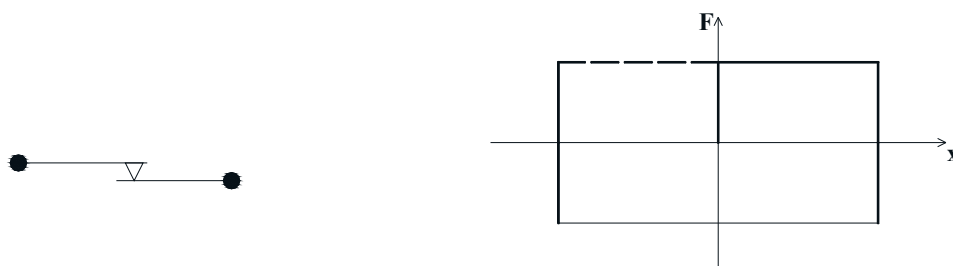
Figure 2.4 Rheological model and hysteresis loop for frictional behavior.

The cyclic hysteretic shapes are twice the size of the skeleton curve, with a starting point at the selected return displacement. The area enclosed within one cycle of the hysteretic curve is the energy dissipated per cycle. The equivalent viscous damping is obtained by setting the area within the hysteretic loop equal to the area within a viscous damper cycle at the same maximum displacement. This is done for each of these characteristic force-displacement shapes in the following discussion, assuming that maximum displacement x_{max} is constant and always larger than the system's yielding displacement.

2.3.1   *Elastoplastic form*

The initial elastic stiffness is determined from experimental yield force and yield displacement as:

$$k_e = F_y / x_y$$

Whenever the device displacement exceeds x_y the force is equal to F_y. The energy dissipated per cycle is equal to the area within the hysteretic loop between (F_y, x_{max}) and $(-F_y, -x_{max})$, which is:

$$E_{ep} = 4F_y(x_{max} - x_y)$$

For the elastoplastic model, setting E_{ep} equal to the energy-viscous value (i.e. $E_v = \pi C_d \omega x_{max}^2$) results in an equivalent viscous damping coefficient of:

$$C_d = 4F_y(x_{max} - x_y)T / (2\pi^2 x_{max}^2)$$

Strain energy at x_{max} is:

$$E_s = \frac{1}{2}F_y x_{max} \tag{2.2}$$

and the corresponding equivalent damping ratio is:

$$\zeta_{eff} = \frac{E_{ed}}{4\pi E_s} = \frac{2}{\pi}(1 - \frac{x_y}{x_{max}}) \tag{2.3}$$

Secant stiffness can be expressed as:

$$k_{eff} = \frac{F_y}{x_{max}} = k_e \frac{x_y}{x_{max}}$$
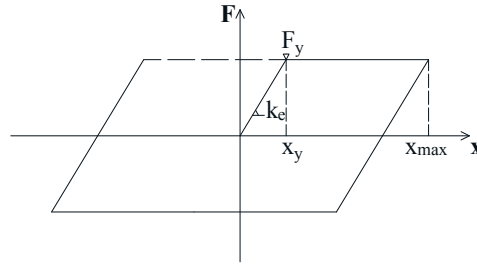
Figure 2.5 Hysteresys loop for elastoplastic case.

Considering the plot of Figure 2.5, dissipated energy can also be expressed as:

$$E_{ep} = 4F_y(x_{max} - x_y) = 4k_e x_y^2(\frac{x_{max}}{x_y} - 1) = 4k_e x_y x_{max} - 4k_e x_y^2 \tag{2.4}$$

To detect the influence of the yielding displacement with respect to the maximum one, eq. (2.4) is derived respect to x_y, thus obtaining:

$$\frac{dE_{ep}}{dx_y} = 4k_e x_{max} - 8k_e x_y$$

By setting $\dfrac{dE_{ep}}{dx_y} = 0$, it is found that maximum value of dissipated energy is attained at the

point

$\bar{x}_y = \dfrac{x_{max}}{2}$ (Figure 2.6), with a corresponding value of $\bar{E}_{ep} = k_e x_{max}^2$.
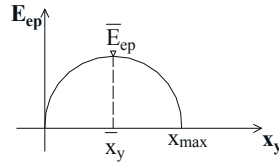
Figure 2.6 Energy dissipated versus yielding displacement.

In the following figures (Figure 2.7), four hysteresis cycles are plotted for different values of

x_y / x_{max}, i.e. 0, 0.25, 0.5 (corresponding to optimum) and 1.
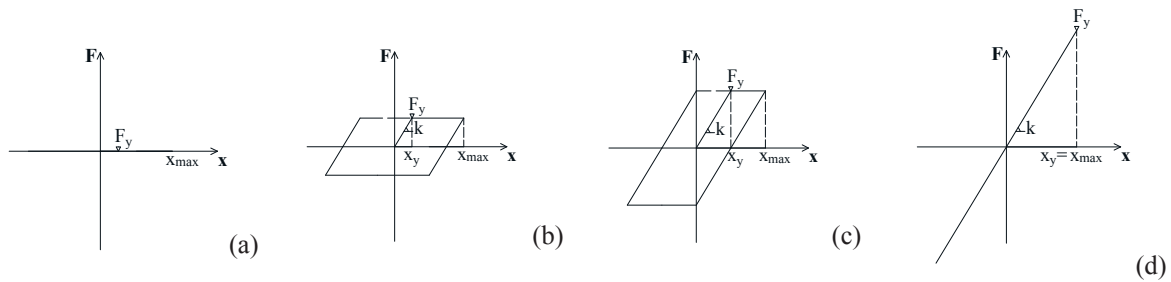
Figure 2.7 Hysteresys cycle for different xy/xmax= 0 (a), 0.25 (b), 0.5 (c), 1 (d).

In both cases $x_y / x_{max} = 0$ and $x_y / x_{max} = 1$, dissipated energy is zero.

Figure 2.8 shows the trend of the damping ratio ζ_{eff} from eq. (2.3), that is maximum in case of

$\dfrac{x_y}{x_{max}} = 0$, i.e. friction behavior.
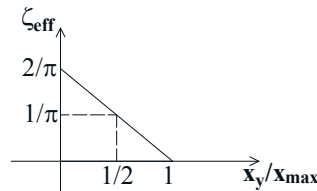
Figure 2.8 Equivalent viscous damping for hysteretic systems.

This trivial example is useful to give the idea of optimum yielding displacement depending on
the system's properties, showing that maximum dissipated energy and maximum damping do
not correspond to the same condition.

For a friction device damper, eq. (2.2), (2.3) and (2.4) with $x_y = 0$ can be adopted.

2.3.2 Bilinear form

As in the elastoplastic case, the initial elastic stiffness is given by:

$$k_e = F_y / x_y$$

The second slope, typically called the strain-hardening slope, is defined as having a stiffness k_p. It should be noted that the strain-hardening stiffness affects both the cyclic energy dissipated and the device restoring force, being respectively:

$$E_b = 4(k_e - k_p)x_y(x_{max} - x_y) \qquad (2.5)$$

$$E_s = \frac{1}{2}\left[F_y + k_p(x_{max} - x_y)\right]x_{max}$$

The equivalent stiffness can be taken as the secant stiffness at the maximum device displacement:

$$k_{eff} = \frac{\left[k_e x_y + k_p(x_{max} - x_y)\right]}{x_{max}}$$

This means that the restoring force increases as the displacement exceeds x_y, and the energy dissipated per cycle decreases as the hardening stiffness increases.

The eq. (2.5) can be properly manipulated to make a comparison with eq. (2.4) and it results, for the same initial stiffness k_e and maximum displacement x_{max}:

$$E_b = (1 - \frac{k_p}{k_e}) \cdot E_{ep}$$

The bilinear form reduces to the elastoplastic model setting $k_p = 0$.

2.3.3 Bouc-Wen model

The Bouc–Wen model is often used to describe hysteretic phenomena. It was introduced by Bouc (Bouc 1967) and extended by Wen (Wen 1976), who demonstrated its versatility by producing a variety of hysteretic patterns. The hysteretic behavior is treated in an unified manner by a single nonlinear differential equation with no need to distinguish different phases, as for example in the various Coulomb friction models.

The non linear restoring force can be expressed as:

$$F(t) = a\frac{F_y}{x_y}x(t) + (1 - a)F_y z(t) \qquad (2.6)$$

where $x(t)$ is the displacement, F_y the yield force, x_y the yield displacement, a the ratio of post-yield to pre-yield (elastic) stiffness and $z(t)$ a dimensionless hysteretic parameter that obeys a single nonlinear differential equation:

$$\dot{z}(t) = \frac{1}{x_y}[A - |z(t)|^n (\beta + sign(\dot{x}(t)z(t))\gamma)]\dot{x}(t),$$

where A, β, γ, n are dimensionless quantities controlling the behavior of the model, $sign(\cdot)$ is the signum function and the overdot denotes the derivative with respect to time. Small values of the positive exponential parameter n correspond to smooth transition from elastic to post-elastic branch, whereas for large values of n the transition becomes abrupt, approaching that of the bilinear model. Parameter A was introduced in the original paper, but it became evident that it is redundant and so is usually set equal to unity. Parameters β, γ control the size and shape of the hysteretic loop. The model is relatively insensitive to the absolute values of β and γ if both are changed proportionally, though very large values (absolute values > 50.0) of both parameters tend to cause significant numeric noise. Absolute values of β and γ inversely influence hysteretic stiffness and strength, as well as the smoothness of the hysteresis loop. However, the magnitude of influence is quite small. Great sensitivity exists as to the relative value of β with respect to γ and vice versa. The combination of β and γ dictates whether the model describes a hardening or softening load-slip relationship (Figure 2.9). However, these parameters do not have clear physical interpretation.
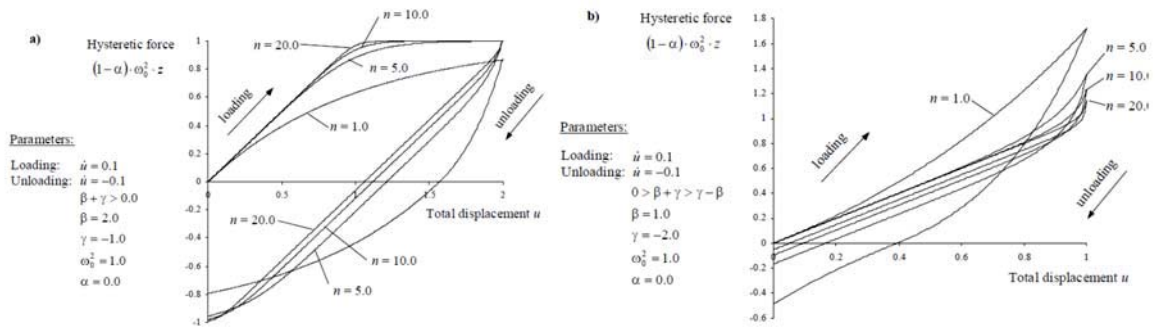
Figure 2.9 a) Hysteretic force versus total displacement: effect of increasing n on softening hysteresis is shown. All other parameters are kept constant. b) Similar to a) but β and γ are set to yield a hardening hysteresis.

It follows from eq. (2.6) that the restoring force $F(t)$ can be analyzed into an elastic and a hysteretic part as follows:

$$F^{el}(t) = a\frac{F_y}{x_y}x(t)$$

$$F^h(t) = (1-a)F_y z(t)$$

Thus, the model can be visualized as two springs connected in parallel (Figure 2.10), where

$k_i = \dfrac{F_y}{x_y}$ and $k_f = ak_i$ are the initial and post-yielding stiffness of the system.
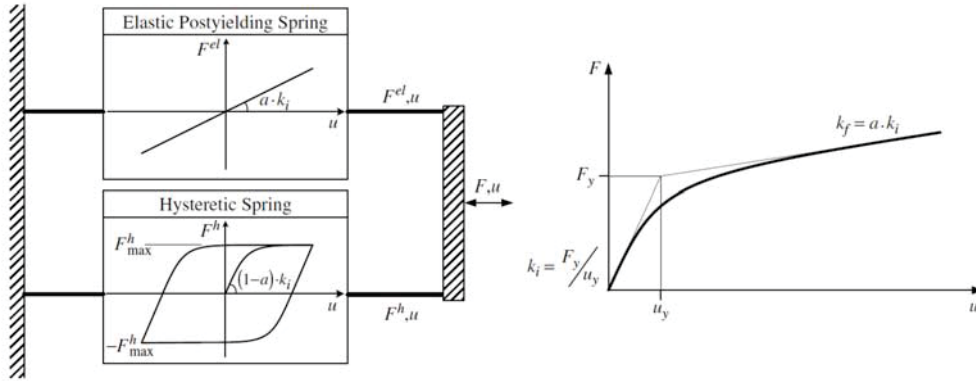
Figure 2.10 Bouc-Wen model.

The dissipated energy is expressed by the area enclosed by hysteretic loops, generally employing numerical evaluation:

$$E = \oint F^h dx$$

Due to problems of numerical accuracy, usually an alternative method based on complementary areas respect to the outer rectangle is adopted. This formulation is numerically stable for both partially and fully yielding systems.

An important modification to the original Bouc–Wen model was suggested by Baber and Wen (Baber and Wen 1981) and Baber and Noori (Baber and Noori 1986), i.e. Bouc-Wen-Baber-Noori model.

This modification included strength, stiffness and pinching degradation effects, by means of suitable degradation functions:

$$\dot{z}(t) = \frac{h(z(t))}{\eta(\varepsilon)}\left\{A(\varepsilon) - \nu(\varepsilon)[\beta sign(\dot{x}(t))|z(t)|^{n-1}z(t) + \gamma|z(t)|^n]\right\}\dot{x}(t)$$

where the parameters $\nu(\varepsilon)$, $\eta(\varepsilon)$ and $h(z)$ are associated with the strength, stiffness and pinching degradation effects, respectively. The $\nu(\varepsilon)$, $\eta(\varepsilon)$ and $A(\varepsilon)$ parameters are defined as linearly-increasing functions of adsorbed hysteretic energy ε.

2.4 Velocity dependent dampers

The force-displacement response of a velocity-dependent device is primarily a function of the relative velocity between each end of the device. In this case associated damping is viscous type.

2.4.1. VE solid devices

The most common rheological model for a visco-elastic material is the Kelvin-Voigt model, made by a spring and a dashpot acting in parallel (Figure 2.11**Errore. L'origine riferimento non è stata trovata.**).

Figure 2.11 Rheological model and hysteresis cycle for a visco-elastic device.

It is seen that the force-displacement relationship is an ellipse with a nonzero slope. The slope is associated with the G' term, and the area of the ellipse is related to the G'' term, so that the former influences the stiffness and hence the frequency of the damper, while the latter relates to the energy dissipated in each cycle.

Consider a sheet of VE material bonded between two plates with area A and thickness t. The effective or equivalent stiffness of the device is:

$$k_d = AG'(\omega)/t$$

and the effective or equivalent viscous damping coefficient is:

$$C_d = AG''(\omega)/t\omega$$

The force in the device is a function of the velocity $\dot{x}$ and the displacement x and can be computed as:

$$F(t) = k_d(\omega)x(t) + C_d(\omega)\dot{x}(t)$$

thus contributing to increase both viscous damping and lateral stiffness.

When the loss factor is used, the effective viscous damping can be expressed as

$$C_d = k_d\eta/\omega$$

2.4.2. Viscous Fluid Devices

Experimental testing (Seleemah and Constantinou 1997) has shown that a suitable mathematical model for describing the behavior of viscous fluid dampers is given by the following nonlinear force-velocity relation:

$$F(t) = C_d(\omega)|\dot{x}|^\alpha \, \text{sgn}(\dot{x}) \tag{2.7}$$

where $C_d(\omega)$ is generalized damping coefficient, which is approximately constant below about 4 Hz, and α takes values in the range of about $0.15 \div 2$. The value $\alpha = 2$ is achieved with cylindrical orifices, a performance which is typically unacceptable.

When $\alpha = 1$, the device exhibits linear behaviour. Small values of α, such as 0.5, are effective in attenuating high-velocity shocks, as those expected in near-fault earthquake excitation; $\alpha = 1$ is usually desirable in structural applications against wind or earthquakes (Figure 2.12).

Lower limits of the exponent cause the damper forces are not out of phase with the displacements and hence are additive to the structural displacements. This coupling effect increases with the amount of damping provided; the more damping provided, the smaller the benefit of having the damper force out of phase with the structure force.
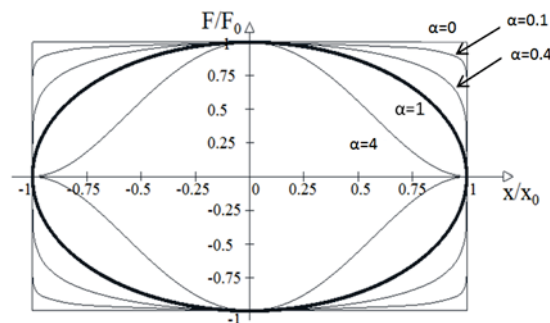
Figure 2.12 Cyclic behavior for a pure viscous dashpot for several values of α.

The force that is generated by the fluid damper is due to a pressure differential across the piston head. However, the fluid volume is reduced by the product of travel and piston rod area. Since the fluid is compressible, this reduction in fluid volume is accompanied by the development of a restoring (spring like) force. This is prevented by the use of the accumulator. Tested devices showed no measurable stiffness for piston motions with frequency less than about 4 Hz. The devices may provide additional viscous type damping to the fundamental mode and additional damping and stiffness to the higher modes. Alternatively, fluid dampers may be constructed

55

with run-through rod. This design prevents compression of the fluid and it does not require an accumulator.

These dampers provide damping forces via fluid orificing and restoring forces via compression of an elastomer. Thus, more accurately, the dampers may be referred to as viscoelastic fluid/solid dampers (Figure 2.13).

(a)

(b)

Figure 2.13 Rheological model for (a) a pure viscous and (b) a viscoelastic fluid damper.

Under steady-state harmonic motion, the hysteresis loops for the linear case ($\alpha=1$) are elliptical (see Figure 2.12) and approach a rectangular shape as α approaches zero. The energy dissipated per cycle of steady-state harmonic motion is obtained by integrating eq. 2.7 over the displacement leading to the following expression (Constantinou et al 1996):

$$E = \lambda C_d x_{max}^{1+\alpha} \omega^{\alpha} = \lambda F_0 x_{max}$$

where

$$\lambda = 4(2^{\alpha}) \frac{\Gamma^2(1+\alpha/2)}{\Gamma(2+\alpha)}$$

and F_0 = peak force developed by the damper; x_{max} peak displacement across the damper; Γ = gamma function; and λ = parameter whose value depends exclusively on the velocity exponent, α.

For a given force and displacement amplitude, the energy dissipated per cycle for a nonlinear fluid damper is larger, by a factor λ/π, than that for the linear case and increases monotonically with reducing velocity exponent (up to a theoretical limit of $4/\pi=1.27$ which corresponds to a velocity exponent of zero). For a given frequency of motion, and displacement amplitude, x_{max}, to dissipate the same amount of energy per cycle, the damping coefficient of the nonlinear damper, C_{NL}, must be larger than that of the linear damper, C_L, as given by:

$$C_{NL} = C_L \frac{\pi}{\lambda} (\omega x_{max})^{1-\alpha}$$

The damper coefficient C_d can assume almost any value by changing orifice configuration: it may be increased or decreased simply by installing more or fewer dampers in the structure.

Certain types of viscous dampers have a relief valve providing a limited velocity. This is useful in limiting forces but reduces out-phase between velocity and displacements which may undermine the effectiveness of the damper on the global structural performance.

It is clear from Figure 2.12 that the equivalent stiffness for a viscous fluid device is 0. Thus, by itself, the device does not add stiffness when applied to a structure.

2.5 Modeling of brace damper assembly

Energy dissipating devices are typically attached to a structure through bracing, which may take the form of a diagonal or a chevron brace. For example, Figure 2.14 illustrates the installation of a damper on top of a chevron brace. The energy dissipation assembly of this story and bay of the structure consists of the chevron brace and the damper installed in series. When the brace has infinite stiffness, the force exerted by the damper on the top girder is related to the relative velocity and/or displacement between the top and bottom girders. In this case, analysis of the damped structure may be performed by assuming models of Section 2.3. and 2.4.

A damper-brace component consists of a damper connecting with a brace in series.

The stiffness of the brace connecting the damper to the structure actually affects the damper efficiency significantly, which depends on the damper parameters and the natural frequencies of the structure. In most cases, its influence on the performance of the damper should not be neglected; in other words the brace stiffness should not be approximately treated as infinite in seismic response analysis of the structure with dampers.
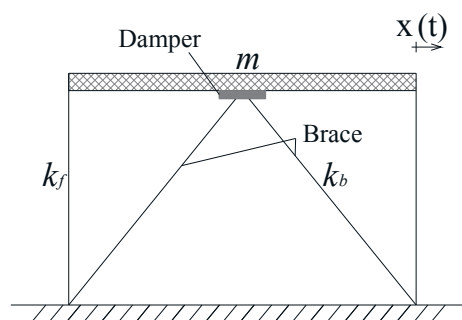
Figure 2.14 SDOF model with dissipative braces.

The behavior of this assembly is best described by the Maxwell model for which the force, F, exerted on the top girder is described by:

$$\begin{bmatrix} F = F_d = F_b \\ x = x_d + x_b = x_1 + x_2 \end{bmatrix}$$

where F_d is the force in the damper, F_b is the force in the brace, $x_d = x_1$ is the damper relative displacement, $x_b = x_2$ is the brace relative displacement, x is the frame relative displacement. The damper provides the most effective reduction in vibration response of the structure with a rather stiff brace, i.e. $x_b \rightarrow 0$ and $x_d \rightarrow x$. Thus, the brace stiffness is found to have significant effect on the vibration control performance of the damper and thus it is an important parameter in designing such an energy dissipation system.

2.5.1 Velocity dependent damper brace assembly

In case of velocity dependent damper, complex response theory is adopted in the following (Fu and Kasai 1998; Ou et al 2007).

The damping force generated by the damper can be expressed as:

$$F_d = (k_d^{'} + ik_d^{''})x_1 \tag{2.8}$$

where $k_d^{'}$ and $k_d^{''}$ are the damper storage modulus and loss modulus, respectively.

For a viscoelastic damper, $k_d^{'} = k_{eff} = \dfrac{G'A}{t}$ and $k_d^{''} = \bar{\omega}C_d = \dfrac{G''A}{t}$; for a viscous damper, $k_d^{'} = 0$ and $k_d^{''} = \bar{\omega}C_d$. In other words, a pure viscous dashpot has no storage stiffness, meaning that exerted force is zero at maximum displacement.

The resistance force of the brace can be expressed as:

$$F_b = (k_b^{'} + ik_b^{''})x_2 \text{ where } k_b^{'} = k_b \text{ and } k_b^{''} = 0 \tag{2.9}$$

The rheololgical models of such viscous and viscoelastic damper–brace component are shown in Figure 2.15.

(a)

(b)

Figure 2.15 Rheological model of brace damper assembly: (a) viscous case, (b) viscoelastic case.

Combining eqs. (2.8) and (2.9), the resistance force of the damper–brace component can be described by the kelvin model as:

$$F_{db} = (k_{db}^{'} + ik_{db}^{''})x = \widetilde{k}x \tag{2.10}$$

where $\widetilde{k} = k_{db}^{'} + ik_{db}^{''}$ is a complex stiffness.

Eq. (2.10) is obtained going through the following passages in frequency domain:

$$(k_d' + ik_d'')x_1 = k_b x_2 = F_{db}$$

$$F_{db} = (k_d' + ik_d'')x_1 = (k_d' + ik_d'')(x - x_2) = (k_d' + ik_d'')(x - \frac{F}{k_b})$$

$$F_{db}(1 + \frac{k_d' + ik_d''}{k_b}) = (k_d' + ik_d'')x$$

$$\frac{F_{db}}{x} = \frac{(k_d' + ik_d'')}{(1 + \frac{k_d' + ik_d''}{k_b})} = \frac{(k_d' + ik_d'')k_b}{(k_d' + k_b) + ik_d''} = \tilde{k}$$

The general form of the complex stiffness $\tilde{k} = k_{db}' + k_{db}''$ is the following:

$$k_{db}' = \frac{k_b k_d'^2 + k_b^2 k_d' + k_b k_d''^2}{(k_d' + k_b)^2 + k_d''^2} \tag{2.11}$$

$$k_{db}'' = \frac{k_b^2}{(k_d' + k_b)^2 + k_d''^2} k_d'' \tag{2.12}$$

For the viscous case ($k_d' = 0$), k_{db}' and k_{db}'' specialize in:

$$k_{db}' = \frac{k_b k_d''^2}{k_b^2 + k_d''^2} = \frac{k_b C_d^2 \overline{\omega}^2}{k_b^2 + \overline{\omega}^2 C_d^2}$$

$$k_{db}'' = \frac{k_b^2 k_d''}{k_b^2 + k_d''^2} = \frac{k_b^2 C_d \overline{\omega}}{k_b^2 + \overline{\omega}^2 C_d^2}$$

The brace-damper restoring force becomes:

$$F_d = \frac{k_b C_d^2 \overline{\omega}^2}{k_b^2 + \overline{\omega}^2 C_d^2} x + i \frac{k_b^2 C_d \overline{\omega}}{k_b^2 + \overline{\omega}^2 C_d^2} x$$

or, in time domain:

$$F_{db} = k'(\omega)x + c'(\omega)\dot{x} \tag{2.13}$$

where $k' = k_{db}'$ and $c' = k_{db}'' / \overline{\omega}$ are, respectively, the storage stiffness and damping coefficient of the brace-damper. These quantities are, in general, frequency dependent.

By definition of the relaxation time $\tau = \frac{C_d}{k_b}$ (Constantinou et al 1996), in case of pure viscous behavior terms of eq. (2.13) become:

$$k'(\overline{\omega}) = \frac{C_d \tau \overline{\omega}^2}{1 + \tau^2 \overline{\omega}^2}$$

and

$$c'(\overline{\omega}) = \frac{C_d}{1 + \tau^2 \overline{\omega}^2}$$ (2.14)

For infinitely stiff bracing, $\tau = 0$, $k'(\overline{\omega}) = 0$ and which describes the case of linear viscous damper with $c'(\overline{\omega}) = C_d$.

For any other case, the energy dissipation assembly exhibits viscoelastic behavior. It can be seen from eq. (2.14) that the greater is the qunatity $\tau^2 \overline{\omega}^2$, the lower is $c'(\overline{\omega})$ with respect to C_d .

It is meaningful to understand the effect of both parameters k_b and C_d on the dynamic properties of the brace-damper assembly.

In the case $k_b \to \infty$, $k'_{db} = k'_d$ and $k''_{db} = k''_d$, thus reducing to the purely viscous or viscoelastic behavior corresponding to viscous dashpot or viscoelastic dashpot, respectively. Thanks to inifinite brace stiffness, there is no loss of efficiency in the brace-damper assembly, i.e. $x = x_1$ and $x_2 = 0$.

In the case $k''_d \to \infty$, i.e. $\overline{\omega} C_d \to \infty$ or $G''(\overline{\omega}) \to \infty$ corresponding to viscous dashpot or viscoelastic dashpot, respectively, $k'_{db} = k_b$ and $k''_{db} = 0$ accounting for a purely elastic behavior without any damping.

In the case $k'_d \to \infty$ for the viscoelastic damper, $k'_{db} = k_b$ and $k''_{db} = 0$ accounting for a purely elastic behavior without any damping.

It is worth to note that both extremely low and high values of the forcing frequency $\overline{\omega}$ yield no damping in the response, resulting:

- $\overline{\omega} \to 0$ $\Rightarrow$ $k'_{db} = 0$ and $k''_{db} = 0$
- $\overline{\omega} \to \infty$ $\Rightarrow$ $k'_{db} = k_b$ and $k''_{db} = 0$

The loss factor of the viscous damper–brace component, η_{db}, is obtained from eqs. (2.11) and (2.12) as:

$$\eta_{db} = \frac{k''_{db}}{k'_{db}} = 2\zeta_d$$ (2.15)

In eq. (2.15), η_{db} is an important parameter which reflects the damping characteristic of the damper–brace component; k'_{db} represents additional stiffness when the damper–brace

component is added to the structure; $k_{db}^{''}$ is associated with the energy dissipation capacity of the damper–brace component. Hence, a rate dependent damper-brace component is equivalently modeled by a Kelvin-Voigt type dashpot – spring model shown in Figure 2.16. In the equivalent model, the viscous coefficient of the dashpot element, C' and the stiffness of the spring element, k', can be expressed as $C' = k_{db}^{''} / \overline{\omega}$ and $k' = k_{db}^{'}$, respectively.
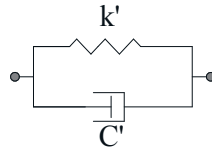
Figure 2.16 Rheological model of velocity dependent – damper assembly.

2.5.2. Frame - velocity dependent damper assembly

Assuming the brace-damper is inserted in a frame with lateral shear stiffness equal to k_f, the system resisting force is:

$$F(t) = F_f(t) + F_{db}(t) = \left[k_f + k'_{db}(\overline{\omega}) + ik''_{db}(\overline{\omega}) \right] x \qquad (2.16)$$

The rheological model is illutrated in Figure 2.17Figure 2.15. The inherent viscous damping is neglected in the following ($c = 0$).
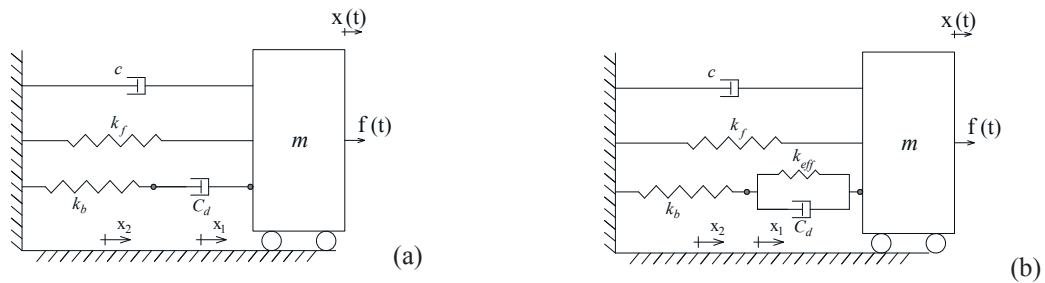
Figure 2.17 Rheological model of SDOF system with dissipative brace: (a) viscous case, (b) viscoelastic case.

As before, the term involving $\left[k_f + k'_{db}(\overline{\omega}) \right] x$ in eq. (2.16) indicates the elastic force of the whole system (i.e. in phase with the system's displacement). Thus, the whole system's stiffness becomes $\left[k_f + k'_{db}(\overline{\omega}) \right]$, where $k'_{db}(\overline{\omega})$ is named added stiffness. The term involving $ik''_{db}(\overline{\omega})x$ indicates the viscous force of the whole sytem (i.e. out-of-phase with the system displacement), thus reflecting the energy dissipation capability of the system.

During one harmonic movement cycle, the maximum strain energy is:

$$E_s = \left[k_f + k'_{db}(\bar\omega) \right] \frac{x^2_{max}}{2}$$

and the dissipated energy:

$$E_d = \pi k''_{db}(\bar\omega) x^2_{max}$$

When the excitation frequency $\bar\omega$ reaches the system's resonance frequency (assuming a mass attached to the right end of the system), the added damping ratio caused by the damper is:

$$\zeta_d = \frac{E_d}{4\pi E_s} = \frac{k''_{db}}{2(k_f + k'_{db})}$$

By previously defined stiffness terms, damping ratio in case of viscous damper becomes:

$$\zeta_{dv} = \frac{k_b^2 C_d \bar\omega}{2(k_f k_b^2 + k_f C_d^2 \bar\omega^2 + k_b C_d^2 \bar\omega^2)} \tag{2.17}$$

It can be noted that in both cases $\bar\omega \to 0$ and $\bar\omega \to \infty$, the equivalent damping ratio is zero. In ideal case of infinitely stiff brace it reduces to:

$$\zeta_{dv} = \frac{C_d \bar\omega}{2k_f} \tag{2.18}$$

When the sytem is vibrating at its natural frequency ω_n, eq. (2.18) becomes the well known:

$$\zeta_{dv} = \frac{C_d}{2\sqrt{k_f m}}$$

Introducing non-dimensional terms $\kappa = \dfrac{k_f}{k_b}$ and $\alpha''_d = \dfrac{k''_d}{k_f}$, equivalent damping ratio is:

$$\zeta_d = \frac{\alpha''_d}{2[1 + \alpha''^2_d \kappa(1+\kappa)]}$$

An added stiffness ratio can also be defined as the ratio between the damped-brace stiffness and the frame stiffness:

$$\alpha_0 = \frac{k'_{db}}{k_f} = \frac{\kappa \alpha''^2_d}{1 + \kappa^2 \alpha''^2_d}$$

When α''_d tends to infinity, α_0 monotonically tends to its maximum value that is $\dfrac{1}{\kappa}$ and ζ_d tends to 0. This phenomenon is understandable because when the damper loss stiffness becomes very large, the damper tends to lock and only the brace deforms. This means that also pure viscous damper, when added to elastic brace, can create added stiffness, that can be as large as brace stiffness, adding to the original system, especially under high mode motion,

because viscous dampers show rigid behavior under high frequency vibration. A stiffer supporting brace ($\kappa \to 0$) can reduce added stiffness while increasing supplemental damping. For a given κ, damping ratio exhibits a maximum for a certain value of $\alpha_d^{''}$: for both extremely low ($\alpha_d^{''} \to 0$) and high ($\alpha_d^{''} \to \infty$) values of the parameter, damping ratio is zero.

The system global resisting force can be rewritten by means of the damping ratio as:

$$F(t) = k_f(1+\alpha_0)x(1+2i\zeta_d)$$

$$F_{max} = x_{max}\sqrt{(k_f + k_{db}^{'})^2 + k_{db}^{''2}} = k_f(1+\alpha_0)x_{max}\sqrt{1+4\zeta_d^2}$$

The frequency of the damped-braced system can thus be expressed as follows:

$$\omega_{db}(\bar{\omega}) = \sqrt{\frac{k_f(1+\alpha_0)}{m}}$$

Depending on the external force frequency, damped-braced system frequency can vary in the range:

$$\sqrt{\frac{k_f}{m}} \leq \omega_{db} \leq \sqrt{\frac{k_f + k_b}{m}}$$

By providing added stiffness and damping, supplemental dampers change the original system's period and damping ratio, and therefore influence the seismic response of the system.

A stiff brace has a positive effect in reducing both maximum acceleration and displacement. By increasing $\alpha_d^{''}$, maximum displacements reduce while accelerations reduce at the beginning but increase after a turning point. Fu and Kasai recommend using $\kappa = 0.1$ or at least $\kappa > 0.2$, since for $\kappa < 0.1$ improvement in reduction is not significative and may even become worse. A value $\alpha_d^{''} = 1 \div 1.5$ is suggested for the best results.

The behavior of the damped system depends on both added stiffness ratio α_0 and added damping ratio ζ_d.

2.5.3. Displacement dependent damper brace assembly (friction case)

In case of hysteretic behaviour, classical force-displacement formulation is adopted.

In case of friction behaviour (Figure 2.18Figure 2.18), the damper force can be expressed as:

$$F_d = F_y \text{ for } x_1 > 0$$

(a)

(b)
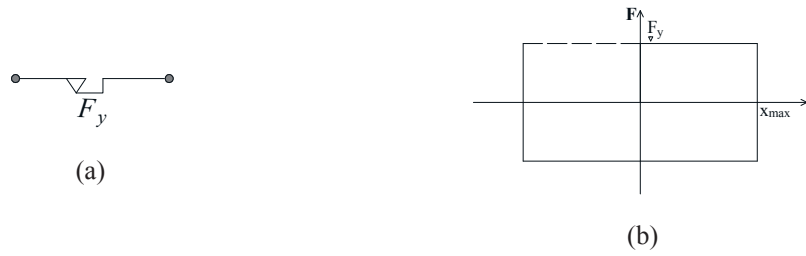
Figure 2.18 Rheological model (a) and hysteretic cycle (b) of a friction damper.

Equivalent viscous damping of a friction damper is always equal to:

$$\zeta_d = \frac{E_d}{4\pi E_s} = \frac{4F_y x_{max}}{4\pi \frac{1}{2} F_y x_{max}} = \frac{2}{\pi}$$

If the brace is connected to the damper (Figure 2.19(a)), the damper-brace component can be described by:

$$F_{db} = k_b x_1 \text{ for } x_1 < \bar{x}_y = \frac{F_y}{k_b}$$

$$F_{db} = F_y \text{ for } x_1 \geq \bar{x}_y$$

(a)

(b)

Figure 2.19 Rheological model (a) and hysteretic cycle (b) of brace+ friction damper.

Assuming the same maximum displacement x_{max}, the damper-brace hystreretic cycle is shown in Figure 2.19(b), and the equivalent viscous damping is:

$$\zeta_d = \frac{E_d}{4\pi E_s} = \frac{4F_y (x_{max} - \frac{F_y}{k_b})}{4\pi \frac{1}{2} F_y x_{max}} = \frac{2}{\pi}(1 - \frac{F_y}{k_b x_{max}})$$

so reduced by a factor $(1 - \frac{F_y}{k_b x_{max}})$ with respect to the pure friciton behavior.

2.5.4. Frame - displacement dependent damper assembly (friction case)

When a friction damper-brace assembly is inserted in a linear elastic frame (Figure 2.20), the rheological model can be represented as follows, assuming inherent viscous damping *c=0* for sake of simplicity.
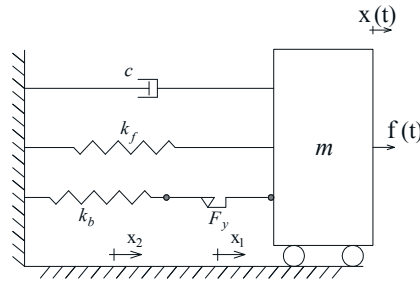
Figure 2.20 Rheological model of SDOF system with friction-dissipative brace.
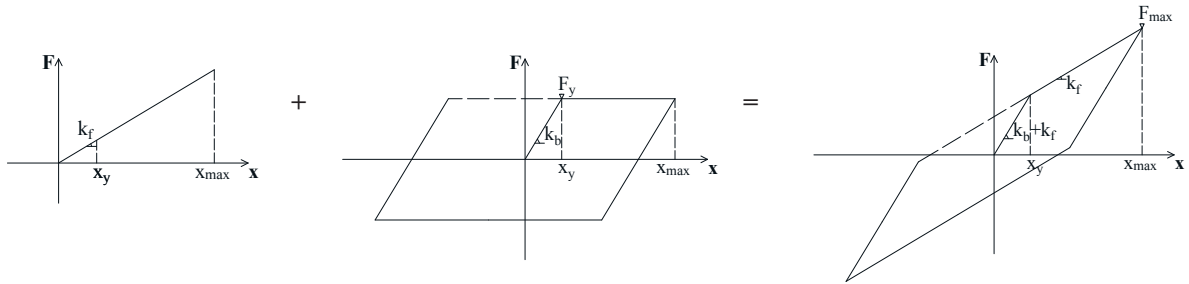
Figure 2.21 Force-displacement behavior of a SDOF system with friction-dissipative brace.

Considering the force-displacement response of Figure 2.21, dissipated energy only accounts for friction contribution and is equal to:

$$E_d = 4F_y(x_{max} - \frac{F_y}{k_b})$$

while strain energy is given by:

$$E_s = \frac{1}{2}(F_y + k_f x_{max})x_{max}$$

Frame stiffness increases elastic strain energy while leaving the same amount of dissipated energy, thus the equivalent damping ratio results:

$$\zeta_d = \frac{E_d}{4\pi E_s} = \frac{2}{\pi} \frac{F_y(1 - \frac{F_y}{k_b x_{max}})}{(F_y + k_f x_{max})}$$

and the secant stiffness is:

$$k_{eff} = \frac{F_y}{x_{max}} + k_f$$

2.5.5. Displacement dependent damper brace assembly (elastoplastic case)

In case of elasto-plastic behaviour (Figure 2.22), the damper force can be expressed as:

$$F_d = k_e x_1 \text{ for } x_1 < x_y$$

$$F_d = F_y \text{ for } x_1 > x_y$$

(a)

(b)
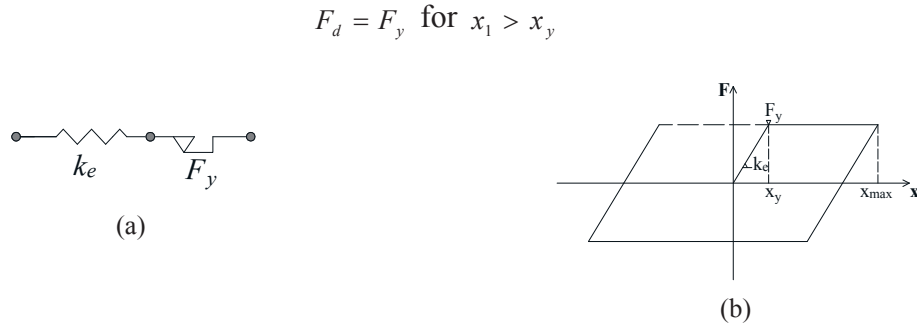
Figure 2.22 Rheological model (a) and hysteretic cycle (b) of an elastoplastic damper.

Equivalent viscous damping of an elasto-plastic damper is equal to:

$$\zeta_d = \frac{E_d}{4\pi E_s} = \frac{4F_y(x_{max} - \frac{F_y}{k_e})}{4\pi \frac{1}{2}F_y x_{max}} = \frac{2}{\pi}(1 - \frac{F_y}{k_e x_{max}})$$

If the brace is connected to the damper (Figure 2.23), the damper-brace component can be described by:

$$F_{db} = \frac{k_e k_b}{k_e + k_b} x_1 = k_{eq} x_1 \text{ for } x_1 < \overline{x}_y = \frac{F_y}{k_{eq}}$$

$$F_{db} = F_y \text{ for } x_1 \geq \overline{x}_y$$

(a)

(b)
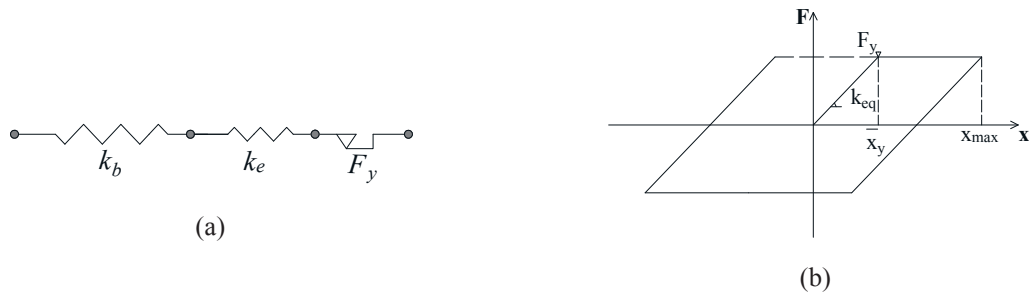
Figure 2.23 Rheological model (a) and hysteretic cycle (b) of brace - elastoplastic damper assembly.

Assuming the same maximum displacement x_{max} and that $F_{db} = F_y$, the damper-brace hystreretic cycle is shown in Figure 2.23 (b), and viscous damping is equal to:

$$\zeta_d = \frac{E_d}{4\pi E_s} = \frac{4F_y(x_{max} - \frac{F_y}{k_{eq}})}{4\pi \frac{1}{2}F_y x_{max}} = \frac{2}{\pi}(1 - \frac{F_y}{k_{eq} x_{max}}) .$$

With respect to friction behavior, a reduction of the provided damping can be appreciated due to the ratio $\frac{k_{eq}}{k_e} < 1$.

66

2.5.6. Frame - displacement dependent damper assembly (elastoplastic case)

If an elastoplastic damper-brace model is inserted in a linear frame (Figure 2.24), the rheological model can be set as:
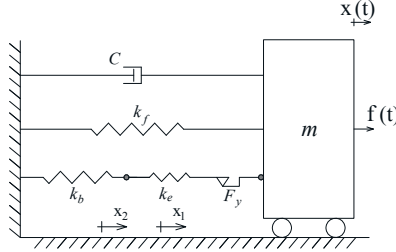
Figure 2.24 Rheological model of SDOF system with elastoplastic dissipative brace.
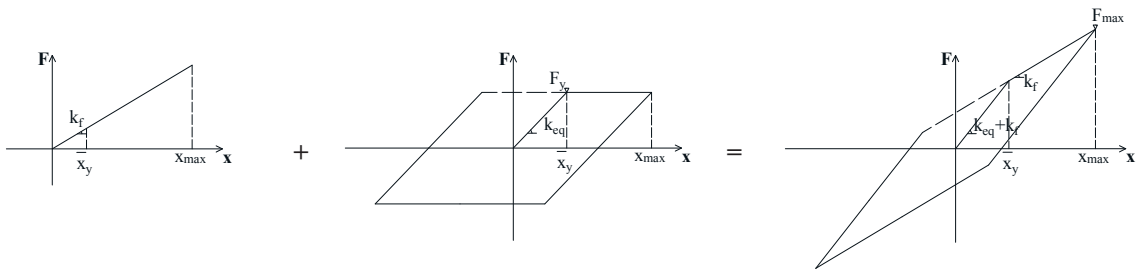
Figure 2.25 Force-displacement behavior of a SDOF system with elastoplastic-dissipative brace.

As in the friction case, bare frame response does not affect energy dissipation but just increases elastic strain energy (Figure 2.25), thus resulting:

$$E_d = 4F_y(x_{max} - \frac{F_y}{k_{eq}})$$

$$E_s = \frac{1}{2}\left[F_y + k_f x_{max}\right]x_{max}$$

Equivalent damping ratio is obviously reduced with respect to the friction case:

$$\xi_d = \frac{E_d}{4\pi E_s} = \frac{2}{\pi}\frac{F_y(1-\frac{F_y}{k_{eq}x_{max}})}{[F_y + k_f x_{max}]}$$

while increasing the secant stiffness by k_f:

$$k_{eff} = \frac{F_y}{x_{max}} + k_f \; .$$

67

2.6 Modeling of isolators' behavior

The role of damping in seismic isolation is complementary: shifting of period is carried out introducing lateral flexibility at a certain level (usually at the foundation) so that a strong reduction of accelerations and interstory drifts on the upper structure is obtained. The price of this benefit is in accepting much larger displacements, usually concentrated at the isolation level. To reduce them to acceptable values, an important contribution is provided by increasing damping up to certain limits (Figure 2.26).
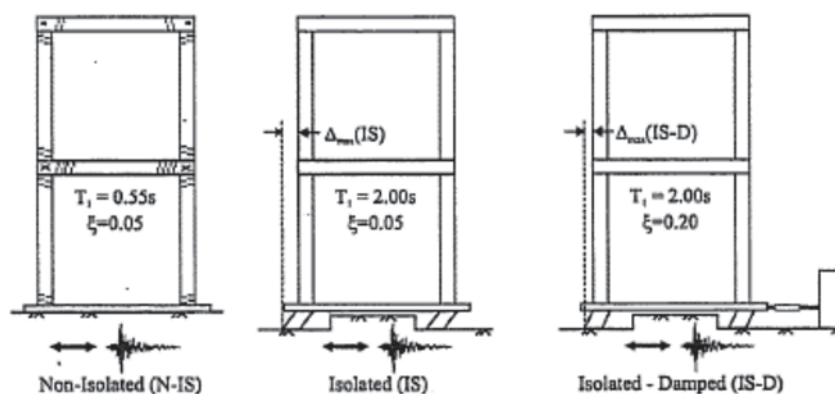
Figure 2.26 Non-Isolated, Isolated and Isolated-Damped Reinforced Concrete Frames.

In the following two main types of systems that have been widely used in the last fifteen years, namely the laminated-rubber bearings systems and the friction pendulum systems, are examined.

2.6.1. Elastomeric isolators

The steel plates vulcanized to the rubber layers limit severely the flexural deformations of a laminated-rubber bearing. Therefore, it can be assumed that pure shear deformations occur in the rubber only. The lateral stiffness of a laminated-rubber bearing can be approximated as:

$$k_b = \frac{G_r A_r}{h_r}$$

where G_r is the shear modulus of rubber at the design strain, A_r is the rubber layer area and h_r is the total rubber height. This equation neglects the reduction in lateral stiffness at large displacements.

Experiments have shown that the energy dissipation through shear deformations in rubber layers of laminated-rubber bearings can be modeled by equivalent viscous damping. Typical

bearings used in bridges provide equivalent viscous damping of the order of 5% to10% of critical. High damping rubbers are now available for bearing applications that can produce viscous damping up to 20% of critical.

Even if the most appropriate model is the Bouc-Wen (Figure 2.27(a)), common practise adopts an equivalent model made by a spring with stiffness k_b acting in parallel with a viscous damper of coefficient C_d (Figure 2.27(b)), representing effective stiffness and damping at the design displacement, respectively.

(a)

(b)
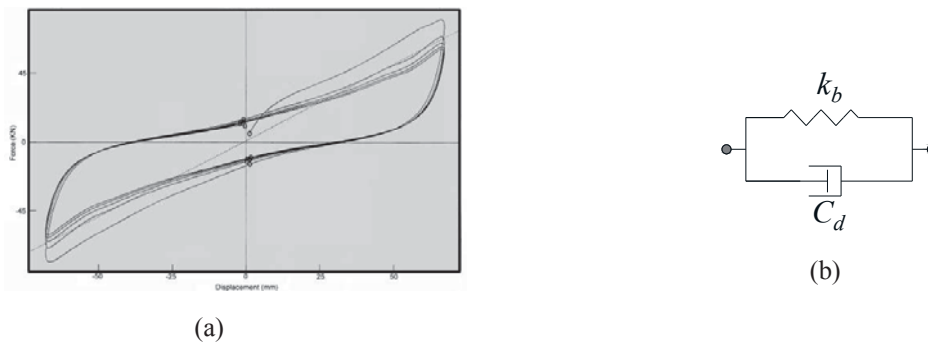
Figure 2.27 (a) Hysteresys plot of an HDRB; (b) rheological model.

Supplemental damping can be provided to a system isolated with laminated-rubber bearings through external supplemental damping devices such as hysteretic or viscous dampers discussed in earlier chapters.

Isolator damping can also be increased by external components such as lead plugs inserted in the center of the bearing. The lead plug is introduced into a laminated rubber bearing to increase the damping by hysteretic shear deformation of the lead. The main reason why lead is chosen as the material for the central plug is that, at room temperature, lead behaves approximately as an elastic-plastic solid and yields in shear at relatively low stress of about 10 MPa.

Figure 2.28 compares the force-displacement hysteresis loop of a laminated-rubber bearing with the one obtained with the same bearing incorporating a lead plug inserted down its center. It can be seen that, before yielding of the lead plug, the lateral stiffness of the lead-rubber bearing is much larger than the lateral stiffness of the laminated-rubber since both the lead and the rubber deform elastically. After yielding of the lead plug, however, the lateral stiffness of both bearings is equal to the elastic shear stiffness of the rubber alone.
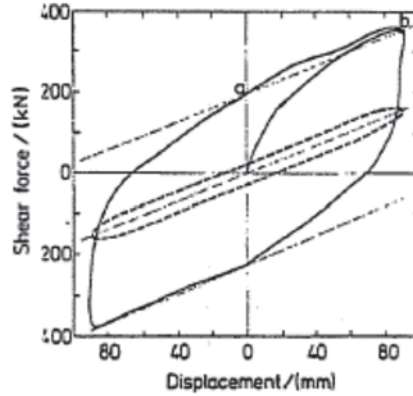
Figure 2.28 Force-Displacement hysteresis loops of a (dashed) Laminated Rubber Bearing and Lead Rubber Bearing (solid).

A reasonable model of the hysteretic behaviour of a lead-rubber bearing is a bilinear solid with elastic stiffness k_1, a post-yield stiffness k_2 and a yield force F_y (Figure 2.29). The elastic stiffness k_1 can be obtained by:

$$k_1 = k_l + k_b = \frac{G_p A_p}{h_r} + \frac{G_r A_r}{h_r}$$

Where:

- h_r is the total rubber height

- A_p is the area of the lead plug

- A_r is the area of the rubber

- G_p is the shear modulus of lead $\approx 150\,MPa$ at room temperature

- G_r is the shear modulus of rubber ≈ 0.5 to $1 MPa$

The post-yield stiffness k_2 is equal to the lateral shear stiffness of the rubber k_b:

$$k_2 = k_b = \frac{G_r A_r}{h_r}$$

For practical size bearings, the lateral stiffness can be estimated as:

$$k_1 \approx 10 k_b$$

The yield force F_y can be estimated by the shear force required to yield the lead plug plus the elastic force carried by the rubber at the corresponding yield displacement:

$$F_y = \tau_{py} A_p (1 + \frac{G_r A_r}{G_p A_p})$$

where $\tau_{py} \approx 10 MPa$ is the shear yield strength of the lead.

For practical size bearings, yield force can be estimated as:

$$F_y = \tau_{py} A_p$$
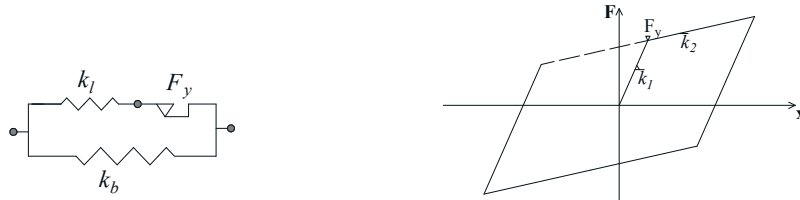
Figure 2.29 Rheological model (a) and hysteretic plot (b) for a Lead Rubber Bearing.

2.6.2. Friction isolators

The lateral force-displacement relationship for a sliding pendulum system is:

$$F = \frac{W}{R} \Delta \qquad (2.19)$$

providing the lateral stiffness of the FPS base isolator $k = W / R$ (Figure 2.30).
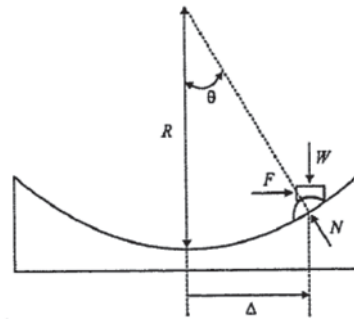
Figure 2.30 Principle of operation of the friction pendulum system.

The natural period of a pendulum system depends only on the radius of the bearing and this would represent a significant advantage of the FPS system since a target isolated period can be achieved independent of the mass of the superstructure.

A particularization of sliding isolator is represented by flat surface, where $R = \infty$ and the device has no post-sliding stiffness. For this reason flat surface isolators have no recentering capabilities.

In reality, friction forces are present at the sliding interface and must be overcome before the bearing can slide. Figure 2.31 shows a typical hysteresis response of a FPS bearing where a

certain amount of friction is present at the interface. The system is near rigid until this friction force is overcome. Then the force increase is proportional to the lateral stiffness of the FPS. The force required to overcome the initial friction is equal to μW where μ is the coefficient of friction of the sliding interface. Because of this initial breakaway friction, the effective stiffness of the isolator is dependent on the friction coefficient of the system μ and the maximum displacement of the isolator x_{max}. This effective stiffness k_{eff}, which is larger than the one described in eq. (2.19), is given by:

$$k_{eff} = W\left(\frac{1}{R} + \frac{\mu}{x_{max}}\right)$$

A friction model with hardening seems quite adequate to capture experimentally obtained hysteretic response of an FPS system:
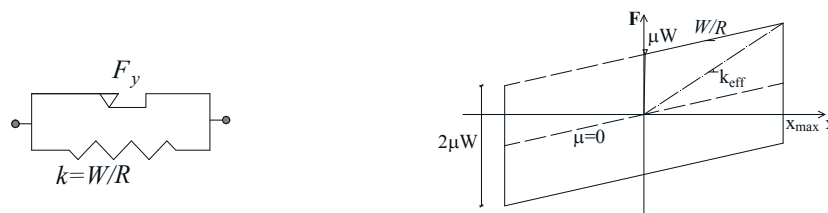
Figure 2.31 Rheological model (a) and hysteretic plot (b) for a FPS isolator.

A further development of the sliding isolator type is represented by double curvature friction pendulum systems, introduced to accommodate the need of larger displacements demand that may increase the cost of the isolation bearings significantly. If both the bottom and the top sliding surfaces have the same curvature and the same friction coefficient, hysteretic behaviour remains unchanged as the one shown in Figure 2.31.

2.6.3. The role of damping in seismic isolation

Recent moderate or large magnitude earthquakes in urban areas have led to significantly increase the current code requirements in many countries. The codes governing the design of seismically isolated structures have always been more conservative than those for conventional structures, and those codes are sometimes so conservative that the benefit of seismic isolation, that provides functionality (elastic response) for large ground motion at an affordable cost, may be jeopardized. For the design of base isolation systems for buildings located at near-fault sites, the design engineer is faced with even larger displacements for the isolators.

In many isolated structures designed according to the most recent Californian design codes, the code requirements are so conservative that the designers are using additional viscous dampers in an attempt to control the large design displacements, and damping factors for the isolation system of the order of 50% are obtained. Clearly, at this level of damping the equations cannot remain uncoupled and a complex modal analysis should be used. Kelly (Kelly 1999) studied the effect of high levels of damping in the isolation system.

These dampers reduce displacements, but at the expense of significant increases in interstorey drifts and floor accelerations in the superstructure.

To prove the effect of additional damping on isolated structure, Kelly proposed a very effective dissertation on the role of damping on isolated structure (Figure 2.32). An elementary analysis based on a simple model of an isolated structure is used to demonstrate this dilemma. The model is linear and is based on modal analysis, but includes the modal coupling terms caused by high levels of damping in the isolation system. At high level of damping the equations of motion cannot remain uncoupled and a complex modal analysis should be used. For this reason a similar approximation will be used in this section to demonstrate the effect of high levels of damping in the isolation system on the response of the structure.
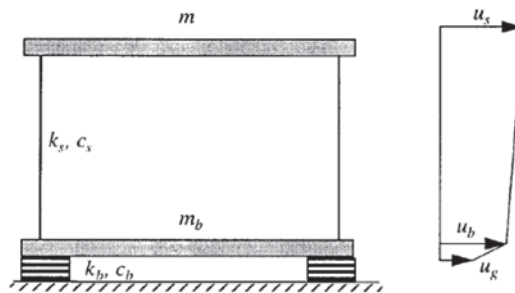
Figure 2.32 Parameters of 2 DOF isolated system.

Referring to the 2DOFs system (Kelly 1990), it was proved the interstorey drift $v_s = u_s - u_b$ can be decomposed in three contributions:

- $\left| v_s^{(1)} \right|_{max}$ produced by the base shear generated by the isolation system;

- $\left| v_s^{(2)} \right|_{max}$ produced by the uncoupled modal equations

- $\left| v_s^{(3)} \right|_{max}$ produced by the coupling terms, generally neglected in most analysis.

For small values of β_b (isolation system critical damping ratio), say $\beta \approx 0.10$, the first term, $\left| v_s^{(1)} \right|_{max}$, is the dominant term. For all values of β_b the second term, $\left| v_s^{(2)} \right|_{max}$ is always much

73

less than the first term and is neglected. The significance of the third term, $\left|v_s^{(3)}\right|_{max}$, depends on the value of β_b. The author of the cited work demonstrated that, under certain reasonable assumptions, moving from $\beta_b = 0.10$ to $\beta_b = 0.50$ the ratio $v_s^{(3)}/v_s^{(1)}$ passed from 0.33 to 1.80, respectively.

This result implies that the addition of dampers (leading to large values of β_b), while controlling the isolator displacement by reducing $v_b = u_b - u_g$, has the counter effect of increasing the interstorey drift and floor accelerations. For a constant velocity design spectrum the accelerations generated by the coupling terms become the dominant term. It is not widely appreciated that in base-isolated structures the higher modes, which carry both the floor accelerations and the interstorey drift, are almost orthogonal to the base shear, so that a low base shear is not a guarantee of an effective isolation system. In this respect the effort to improve the performance of the system by adding damping is a misplaced effort and inevitably self-defeating.

A further consequence of the present US codes is that by identifying a MCE, i.e. an event with a return period of 1000 years, level for design of the isolators that is a very large and very rare event, it raises the possibility that in the more probable, lower-level earthquake, the isolation system will be too stiff and so heavily damped that it will not move. The result would be much less isolation than promised. While not an issue of life safety, it is possible that large enough floor accelerations could be generated to damage non-structural elements and equipment, in addition to disturbing occupants. The solutions to this dilemma of how to control displacements for large input level earthquakes while maintaining good performance for low-to-moderate input level earthquakes are several, but mainly reduce to designing a system that is very stiff at low input shaking, softens with increasing input reaching a minimum at the DBE, i.e. an event with a probability of exceedance of 10% in 50 years, and then stiffens again at higher levels of input. With frictional systems such as the FPS, this can be achieved by gradually increasing the curvature of the disc at radii larger than the DBE displacement and increasing the surface roughness. For elastomeric isolators it requires using the increased stiffness and increased damping that is associated with the strain-induced crystallization that occurs in the elastomer at strains around 150 to 200 % shear strain (depending on the compound). Other possibilities are to use a compound seismic isolator.

REFERENCES

Baber TT, Noori MN (1986) Modeling General Hysteresis Behavior and Random Vibration Application. J Vib Acoust 108:411–420.

Baber TT, Wen YK (1981) Random Vibration Hysteretic, Degrading Systems. J Eng Mech Div 107:1069–1087.

Bouc R (1967) Forced vibration of mechanical systems with hysteresis. Proc. Fourth Conf. Nonlinear Oscil.

Chopra AK (2011) Dynamics of Structures: Theory and Applications to Earthquake Engineering. Prentice Hall/Pearson Education

Constantinou MC, Soong TT, Dargush GF (1996) Passive Energy Dissipation Systems for Structural Design and Retrofit. Buffalo, N.Y.

Fu Y, Kasai K (1998) Comparative Study of Frames Using Viscoelastic and Viscous Dampers. J Struct Eng 124:513–522. doi: 10.1061/(ASCE)0733-9445(1998)124:5(513)

Kelly JM (1999) The role of damping in seismic isolation. Earthq Eng Struct Dyn 28:3–20. doi: 10.1002/(SICI)1096-9845(199901)28:1<3::AID-EQE801>3.0.CO;2-D

Kelly JM (1990) Base Isolation: Linear Theory and Design. Earthq Spectra. doi: DOI: 10.1193/1.1585566

Ou JP, Long X, Li QS (2007) Seismic response analysis of structures with velocity-dependent dampers. J Constr Steel Res 63:628–638. doi: 10.1016/j.jcsr.2006.06.034

Wen YK (1976) Method for Random Vibration of Hysteretic Systems. J Eng Mech Div 102:249–263.

Chapter 3

3.   DESIGN OF SUPPLEMENTAL DAMPING SYSTEMS

3.1   Introduction

The presence of some damping (energy dissipation) in conventional buildings has long been recognized and accepted by practicing professional engineers. Although the nature of the energy dissipation inherent in buildings has not been explicitly identified, inherent equivalent viscous damping in the range of two percent to five percent of critical has become accepted in practice for linear response analysis of typical buildings. In fact most of the design spectra are developed assuming about five percent of critical viscous damping in the system.

If there were no damping, vibrations would exist for all time. However, there is always some level of inherent damping which withdraws energy from the system and therefore reduces the amplitude of vibration until the motion ceases.

However, the addition of supplemental damping systems can substantially increase damping (Figure 3.1).
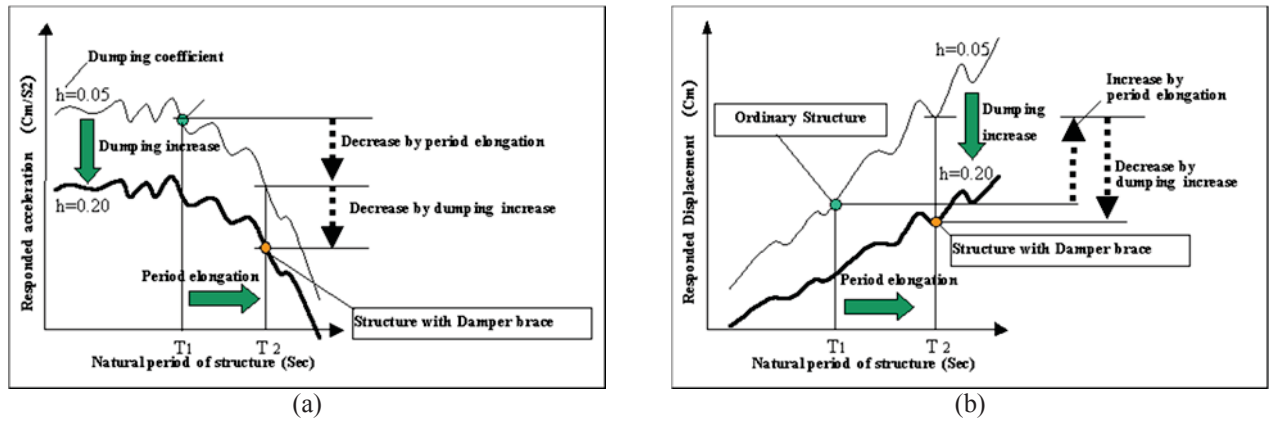
Figure 3.1 Effects of damping increase on spectral acceleration (a) and spectral displacement (b).

The following discussion is intended to propose a dissertation on design issues for buildings with supplemental damping systems, including more advanced code provisions and proposed analysis methods.

3.2 Effects of damping on SDOF structural dynamics

Consider a single-degree-of-freedom system (SDOF – Figure 3.2) assumed to be linear elastic (lateral stiffness k), with a linear viscous damper (damping coefficient c), and a top mass (storey mass m).
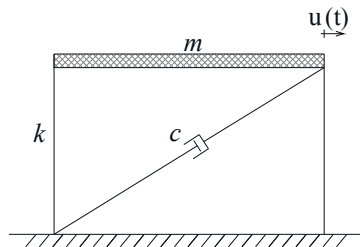
Figure 3.2 SDOF linear elastic frame with viscous damper.

The present chapter is devoted to summarize the effects of damping on this simple system in case of free vibration, harmonic excitation, unit impulse and ground motion (Chopra 2011).

3.2.1. Free Vibration

It is known that, when this system initially at rest and assumed to be linear elastic with less than critical viscous damping, is released from a displaced position, it will vibrate with decreasing amplitudes as shown in Figure 3.3 for increasing values of critical damping.

77
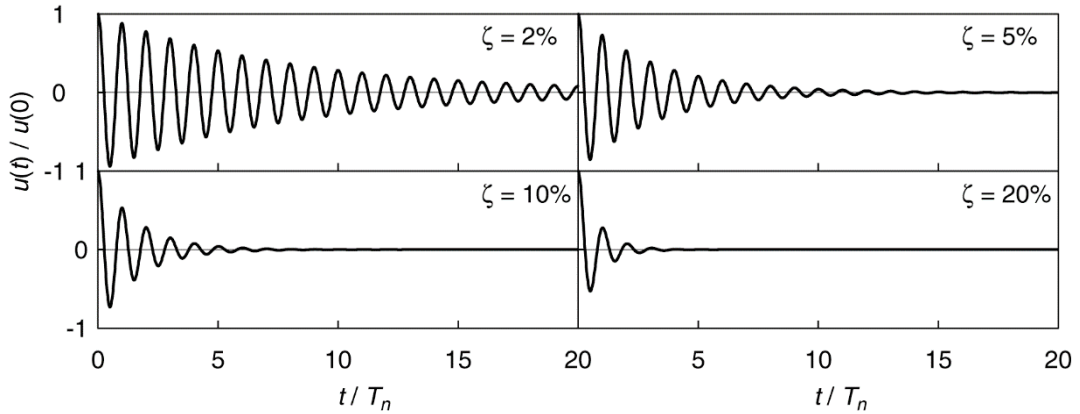
Figure 3.3 Free vibration for ζ=2,5,10 and 20%.

In condition of damped free vibration, the differential equation governing the motion is:

$$m\ddot{u} + c\dot{u} + ku = 0$$

Dividing by m gives:

$$\ddot{u} + 2\zeta\omega_n\dot{u} + \omega_n^2 u = 0 \qquad (3.2)$$

where $\omega_n = \sqrt{k/m}$ is the system natural frequency and $\zeta = \dfrac{c}{2m\omega_n} = \dfrac{c}{c_{cr}}$ is the damping ratio

or fraction of critical damping. The damping constant is a measure of the energy dissipated in a cycle of free vibration or in a cycle of forced harmonic vibration. However, the damping ratio - a dimensionless measure of damping - is a property of the system that also depends on its mass and stiffness.

Figure 3.4 shows a plot of the motion $u(t)$ due to initial displacement $u(0)$ for three values of ζ. If $c = c_{cr}$ or $\zeta = 1$, the system returns to its equilibrium position without oscillating. If $c > c_{cr}$ or $\zeta > 1$, again the system does not oscillate and returns to its equilibrium position, as in the $\zeta = 1$ case, but at a slower rate (Figure 3.4(a)). If $c < c_{cr}$ or $\zeta < 1$, the system oscillates about its equilibrium position with a progressively decreasing amplitude.

For underdamped systems, free vibration solution to eq. (3.2) is:

$$u(t) = e^{-\zeta\omega_n t}\left[u(0)\cos\omega_D t + \left(\frac{\dot{u}(0) + \zeta\omega_n u(0)}{\omega_D}\right)\sin\omega_D t\right]$$

where

$\omega_D = \omega_n\sqrt{1-\zeta^2}$ is the natural frequency of damped vibration.

The natural period of damped vibration is $T_D = 2\pi/\omega_D$ and is related to the natural period T_n without damping by:

78

$$T_D = \frac{T_n}{\sqrt{1-\zeta^2}}$$

(a)

(b)
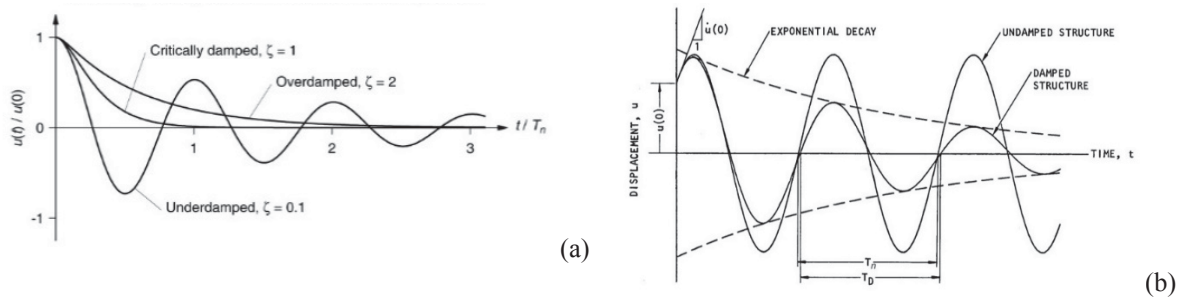
Figure 3.4 (a) Free vibration of underdamped, critically-damped, and overdamped systems; (b) exponential decay in free vibration of an underdamped system.

Effect of increasing damping is manifold:

- amplitude of oscillation decreases with every cycle of vibration;

- the natural frequency is lowered from ω_n to ω_D, so lengthening the natural period from T_n to T_D.

Effect of lengthening natural period is negligible for damping ratios below 20%, a range that includes most structures (Figure 3.5). The most important effect of damping is on the rate at which free vibration decays.
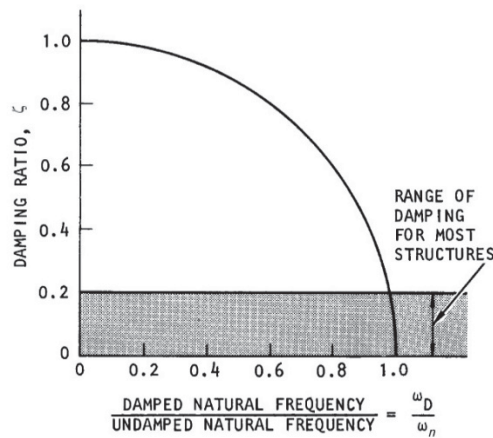
Figure 3.5 Effects of damping on the natural vibration frequency.

3.2.2. Harmonic excitation

The equation of motion for SDOF systems under harmonic force can be formulated as follows:

$$m\ddot{u}(t) + c\dot{u}(t) + ku(t) = p_o\,sen\,\overline{\omega}t$$

where p_o and $\overline{\omega}$ are the amplitude and the frequency of the external force, respectively.

The solution is given by:

79

$$u(t) = e^{-\zeta \omega_n t}\left(A \operatorname{sen} \omega_D t + B \cos \omega_D t\right) + u_{st} D \operatorname{sen}\left(\overline{\omega} t - \theta\right)$$

where $u_{st} = \dfrac{p_o}{k}$.

Solution shows that $u(t)$ contains two distinct vibration components: (1) the $\operatorname{sen}\overline{\omega}t$ term, giving an oscillation at the forcing or exciting frequency, and (2) the $\operatorname{sen}\omega_D t$ and $\cos \omega_D t$ terms, giving an oscillation at the damped frequency of the system. The first of these is the forced vibration or steady-state vibration, it is present because of the applied force no matter what the initial conditions. The latter is the transient vibration, which depends on the initial displacement and velocity.

After a while, essentially the forced response remains, and we therefore call it steady-state response. It should be recognized, however, that the largest deformation peak may occur before the system has reached steady state.

Amplitude of forced vibration is $D \cdot u_{st}$, where D is the response amplification factor depending on both β and ζ defined as:

$$D = \frac{1}{\sqrt{\left(1 - \beta^2\right)^2 + \left(2\zeta\beta\right)^2}}$$

A plot of the amplitude of a response quantity against the excitation frequency is called a frequency-response curve. Such a plot for deformation u is given by Figure 3.6, wherein the deformation response factor D is plotted as a function of β for a few values of ζ ; all the curves are below the $\zeta = 0$ curve. Damping reduces D and hence the deformation amplitude at all excitation frequencies.
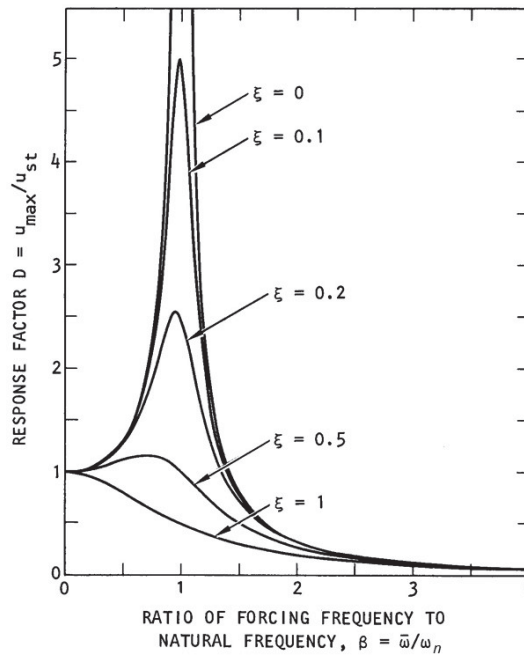
Figure 3.6 Dynamic amplification factor for harmonic excitation.

In case of motion, the role of damping comes out both in the rate at which steady-state response is attained and in limiting the magnitude of this response when the forcing frequency is close to the natural frequency.

The lighter the damping, the larger is the number of cycles required to reach a certain percentage of the steady-state amplitude. Even if frequency response curves clearly show that damping reduces the deformation amplitude at all excitation frequencies, it should be observed that increasing damping has a significant effect on the dynamic response of the system only when the excitation frequency is nearly the same as the natural frequency of the system (within about plus or minus 20%). Thus, if the frequencies of the system are not close to the expected frequencies of the input motions, added viscous damping will not have a significant impact on the response.

3.2.3. Unit impulse

A unit impulse causes free vibration of the SDOF system due to the initial velocity (Figure 3.7). The response for viscously damped systems is:

$$h(t-\tau) = u(t) = \frac{1}{m\omega_D} e^{-\zeta\omega_n(t-\tau)} \sin[\omega_D(t-\tau)] \qquad t \geq \tau$$
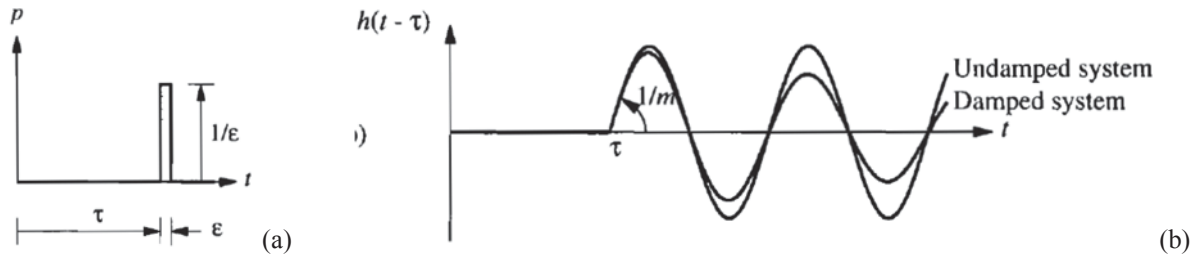
Figure 3.7 (a) Unit impulse and (b) unit impulse response.

When the excitation is a single pulse, the effect of damping on the maximum response is usually not important unless the system is highly damped (Figure 3.8).
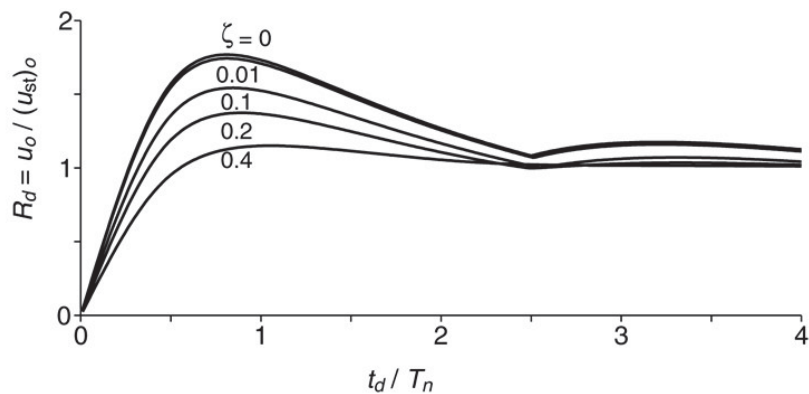
Figure 3.8 Shock spectra for a half-cycle sine pulse force.

If the earthquake response of a building is thought as a series of responses to individual earthquake pulses, it would be concluded that the response of higher damped systems will be less because the individual response decay quickly and cannot accumulate (Hanson 1993). The response of more highly damped systems will be smaller than that of the lightly damped systems, because the initial amplitudes are smaller, and the responses decays more quickly.

3.2.4. Ground motion

As far as effects of a real ground motion on a SDOF system are concerned, Figure 3.9 shows an acceleration response spectra for three values of damping: moving from 2 to 5 and 10 % of equivalent viscous damping gradually reduces maximum acceleration. For earthquake ground motion inputs, the displacement response spectra decreases for elastic systems with changes in viscous damping.
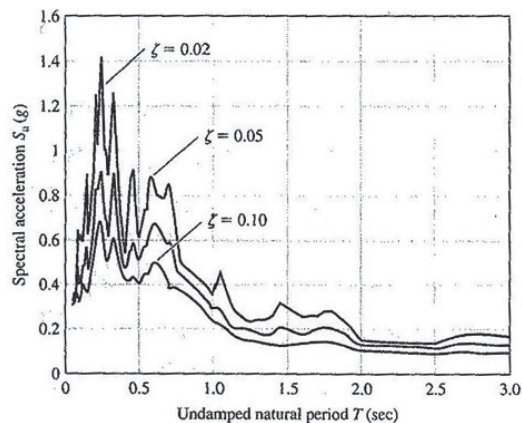
Figure 3.9 Ground motion pseudo-acceleration response spectra for increasing values of damping.

It is worth to note that the spectral acceleration S_{pa}, which is exactly the acceleration at maximum displacement and is equal to the maximum displacement times the frequency squared, well approximates the maximum acceleration only for low damped systems.

Figure 3.10 compares pseudo acceleration and maximum acceleration response spectra for the 1940 El Centro earthquake (S00E) where it is demonstrated that, for large values of damping (i.e, 30% of critical and larger), the pseudo acceleration is typically less than the maximum acceleration. The maximum acceleration occurs at a time in which the displacement is less than maximum.
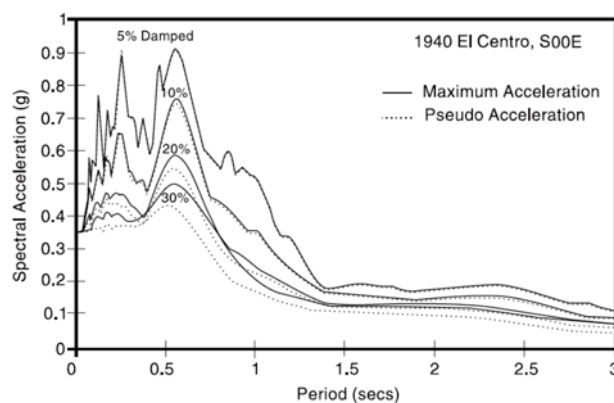
Figure 3.10 Response spectra of maximum and pseudo acceleration.

Consider a frame to have been designed for ductile behaviour following the capacity design approach. The yielding frame has substantial ability to dissipate energy. Approximately, one can determine an effective damping ratio of at least 30% of critical for this frame. With such ability to dissipate energy, an increase in this ability due to the added energy dissipation system will not be very effective in further reducing the displacement of the frame.

To approximately quantify this further response reduction, Figure 3.11 was prepared from data in FEMA 273 (ATC 1997a). It presents plots of the displacement response ratio of a structure

in which an energy dissipating system caused an increase in the damping ratio by either 10 or 20 or 30% of critical. The damping ratio of the structure without the energy dissipation system is shown to be in the range of 1 to 30% of critical. The response ratio shown here is valid for the so-called velocity domain of the response spectrum (long period range). As shown in Figure 3.11, a structure with a damping ratio of 1 to 3% of critical will have its response reduced to approximately one half (reduction by 50%) when an energy dissipating system enhances damping by 20 to 30% of critical. However, when the structure has a damping ratio of 30%, an increase of damping by 20 to 30% of critical will cause a reduction of response to approximately 0.85 of the value without the energy dissipation system (reduction by 15%).

Actually, the reduction in response will be larger due to the increased effective stiffness of the structure, which is caused (a) by the reduction in drift, and (b) by the addition of stiffness in certain energy dissipation systems.
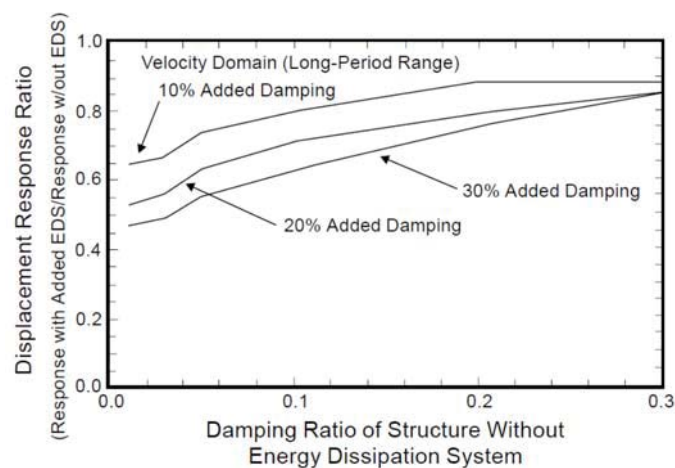
Figure 3.11 Response reduction of structure with added damping of 10, 20 or 30 % of critical.

3.3 Design considerations for structures with passive energy dissipation systems

Seismic Drift-Controlled Structures (New Construction)

For structures located in high seismic regions, member sizes of steel moment frames are usually determined by drift restrictions. Since passive energy dissipation systems are effective in reducing drifts, the use of such systems can lead to significant reductions in the size of framing members. Adding damping devices in each story, as it is generally recommended, creates a system that resembles a supplemental braced frame within the structure. This can be problematic since it may be difficult to convince owners and architects to disrupt an open floor plan with these elements. However, discreet locations can often be found to position these

elements within a floor plan. The inclusion of passive damping elements within steel moment frames offers the following advantages for seismic loading:

- when compared with the alternative of using a conventional moment frame, the required weight of the steel moment frame will generally be reduced, often more than offsetting the cost of adding the damping elements;

- when compared with the alternative of using a conventional braced frame, the various height limitations and seismic R factors of the various ordinary braced frame, special concentrically braced frame, and eccentricity braced frame systems can cause some of the systems to be prohibited or more heavy than a passive-damped steel moment frame. The overturning moment and resulting foundation sizes beneath the conventional braced frames will almost always be larger; and

- the passive-damped steel moment frame can be designed to provide a reduced damage, performance-based earthquake design in which minimal inelastic deformation is required in the steel frame. In comparison, either a conventional moment frame or braced frame may be subjected to significant damage following a major earthquake. This is arguably the most important benefit resulting from the inclusion of dampers in flexible moment frame structures;

- it is important to note that applications of passive energy dissipation devices are not restricted to flexible steel moment frames. In fact, such devices have been implemented in concrete buildings and have been studied for application to light wood frame construction. Furthermore, application of such devices is not limited to office/residential construction. For example, the retractable roof structure of the Seattle, WA Mariners baseball stadium in Seattle employs large capacity viscous fluid dampers in the bottom chords of long-span roof trusses.

Seismic Drift-Controlled Structures (Retrofit Construction)

Retrofit applications of passive damping systems have been used to limit inelastic demands of connections in both steel and concrete moment frames. For existing steel and concrete buildings having framing connections, maximum inelastic rotation capacities can be used to define structure drift limitations that form the basis for design of a passive damping system, to be designed to meet this requirement.

Assuming perfectly rigid damper bracing and associated connections and assuming elastic structural response, linear viscous dampers produce forces within a given story that are 90° out of phase with respect to the restoring forces in the same story. In this case, for retrofit applications in which the damping is proportionally distributed, and considering only the response in the fundamental mode, the impact of the damping forces on the existing foundation may be minor and therefore the foundation, which is usually very difficult and expensive to retrofit, may require minimal, if any, strengthening. In reality, elastic structure forces and viscous damping forces are usually partially in phase, leading to the possibility of increased forces at the foundation level. The partially in-phase relation for the elastic and viscous damping forces can be induced by damper bracing and connection flexibility (Fu and Kasai 1998), higher mode effects, and non-proportional damping effects. It is also important to recognize that, for strong earthquakes, most structures employing viscous dampers will experience some level of inelastic response in the structure framing system. In this case, damping forces and inelastic restoring forces may be additive, causing significant increases in the base shear. Adding dampers to a structure introduces a new and very important design requirement in that the deformations along the load path between all dampers and the main structural elements must be included in the analysis (e.g., rigid diaphragm action cannot be assumed).

Pros and Cons of Viscous Damper Velocity Exponent Value

For a given peak force and displacement amplitude, as the velocity exponent of nonlinear fluid viscous dampers is reduced below unity, the energy dissipated per cycle of motion is increased since the area within the force-displacement hysteresis loop is larger. However, the additional energy dissipation afforded by the nonlinear dampers is minimal (at the extreme, the increase in energy dissipation afforded by a damper with velocity exponent of zero over that with a velocity exponent of 1.0 is by a factor of $4/\pi$). As compared to a linear viscous damper (velocity exponent of unity), the forces transferred by a nonlinear damper to the structure will be more nearly in phase with the structure restoring forces such that the resulting design more nearly resembles that of a braced frame within the structure (albeit, a braced frame would have a limiting base shear whereas a structure with nonlinear viscous dampers may not, particularly if the velocity exponent is in the higher range of 0.6–1.0). The main advantage of using nonlinear viscous dampers with a low velocity exponent (say 0.5 or less) is that peak damping forces will be limited and smaller leading to limited base shears. On the other hand, using a more linear force-velocity relationship will generally result in somewhat lower effective

damping and somewhat greater damper forces (depending, of course, on the magnitude of the damping coefficient for the linear and nonlinear cases). The main advantage of using a more linear force-velocity relationship is that modeling of the damper is simplified and, for weak to moderate earthquakes that do not induce inelastic structural response, the damper forces within a given story are nearly 90° out of phase with respect to the elastic structural forces. As explained above, under certain special conditions, this may result in damper forces that have minimal effect on the forces at the foundation level.

Improvement of Irregularity Conditions

Mostly in retrofit situations, passive damping systems have been added to improve the response of irregular buildings (e.g., buildings having a soft story or a geometrical configuration in which excessive deformations are concentrated in local areas). By arranging damper locations and selecting damping values so that the resulting damper forces are in proportion to structure deformations, displacements in these areas can be reduced and overall response improved. For example, if a low-to midrise structure has a vertical irregularity in the form of a soft first story, dampers located in that story would experience significant deformations and thus produce significant damping forces. However, if the dampers were located only in that story, the Provisions require that nonlinear analysis be performed. Linear static and response spectrum analysis can only be performed if the damping system is distributed over the full height of the structure with at least two dampers per story. The performance of structures with plan irregularities that induce torsion can also be improved via strategic placement of dampers (Goel 2000).

Damper Placement and Damper Installation Configuration

In general, the effectiveness of each damper in a structure is proportional to its maximum displacement and/or velocity and the damper design parameters. For a single mode of vibration, the effectiveness of the dampers can be maximized by positioning devices in accordance with the largest interstory displacements of the corresponding mode shape (or, conversely, the effectiveness of dampers for any single mode of vibration will be reduced if the dampers are located in stories having little interstory displacement for that mode). As an example, locating devices at each story within the core of a building may be effective for regular, symmetric structures, but might be ineffective for torsionally irregular structures since, although the fundamental translational vibration modes may be effectively damped, the torsional modes

might have little added damping (Goel 2000). Of course, the above approach to damper placement is based on the assumption that the mode shapes remain constant which is only valid if the structure remains elastic and the damping is distributed in a proportional manner. Other approaches to damper placement, including formal optimization of damper placement, have been developed (Lopez Garcia and Soong 2002).

Dampers are attached to the main structural framing system via a bracing system. The bracing system may be diagonal bracing, chevron bracing, or cross-bracing. If the main structural framing is relatively stiff (e.g., reinforced concrete structures), the damper effectiveness is limited due to low displacements and velocities across the damper. This is particularly problematic when the damping system is also used to resist wind loading since wind-induced interstory drifts are usually much smaller than seismically induced drifts. To improve the effectiveness of dampers under such conditions, alternative damper bracing systems have been developed to amplify the motion of the damper. Examples of such amplification systems include toggle bracing and scissor-jack bracing.

As mentioned previously, all bracing systems introduce flexibility into the damper assembly which reduces effectiveness of dampers.

3.4 Load path in damping braced frames

Energy dissipation devices will typically be attached to moment frames. While the energy dissipation system can result in significant reduction in drift (and, thus, reduction in column bending moment and/or reduction in inelastic deformation), it also affects load paths.

Specifically, the change from a moment frame to a braced configuration can result in substantial increase in column axial forces. In addition to this, base shear can be affected due to larger lateral stiffness of the resisting system.

3.4.1 Axial forces in columns

Let us consider the implications of the use of energy adsorbing systems in an existing moment-resisting frame building. The energy adsorbing devices are installed in new bracing systems and, say, are capable of reducing drifts to half of those of the original system in a severe earthquake. In the friction and steel yielding devices, the peak brace force occurs at the time of peak displacement. Accordingly, the additional column force, which is equal to $F \sin \varepsilon$ (ε is the brace angle with respect to the horizontal), is in-phase with the bending moment due to

column drift. Similarly, in the viscoelastic device a major portion of the additional column force is in-phase with the bending moment. In contrast, in the viscous device the additional column force is put-of-phase with the bending moment.

The drift is not the only concern in design. Energy adsorbing devices may reduce drift and thus reduce inelastic action. However, depending on their force-displacement characteristics, they may induce significant axial column forces which may lead to significant column compression or even column tension. This concern is particularly important in the seismic retrofitting of structures which suffered damage in previous earthquakes. After all, it may not always be possible to upgrade the seismic resistance of such structures by the addition of energy adsorbing devices alone. It may also be necessary to strengthen the columns.

3.4.2 Base shear

It should be noted that, as shown in Figure 3.12(a), the base shear force response of the structure with energy dissipation systems may be larger than that of the structure without these systems.
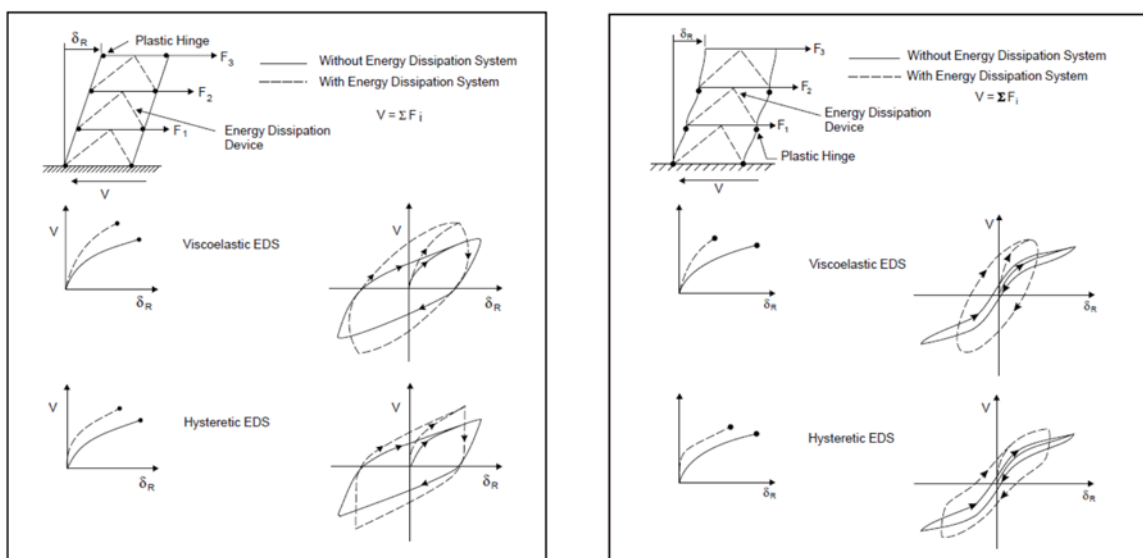
Figure 3.12 Pushover curves and force-displacement hysteresis loops of a yielding structure with and without energy dissipation systems: (a) having proper plastic hinge formation and (b) having improper plastic hinge formation.

This would be the case when the pushover curve of the structure without an energy dissipation system exhibits essentially elastoplastic behavior. It is possible to have reduction in base shear force when the pushover curve exhibits significant post-yielding stiffness.

Energy dissipation devices will also reduce force in the structure, provided the structure is responding elastically, but would not be expected to reduce force in structures that are responding beyond yielding.

89

Structures designed for low lateral forces without proper distribution of stiffness and detailing for ductility typically develop improper plastic hinge mechanisms and undesirable modes of deformation. Figure 3.12(b) shows a frame with such characteristics, where plastic hinges can form in the columns and lead to hysteresis loops with low energy absorption capability. Such a mechanism may lead to excessive hinge rotations which cannot be accommodated, resulting in deterioration of strength and stiffness and eventually failure. Figure 3.12(b) depicts a case in which neither significant deterioration nor failure has occurred. The addition of an energy dissipation system to this frame results in significant improvement in energy absorption capability and large reduction in displacement. This reduction in displacement is associated with reduction in plastic hinge rotation and possible elimination of some plastic hinges. However, the total force on the frame may be increased as a result of the increase in stiffness and/or strength provided by the energy dissipation system.

It is apparent that energy dissipation systems are most useful in applications of seismic retrofit.

3.5 Analysis of damper added structure *vs* traditional structure

From the viewpoint of multistory structural analysis, significant differences can exist between the structural properties of a traditional structure and those of a damper added structure. For these cases, the traditional methods of analysis may need to be modified to account for these differences. Some potentially significant differences are listed below.

Significant increase in damping

Damper added structures exhibit significantly higher modal damping ratios than those associated with traditional structures. This is particularly true in higher modes, where damping ratios can reach values close to or even exceeding their critical values. Hence, the damping term in the equation of motion of a damper-added structure becomes important in determining the structure's modal properties.

Non proportional damping

For analytical convenience proportional damping is usually assumed in the analysis of a traditional structure. This simplifies the structural analysis by using modal superposition. The consequence of adding dampers to a traditional structure depends on the location and characteristics of the selected devices. If the added damping is proportional – that is, if the undamped mode shapes of the structure with added stiffness that are due to damping devices diagonalize the structure's damping matrix – then the structure has proportional damping. In

this case, the traditional modal analysis approaches work well. That is, the normal modes of vibration of the damped system are identical to those for the undamped structure, making the calculation of modal properties a routine procedure.

The proportional damping assumption, however, is generally not valid for damper added structures, because it may not be practical to try to match added damper characteristics to the vibrations in the structural stiffness and mass of the building. In fact, in some cases it may be desirable to add dampers only at specific floors in the building. Thus, the distribution of the damping properties within the structure will probably not be proportional. In this situation, modifications of the traditional model analysis must be considered.

Damping devices nonlinearities

Whether a traditional structure behaves linearly or non linearly (because of yielding) under a given loading condition, a damper-added structure generally exhibits nonlinear behavior because damper dynamics are generally non linear in local displacements and velocities. This fact complicates exact structural analysis procedures considerably. Although a rigorous nonlinear time history analysis can be performed to verify the final design, simple approximation methods of analysis are needed for preliminary design and desirable for final design.

Damper device nonlinerities and their "linearized" properties have been discussed in Chapter 2.

3.6 Code provisions for supplementally damped structures

The effectiveness of seismically isolated structures or structures with supplemental damping has been recently codified in international seismic regulations and recommendations. The present paragraph provides an overview of the historical developments of building codes, with particular focus on American state of art, whose Provisions (BSSC 2004) probably represent cutting-edge of developments.

3.6.1. Development of Guidelines and Design Philosophy

Guidelines for the implementation of energy dissipation or damping devices in new buildings were first proposed by the Structural Engineers Association of Northern California (SEAONC) to provide guidance to structural engineers, building officials, and regulators who were tasked with implementing such devices in building frames. These guidelines were prepared in response

to the increased interest shown in damping devices following widespread damage to building frames in the 1989 Loma Prieta earthquake in Northern California and the emergence of vendors of damping hardware. The intent of the authors of that document was to direct the dissipation of earthquake-induced energy into the damping devices and away from components of the gravity-load-resisting system, thereby reducing repair costs and business interruption following severe earthquake shaking.

In the mid 1990s, the Federal Emergency Management Agency (FEMA) funded the development of guidelines for the seismic rehabilitation of buildings. Four new methods of seismic analysis and evaluation were presented in the NEHRP Guidelines for the Seismic Rehabilitation of Buildings; FEMA Reports 273 (ATC 1997a) and 274 (ATC 1997b): (1) linear static procedure, (2) linear dynamic procedure; (3) nonlinear static procedure; and (4) nonlinear dynamic procedure. All four methods were displacement based and all directly or indirectly made use of displacement-related information for component checking (as such the FEMA 273 and 274 procedures represented a paradigm shift in the practice of seismic design because the focus of analysis, design, and evaluation shifted from forces to deformations). Actions in components of a building frame were characterized as either deformation controlled (for ductile actions such as bending moments in beams) or force controlled (for brittle actions such as shear forces in columns). Rotation limits for deformation controlled actions were presented in the materials chapters of FEMA 273 for comparison with rotation demands estimated using the displacement-based methods of analysis. Strength limits were established for force-controlled actions using procedures similar to those in codes and manuals of practice. With regard to structures incorporating passive energy dissipation devices, the basic principles to be followed included: (1) spatial distribution of dampers (at each story and on each side of building); (2) redundancy of dampers (at least two dampers along the same line of action); (3) for maximum considered earthquake, dampers, and their connections designed to avoid failure (i.e., not the weak link in system); and (4) members that transmit damper forces to foundation designed to remain elastic.

In 1997, Technical Subcommittee 12 (TS-12) of the Building Seismic Safety Council was tasked with developing analysis, design, and testing procedures for damping systems and devices for inclusion in the NEHRP Recommended Provisions for Seismic Regulations for New Buildings and Other Structures. The resultant provisions were required to be 100% consistent with those presented in the NEHRP Recommended Provisions for conventional construction. The equivalent lateral force and modal analysis procedures for damped buildings that were

developed are based in large part on the procedures of the NEHRP Rehabilitation Guidelines (FEMA 273 and 274) but assumed that: (1) the collapse mechanism for the building is a single-degree-of freedom mechanism so that the drift distribution over the height of the building can be reasonably estimated using either the first mode shape or another profile such as an inverted triangle; (2) the building is analyzed in each principal direction with one degree of- freedom per floor level; (3) the nonlinear response of the building can be represented by an elastoplastic relationship; and (4) the yield strength of the building can be estimated by either simple plastic analysis or using the specified minimum seismic base shear and values of the response modification (R), the reserve strength of the framing system Ω_0 and the deflection amplification (C_d) factors presented in the NEHRP Recommended Provisions. The work of TS-12 resulted in a chapter entitled "Structures with Damping Systems" as a new addition to the 2003 NEHRP Recommended Provisions FEMA 450 (BSSC 2004), having first appeared as an appendix of the 2000 NEHRP Recommended Provisions. Recently, the 2003 NEHRP Recommended Provisions were reformatted and included in the 2005 edition of the ASCE/SIE 7-05 Standard entitled "Minimum design loads for buildings and other structures" (ASCE 2005). The earthquake load provisions in the ASCE/SEI 7-05 standard are substantially adopted by reference in the 2006 International Building Code (ICC 2006) and the Building Construction and Safety Code (NFPA 2006), the two model building codes used in the United States.

As far as European regulations are concerned, both in force Europeran (1998-1 EN 2004) and Italian building Codes (NTC 2008) are still lacking an adequate dissertation on constructions with supplemental damping devices.

Eurocode 8 does not provide any provision for design of supplemental damping systems, while NTC 2008 in section § 7.10 mainly deals with seismic isolated structures for which supplemental damping is considered an additional feature to reduce displacements to acceptable values. Italian commentary to building code (Circ.617 2009) just clarifies some general aspects of the design of buildings with supplemental damping braces. Guidelines (Reluis 2014) have just been published by Italian Department of civil Protection for analysis and modeling of structures with damping braces. European approach defines a damping reduction factor for effective damping larger than conventional 5%:

$$\eta = \sqrt{\frac{10}{5+\zeta}} \leq 0.55$$

With the aim of traducing the coefficient η into an equivalent damping factor B_{eq} as included by US Provisions (Figure 3.13), it is found that $B_{eq}=1/\eta$ is in very good agreement with those of Figure 3.13. A dilemma of European codes is the limitation of damping benefits to maximum values of 25÷30%, for which the minimum value of the code provided coefficient $\eta=0.55$ is attained, thus corresponding to a value B_{eq} of the order of 1.8.

3.6.2. Design Philosophy

The basic approach followed in developing regulations on structures with damping systems in the aforementioned Provisions is based on the following concepts:

-   The methodology is applicable to all types of damping systems, including displacement-dependent damping devices (hysteretic or friction systems) and velocity-dependent damping devices (viscous or viscoelastic systems);

-   The methodology provides minimum design criteria with performance objectives comparable to those for a structure with a conventional seismic-force-resisting system (but also permits design criteria that will achieve higher performance levels);

-   The methodology requires structures with a damping system to have a seismic-force-resisting system that provides a complete load path. The seismic-force-resisting system must comply with the requirements of the Provisions, except that the damping system may be used to meet drift limits. Thus, the detailing requirements that are in place for structures without damping systems may not be relaxed for structures which include damping systems;

-   The methodology requires design of damping devices and prototype testing of damper units for displacements, velocities, and forces corresponding to those of the maximum considered earthquake; and

-   The methodology provides linear static and response spectrum analysis methods for design of most structures that meet certain configuration and other limiting criteria (for example, at least two damping devices at each story configured to resist torsion). In addition, nonlinear response history analysis is required to confirm peak response for structures not meeting the criteria for linear analysis (and for structures close to major faults). Note that the procedures in the 2003 NEHRP Recommended Provisions (BSSC 2004) and the 2005 ASCE/SEI-7-05 standard (ASCE 2005) for analysis and design of structures with damping systems were largely based on studies that do not consider the

effects of near-field (close to the fault) seismic excitations. However, as demonstrated by Pavlou and Constantinou (Pavlou and Constantinou 2004), the 2000 NEHRP simplified methods of analysis for single-degree-of-freedom systems yield predictions of peak response of structures with damping systems that are generally accurate or conservative for the case of near-field seismic excitation (with a correction factor required for predicting peak velocity).

3.7   Analysis of Structures with Energy Dissipation Systems

Seismic isolation and energy dissipation systems are relatively new and sophisticated concepts that require more extensive design and detailed analysis than other structural typologies. The mathematical model of the damper-added building should include the plan and vertical distribution of the energy dissipation devices. This section specifies analysis methods and design criteria for energy dissipation systems. Simplified non linear analysis, i.e. linear static or dynamic analysis, even if more approximated, have enormous benefits for the preliminary analysis and design of damper added structure but require the definition of equivalent damping and equivalent stiffness.

3.7.1 Design Effective Damping

For structures with damping systems, the 2003 NEHRP Recommended Provisions FEMA 450 (BSSC 2004) specifies that the response of the structure be reduced by the damping coefficient, B, based on the effective damping ratio, β, of the mode of interest:

$$S_a(T,\beta) = \frac{S_a(T,5\%)}{B(\beta)}$$

This is the same approach that is used by the Provisions for isolated structures. The recommended values of the B coefficient for design of damped structures are the same as those in previous Provisions FEMA 274 (Figure 3.13(b)) for isolated structures at damping levels up to 30%, but now extend to higher damping levels (Figure 3.13(a)) based on the results presented in Ramirez et al (Ramirez et al 2001).

Table 15.6-1
Damping Coefficient, B_{V+I}, B_{1D}, B_R, B_{1M}, B_{mD}, or B_{mM}

Effective Damping, β (percentage of critical)	B_{V+I}, B_{1D}, B_R, B_{1M}, B_{mD} or B_{mM} (where period of the structure $\leq T_0$)
≤ 2	0.8
5	1.0
10	1.2
20	1.5
30	1.8
40	2.1
50	2.4
60	2.7
70	3.0
80	3.3
90	3.6
≤ 100	4.0

(a)

Table 2-15   Damping Coefficients B_S and B_1 as a Function of Effective Damping β

Effective Damping β [1] (percentage of critical)	B_S	B_1
< 2	0.8	0.8
5	1.0	1.0
10	1.3	1.2
20	1.8	1.5
30	2.3	1.7
40	2.7	1.9
> 50	3.0	2.0

1. The damping coefficient should be based on linear interpolation for effective damping values other than those given.

(b)

Figure 3.13 Damping coefficient for different levels of damping: (a) FEMA 450 and (b) FEMA 274.

FEMA 274 provided a general design spectrum for a conventional 5% damped system, to be scaled with damping coefficient B_s and B_1, with a maximum allowable effective damping of 50%. A further limitation was given by the fact that, these parameters usually underestimated the effective response reduction, as demonstrated by Ramirez (Ramirez et al 2001). For this reason an upgraded version came out in 2003 with FEMA 450.

As for isolated structures, effective damping of the fundamental-mode of a damped structure is based on the nonlinear force-deflection properties of the structure. For use with linear analysis methods, nonlinear properties of the structure are inferred from overstrength, Ω_0, and other terms of the Provisions. For nonlinear analysis methods, properties of the structure are based on explicit modeling of the postyield behavior of elements.
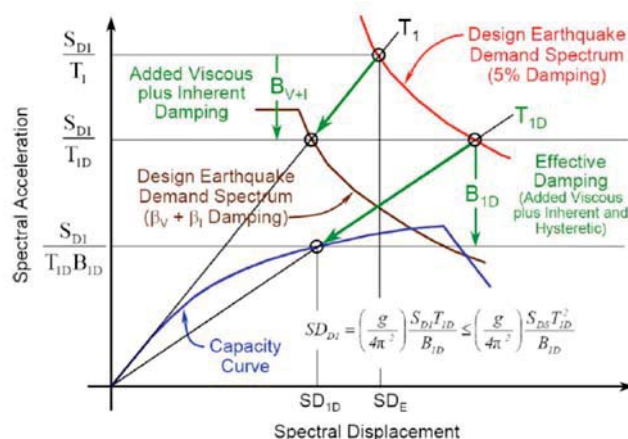
Figure 3.14 Reduction of the design demand due to effective damping.

Figure 3.14 illustrates the reduction in design earthquake response of the fundamental mode due to the effective damping coefficient, B_{1D}, at the design displacement. In this figure, two

demand spectra are shown, one for a structure with 5% nominal inherent damping (characterized by the 5% damped design spectral response acceleration parameter at a period of one second, S_{D1}) and the other for a structure with additional damping provided by inherent damping beyond the nominal 5% and added viscous damping from a damping system. The structure capacity curve is also shown and represents the nonlinear behavior of the structure responding in the fundamental mode and plotted in spectral acceleration/displacement coordinates. An intersection point (or *performance point*) exists between the demand and capacity curves which defines the expected performance of the structure. If the structure were assumed to remain elastic, the performance point would lie along the line marked T_1 where T_1 represents the elastic fundamental period of the structure in the direction under consideration. Accounting for inelastic behavior, the performance point lies along the line marked T_{1D} where T_{1D} represents the effective period of the fundamental mode at the design spectral displacement (SD_{1D}) in the direction under consideration (i.e., T_{1D} is based on the secant stiffness at the design displacement). As shown in Figure 3.14, the demand spectrum at the effective period (not sketched in Figure 3.14) is reduced in accordance with the effective damping coefficient, B_{1D}, which has contributions from three components: (1) inherent damping B_I - inherent damping of structure at or just below yield, excluding added viscous damping (B_I is typically assumed to be 5% of critical); (2) hysteretic damping B_H - postyield hysteretic damping of the seismic-force-resisting system and elements of the damping system at the amplitude of interest (taken as 0% of critical at or below yield); and (3) added viscous damping B_V - viscous component of energy dissipation in elements of the damping system (taken as 0% for hysteretic or friction-based damping systems).

Both hysteretic damping and the effects of added viscous damping are amplitude dependent and the relative contributions to total effective damping changes with the amount of postyield response of the structure. For example, adding dampers to a structure reduces postyield displacement of the structure and hence reduces the amount of hysteretic damping provided by the seismic-force-resisting system. If the displacements were reduced to the point of first yield, the hysteretic component of effective damping would be zero and the effective damping would be equal to inherent damping plus added viscous damping.

3.7.2 Evaluation of effective damping

The effective damping at the design displacement, β_{mD} (BSSC 2004) of the mth mode of vibration of the structure in the direction under consideration shall be calculated using the following equation:

$$\beta_{mD} = \beta_I + \beta_{Vm}\sqrt{\mu_D} + \beta_{HD} \qquad (3.3)$$

where

- β_{HD} = component of effective damping of the structure in the direction of interest due to post-yield hysteretic behavior of the seismic-force-resisting system and elements of the damping system at effective ductility demand, μ_D;

- β_I = component of effective damping of the structure due to the inherent dissipation of energy by elements of the structure, at or just below the effective yield displacement of the seismic force-resisting system;

- β_{Vm} = component of effective damping of the mth mode of vibration of the structure in the direction of interest due to viscous dissipation of energy by the damping system, at or just below the effective yield displacement of the seismic-force-resisting system;

- μ_D = effective ductility demand on the seismic-force-resisting system in the direction of interest due to the design earthquake.

Unless analysis or test data supports other values, the effective ductility demand of higher modes of vibration in the direction of interest shall be taken as 1.0.

Inherent damping, β_I, shall be based on the material type, configuration, and behavior of the structure and non-structural components responding dynamically at or just below yield of the seismic-force-resisting system. Unless analysis or test data supports other values, inherent damping shall be taken as not greater than five percent of critical for all modes of vibration.

Hysteretic damping of the seismic-force-resisting system and elements of the damping system shall be based either on test or analysis, or shall be calculated as follows:

$$\beta_{HD} = q_H(0.64 - \beta_I)(1 - \frac{1}{\mu_D}) \qquad (3.4)$$

Where

- q_H = hysteresis loop adjustment factor;

- μ_D = effective ductility demand on the seismic-force-resisting system in the direction of interest due to the design earthquake.

It must be noted that meaning of eq. (3.4) can be related to eq. (2.3).

Unless analysis or test data supports other values, the hysteretic damping of higher modes of vibration in the direction of interest shall be taken as zero.

The calculation of hysteretic damping of the seismic force-resisting system and elements of the damping system shall consider pinching and other effects that reduce the area of the hysteresis loop during repeated cycles of earthquake demand. Unless analysis or test data support other values, the fraction of full hysteretic loop area of the seismic-force-resisting system used for design shall be taken as equal to the factor, q_H that shall not be taken as greater than 1.0 and not less than 0.5.

Viscous damping of the mth mode of vibration of the structure, β_{Vm}, shall be calculated as follows:

$$\beta_{Vm} = \frac{\sum_j W_{mj}}{4\pi W_m} \tag{3.5}$$

where

- W_{mj} = work done by jth damping device in one complete cycle of dynamic response corresponding to the mth mode of vibration of the structure in the direction of interest at modal displacements, ϕ_{mrj} ;

- $W_m = \dfrac{1}{2}\sum_i F_{im}\phi_{mi}$ = maximum strain energy in the mth mode of vibration of the structure in the direction of interest at modal displacements, ϕ_{mi} ;

- F_{im} = mth mode inertial force at Level i ;

- ϕ_{mi} deflection of Level i in the mth mode of vibration at the center of rigidity of the structure in the direction under consideration.

Eq. (3.5) can also be formulated as:

$$\beta_{Vm} = \frac{T_m \sum_j C_j \cos^2 \theta_j \phi_{mrj}^2}{\pi \sum_i (\frac{W_i}{g}) \phi_{mi}^2} \tag{3.6}$$

where

- T_m = natural period of the mth mode of vibration;

- C_j = damping coefficient of the jth damping device;

- W_i = seismic weight at Level i.

It must be noted that, due to inelastic system deformation, the role of effective viscous damping contribution in eq. (3.3) is magnified by a factor $\sqrt{\mu_D}$ due to increase of the effective period T_m or, equivalently, to reduction of elastic strain energy at the denominator of eq. (3.5).

3.7.3 Linear Analysis Methods

In the 2003 NEHRP Recommended Provisions (BSSC 2004), the design earthquake displacements, velocities, and forces are specified in terms of design earthquake spectral acceleration and modal properties.

The equivalent lateral force procedure is permitted to be used for design of structures with damping systems provided that:

- in the direction of interest, the damping system has at least two damping devices in each story, configured to resist torsion; and

- the total effective damping of the fundamental mode, β_{mD} (m = 1), of the structure in the direction of interest is not greater than 35 percent of critical.

- the seismic-force-resisting system does not have plan irregularity or vertical irregularity;

- floor diaphragms are rigid as defined in Sec. 4.3.2.1; and

- the height of the structure above the base does not exceed 100 ft (30 m).

The response spectrum procedure is permitted to be used for design of structures with damping systems provided that:

- in the direction of interest, the damping system has at least two damping devices in each story, configured to resist torsion; and

- the total effective damping of the fundamental mode, β_{mD} (m = 1), of the structure in the direction of interest is not greater than 35 percent of critical.

The elastic stiffness of elements of the damping system other than damping devices shall be explicitly modeled. Stiffness of damping devices shall be modeled depending on damping device type as follows:

- Displacement-Dependent Damping Devices shall be modeled with an effective stiffness that represents damping device force at the response displacement of interest (e.g., design story drift). Alternatively, the stiffness of hysteretic and friction damping devices may be excluded from response spectrum analysis provided design forces in displacement-dependent damping devices are applied to the model as external loads.

- Velocity-Dependent Damping Devices that have a stiffness component (e.g., visco-elastic damping devices) shall be modeled with an effective stiffness corresponding to the amplitude and frequency of interest.

In order to determine design displacements, lowest effective stiffness and damping should be used. By contrast, design forces correspond to greatest stiffness values and lowest damping.

For equivalent lateral force (ELF) analysis (linear static analysis), the response is defined by two modes: the fundamental mode and the residual mode. The residual mode is a new concept used to approximate the combined effects of higher modes. While typically of secondary importance to story drift, higher modes can be a significant contributor to story velocity and hence are important for design of velocity-dependent (rate dependent) damping devices. For response spectrum analysis (linear dynamic analysis), higher modes are explicitly evaluated. For both the ELF and the response spectrum analysis procedures, the response in the fundamental mode in the direction of interest is based on assumed nonlinear (pushover) properties of the structure. Nonlinear (pushover) properties, expressed in terms of base shear and roof displacement, are related to building capacity, expressed in terms of spectral acceleration and displacement, using mass participation and other fundamental-mode factors. When using linear analysis methods, the shape of the fundamental-mode pushover capacity curve is not known and an idealized elastoplastic pushover curve is assumed, as shown in Figure 3.15.
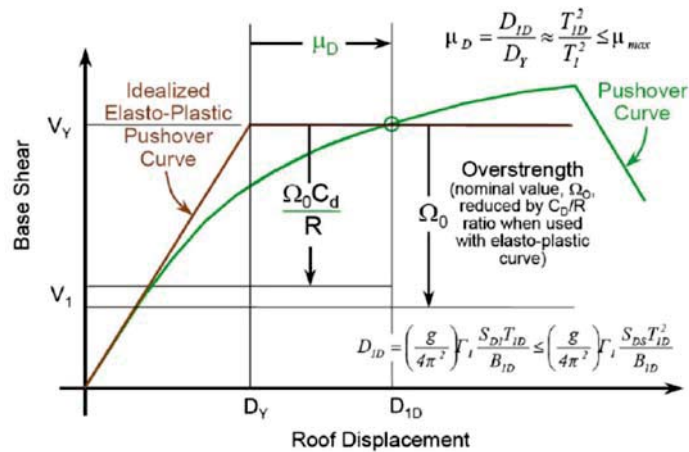
Figure 3.15 Idealized elastoplastic pushover curve used for linear analysis.

The idealized pushover curve shares a common point with the actual pushover curve at the fundamental mode design earthquake displacement, D_{1D}. Note that, in Figure 3.15, the parameters Γ_1 and S_{DS}, which are used to compute D_{1D}, represent the modal participation factor for the fundamental mode and the 5% damped design spectral response acceleration at short periods, respectively. The idealized pushover curve permits defining the effective global ductility demand due to the design earthquake, μ_D, as the ratio of design roof displacement, D_{1D}, to the yield displacement, D_Y. This ductility factor is used to calculate various design factors (e.g., it is used in the computation of the effective period, T_{1D}, and the hysteretic damping ratio, β_H) and to limit the maximum ductility demand, μ_{max}, in a manner that is consistent with conventional building response limits. Design examples for structures with passive energy dissipation systems and using linear analysis methods have been developed and found to compare well with the results of nonlinear response-history analysis (Ramirez et al 2001).

The Provisions require that elements of the damping system be designed for actual fundamental-mode design earthquake forces corresponding to a base shear value of V_Y (except that damping devices are designed and prototypes tested for maximum considered earthquake response) (see Figure 3.15). Elements of the seismic-force- resisting system are designed for a reduced fundamental mode base shear, V_1, where the force reduction is based on system overstrength, Ω_0, conservatively decreased by the ratio C_d / R (C_d is the deflection amplification factor, R is the response amplification factor), for elastic analysis (when actual pushover strength is not known).

In a simplified nonlinear method of analysis, response in the higher modes may be determined by application of the response spectrum method using the effective stiffness properties of the structure at the actual displacement of the structure.

Under certain conditions, the damping ratio in higher modes may be very large and can reach critical values. The origin of this interesting phenomenon may be found in eq. (3.6): for higher modes, the device relative modal displacement ϕ_{rj} assume large values. It should be noted that this phenomenon cannot, generally, occur in structures having viscoelastic or hysteretic energy dissipation devices since such devices contribute stiffness and, therefore, cause an increase in the strain energy.

Linear procedures require iterations for evaluation of the effective damping and stiffness. It is a trial and error process because effective damping and stiffness depend on structural response, both for rate dependent or independent devices.

3.7.4 Nonlinear Analysis Methods

The Provisions specify procedures for nonlinear static analysis and nonlinear dynamic (response-history) analysis. The nonlinear procedures are permitted to be used for design of all structures with damping systems.

The nonlinear static analysis procedure is similar to the linear static analysis procedure in that the pushover capacity curve is used to define the nonlinear behavior of the structure.

However, in the nonlinear static analysis procedure, the actual nonlinear force-displacement relation is used, rather than an idealized elastoplastic curve as shown in Figure 3.15. In addition, since actual pushover strength is known from the nonlinear pushover analysis, the force reduction for design of the seismic-force resisting system is based on overstrength alone with no additional reduction (i.e., in Figure 3.15, C_d/R is taken as 1.0).

Non linear static procedure requires the definition of a "spectral capacity curve" (conceptually similar to the pushover curve) and a "design demand curve". The design demand curve is derived from the elastic response spectrum using a level of equivalent damping consistent with the energy dissipated by the building in one cycle of loading to the assumed target displacement. Also in this case, even if the designer is required to run just one analysis to get the capacity curve, he needs to perform some iterations for the evaluation of the effective damping and so the effective design demand curve.

In general, nonlinear dynamic analysis procedure is the most robust procedure available for evaluating the behavior of systems that incorporate passive energy dissipation devices. Such analysis allows explicit modeling of individual devices, the elements connecting the devices to the structure, and the structure itself. If the connecting elements or the structural framing yields during the response, this behavior must be incorporated into the analytical model. It is noted that accurate modeling of the flexibility of the floor diaphragm and of the connecting elements (braces) is essential since a loss of effective damping may occur if these elements are overly flexible. To determine the effect of such flexibility on response, analyses should be run with both rigid and flexible diaphragms and connectors. If the difference in response for these two cases is significant, the designer should consider stiffening the connecting elements, or changing the deployment configuration of the devices.

Nonlinear dynamic analysis may be performed using a variety of commercially available software and several academic programs. Most of these programs can readily be used to model the behavior of linear fluid viscous dampers, viscoelastic dampers, friction dampers, or metallic yielding dampers. However, modeling of some damping devices (e.g., nonlinear viscous dampers and dampers with temperature-dependent or frequency-dependent mechanical properties) can be more challenging or, in some cases, not possible with a given program. When the modeling of such behavior is not possible, the expected response may be bounded by analyzing the structure over a range of behaviors. For example, the properties of viscoelastic dampers are a function of the temperature of the viscoelastic material, with the temperature generally increasing during the response. The effect of the temperature increase is to reduce the effective damping capacity of the device. Hence, analyses should be run with the viscoelastic material at the ambient temperature and at the peak expected temperature (peak base shears may be obtained from the first analysis and peak displacements from the second). Note that this approach of performing analysis for upper and lower bound damper properties is recommended by the Provisions. According to the Provisions, a minimum of three ground motions are required for linear or nonlinear dynamic analysis, although it is usually beneficial to analyze the system for seven or more ground motions. The main benefit of using seven or more motions is that the system may be evaluated on the basis of the average among the seven responses, whereas if less than seven motions are used, the maximum values among all analyses must be used. The Provisions provide guidelines for appropriately scaling the ground motions.

Only non linear dynamic analysis avoid iterations for the definition of the structural performance, since spectrum-matching acceleration records are usually obtained for a 5%

elastic design spectra. By proper modeling devices'mechanical behavior, the effective non-linear response will be accounted for. The definition of effective stiffness and damping is not required for the purpose of design but can just be estimated for performance considerations.

3.8   Design procedures: an overview

Hanson and Soong imparted to design engineers and building officials basic concepts of the supplemental energy dissipation technology in the monograph series published by EERI in 2001 (Hanson and Soong 2001). The authors focused on the concept that the design of a damper-added structure is, in general, an iterative process: in step 1 an analysis of the bare frame is carried out, in step 2 the desired overall damping ratio is determined, in step 3 the available damper locations are selected, in step 4 the damper-induced damping and stiffness is calculated, in step 5 the equivalent modal damping ratios, stiffnesses and mode shapes associated with the damper-added structure are computed, in step 6 the analysis of the damper-added structure is performed. When steps 5 and 6 satisfy the desired damping ratio and the structural performance criteria the design is complete, otherwise a new design cycle has to be made, which may lead to new structural properties, damper locations, or damper properties. They presented two design examples of damper-added structure with viscoelastic and friction dampers, respectively.

The optimum distribution of dampers can be cast in a context of optimum control theory, maximizing a given set of optimum location indices. A simplified method based on the sequential search algorithm (SSA) was developed by Garcia (Garcia 2001). Only linear viscous damper type is considered.

For the case of linear viscous dampers, the optimum location index is simply given by the maximum interstorey velocity, which indicates that the optimum location is between two adiacent stories of the structure. In the case of regular buildings, the SSA will generally lead (Lopez Garcia and Soong 2002) to efficient damper configurations, particularly for low-to-medium-rise buildings and for a number of dampers equal to or greater than 1.5–2 times the number of storeys. The resulting damper configurations are found to be sensitive to ground motion characteristics, especially for low levels of supplemental damping.

3.8.1. Displacement dependent dampers

The design of structures equipped with metallic or friction dampers is similar. Only the yield loads of the metallic dampers need to be substituted for the slip loads of the friction dampers.

A number of design procedures exists in literature and some general concepts are illustrated in this Chapter.

Some procedures are based on maximization of dissipated energy (Baktash and Marsh 1987) by means of hysteretic dampers. Optimum performance from an energy point of view is not necessarily associated with maximum energy dissipation by the hysteretic dampers but rather with the minimization of the difference between the seismic input energy and the energy dissipated by the dampers.

Ciampi et al. (Ciampi et al 1995) considered the design of hysteretic bracing systems using an approach based on inelastic response spectra. The design is defined by the choice of two characteristic parameters: the bracing stiffness k_b and the activation load of the bracing members F_a. The authors recognized that the hysteretic bracing system needs to be activated much before yielding of the frame takes place. Consequently, the ratio of the displacement which causes yielding (or slipping) in the brace to the displacement which induces yielding of the frame is always equal to or less than one and is suggested to be taken close to 0.5. The application of this methodology to MDOF systems requires the selection of proper distributions of stiffness and yield force along the height of the building, aiming at uniform engagement of the bracing system in the energy dissipation process, and to avoid concentration of damage at specific locations in the frame.

Filiatrault and Cherry (Filiatrault and Cherry 1990) determined an optimum activation shear distribution based on a numerical parametric study that takes into account the frequency content of the ground motion and the dynamic properties of the structure with and without the added bracing system. For a given ground motion, the optimum activation shear distribution is determined by minimizing a Relative Performance Index (RPI) derived from energy concepts. These authors recommended the selection of diagonal cross braces such that the ratio between the stiffness of the braced structure is about 6 times that of the unbraced one. Therefore the diagonal cross-braces should be chosen with the largest possible cross-sectional area within the limits of cost and availability of material. The procedure than requires the estimation of the design peak ground acceleration and the predominant period of the design ground motion for the site.

The significance of optimal design was put forward by Filiatrault and Cherry (Filiatrault and Cherry 1988): it was suggested that the seismic response of friction damped braced frames is the least sensitive to variations in the slip load (as large as 20%) when they are tuned to the

optimal slip load value. This is schematically shown in Figure 3.16. Variations in the slip load in the friction device may occur due to environmental and constructional factors such as temperature change, adjustment and other uncertainties. Therefore, design procedure that target the optimal (minimum) response are likely to yield structures with a reduced sensitivity to variations in their actual slip load. Optimum activation loads of the hysteretic dampers are dependent on both the structural and ground motion characteristics.
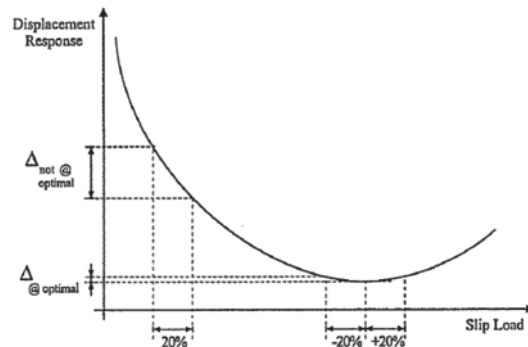
Figure 3.16 Effect of variation in slip load on displacement response.

In general, the optimized performance indices used are either the maximum displacement response or the maximum acceleration response, or factored combinations of both to suggest a single optimized solution. However, both these families of design methods offer limited information about the possible range of different seismic performance that can be achieved by changing the added brace stiffness and/or the damper activation load, and do not allow the designer to explicitly target a desired performance level. It can be seen that generally, lower activation loads result in lower accelerations while the displacement response is variable for different values of the braced period. It can also be seen that for braced periods lower than 0.5s, the elastic response is the one which optimizes the displacement so that if the acceleration levels are acceptable, the retrofit strategy can simply consist of adding bracing members without the additional cost of adding the dampers. The best possible acceleration response of a structure equipped with hysteretic dampers is very close to the spectral acceleration of the unbraced structure and can be reached by using a low stiffness of the added bracing or by using a low activation load of the added damper such that the structure's effective stiffness is similar to that of the unbraced frame during most of the response. In the former case, the displacement response will remain large because of the longer period of the braced frame, whereas in the latter case, when a higher brace stiffness is used in conjunction with a low slip load, not only the accelerations are reduced but the maximum displacement response is also controlled.

Procedures to extend SDOF approach to MDOF structures have also been suggested using a transformation based on the fundamental mode of vibration of the structure. The effect of the distribution of the activation load along the height of the building was also investigated by considering both a uniform activation load and an activation load distribution aimed at achieving simultaneous activation of the hysteretic dampers under the first mode of vibration of the structure. The distributed activation loads were found to improve the response of the structure and to better correspond with the expected response of the structure once it was designed with the method described above.

3.8.2. Velocity dependent dampers

In the design of structures equipped with viscoelastic dampers, the primary parameters to be evaluated are the required viscous damping ratio and the stiffness of the damping system. Since it is expected that structures equipped with viscoelastic dampers will respond with minimal yielding of the main structural elements under design level earthquakes, most design methods are based on elastic modeling of the main structure.

The desired damping ratio in the fundamental mode of vibration of the structure ζ_1 must be set.

The stiffness k_d and the loss factor η of each viscoelastic damper must be selected based on the available viscoelastic material and the geometry of the damper. These parameters are usually determined based on the assumption that the added stiffness due to the viscoelastic dampers at each storey is proportional to the storey stiffness of the initial structure.

This could be a trial and error procedure: even in case of proportional stiffness, viscoelastic damper properties are frequency, temperature and strain amplitude dependent.

As fare as viscous dampers are concerned, since they are usually inserted in bracing members between diaphragms of the structures, the global damping matrix generated by the linear viscous dampers $\left[\overline{C_L}\right]$ may be assumed proportional to the global stiffness matrix of the structure $\left[K\right]$ (Chopra 2011):

$$\left[C_L\right] = \alpha_0 \left[K\right] \tag{3.5}$$

From modal analysis, the generalized damping coefficient in the ith mode of vibration $\overline{C}_i$ is given by:

$$\overline{C}_i = \left\{ A^{(i)} \right\}^T [\overline{C}_L] \left\{ A^{(i)} \right\} = \left\{ A^{(i)} \right\}^T \alpha_0 [K] \left\{ A^{(i)} \right\} = \alpha_0 K_i = 2 \zeta_i \omega_i M_i \tag{3.6}$$

where $\left\{ A^{(i)} \right\}$ is the ith mode of vibration, ζ_i is the damping ratio in the ith mode, K_i is the generalized stiffness in the ith mode of the original structure without damper, ω_i is the circular frequency associated with the ith mode of vibration, and M_i is the generalized mass in the ith mode of vibration.

From eq. (3.6) the proportionality constant α_0 can be easily obtained as:

$$\alpha_0 = \frac{2 \zeta_i}{\omega_i}$$

Conceptually, the design process is simple. Once a desired viscous damping ratio in a particular mode is established (usually in the first mode), the proportionality constant α_0 can be computed by Equation 3.6. The resulting global damping matrix $[C_L]$ can then be obtained by 3.5.

This conceptually simple approach is, however, difficult to apply for large structural systems for which the explicit form of the global damping matrix may not be obtained easily. Therefore, in most practical design situations, the damping constant for each damper is obtained by trial-end-error.

Some design procedure have been proposed by several authors to provide, for a target equivalent damping ratio, the corresponding damping coefficients and their distribution along the height (Christopoulos and Filiatrault 2006). Christopoulos and Filiatrault [Ch. 6.8.2] suggested a practical design procedure for estimating the damping constants of individual dampers on the basis of the knowledge of the interstory lateral stiffness and the introduction of a generalized stiffness coefficient of a fictitiously braced structure.

Silvestri et. al (Silvestri et al 2010) proposed a practical procedure for the seismic design of building structures equipped with viscous dampers. It is based on five consecutive steps which move from the selection of a target reduction in the seismic response of the system (with respect to that of a system without any additional viscous dampers) to the identification of the characteristics (final design specifications) of viscous dampers which allow to obtain target reduction factors in the seismic response of the system. According to the analytical nature of the proposed procedure, very close correlations between damping coefficients and target reduction factors do exist only for structures which satisfy the shear-type, equal floor mass, and equal lateral stiffness hypotheses. Nonetheless, in case of structures which drift from the above

hypothesis, in the applicative examples there presented, it is observed that the correlation is still close and the results conservative.

The proposed procedure allows to obtain the damping coefficient of each linear viscous damper by means of just a single and very easy formula starting from the knowledge of the target damping ratio, the fundamental frequency of the system, total mass, total number of stories, and total number of dampers at each story for each direction. This formula leads to a first dimensioning of the linear damping coefficients which leads to a damping ratio which is sufficiently close to the target one.

Typical design procedures commonly refer to linear viscous dampers. In case of non-linear behavior (i.e. $\alpha_{vd} \neq 1$) energy considerations lead to the equivalence of the energy dissipated by equivalent linear and non-linear damper as a function of the velocity exponent and the displacement amplitude.

Most of design procedures are based on preserving the classical normal modes. This design approach leads to a distribution of damping constants proportional to the lateral stiffness of the original structure, which may lead to several different dampers in the structure. Although this approach is very simple, it may not be optimum from an economical point of view where same size dampers should be used as much as possible. Furthermore, the constraint on maintaining classical normal modes is not required particularly if nonlinear time-history dynamic analysis is used in the design process.

3.9 Force reduction factor for yielding systems equipped with added viscous dampers

An open issue is related to the effects of supplemental damping on the inelastic response of structural systems. Modern earthquake resistant design codes use earthquake spectral reduction factors to account for building inelastic response capabilities (strength reduction factor R in the American codes or q in the European codes): numerical values of the force reduction factor are generally given by codes only for the case of structures without added dissipative devices (thus considering only the inherent damping ratio, conventionally equal to 0.05).

It is important to consider the consequences of including the effects of increased viscous damping on the inelastic response of structural systems so that appropriate supplemental damping reductions can be included in these code design procedures. Code design procedures which acknowledge spectral reductions due to inelastic deformations and other factors can be

retained while incorporating a separate reduction factor for added energy dissipation devices (Hanson 1993).

For the case of structures equipped with added dampers, the actual codes do not allow to reduce the seismic demand by applying the force reduction factor, while it is suggested to reduce the seismic actions by means of the so-called reduction coefficient η, which accounts for damping ratios ζ larger than 0.05.

The objective of a recent research work (Palermo et al 2013) is to investigate the influence of higher damping ratios on the force reduction factor R. In more detail, the main goal is to obtain a relationship between the force reduction factor given by the codes (referred to as R_5) for a structure characterized only by the inherent damping, and the one for the same structure equipped with added dampers (R_ζ).
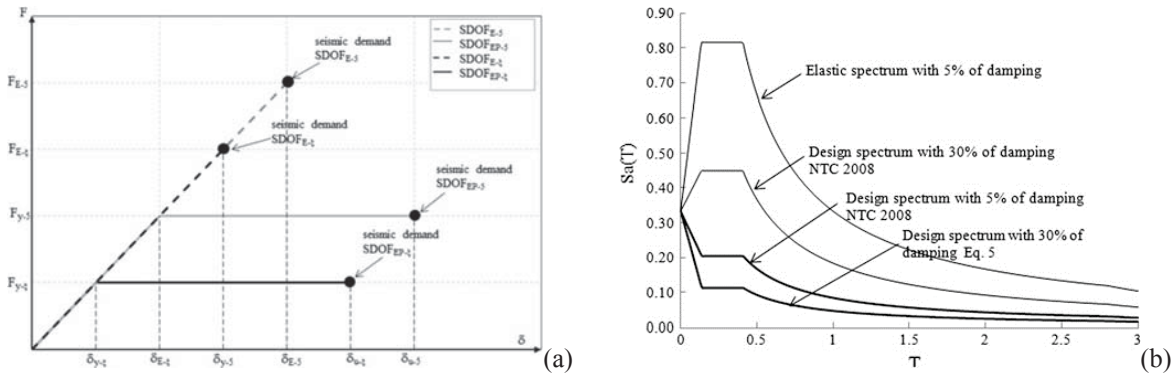
Figure 3.17 (a) Seismic demand for elastic and inelastic SDOF systems (with and without added damping); (b) Elastic spectrum for 0.05 and 0.30 of damping ratio and corresponding design spectrum for a behavior factor equal to 4.0.

The authors of this work proposed a global reduction factor for building structures equipped with added viscous dampers η_{tot} in order to couple both the effects due to the ductility of the structural elements and to the dissipation in the viscous dampers. In detail, η_{tot} can be expressed as a function of the behaviour factor q (typically provided by codes and expressed as $q_5 = a \cdot R_5$, where a is the overstrength factor), the reduction coefficient $\eta(\zeta)$ (typically provided by codes) and the $\alpha(\zeta)$ coefficient (introduced in the cited work):

$$\eta_{tot}(\zeta) = \eta_{visc}(\zeta) \cdot \eta_{hyst}(q) = \sqrt{\frac{10}{5+\zeta}} \cdot \frac{1}{q_\zeta} = \sqrt{\frac{10}{5+\zeta}} \cdot \frac{1}{\alpha_\zeta \cdot q_5}$$

$$S_{e,\zeta} = S_{e,5} \cdot \eta_{tot}(\zeta) = S_{e,5} \cdot \frac{\eta(\zeta)}{\alpha(\zeta)q_5} \tag{3.7}$$

In order to quantify the magnitude of the reduction, Figure 3.17 gives a comparison of the elastic and inelastic design spectra as per Italian building code (NTC 2008) and the here proposed design spectrum given by Eq. (3.7), for the specific case of a behaviour factor $q = 4$, a damping ratio equal to 0.30 and a peak ground acceleration equal to 0.35 g. For this case, the ordinate of the inelastic design spectrum with a damping ratio equal to 0.30 (i.e. Eq. (3.7) is reduced approximately to 0.5 of the ordinate of the inelastic design spectrum with a damping ratio equal to 0.05.

3.10 Estimating response of yielding systems with energy dissipation devices

The simplified non linear analysis methods discussed in Section 3.7.3 have been evaluated using design examples for structures with passive damping systems. The seismic response calculated using linear analysis was found to compare well with the results of nonlinear response history analysis (Ramirez et al 2001): the main features of the investigation are explained hereafter.

Important steps in the simplified nonlinear method of analysis is the establishment of the design demand spectrum and the determination of response by overlaying this spectrum on the spectral capacity curve. In essence, this approach is one of replacing the nonlinear system by an "equivalent" linear system, defined by an equivalent stiffness and equivalent damping ratio. The method here used is the one proposed in FEMA for establishing equivalent linear systems based on the geometric stiffness approximation. That is, the effective period is determined from the secant (or effective) stiffness at maximum displacement u, whereas the effective damping is determined assuming the external strain energy equal to $\frac{1}{2}K_s u^2$. The validity of this approximation was investigated by Ramirez.

In this work, a single-degree-of-freedom system with the characteristics shown in Figure 3.18 is analyzed. The system is characterized by ideal bilinear hysteretic behaviour, added linear viscous damping ratio β_v representing the energy dissipation devices, inherent viscous damping ratio β_i equal to 0.05 in both the elastic and inelastic ranges of displacement.

The system was excited with the 20 horizontal components of the ten scaled earthquake motions. Also, Figure 3.19 shows average damped response spectra of these 20 scaled components. Note that the spectra present the spectral acceleration: they are useful in directly

112

obtaining the maximum displacement and acceleration at maximum displacement, but not the maximum acceleration.

Elastic Period $T_{el} = 2\pi\sqrt{\dfrac{D_y}{A_y}}$

Added Viscous Damping $\beta_v = \dfrac{C\,T_{el}}{4\pi m}$

Strength to Elastic Demand Ratio $e = \dfrac{A_y}{S_{ae}}$

(S_{ae} = Spectral Acceleration of Elastic System of Period T_{el} and 5% Damping)
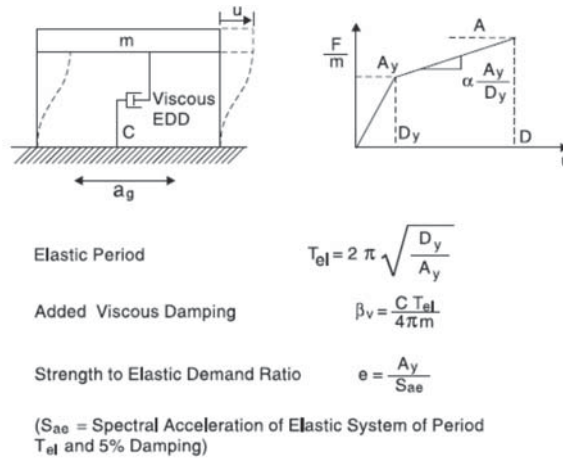
Figure 3.18 Analyzed SDOF inelastic system with linear viscous energy dissipation system.
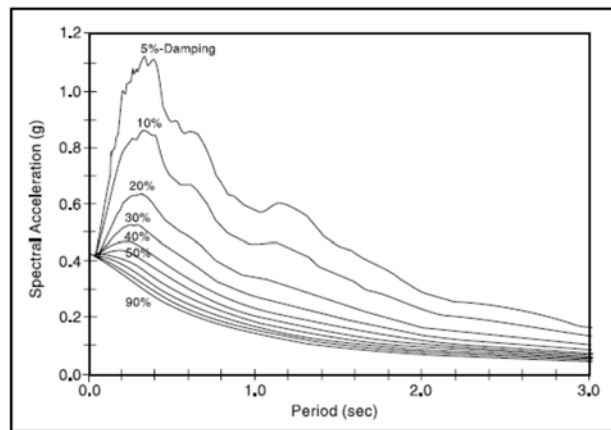
■ Figure 2.17 Average Damped Response Spectra of Scaled Motions

Figure 3.19 Avarage damped response spectra of scaled motions.

The spectra of Figure 3.19 may be used to obtain response modification factors B and compare these with those of Provisions.

Dynamic response time history analyses of the system of Figure 3.18 were conducted for a wide range of parameters (strength to elastic demand ratio, post-yielding stiffness, linear added viscous damping, elastic period) and for 20 scaled earthquake components for each analyzed system. Values of effective period T_{eff} and effective damping β_{eff} for each system were determined from the calculated average peak displacement D and the corresponding acceleration response A (see Figure 3.18). Based on the geometric stiffness approach for approximating the system by an equivalent linear one and use of eq. (2.1), expressions for T_{eff} and β_{eff} are:

$$T_{eff} = 2\pi \left(\frac{D}{A} \right)^{\frac{1}{2}}$$

$$\beta_{eff} = \frac{2(A_y D - A D_y)}{\pi A D} + \beta_v \frac{T_{eff}}{T_{el}} + \beta_i \qquad (3.8)$$

Note that in Eq. (3.8), the first term represents the contribution from yielding of the framing system (assumed to be perfect bilinear hysteretic), the second term represents the contribution of viscous damping force associated with the energy dissipation devices and the third represents the inherent damping ($\beta_i = 0.05$).

The results of the investigation demonstrated that the simplified method of analysis predicts well the average of peak displacement response, although it occasionally under predicts the response by as much as 20%. Under prediction of displacement response typically occurs in situations where the contribution of hysteretic damping is significant.

REFERENCES

1998-1 EN (2004) EN 1998-1. Eurocode 8: Design of structures for earthquake resistance – Part 1: General rules, seismic actions and rules for buildings

ASCE (2005) Minimum design loads for buildings and other structures.

ATC (1997a) Applied Technology Council. FEMA 273 - NEHRP Guidelines for the seismic rehabilitation of buildings, U.S.A.

ATC (1997b) Applied Technology Council. FEMA 274 - NEHRP Commentary on the Guidelines for the seismic rehabilitation of buildings, U.S.A.

Baktash P, Marsh C (1987) Damped Moment_Resistant Braced Frames: A Comparative Study. Can J Civ Eng 14:342–346.

BSSC (2004) Building Seismic Safety Council. FEMA 450 - NEPHR Recommended Provisions For Seismic Regulations For New Buildings and Other Structures, U.S.A.

Chopra AK (2011) Dynamics of Structures: Theory and Applications to Earthquake Engineering. Prentice Hall/Pearson Education

Christopoulos C, Filiatrault A (2006) Principles of Passive Supplemental Damping and Seismic Isolation. IUSS Press, Pavia

Ciampi V, De Angelis M, Paolacci F (1995) Design of yielding or friction-based dissipative bracings for seismic protection of buildings. Eng Struct 17:377–396.

Circ.617 (2009) Ministero delle Infrastrutture e dei Trasporti. Circolare 02 febbraio 2009 n. 617/C.S.LL.PP.: Istruzioni per l'applicazione delle «Nuove norme tecniche per le Costruzioni» di cui al Decreto Ministeriale 14 gennaio 2008

Filiatrault A, Cherry S (1990) Seismic Design Spectra for Friction-Damped Structures. J. Struct. Eng. 116:

Filiatrault A, Cherry S (1988) Seismic Design of Friction Damped Steel Plane Frames by Energy Methods. Vancouver, Canada

Fu Y, Kasai K (1998) Comparative Study of Frames Using Viscoelastic and Viscous Dampers. J Struct Eng 124:513–522. doi: 10.1061/(ASCE)0733-9445(1998)124:5(513)

Garcia DL (2001) A Simple Method for the Design of Optimal Damper Configurations in MDFO Structures. Earthq. Spectra 17:

Goel RK (2000) Seismic behaviour of asymmetric buildings with supplemental damping. Earthq Eng Struct Dyn 29:461–480. doi: 10.1002/(SICI)1096-9845(200004)29:4<461::AID-EQE917>3.0.CO;2-6

Hanson RD (1993) Supplemental Damping for Improved Seismic Performance. Earthq Spectra 9:319–334. doi: 10.1193/1.1585719

Hanson RD, Soong TT (2001) Seismic design with supplemental energy dissipation devices. EERI Monograph No.8. Earthquake Engineering Research Institute, Oakland(CA)

ICC (2006) International Building Code. USA

Lopez Garcia D, Soong TT (2002) Efficiency of a simple approach to damper allocation in MDOF structures. J Struct Control 9:19–30. doi: 10.1002/stc.3

NFPA (2006) NFPA 5000: Building Construction and Safety Code.

NTC (2008) Ministero delle Infrastrutture. D.M. 14 gennaio 2008: Nuove norme tecniche per le costruzioni

Palermo M, Silvestri S, Trombetti T, Landi L (2013) Force reduction factor for building structures equipped with added viscous dampers. Bull Earthq Eng 11:1661–1681. doi: 10.1007/s10518-013-9458-z

Pavlou EA, Constantinou MC (2004) Evaluation of Accuracy of Simplified Methods of Analysis and Design of Buildings with Damping Systems for Near-Fault and for Soft-Soil Seismic Motions.

Ramirez OM, Constantinou MC, Kircher C, et al (2001) Development and evaluation of simplified procedures of analysis and design for structures with passive energy dissipation systems. Buffalo, N.Y.

Reluis (2014) Linee guida sulla progettazione di strutture con controventi dissipativi.

Silvestri S, Gasparini G, Trombetti T (2010) A Five-Step Procedure for the Dimensioning of Viscous Dampers to Be Inserted in Building Structures. J Earthq Eng 14:417–447. doi: 10.1080/13632460903093891

Chapter 4

4.   A PROCEDURE FOR OPTIMAL DESIGN OF A SDOF FRAME

4.1   Introduction

The purpose of the chapter is the definition of a design procedure to determine the optimal design parameter of dissipative braces installed in a simple one story–one bay frame (Figure 4.1), whose behavior has to remain elastic (Losanno et al 2014). External supplemental devices are assumed to be viscous dampers (linear viscous behavior – VD case) or friction dampers (rigid plastic behavior – FD case). The proposed methodology provides closed-form expressions of suitably defined adimensional damping parameters (i.e., adimensionalized viscous damping and adimensionalized yielding displacement), and points out the fundamental influence of a properly dimensioned braces stiffness on the optimal design of the dissipation devices, while current state of art usually assumes the supporting brace as infinitely rigid and models also the damper as directly connecting two stories. The analytical treatment at the base of the proposed method considers the response to a simple harmonic excitation with sweeping frequency, thus determining the frequency response functions (FRFs) for different values of the adimensional design parameters: theoretical optimal damping parameters are provided as the ones corresponding to a minimum of the resonance peak frame displacement and base shear, in

117

the overall range of frequencies. Then, the theoretical results are validated by means of numerical integration of the framed structure under real ground motions, thus giving just the required effectiveness to the design procedure.

4.2 Steady-state response of a dissipative braced frame subjected to harmonic base motion

The structural model (Figure 4.1) is a two degrees of freedom (DOF) system (x, x_b), where the parameters k_f and k_b are, respectively, the lateral frame and the elastic brace stiffness. The supplemental damping device is defined by the damping coefficient C_d (in the VD case) or by the yield strength F_{dy} (in the FD case), while the frame has no inherent damping. The only mass accounted for is the floor mass m, so that the model reduces to a single dynamic DOF with two kinematic DOFs. It is worth to point out that the assumptions of frame elastic behavior with negligible damping contribution are based on the following consideration: an optimally designed supplemental damping system is able to produce a strong reduction of stresses in the structural and non-structural components, even for design earthquakes, so to keep them in the elastic field.

The dynamic problem of the frame subjected to a harmonic base excitation can be formulated and solved as shown in the following. The equations of motion are derived together with the definition of the relevant design parameters and response quantities, and the optimal damper characteristics are obtained under the hypothesis that the ratio $\kappa = k_f / k_b$ and the mass m are known. For both VD and FD cases, a closed-form solution of the response is obtained.

Even if earthquake motion is usually random, by means of the Discrete Fourier Transform Function (DFT), properly working on non-periodic data, it can be decomposed into a linear combination of harmonic functions. Typical ground motions contain a wide range of frequencies while system displacement response shows a dominant period very close to its natural period. A sweeping frequency (i.e., harmonic function with $0 \leq \overline{\omega} \leq \infty$) of the excitation at the base is assumed, since due to extremely different values of the damping parameter, the effective frequency of the system vary significantly. In addition to this, for a damped system, the higher is the damping the shorter is the transitory condition, so that structural response tends to a single period harmonic function.
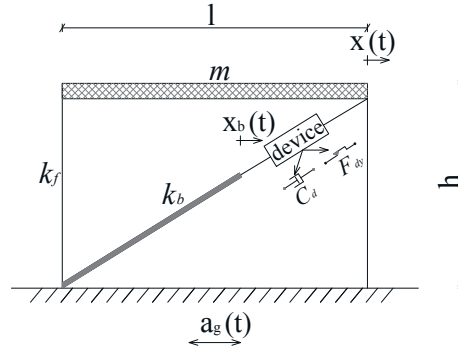
Figure 4.1 Braced frame model with viscous (VD) or friction (FD) device.

The problem is first solved referring to the frame displacement x: the optimization procedure is developed with the aim of determining the value of the control device parameter corresponding to the minimum story drift ($C_{d,opt}$ or $F_{dy,opt}$) and base shear ($C_{d,f,opt}$ or $F_{dy,f,opt}$) over the whole range of frequency excitation.

Moreover, one of the more effective way to understand the effects of dissipative braces on the structural dynamics, is by means of the energy balance equation, that is thus formulated for a controlled structure with linear elastic behavior and negligible viscous damping as $E_k^a + E_{sd} + E_a = E_{vb} + E_{sd} = E_{in}^a$. The energy E_k^a is the absolute kinetic energy, E_{sd} is the energy dissipated by the dissipative braces, E_a is the energy adsorbed by the frame (equal to the elastic recoverable strain energy), E_{vb} is the vibrational energy (equal to the sum of the kinetic energy and the elastic strain energy), and E_{in}^a is the absolute input energy. Maximizing the energy dissipated by the supplemental dampers does not necessarily lead to a minimum vibrational energy, since the amount of input energy can also increase significantly. The optimal design strategy of a supplemental damping system should be based on the minimization of the difference between the seismic input energy and the vibrational energy (Christopoulos and Filiatrault 2006). Only in this case, the variation of the input energy with the specific control system, defined by (k_b, C_d) or (k_b, F_y), is properly accounted.

4.2.1   *Formulation of the equation of motion*

The general expression of the equation of motion for the model illustrated in Figure 4.1, subjected to a harmonic base acceleration $a_g(t) = a_{g,max} \cdot \cos \overline{\omega} t$, is simply the following:

$$m\ddot{x} + F(x, x_b, \dot{x}, \dot{x}_b, ...) = -ma_{g,max} \cos \overline{\omega} t \tag{4.1}$$

119

where x is the relative floor displacement, x_b is the relative displacement of the elastic element of the dissipative brace (in the following referred to as the brace), *dot* notation represents the derivative respect to time and $F(x,x_b,\dot{x},\dot{x}_b,...)$ is the global restoring force.

In order to single out the relevant design parameters of the control devices and the structural response parameters, it is needed to write Eq. (4.1) in a non-dimensional form. Considering the time parameter $\tau = \omega_b t$ and the reference displacement $x_{g,max} = a_{g,max}/\omega_b^2$, where $\omega_b = \sqrt{(k_f + k_b)/m_f}$, Eq. (1) can be expressed as follows:

$$\zeta''(\tau) + \frac{F(x,x_b,\dot{x},\dot{x}_b,...)}{ma_{g,max}} = -\cos\beta\tau \quad \rightarrow \quad \zeta''(\tau) + f(\zeta) = -\cos\beta\tau \tag{4.2}$$

where (') represents the derivative respect to τ, $\zeta = x/x_{g,max}$ is the normalized frame displacement, $f(\zeta) = F(x,x_b,\dot{x},\dot{x}_b,...)/\left[(k_b + k_f)\cdot x_{g,max}\right]$ is the normalized restoring force, and $\beta = \overline{\omega}/\omega_b$ is the normalized frequency. Eq. (4.2) represents the final form of the normalized equation of motion and it is developed in the following paragraphs for the two defined cases.

It is worth to point out that, in general terms, such kind of manipulation (i.e., a normalization with respect to both a stiffness and a displacement term) allows to derive an adimensionalized set of equations and adimentional solutions, as shown in the paragraphs 4.2.2 and 4.2.3.

4.2.2 Solution of the equation of motion for the VD case

In the case of an added linear viscous device having damping coefficient C_d (Figure 4.2(a)), the equivalent damping ratio is defined as:

$$\nu = \frac{C_d}{2\sqrt{m\cdot k_f}} \tag{4.3}$$

The restoring force in Eq. (1) may be expressed as $F(x,x_b,\dot{x},\dot{x}_b,...) = k_f x + F_d$, where $F_d = k_b \cdot x_b = C_d \cdot(\dot{x} - \dot{x}_b)$.

The force–displacement relationship for the Maxwell element composed by the spring k_b and the viscous dashpot C_d in series is given by the well-known expression $F_d(x) = K_d(\overline{\omega})\cdot x$, where the complex stiffness $K_d(\overline{\omega})$ is obtained as follows:

$$x = x_b + \frac{\dot{x} - \dot{x}_b}{i\overline{\omega}} = F_d\left(\frac{1}{k_b} + \frac{1}{i\overline{\omega}C_d}\right) \quad \Rightarrow \quad F_d = \frac{k_b C_d^2 \overline{\omega}^2 + ik_b^2 C_d \overline{\omega}}{k_b^2 + \overline{\omega}^2 C_d^2}x \quad \Rightarrow$$

$$\Rightarrow \quad K_d(\overline{\omega}) = \frac{k_b C_d^2 \overline{\omega}^2}{k_b^2 + \overline{\omega}^2 C_d^2} + i\frac{k_b^2 C_d \overline{\omega}}{k_b^2 + \overline{\omega}^2 C_d^2} = K_d'(\overline{\omega}) + iK_d''(\overline{\omega})$$

(4.4)

The quantities $K_d'(\overline{\omega})$ and $K_d''(\overline{\omega})$ are, respectively, the storage and the loss modulus of the Maxwell element. The restoring force $F(x) = (k_f + K'_d(\overline{\omega}) + K'_d(\overline{\omega})) \cdot x$ corresponds to $f(\varsigma) = \left[k_f + K'_d(\overline{\omega}) + K'_d(\overline{\omega})\right] \cdot x / \left[(k_f + k_b) \cdot x_{g,\max}\right] = \overline{K}_s(\beta) \cdot \varsigma(\tau)$ (Figure 4.2(b)), where the normalized complex stiffness of the system $\overline{K}_s(\beta)$ is:

$$\overline{K}_s(\beta) = \frac{\kappa}{1+\kappa} + \frac{\kappa}{1+\kappa}\frac{4\beta^2 v^2 \kappa(1+\kappa)}{[1+4\beta^2 v^2 \kappa(1+\kappa)]} + i\frac{\kappa}{1+\kappa}\frac{2\beta v\sqrt{\kappa(1+\kappa)}}{[1+4\beta^2 v^2 \kappa(1+\kappa)]} =$$

$$= \overline{K}_s'(\beta) + i\overline{K}_s''(\beta)$$

(4.5)

with $\overline{K}_s'(\beta)$ and $\overline{K}_s''(\beta)$ the overall storage and the loss modulus of the controlled structure.
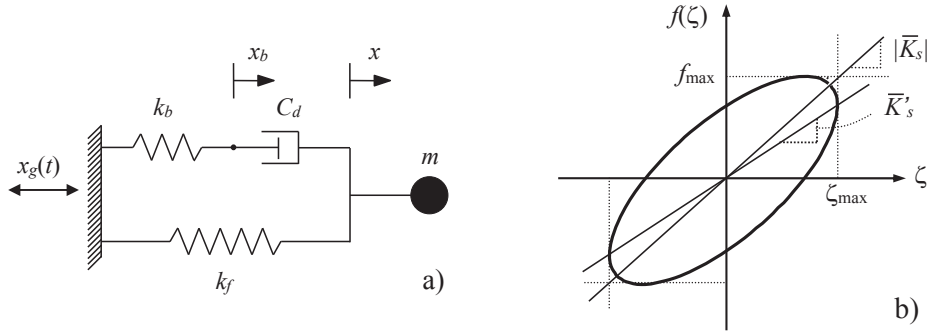
Figure 4.2 SDOF with purely viscous damper: (a) rheological model, (b) hysteretic cycle.

Given that the system is linear, an exact solution can be easily evaluated. The steady-state response $\varsigma(\tau) = \varsigma_{\max}e^{i\beta\tau}$ is periodic with frequency β, giving the equation of motion:

$$-\beta^2 \varsigma_{\max}(\beta) + \overline{K}_s(\beta)\varsigma_{\max}(\beta) = -1$$

(4.6)

where the amplitude of motion is the modulus of the complex number $\varsigma_{\max}(\beta)$:

$$\zeta_{max}(\beta) = \frac{-1}{\dfrac{\kappa}{1+\kappa} + \dfrac{4\beta^2\nu^2\kappa}{1+4\beta^2\nu^2\kappa(1+\kappa)} - \beta^2 + i\dfrac{2\beta\nu\sqrt{\kappa(1+\kappa)}}{(1+\kappa)[1+4\beta^2\nu^2\kappa(1+\kappa)]}} \Rightarrow$$

$$\Rightarrow \quad |\zeta_{max}(\beta)| = \frac{1}{\sqrt{\left(\dfrac{\kappa}{1+\kappa} + \dfrac{4\beta^2\nu^2\kappa}{1+4\beta^2\nu^2\kappa(1+\kappa)} - \beta^2\right)^2 + \dfrac{4\beta^2\nu^2\kappa}{(1+\kappa)[1+4\beta^2\nu^2\kappa(1+\kappa)]^2}}}$$

(4.7)

The two limit cases, for which the behavior reduces to an elastic undamped system, are the following:

- $\nu = 0 \quad \Rightarrow \quad C_d = 0$ (no damper) $\Rightarrow \quad |\zeta_{max}(\beta)| = \dfrac{1}{\left|\kappa/(1+\kappa) - \beta^2\right|}$;

$$\beta_{resonance} = \sqrt{\frac{\kappa}{(1+\kappa)}}$$

- $\nu \to +\infty \quad \Rightarrow \quad C_d \to +\infty$ (infinitely stiff damper) $\Rightarrow \quad |\zeta_{max}(\beta)| = \dfrac{1}{\left|1-\beta^2\right|}$

$$\beta_{resonance} = 1$$

The quantity $|\zeta_{max}(\beta)|$ is plotted in Figure 4.3 for $\kappa = 0.1, 1.0$ ($k_b = 10k_f, k_f$) and for several different values of ν: the strong influence of the device damping coefficient on the system response comes out, i.e. a deep modification in the dynamic behavior of the structure can be produced by a change in the viscous constant of the device. A very low value of ν produces a peak of the curve near to the one of the no damping limit case. This peak decreases as far as ν increases but a large increase of the damping coefficient induces a shift of the resonance frequency toward the infinite damping limit case, with an increment, at the same time, of the peak amplitude.

All the curves have a common point, corresponding to the intersection of the two limit curves for $\nu = 0$ and $\nu \to +\infty$, whose coordinates are $\overline{\beta} = \sqrt{(1+2\kappa)/[2(1+\kappa)]}$ and $|\zeta_{max}(\overline{\beta})| = 2 + 2\kappa$. For $\beta = \overline{\beta}$, Eq. (4.8) gives $\zeta_{max}(\overline{\beta}) = 2 + 2\kappa$ for any value of ν, thus demonstrating that the point of coordinates $(\overline{\beta}, \zeta_{max}(\overline{\beta}))$ is a common point for all curves. Therefore, the intersection point of the FRF curves, and consequently the optimal parameter ν_{opt}, the optimal displacement $\zeta_{max}(\overline{\beta})$ and the corresponding frequency $\overline{\beta}$, are function of the structural parameter κ.

$$\left|\zeta_{max}\left(\bar{\beta}\right)\right| = \cfrac{1}{\sqrt{\left(\cfrac{\kappa}{1+\kappa} + \cfrac{2\cfrac{1+2\kappa}{(1+\kappa)}v^2\kappa}{1+2(1+2\kappa)v^2\kappa} - \cfrac{1+2\kappa}{2(1+\kappa)}\right)^2 + \cfrac{2\cfrac{1+2\kappa}{(1+\kappa)}v^2\kappa}{(1+\kappa)\left[1+2(1+2\kappa)v^2\kappa\right]^2}}} = 2+2\kappa, \quad (4.8)$$
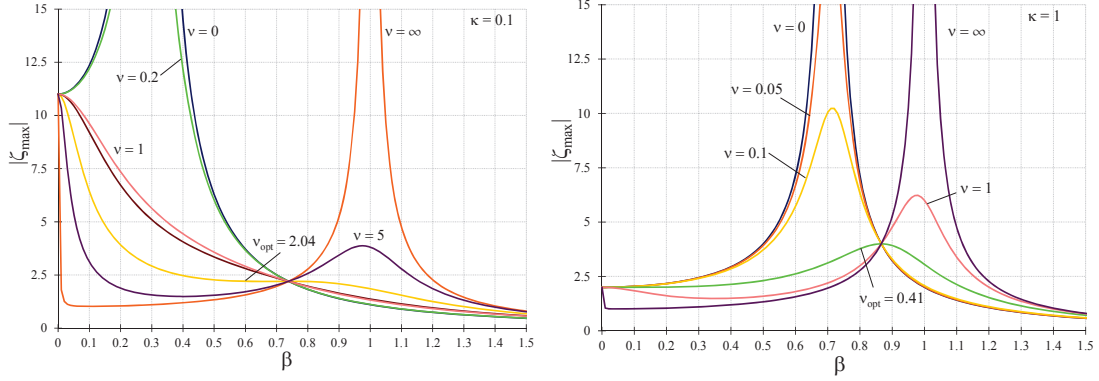
Figure 4.3 FRFs ζ_{max} for κ=1,0.1 (VD case).

For any value of v, the cases $\beta = 0$ and $\beta \to \infty$ give a maximum displacement equal to $(1+\kappa)/\kappa$ (static displacement) and zero, respectively. For $\kappa < 0.5$ and for $0 < v < \infty$, the static displacement is the largest one in the overall range of frequency, even if, for increasing β, the larger is v the faster is the system growing in complex stiffness, then reducing $\zeta_{max}(\beta)$.

Assuming that major frequency content of earthquake occurs toward $\bar{\beta}$, we can compute the value of v for which the intersection point corresponds to the local maximum of the curves, by imposing $\zeta'_{max}(\bar{\beta}) = 0$. In this way, we get the following 3rd degree equation in the unknown v^2: $8\kappa^3(1+2\kappa)^3(v^2)^3 + 4\kappa^2(1+2\kappa)^2(v^2)^2 - 2\kappa(1+2\kappa)v^2 - 1 = 0$.

The physically acceptable real solution, provided by the formula of Tartaglia-Cardano, represents the optimal value v_{opt} of the parameter v, for each assumed value of the parameter κ:

$$v_{opt} = \sqrt{\frac{1}{2\kappa(1+2\kappa)}}, \quad (4.9)$$

The brace's and device's non-dimensional displacements, and the consequent relative frame-to-brace displacement can be obtained through the following passages:

$$x_b = \frac{F_d}{k_b} = \frac{C_d^2\bar{\omega}^2 + ik_bC_d\bar{\omega}}{k_b^2 + C_d^2\bar{\omega}^2}x$$

$$\zeta_b(\tau) = \frac{x_b}{x_{g,\max}} = \frac{4\beta^2\nu^2\kappa(1+\kappa) + i2\beta\nu\sqrt{\kappa(1+\kappa)}}{1+4\beta^2\nu^2\kappa(1+\kappa)}\zeta(\tau) \qquad (4.10)$$

$$\zeta(\tau) - \zeta_b(\tau) = \frac{1 - i2\beta\nu\sqrt{\kappa(1+\kappa)}}{1+4\beta^2\nu^2\kappa(1+\kappa)}\zeta_f(\tau)$$

and their amplitudes are the moduli of the complex numbers $\zeta_{b,\max}(\beta)$ and $\zeta_{\max}(\beta) - \zeta_{b,\max}(\beta)$:

$$\left|\zeta_{b,\max}(\beta)\right| = \frac{2\beta\nu\sqrt{\kappa(1+\kappa)}}{\sqrt{1+4\beta^2\nu^2\kappa(1+\kappa)}}\left|\zeta_{\max}(\beta)\right|$$

$$\left|\zeta(\beta) - \zeta_b(\beta)\right|_{\max} = \frac{1}{\sqrt{1+4\beta^2\nu^2\kappa(1+\kappa)}}\left|\zeta_{\max}(\beta)\right|$$

$$(4.11)$$

Figure 4.4 shows the quantities $\left|\zeta_{b,\max}(\beta)\right|$ and $\left|\zeta_{\max}(\beta) - \zeta_{b,\max}(\beta)\right|$ as function of β for $\kappa = 1.0$. It is worth to notice that each of these curves has only one of the two resonance peaks of $\left|\zeta_{\max}(\beta)\right|$, since $\left|\zeta_{b,\max}(\beta)\right|$ is zero for $\nu = 0$ while $\left|\zeta_{\max}(\beta) - \zeta_{b,\max}(\beta)\right|$ is zero for $\nu \to \infty$.
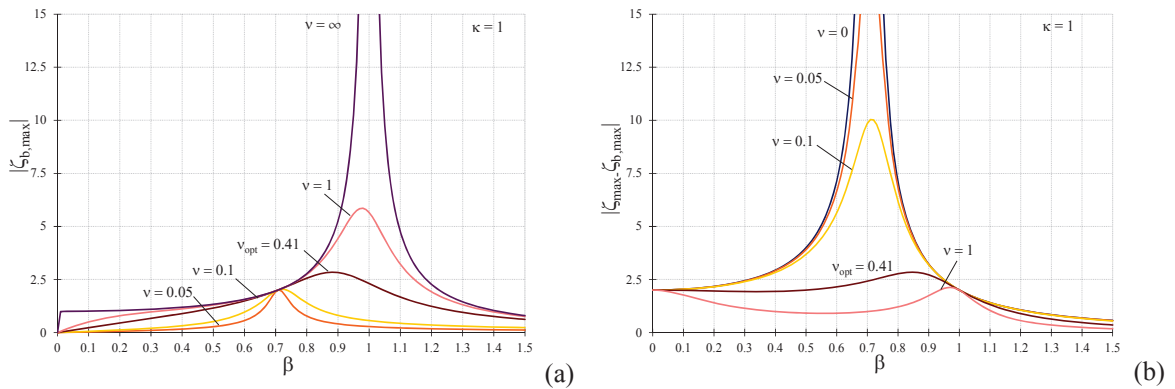
Figure 4.4 (a) FRFs $\zeta_{b,\max}$, and (b) $\left|\zeta_{\max}(\beta) - \zeta_{b,\max}(\beta)\right|$ for $\kappa = 1$ (VD case).

As far as the maximum base shear in the frame is concerned, it can be expressed as $f_{\max}(\zeta) = \overline{K}_s(\beta)\cdot\zeta_{\max}(\beta)$. In Figure 4.5 the curves $\left|f_{\max}\right|$ versus β are plotted for $\kappa = 0.1, 1$.
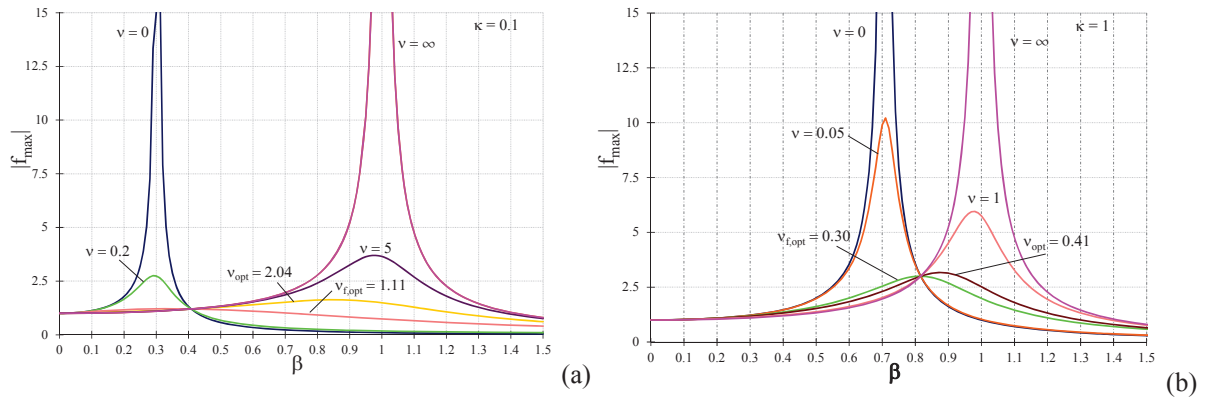
Figure 4.5 FRFs f_{max} for (a) $\kappa = 0.1$ and (b) $\kappa = 1$ (VD case).

An optimization criterion for the design of the control system is the minimization of the maximum displacement $\zeta_{max}(\beta)$ in the whole range of β, and the successive check of response in terms of base shear. This means to select the value v_{opt} given by Eq. (4.9) as design parameter.

A different criterion can provide the optimal value $v_{f,opt}$ as the one corresponding to the minimum resonance peak of the function f_{max}. The value $v_{f,opt}$, numerically determined, is always lower than v_{opt}. Results in terms of $v_{opt}(\kappa)$ and $v_{f,opt}(\kappa)$ are provided in the design spectrum of Figure 4.6(a). Higher values of damping ratios are required for small values of κ and, for a given κ, larger damping ratio is needed to optimize the frame displacement with respect to the base shear optimization. It is interesting to note that, in Figure 4.6(b), the optimum frame displacement and base shear, i.e. the minimum resonance peaks corresponding to v_{opt} and $v_{f,opt}$, increase linearly with κ.
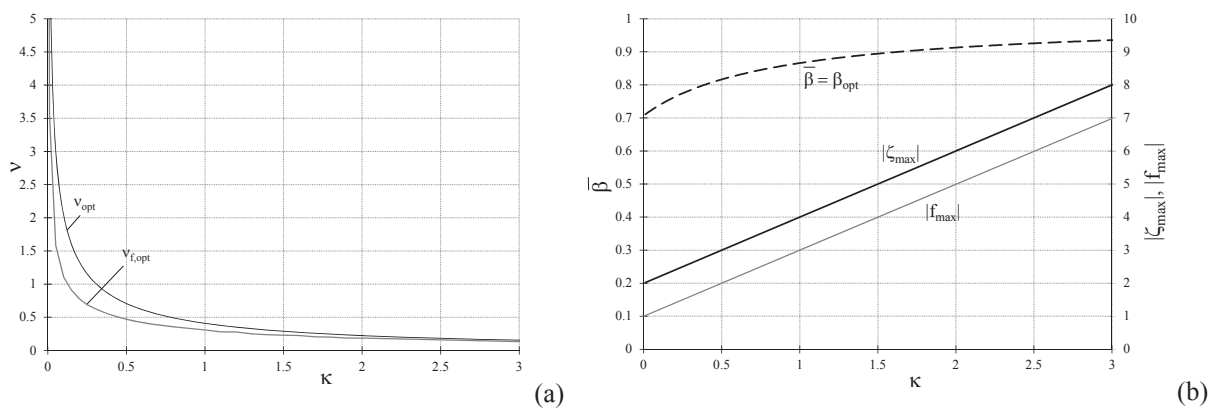
Figure 4.6 (a) VD optimal parameter and (b) story optimal displacement and optimal frequency ratio versus κ.

125

Some further considerations are made in the following in terms of normalized energy dissipated by the viscous devices. The dissipated energy during one cycle has been calculated as the area enclosed by the normalized force-displacement curve at the maximum displacement ζ_{max}:

$$\overline{E}_{VD} = \pi \cdot \frac{1}{1+\kappa} \frac{2\beta\nu\sqrt{\kappa(1+\kappa)}}{\left[1+4\beta^2\nu^2\kappa(1+\kappa)\right]} \cdot \zeta_{max}^2 \tag{4.12}$$

The optimal damping parameter ν_{opt} is practically the value corresponding to the minimum of the maximum values attained by the energy curves, whose envelope is dashed in Figure 4.7(a). For both extremely low and high values of ν (i.e. $\nu \to 0$ and $\nu \to \infty$), large peak values of ζ_{max} are reached and this produces large amounts of dissipated energy. Obviously, no energy is dissipated in the two aforementioned limit cases ($\nu = 0$ and $\nu = \infty$).

Due to the fact that each value of ζ_{max} may correspond more than one value of β (see Figure 4.3(b)), $\overline{E}_{VD}$ is not a one to one correspondence with ζ_{max}. In Figure 4.7 the trend of $\overline{E}_D$ as function of ζ_{max} (Figure 4.7(a)) and β (Figure 4.7(b)) is shown.
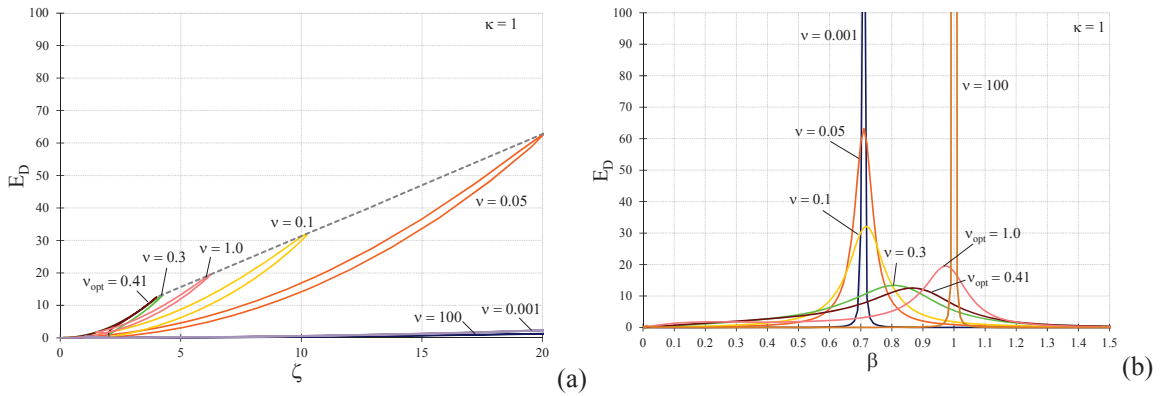
Figure 4.7 Viscous dissipated energy as function of (a) ζ_{max} and (b) β, for $\kappa = 1$.

Considering Eq. (2.17):

$$\nu_d = \frac{k_b^2 C_d \overline{\omega}}{2(k_f k_b^2 + k_f C_d^2 \overline{\omega}^2 + k_b C_d^2 \overline{\omega}^2)}$$

and substituting non-dimensional parameters, equivalent damping ratio is expressed as:

$$\nu_d = \frac{\nu\beta}{1+4\nu^2\beta^2(1+\kappa)^2} \sqrt{\frac{1+\kappa}{\kappa}}$$

It is found that, for the case $\kappa = 1$, the optimal value $\nu_{opt}(\kappa = 1)$ yields a maximum equivalent damping ratio approximately 18% of critical.

Assuming $\kappa = 0.1$, for the corresponding optimal value $v_{opt}(\kappa = 0.1)$, the maximum equivalent damping ratio would become 75% of critical, thus confirming the influence of the supporting brace stiffness on the overall damping capacity.

4.2.3   Solution of the equation of motion for the FD case

In the case of a friction damper (Figure 4.8(a)), the expression of the restoring force is $F(x, x_b, \dot{x}, \dot{x}_b, ...) = k_f x + F_d$, where $F_d = k_b \cdot x$ for $|x| < x_y$, and $F_d = F_{dy} = k_b \cdot x_y$ for $|x| > x_y$.

It results $F(x, \dot{x}, ...) = k_{eq} \cdot x$, i.e. a bilinear relationship characterized by an initial stiffness $k_f + k_b$ and a post-yielding stiffness k_f. The normalized restoring force is shown in Figure 4.8(b). It depends on two dimensionless parameters $\kappa = k_f / k_b$ and δ. The normalized initial stiffness is equal to unity while the post-elastic stiffness becomes $\kappa / (1 + \kappa)$. The parameter δ is the normalized frame displacement $x_y / x_{g,\max}$ corresponding to the achievement of yielding in the device, with a normalized frame yield strength f_y corresponding to $F_y = (k_b + k_f) \cdot x_y = F_{dy} \cdot (1 + \kappa)$.
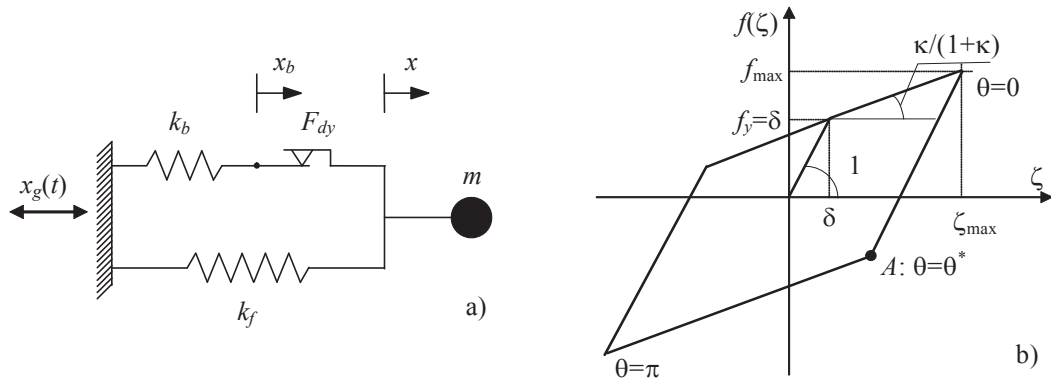
Figure 4.8 SDOF with purely friction damper: (a) rheological model, (b) $f(\zeta) - \zeta$ hysteretic cycle.

On the basis of the observations above, it is possible to state that the dynamic behavior of the simple frame equipped with elastic-perfectly plastic devices is completely defined by the following three parameters: κ, δ and β. In this case, the equation of motion (4.2) is non-linear, and a closed form solution cannot be easily derived as in the previous case. In the following, the slowly varying parameters method (Caughey 1960) is adopted. It can be

127

reasonably assumed that, under a harmonic base motion, the steady-state response is periodic with frequency β:

$$\zeta(\tau) = \zeta_{max}(\tau)\cos[\beta\tau + \phi(\tau)] = \zeta_{max}\cos\theta \qquad (4.13)$$

where ζ_{max} and ϕ are slowly varying functions of τ, and $\theta = \beta\tau + \phi(\tau)$. Differentiating Eq. (4.13) with respect to τ, one obtains that $\zeta'(\tau) = -\beta\zeta_{max}\sin\theta + \zeta'_{max}\cos\theta - \zeta_{max}\phi'\sin\theta$. For the hypothesis of the slowly varying parameters method, it is possible to approximate the values of ζ_{max} and $\phi(\tau)$ by their mean values and to assume that the velocity $\zeta'(\tau)$ is harmonic, i.e. $\zeta'_{max}\cos\theta - \zeta_{max}\phi'\sin\theta = 0$. Differentiating again the expression of $\zeta'(\tau)$ with respect to τ, one leads the expression of $\zeta''(\tau)$: $\zeta''(\tau) = -\beta^2\zeta_{max}\cos\theta - \beta\zeta'_{max}\sin\theta - \beta\zeta_{max}\phi'\cos\theta$. Substituting this latter in Eq. (4.2), leads to:

$$-\beta^2\zeta_{max}\cos\theta - \beta\zeta'_{max}\sin\theta - \beta\zeta_{max}\phi'\cos\theta + f(\zeta) = -\cos(\vartheta - \phi) \qquad (4.14)$$

We can multiply the expression of $\zeta'(\tau)$ by $\beta\cos\theta$, Eq. (4.14) by $\sin\theta$, subtract them and make the average over one cycle of θ, thus obtaining:

$$-\beta\zeta'_{max} + \frac{1}{2\pi}\int_0^{2\pi} f(\zeta)\sin\theta d\theta = -\frac{1}{2}\sin\phi \qquad (4.15)$$

Now, multiplying Eq. (4.14) by $\beta\sin\theta$, Eq. (4.15) by $\cos\theta$, adding them and averaging over one cycle of θ, one obtains:

$$-\beta\zeta_{max}\phi' - \frac{\beta^2}{2}\zeta_{max} + \int_0^{2\pi} f(\zeta)\cos\theta d\theta = -\frac{1}{2}\cos\phi \qquad (4.16)$$

If the quantities $S(\zeta_{max}) = \frac{1}{\pi}\int_0^{2\pi} f(\zeta)\sin\theta d\theta$ and $C(\zeta_{max}) = \frac{1}{\pi}\int_0^{2\pi} f(\zeta)\cos\theta d\theta$ are defined, Eqs. (4.15) and (4.16) become:

$$\begin{aligned} -2\beta\zeta'_{max} + S(\zeta_{max}) &= -\sin\phi \\ -2\beta\zeta_{max}\phi' - \beta^2\zeta_{max} + C(\zeta_{max}) &= -\cos\phi \end{aligned} \qquad (4.17)$$

Using Figure 4.8(b), if $\theta* = \cos^{-1}\left(1 - \frac{2\delta}{\zeta_{max}}\right)$, the quantities $S(\zeta_{max})$ and $C(\zeta_{max})$ may be readily evaluated:

$$\begin{cases} S(\zeta_{max}) = -\dfrac{1}{1+\kappa}\dfrac{\zeta_{max}}{\pi}\sin^2\theta* & if \quad \zeta_{max} > \delta \\[3mm] S(\zeta_{max}) = 0 & if \quad \zeta_{max} \le \delta \end{cases}$$

(4.18)

$$\begin{cases} C(\zeta_{max}) = \dfrac{\zeta_{max}}{\pi}\left[\dfrac{1}{1+\kappa}\theta* + \dfrac{\kappa\pi}{1+\kappa} - \dfrac{1}{2(1+\kappa)}\sin 2\theta*\right] & if \quad \zeta_{max} > \delta \\[3mm] C(\zeta_{max}) = \zeta_{max} & if \quad \zeta_{max} \le \delta \end{cases}$$

(4.19)

The steady state response, in terms of displacement and phase angle *vs* frequency, is obtained from Eq. (4.17) by setting $\zeta'_{max}(\tau)$ and $\phi'(\tau)$ equal to zero, and by eliminating ϕ and β^2:

$$\left[C(\zeta_{max}) - \beta^2\zeta_{max}\right]^2 + \left[S(\zeta_{max})\right]^2 = 1$$

(4.20)

$$\tan\phi = \dfrac{S(\zeta_{max})}{C(\zeta_{max}) - \beta^2\zeta_{max}}$$

(4.21)

Differently from the VD case, now it is more convenient to express the quantity ζ_{max} implicitly as a function of β from Eq. (4.20):

$$\beta^2 = \left[\zeta_{max}C(\zeta_{max}) \pm \sqrt{-\zeta_{max}^2 S^2(\zeta_{max}) + \zeta_{max}^2}\right]\Big/\zeta_{max}^2$$

(4.22)

The maximum floor displacement ζ_{max} is attained at the point where β^2 has a double root, that is, for the value $\tilde{\zeta}_{max} > \delta$ which makes void the radical quantity in Eq. (4.22), thus satisfying the equation:

$$S^2(\tilde{\zeta}_{max}) = 1$$

(4.23)

and the corresponding frequency is $\tilde{\beta} = \sqrt{C(\tilde{\zeta}_{max})/\tilde{\zeta}_{max}}$.

The limit cases ($\delta = 0$ and $\delta \to +\infty$) again correspond, respectively, to the case of one spring (k_f) or two springs connected in parallel (k_f and k_b), and are expressed as $\beta(\zeta_{max})$:

$$\bullet \; \delta = 0 \quad \Rightarrow \quad F_{dy} = 0 \quad \Rightarrow \quad \beta^2 = \dfrac{\zeta_{max}\dfrac{\kappa}{1+\kappa} \pm 1}{\zeta_{max}};$$

$$\beta_{resonance} = \sqrt{\dfrac{\kappa}{(1+\kappa)}}$$

• $\delta \to +\infty$ $\quad \Rightarrow \quad$ $F_{dy} \to +\infty$ $\Rightarrow$ $\quad \beta^2 = \dfrac{\zeta_{max} \pm 1}{\zeta_{max}}$

$$\beta_{resonance} = 1$$

The function $\beta^2(\zeta_{max})$ in Eq. (4.22) is a continuous function whose derivative is discontinuous when $\zeta_{max} = \delta$, being the response linear for any value of $\zeta_{max} < \delta$. The quantity ζ_{max} as a function of β is plotted in Figure 4.9 for $\kappa = 0.1$, 1.0 ($k_b = 10k_f, k_f$) and for several different values of δ: the point of coordinates $\overline{\beta} = \sqrt{(1+2\kappa)/[2(1+\kappa)]}$ and $\zeta_{max}(\overline{\beta}) = 2 + 2\kappa$ still represents the intersection of the two limit cases but does not belong to all other curves. One notes that a very low value of δ produces a peak of the curve near to the one relative to $\delta = 0$, and its value decreases as far as the previous parameter increases; however, a further increase of the yield displacement induces a shift of the resonance frequency toward the value $\beta = 1$ with an increment of the peak amplitude. Therefore, the resonance peak within the range $\delta = [0, +\infty]$ has a minimum value in correspondence of the frequency β_{opt}, equal to $\overline{\beta}$ relative to the intersection point between the limit curves: the value δ_{opt} is defined as the one corresponding to the curve $\zeta_{max}(\beta)$ having the minimum resonance peak, settled a certain κ.
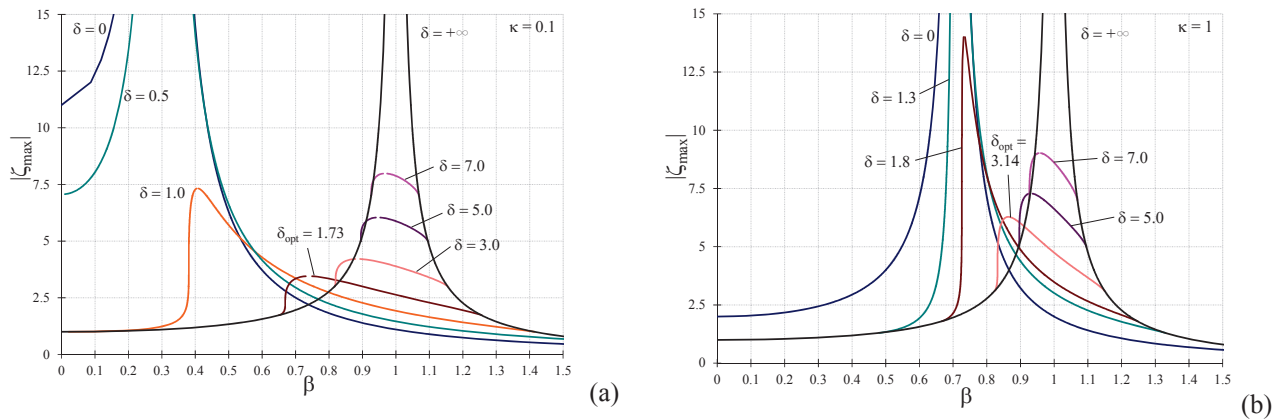
Figure 4.9 FRFs ζ_{max} **for (a)** $\kappa = 0.1$ **and (b)** $\kappa = 1$ **(FD case).**

Brace displacements are trivial: there is no relative displacement respect to the frame up to the yielding point δ, while after that the brace does not move anymore and the relative displacement is $\zeta_{max}(\beta) - \delta$ (Figure 4.10).
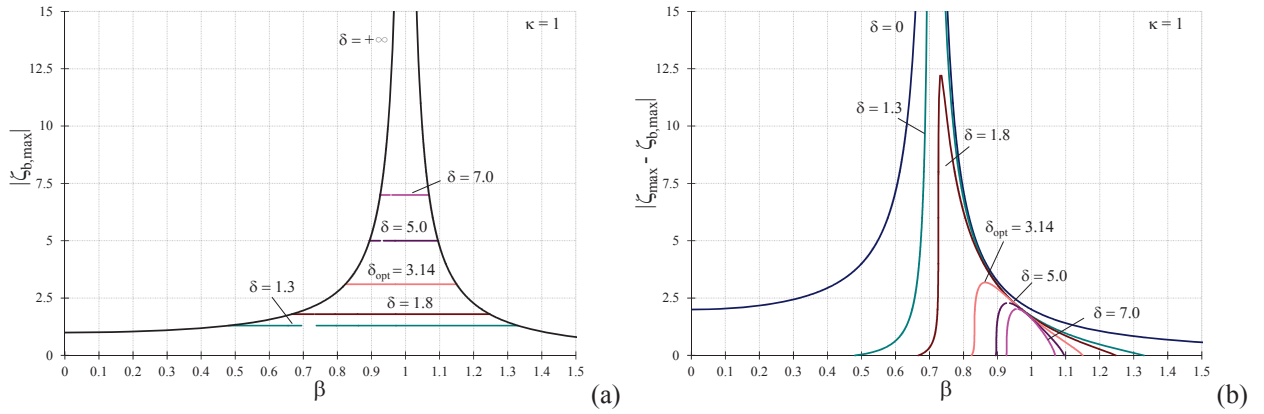
Figure 4.10 (a) FRFs $\zeta_{b,max}$ and (b) $\left|\zeta_{f,max}(\beta) - \zeta_{b,max}(\beta)\right|$ for $\kappa=1$ (FD case).

In order to get the maximum base shear, simple expressions are introduced. When $\zeta_{max} > \delta$, the maximum force assumes the expression $f_{max} = \delta + (\zeta_{max} - \delta) \cdot \dfrac{k}{1+k}$, while $f_{max} = \zeta_{max}$ for $\zeta_{max} < \delta$.

In Figure 4.11 the curves $\left|f_{max}\right|$ versus β are plotted for $\kappa = 0.1, 1$. It can be noted that, for low values of κ, maximum base shear is almost equal to δ.
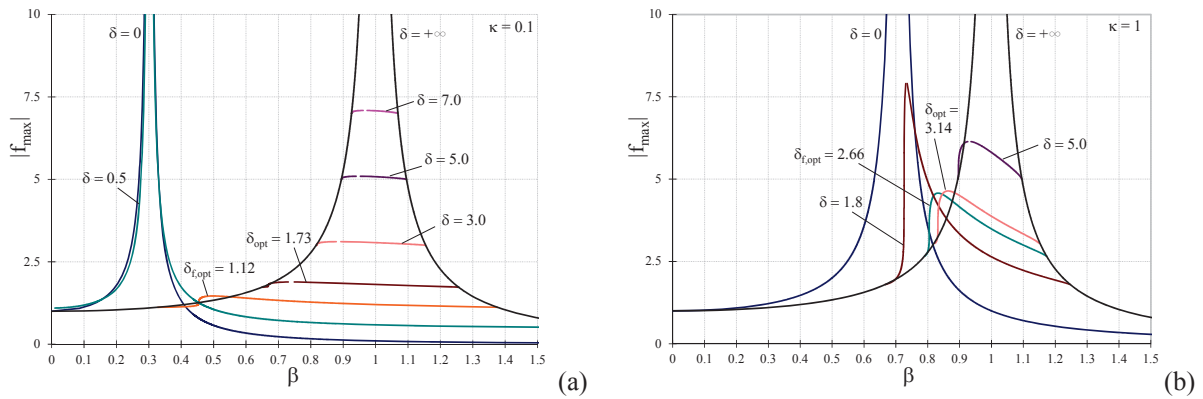
Figure 4.11 FRFs f_{max} for (a) $\kappa = 0.1$ and (b) $\kappa = 1$ (FD case).

Both parameters corresponding to minimum frame displacement and base shear in the overall range of frequency, namely respectively $\delta_{opt}(\kappa)$ and $\delta_{f,opt}(\kappa)$, have been numerically determined: a design spectrum is plotted in Figure 4.12(a). In Fig. Figure 4.12(b), the quantities $\zeta_{max}(\delta_{opt})$, $f_{max}(\delta_{f,opt})$ and $\beta_{opt} = \overline{\beta}$ are plotted versus κ.

131
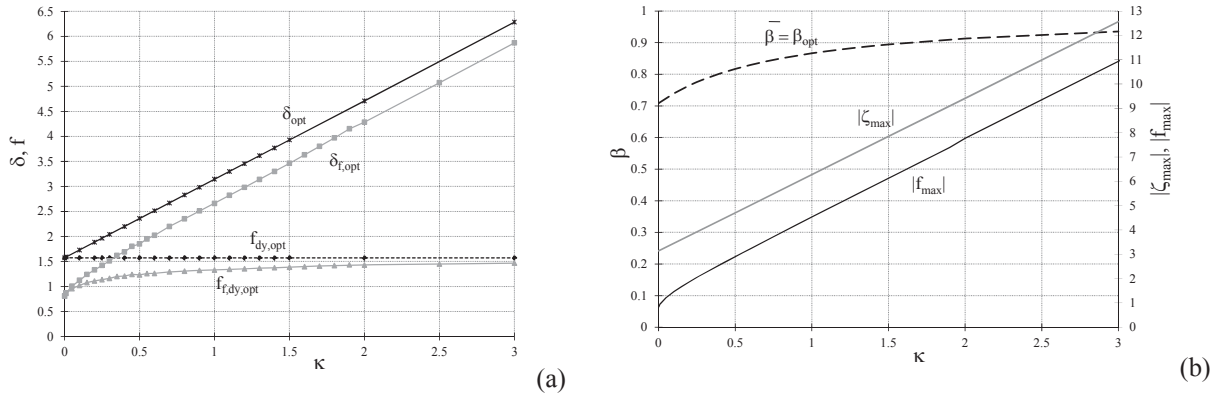
Figure 4.12 (a) FD optimal parameter versus κ, (b) story optimal displacement and optimal frequency ratio versus κ.

From Figure 4.12 it is clear that, as far as κ increases, both optimal parameters and maximum response increase too.

As in the VD case, the quantities $\zeta_{max}(\delta_{opt})$ and $f_{max}(\delta_{f,opt})$ linearly increase with κ, and the value of the optimal parameter corresponding to minimum base shear is always lower than the one corresponding to minimum story drift. It also appears that the optimal sliding force in the device is lightly varying with κ, being practically constant when the frame displacement is minimized ($f_{dy,opt} = \dfrac{f_{d,opt}}{1+k} = \dfrac{\delta_{opt}}{1+k}$ for minimum displacement; $f_{f,dy,opt} = \dfrac{f_{f,d,opt}}{1+k} = \dfrac{\delta_{f,opt}}{1+k}$ for minimum base shear).

Energy dissipated by yielding dampers can be calculated as:

$$\overline{E}_{FD} = 4 \cdot \delta \cdot (\zeta_{max} - \delta) \cdot \frac{1}{1+k} \tag{4.24}$$

As in the VD case, the optimal damping parameter δ_{opt} corresponds to the minimum of the maximum values attained by Eq. 4.24 (dashed line in Figure 4.13(a)) and remarkable dissipated energy corresponds to both extremely low and high values of δ. In Figure 4.13, the trend of $\overline{E}_{FD}$ is shown as function of ζ_{max} (Figure 4.13(a)), with a minimum value on the *x* axis equal to δ, and as function of β (Figure 4.13(b)).

132
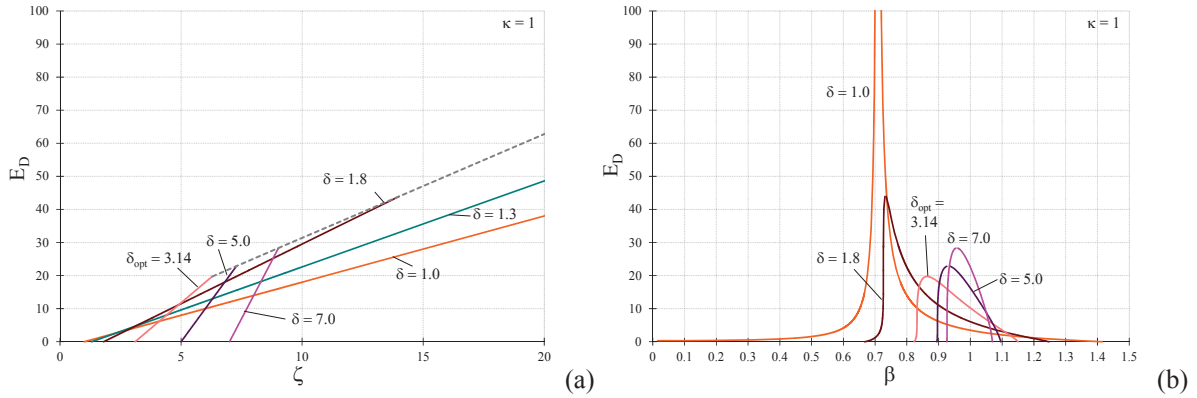
Figure 4.13 Friction dissipated energy as function of (a) ζ_{max} and (b) β, for $\kappa = 1$.

By adapting the general formula

$$v_d = \frac{E_d}{4\pi E_s}$$

to the adimensionalized form of force-displacement relationship, equivalent damping ratio becomes:

$$v_d = \frac{2\delta(\zeta_{max} - \delta)}{(1+\kappa)\pi\left[\delta + \frac{\kappa}{1+\kappa}(\zeta_{max} - \delta)\right]\zeta_{max}}$$

It is found that, for the case $\kappa = 1$, the optimal value $\delta_{opt}(\kappa = 1)$ yields a maximum equivalent damping ratio approximately 22% of critical.

Assuming $\kappa = 0.1$, for the corresponding optimal value $\delta_{opt}(\kappa = 0.1)$, the maximum equivalent damping ratio would increase to 53% of critical, thanks to beneficial effect of stiffer supporting brace.

4.3   Numerical validation of proposed design procedure

The design procedure proposed in the previous paragraphs has been verified through a numerical investigation performed on a steel frame (of $l = 5$ m span and $h = 3$ m height), having a I-shaped columns' cross section (European HEM 300) and a 25 tons mass, assumed as representative of a retrofitting design problem. Depending on the stiffness of the transversal beam, the period of the bare frame T_b varies in the range 0.09÷0.18 s, where the boundary values correspond to a shear type frame and a cantilevered columns frame, respectively. Both the latter frame configurations are considered, having lateral stiffness $k_f = 2 \cdot \frac{12EI}{h^3} = 93333$ kN/m and

133

$k_f = 2 \cdot \dfrac{3EI}{h^3} = 23333$ kN/m, respectively. A diagonal brace, with slope $\varepsilon = arctg(\dfrac{h}{l})$ and lateral stiffness k_b, is inserted to support the damping device (viscous or friction damper), so that the parameter κ is immediately defined. The equation of motion has been solved by implementing the Newton-Raphson integration method (Chopra 2011) in Matlab® environment (Mathworks 2010). In order to improve the accuracy of results, the time step has been set equal to 0.0001s and the parameters γ and β to 1/2 and 1/6, respectively.

To be representative of an actual design problem, the input at the base has been defined by means of ground motion records instead of harmonic excitation. For the latter case, numerical results have been verified to be in perfect agreement with the analytical ones, both in the VD and FD case. According to the Italian building code (NTC 2008), the design spectra (Figure 4.14Figure 4.12) with 5% of critical damping have been defined for the life safety limit state (SLV) of a conventional building (functional class II) located in L'Aquila, Italy (13.37° longitude, 42.37° latitude) on soil type B (360≤Vs,30≤800 m/s) with a nominal life of 50 years, corresponding to a return period of 475 years, and providing a Peak Ground Acceleration equal to 0.35 g. A set of seven unscaled accelerograms matching the reference spectrum (Figure 4.14, Table 4.1) was found in the European ground motion database using Rexel v3.4 beta (Iervolino et al 2010). The average spectrum has 10% lower and 30% upper tolerance in the period range 0.15-2 s. Peak Ground Displacements reported in Table 1 have been obtained by numerical integration of acceleration time histories in Seismosignal, with the constraint of velocities oscillating around zero after the end of the strong shaking (Seismosoft 2013).
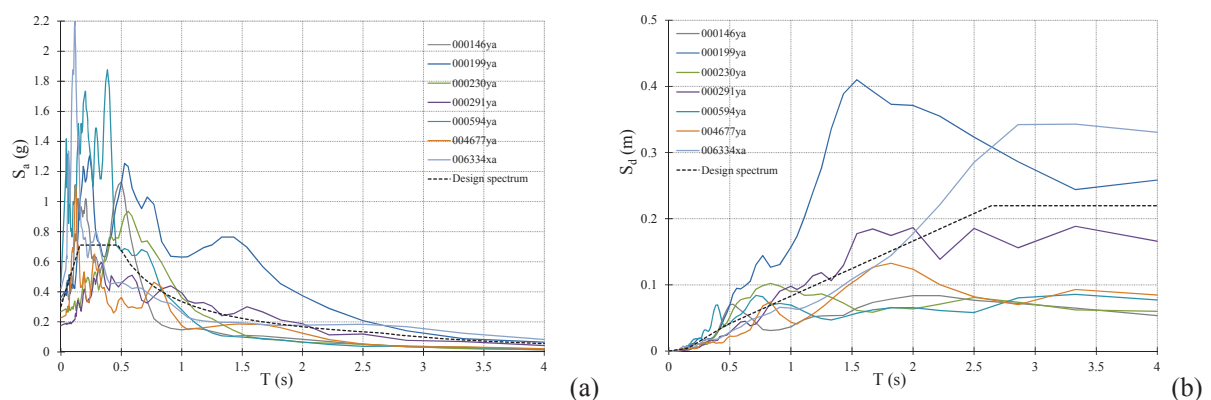
Figure 4.14 (a) Code provided (ν =5%) and selected ground motion acceleration and (b) displacement spectra.

Table 4.1 Selected spectrum-compatible accelerograms for site class B (as = aftershock).

Waveform ID	Earthquake ID	Station ID	Earthquake Name	M_w	Epicentral Distance [km]	PGA [m/s²]	PGV [m/s]	PGD [m]
6334	2142	ST2488	South Iceland (as)	6.4	11	4.12	0.97	1.47
146	65	ST24	Friuli (as)	6	14	3.30	0.23	0.35
291	146	ST276	Campano Lucano	6.9	16	1.72	0.27	0.73
230	108	ST73	Montenegro (as)	6.2	8	2.62	0.27	0.38
4677	1635	ST2562	South Iceland	6.5	21	2.23	0.21	0.82
594	286	ST60	Umbria Marche	6	11	4.54	0.29	0.33
199	93	ST67	Montenegro	6.9	16	3.56	0.42	1.49
mean:				6.4	13.9	3.16	0.38	0.80

The response of the frame including VD and FD systems has been evaluated under the above mentioned ground motions characterized by different frequency content, to numerically determine the optimal values of the parameters ν and δ, and compare them with those obtained from the analytical approach presented in the previous paragraph. The numerical investigation has been repeated for two different values of κ (0.25 and 1) and for the aforementioned values of k_f (93333 kN/m and 23333 kN/m), corresponding to the following dynamic properties in case of rigid frame-to-brace connection (limit case $\nu \to \infty$ or $\delta \to \infty$ - Table 4.2):

Table 4.2 Frame dynamic properties for rigid frame-to-brace connection.

k_f [kN/m]	κ [-]	k_b [kN/m]	T [s]	ω_b [rad/s]	f_b [hz]
23333	**1.00**	23333	0.15	43.20	6.88
23333	**0.25**	93333	0.09	68.31	10.88
93333	**1.00**	93333	0.07	86.41	13.76
93333	**0.25**	373333	0.05	136.63	21.76

The frequency $\omega_b = \sqrt{\dfrac{k_f + k_b}{m}}$ and the corresponding normalized frequency β at resonance is equal to 1.

A parametric investigation has been performed for each ground motion and for each value of κ, by assigning extremely different values to both ν (200 logarithmically spaced values between 10^{-3} and 10^5) and δ (200 logarithmically spaced values between 10^{-6} and 100): the maximum response values have been computed for each time history case. As suggested by current seismic codes in case of selection of seven records (1998-1 EN 2004), structural response is defined in terms of average values of both maximum displacements (frame displacement x, displacement of the elastic brace x_b, relative displacement x-x_b) and forces (base shear force V, axial force N produced by the brace). The numerical optimum parameter ($\overline{\nu}_{opt}$ or $\overline{\delta}_{opt}$) is the value corresponding to the minimum averaged structural response, for any given κ. The following figures summarize some relevant results of the numerical analysis performed on the case study for both control systems: the normalized average maximum response (frame displacement d, displacement of the elastic brace b, relative displacement r, base shear force v, axial force n) is plotted versus the value of the damping parameter in a semi-logarithmic scale. Time history analysis allowed also to determine the effect of the dissipative diagonal braces, having slope ε and lateral stiffness k_b, in terms of additional axial force in the columns. For a given stiffness k_b of the diagonal brace, the increase of the damping parameter from zero to infinite is always detrimental: the axial force goes from zero in case of no brace-frame coupling ($\nu_i = 0$ or $\delta = 0$), to a maximum value resulted in case of complete coupling ($\nu_i \rightarrow \infty$ or $\delta \rightarrow \infty$). In addition to this, being axial force proportional to brace displacement, normalized functions N and x_b are practically overlapping. On the other hand, a limitation in the use of bracing systems is also related to detrimental effects on the foundation both in terms of incremental base shear and axial force. This problem is a main drawback for all conventional bracing systems but must be taken into account also in case of dissipative braces that, generally speaking, provide both damping and stiffness.

4.3.1 VD case

In the VD case, the structural model is defined as a two DOFs system (x, x_b - see § 4.2.2), where the only dynamic DOF is associated to the floor displacement. The equation of motion has been formulated as follows:

$$\mathbf{M} \cdot \ddot{\mathbf{x}} + \mathbf{C} \cdot \dot{\mathbf{x}} + \mathbf{K} \cdot \mathbf{x} = -\ddot{x}_g \mathbf{M} \cdot \mathbf{l}$$

where $\mathbf{x}^T = \begin{bmatrix} x & x_b \end{bmatrix}$, $\dot{\mathbf{x}}^T = \begin{bmatrix} \dot{x} & \dot{x}_b \end{bmatrix}$, $\ddot{\mathbf{x}}^T = \begin{bmatrix} \ddot{x} & \ddot{x}_b \end{bmatrix}$, $\mathbf{M} = \begin{bmatrix} m & 0 \\ 0 & 0 \end{bmatrix}$, $\mathbf{K} = \begin{bmatrix} k_f & 0 \\ 0 & k_b \end{bmatrix}$, $\mathbf{C} = \begin{bmatrix} c & -c \\ -c & c \end{bmatrix}$,

$\mathbf{I} = \begin{bmatrix} 1 \\ 1 \end{bmatrix}$ and $\ddot{x}_g$ is the base acceleration.

Figure 4.15 and Figure 4.16 show the normalized average of the peak response values under the seven records, for several values of v. In the same figures, the grey vertical straight line indicates the optimal value for the minimization of the story drift, ($v_{opt} = 2.04$ for $\kappa = 0.25$, $v_{opt} = 0.41$ for $\kappa = 1$), while the black one indicates the optimal value for the minimization of the base shear ($v_{opt} = 0.69$ for $\kappa = 0.25$, $v_{opt} = 0.30$ for $\kappa = 1$), both determined from the theoretical treatment. (Figure 4.6 (a))
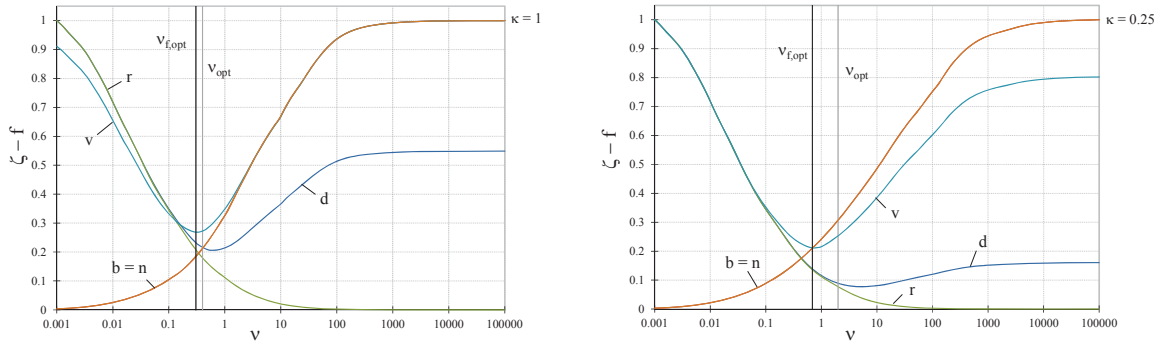
Figure 4.15 VD case: numerical results for k_f=23333 kN/m.
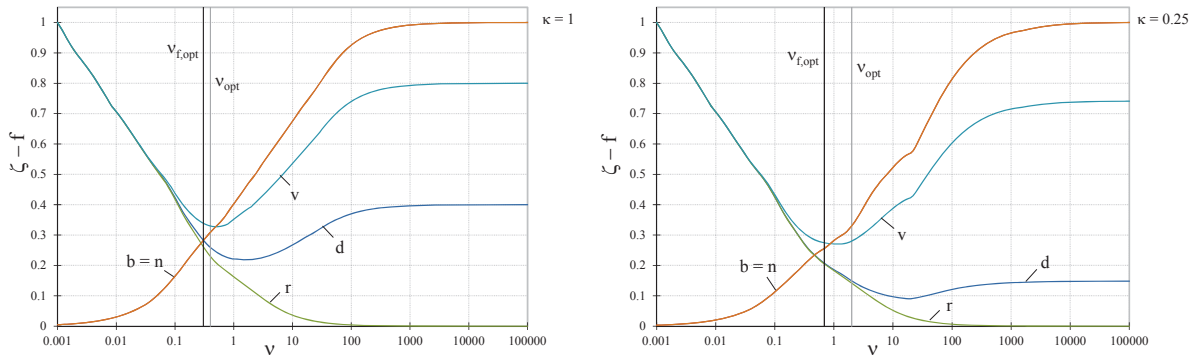
Figure 4.16 VD case: numerical results for k_f=93333 kN/m.

As expected, in all the analyzed cases, the response in terms of story drift and base shear shows a minimum value. The minimum frame displacement ζ_{min} occurs for a value of v larger than v_{opt}, and is , for low values of κ, close to the value of ζ corresponding to the limit case $v \to \infty$ (rigid frame-to-brace connection). The maximum displacement $\zeta(v_{opt})$ is strongly reduced with respect to the undamped case ($v = 0$).

137

However, it is worth to note that the minimum base shear V_{min} occurs for a value practically equal to $v_{f,opt}$. Higher values of v would be responsible for a worse condition due to a higher additional force transmitted by the damping brace.

For the considered cases, the value v_{opt} represents a good compromise which allows to optimize at the same time both the frame displacement and the base shear, with a limited effect in terms of additional axial stress in the columns, about 20 to 30 % of the force that would arise in case of rigid frame to brace connection. Differently from the present one, most common optimization procedures are based on the dimensioning of viscous dampers once a threshold equivalent damping ratio has been set.

4.3.2   FD case

In the FD case, the structural model is defined as a bilinear single DOF system (see § 4.2.3). Figure 4.17 and Figure 4.18 show the average frame response under the applied earthquake records for different values of δ. In the same figures, vertical straight lines indicate the theoretically determined optimal value for the minimization of the story drift (grey line at δ_{opt} =1.97 for κ=0.25 , δ_{opt} = 3.14 for κ= 1), and the base shear (black line at $\delta_{f,opt}$ = 1.42 for κ=0.25 , $\delta_{f,opt}$ = 2.66 for κ= 1).
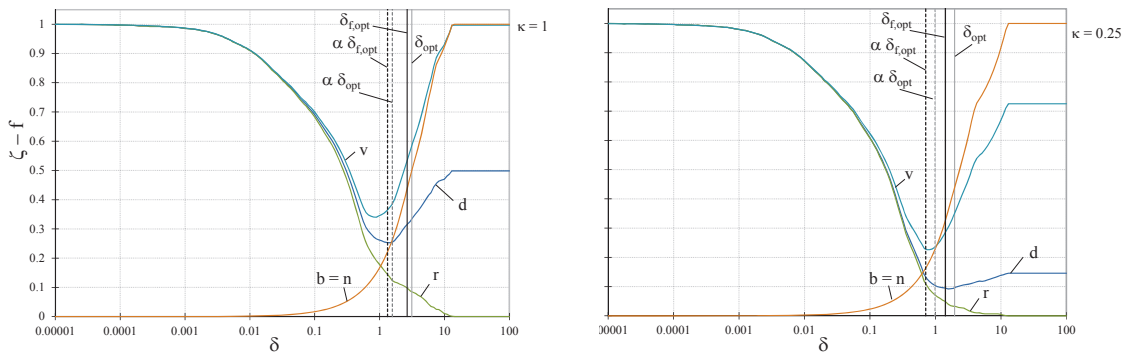
Figure 4.17 FD case: numerical results for k_f=23333 kN/m.
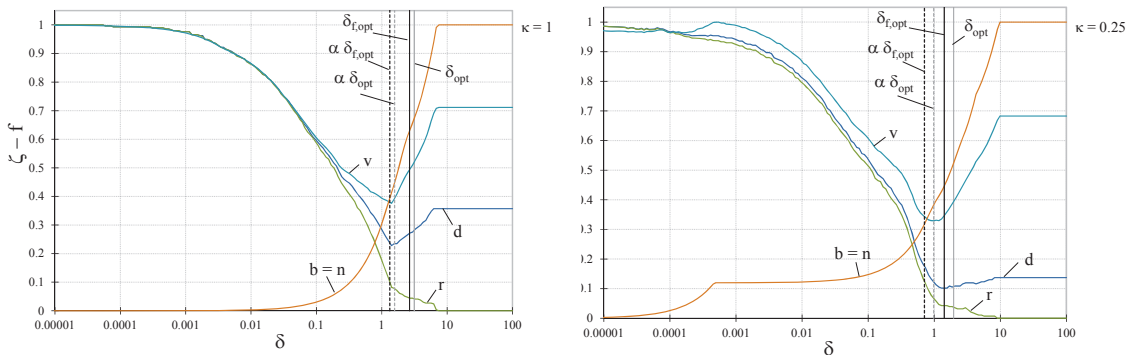
Figure 4.18 FD case: numerical results for k_f=93333 kN/m.

138

As in the VD case, the minimum frame displacement is in between the two boundary conditions, and for low values of κ is almost equal to the rigid frame-to-brace connection scheme. The base shear shows a clear minimum too, for a value of δ that is lower than numerical one. Optimum response corresponds to an acceptable increase of axial force in the columns (from 20 to 40% of the rigid connection case). Even if theoretically suggested values δ_{opt} and $\delta_{f,opt}$ are beneficial with respect to both limit cases ($\delta = 0$, $\delta \to \infty$), they are higher than the numerical optimum. A corrective factor α, able to tune the theoretical response to the effective one, can be introduced with the aim of reducing theoretical optimal values, so providing corrected values $\alpha \cdot \delta_{opt}$ and $\alpha \cdot \delta_{f,opt}$. The role of the parameter α can be seen in terms of providing an "equivalent" maximum ground acceleration $\alpha \cdot a_{g,max}$ with respect to the harmonic base motion. It is well known that, during a seismic event, the maximum acceleration $a_{g,max}$ just occurs at a certain instant, as a single pulse instead of harmonic excitation, not allowing the device to reach a steady state response condition. A value of $\alpha = 0.5$ is proved to be suitable for this task, as shown by dashed vertical grey (at $0.5 \cdot \delta_{opt}$) and black lines (at $0.5 \cdot \delta_{f,opt}$) in the above Figure 4.17 and Figure 4.18. In particular, the tuned value $0.5\delta_{opt}$ is able to significantly reduce both frame displacement and base shear and is deemed a satisfactory design value.

In a FD system, it has been also verified what is the effect on structural response of the equivalent viscous damping due to bare frame and non-structural components: to this aim, the model of Figure 4.8(a) has been provided with a viscous dashpot acting in parallel with the spring elements. The equivalent viscous damping ratio is defined as $\nu = \dfrac{C_d}{2\sqrt{m \cdot k_f}}$. Values of ν = 2% and ν = 5% strongly reduce the response in case of elastic behavior ($\delta = 0$ or $\delta \to \infty$) while, in case of significant yielding in the damper, maximum displacements and base shear are mainly dependent on hysteretic dissipation (Figure 4.19).
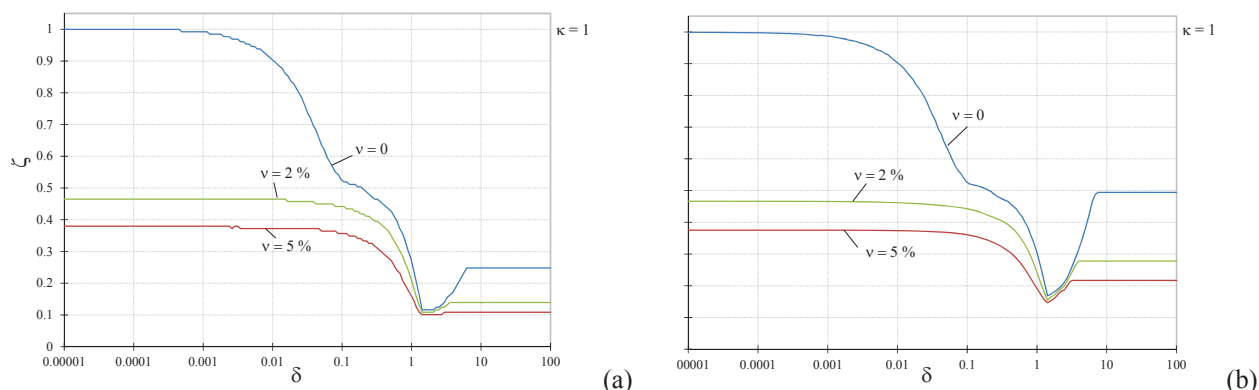
Figure 4.19 Numerical results with additional viscous damping of (a) 2% and (b) 5% (k_f = 93333 kN/m), for record 6334 xa.

The obtained optimal damping parameters could be compared with those computed by applying a design method presented in (Christopoulos and Filiatrault 2006). In order to obtain the minimum resonant amplitude, Christopoulos et Filiatrault suggested the following lateral load required to activate the damper: $F_{dy} = \pi \cdot a_g \cdot W / (2 \cdot g)$. This closed-form expression, where W is the weight of the structure, has been derived from a FRF analysis and is not dependent on the relative brace to frame stiffness, since the elastic supporting brace was assumed to be rigid. The application of the above expression to the case study considered in the proposed case would provide a yielding force of 136 kN. Such a value overestimates the effective optimal values determined through the above described procedure (Table 4.3) for the value $\bar{\delta}_{opt} = \alpha \cdot \delta_{opt}$.

Table 4.3 Optimal sliding force from proposed design procedure.

k_f [kN/m]	κ [-]	k_b [kN/m]	δ_{opt}	α	F_Y [kN]	F_{dy} [kN]
23333	1.00	23333	3.14	50%	133	67
23333	0.25	93333	1.97	50%	84	67
93333	1.00	93333	3.14	50%	133	67
93333	0.25	373332	1.97	50%	84	67

As obtained theoretically, it has been proved that the optimal yielding force F_{dy} does not depend on κ.

4.4   Effective design procedure

The proposed operative design procedure is schematically summarized in the following flowchart of Figure 4.20. It is especially effective joining results of both theoretical treatment and numerical validation.
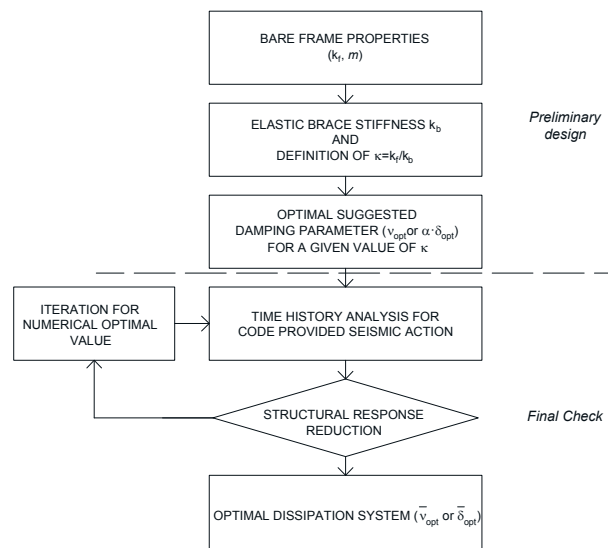
Figure 4.20 Flowchart of the suggested design procedure.

Given the bare frame properties, the stiffness of the elastic brace k_b is defined taking into account that the higher is the relative brace to frame stiffness, the more effective is the control system. A starting value of the damping parameter is assumed equal to v_{opt} or $\alpha \cdot \delta_{opt}$, where v_{opt} and δ_{opt} are the analytical results taken from Figure 4.6(a) or Figure 4.12(a), respectively, and $\alpha = 0,5$. Time history analysis are then performed under the code provided seismic action at ultimate limit state. Then, the response reduction level is checked, by verifying if the assumption of the values v_{opt} or $\alpha \cdot \delta_{opt}$ corresponding to a specific κ is able to produce an acceptable response reduction in terms of frame displacement and base shear, with an allowable level of column axial force. If the result is not satisfactory, a modification of the damping parameter can be made in order to get an improvement in the achievement of the desired response reduction level. Some iterations could be needed to define the effective optimal values ($\bar{v}_{opt}$ or $\bar{\delta}_{opt}$), because the latters depend on both the properties of the ground motion and of the structural system. At the end of the procedure, when the optimal damping parameters $\bar{v}_{opt}$ or $\bar{\delta}_{opt}$ have been determined, if a certain response reduction target level is not fulfilled, a different solution can be pursued varying the brace stiffness k_b, so reducing κ, in order to get a higher efficiency of the passive control system. Actually, real strong motion properties (magnitude, duration, frequency content, etc.) may play an important role in the determination of the effective design optimal value.

The next goal of the topic is to develop the current optimization procedure for a multi-degree-of-freedom (MDOF) system. A case study MDOF system could be a *n*-story elastic frame with lateral story stiffness k_f, equipped with *n* equivalent dissipative braces. The latters are obtained by connecting in series an elastic component of lateral stiffness k_b to a viscous (C_d) or friction damper (F_y). The analytical treatment presented in this work could be simply extended to a MDOF system, for both VD and FD cases, by adopting matrix instead of scalar quantities. Of course, the design objective would still represent the value of the optimal parameter able to yield a minimum response of the structure.

4.5 Design example

A design example is proposed to further validate the object of the Chapter. In this case, the simple frame (of $l = 5$ m span and $h = 3$ m height) has square cross section 40x40 cm with 25 tons mass. Assuming a shear type model, lateral stiffness k_f is equal to 56889 kN/m. The ratio κ is fixed equal to 0.5, thus providing a diagonal brace (inclined by ε) with horizontal stiffness $k_b = 2 \cdot k_f$.

According to the Italian building code (NTC 2008), the design spectra (Figure 4.21) with 5% of critical damping have been defined for the collapse prevention limit state (SLC) of an important building (functional class III) located in Napoli, Italy (14.19° longitude, 40.83° latitude) on soil type B ($360 \leq V_{s,30} \leq 800$ m/s) with a nominal life of 100 years, corresponding to a return period of 2475 years, providing a Peak Ground Acceleration equal to 0,31 g. An ensemble of seven unscaled accelerograms matching the reference spectrum (Figure 4.21, Table 4.4) was found in the European ground motion database using Rexel v3.4 beta (Iervolino et al 2010). The average spectrum has 10% lower and 30% upper tolerance in the period range 0.15-2 s.
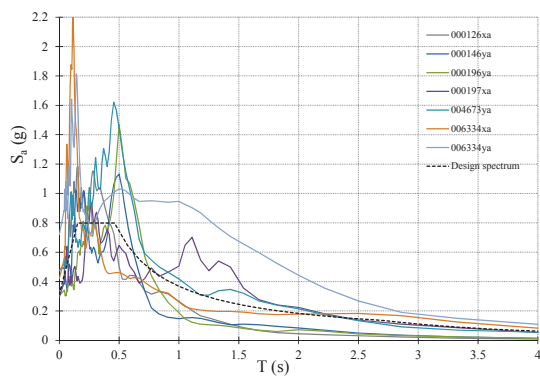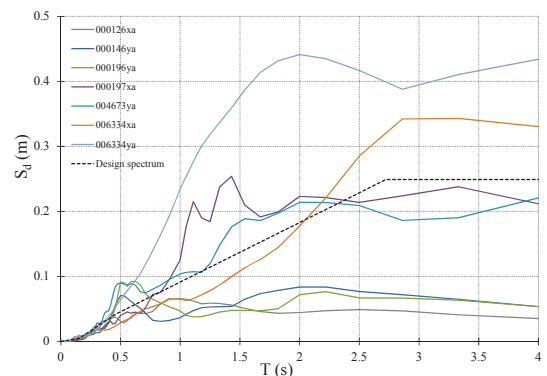
(a)   (b)

Figure 4.21 (a) Code provided (v =5%) and selected ground motion acceleration and (b) displacement spectra – Case study.

Table 4.4 Selected spectrum-compatible accelerograms for site class B (as = aftershock) – Case study.

Waveform ID	Earthquake ID	Station ID	Earthquake Name	Mw	Epicentral Distance [km]	PGA [m/s^2]	PGV [m/s]	PGD [m]
6334	2142	ST2488	South Iceland (as)	6.4	11	4.10	0.38	0.022
146	65	ST24	Friuli (as)	6	14	3.30	0.23	0.039
126	63	ST35	Friuli (as)	6	21	4.96	0.22	0.033
197	93	ST63	Montenegro	6.9	24	2.88	0.39	0.102
196	93	ST62	Montenegro	6.9	25	3.00	0.25	0.100
4673	1635	ST2482	South Iceland	6.5	15	4.12	0.38	0.149
6334	2142	ST2488	South Iceland (as)	6.4	11	4.63	0.51	0.230
mean:				6.4	17.3	3.86	0.34	0.10

Seven time history analysis have been run for both VD and FD protection systems: normalized average of maximum results are then plotted in Figure 4.22 as function of the damping parameter (v or δ).
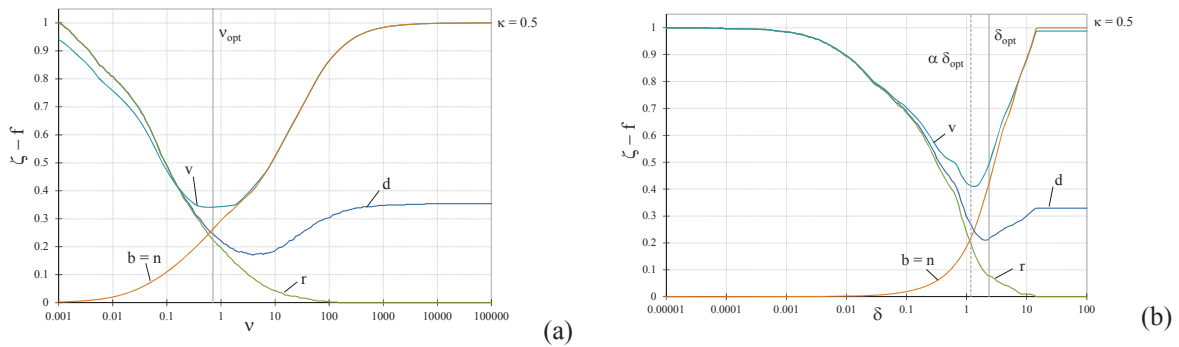
Figure 4.22 Design example for (a) VD case and (b) FD case.

The design procedure is confirmed: both suggested values v_{opt} and $\overline{\delta}_{opt} = \alpha \cdot \delta_{opt}$ provide the absolute minimum of the base shear and a value of the frame displacements close to its absolute minimum and lower than that corresponding to the rigid frame to brace connection condition. Better performance could be pursued lightly varying these parameters, i.e. increasing them, in order to further reduce displacements but accounting for increase in base shear force.

143

4.6   Conclusions

The present Chapter dealt with an optimal design problem for a simple linear-elastic frame equipped with dissipative braces (steel diagonal brace in series with a dissipative viscous or friction device). Aim of the work is the definition of the optimal device parameter (respectively C_d for the viscous case VD and F_y for the friction case FD) able to provide the minimum frame displacement or base shear.

A theoretical approach was suggested for determining an analytical optimal value of the viscous damping in VD case, or the yielding force in FD case, for a braced one-bay one-story frame subjected to a harmonic base motion. It was demonstrated that, given a certain frame to brace relative stiffness κ, for different values of the design parameters (adimensionalized viscous damping ν or adimensionalized yielding displacement δ), the behavior would span between two extreme cases both corresponding to an undamped response with an unbounded resonance. The process of adding damping would not be beneficial to any extent but just up to a certain level, depending on the objective of the optimization process. Within this field, the optimal values of ν and δ have been assumed as the ones corresponding to a minimum of the response curve in the overall frequency range for the frame displacement and the base shear. Design spectra are provided, where theoretical optimal values are given as a function of κ.

Then, numerical analysis were performed to validate the proposed design method in case of a seismic retrofit problem for a simple frame subjected to seven spectrum-compatible earthquake records for a life safety limit state, according to the NTC. Both theoretical and numerical results demonstrated that:

∗ The brace stiffness k_b is an additional design parameter that has to be properly selected taking into that that the higher is the brace stiffness the more effective is the control system in reducing inter-story drifts, but it may be detrimental in terms of base reaction.

∗ In the VD case, the value ν_{opt} minimizing the peak amplitude of the frame FRF curve is usually lower than the one corresponding to the actual numerical optimum for the frame. This can be explained taking into account that the frequency content of a ground motion can vary significantly and does not correspond to a white noise exciting the overall range of frequencies of the system. Despite that, the theoretical value ν_{opt} is very close to the numerical optimum for

the base shear, being also able at the same time to significantly reduce the frame response, so representing a reliable design parameter.

∗In the FD case, theoretical values δ_{opt} and $\delta_{f,opt}$ tend to be higher than numerical optimum minimizing frame displacement and base shear, respectively, both occurring for a value that is about one half of the one theoretically determined. A correction parameter $\alpha = 0.5$ has been introduced with the aim of considering as design parameter the value $\alpha \cdot \delta_{opt}$, practically reducing the maximum ground acceleration $a_{g,max}$ to an "equivalent" value $\alpha \cdot a_{g,\max}$ with respect to the harmonic excitation.

∗Both theoretically and numerically, it comes out that the optimal damping parameter corresponding to minimum base shear is lower than the one giving the minimum story frame. Therefore, in the proposed design procedure, the suggested reference values can be assumed as a starting point in a case-dependent optimization process, then being necessary to perform iterative analysis under code provided seismic action, in order to check and find out the effective optimum value for the minimization of the desired response.

It has also been observed that, for a given κ and ground motion, the absolute minimum frame displacement and base shear are obtained by means of viscous damping rather than hysteretic damping.

REFERENCES

1998-1 EN (2004) EN 1998-1. Eurocode 8: Design of structures for earthquake resistance – Part 1: General rules, seismic actions and rules for buildings

Caughey T (1960) Sinusoidal Excitation of a System with Bilinear Hysteresis. J Appl Mech 32:640–648.

Chopra AK (2011) Dynamics of Structures: Theory and Applications to Earthquake Engineering. Prentice Hall/Pearson Education

Christopoulos C, Filiatrault A (2006) Principles of Passive Supplemental Damping and Seismic Isolation. IUSS Press, Pavia

Iervolino I, Galasso C, Cosenza E (2010) REXEL: computer aided record selection for code-based seismic structural analysis. Bull Earthq Eng 8:339–362. doi: 10.1007/s10518-009-9146-1

Losanno D, Spizzuoco M, Serino G (2014) An optimal design procedure for a simple frame equipped with elastic-deformable dissipative braces.

Mathworks T (2010) Matlab.

NTC (2008) Ministero delle Infrastrutture. D.M. 14 gennaio 2008: Nuove norme tecniche per le costruzioni

Seismosoft (2013) A computer program for signal processing of strong-motion data. http://www.seismosoft.com.

Chapter 5

5. A PROCEDURE FOR OPTIMAL DESIGN OF A MDOF FRAME

5.1 Introduction

Viscous dampers (VDs) have been employed for retrofit of existing structures or seismic protection of new buildings. They are generally attached to steel supporting braces. In most analysis, these braces are neglected and assumed to have infinite stiffness compared with that of the structure and dissipative devices. But, the dimensions of the steel braces often need to be limited for functional and aesthetic requirements, so that their stiffness cannot be considered infinite. Nevertheless, a certain brace stiffness is important for activating the energy dissipative mechanism of viscous dampers.

The procedure of Chapter 4 is now extended to the MDOF case with reference to viscous damper braces following the same approach.

5.2 State of the art

In the following, some results are cited, which have been produced by some researchers in the last few years. They are focused on the influence of the braces stiffness on the optimal design of the dissipative devices in a protected multi-story building.

Chen and Chai (Chen and Chai 2011) studied shear-type buildings with Maxwell model-based brace-damper systems: after showing the closed-form solutions derived for a single-story building, an iterative numerical procedure was described for a multi-story building, to the aim of obtaining the minimum brace stiffness together with a set of optimal damper coefficients for a targeted reduction in terms of interstory drift, floor acceleration or base shear force. They concluded that a brace stiffness equal to the first story stiffness is adequate for the desirable levels of response reduction in typical applications. For example, in a ten-story building, the maximum response reduction was found to reach around 80% for story acceleration and base-shear force-based indices, and around 90% for interstory drift-based index.

Londono et al. (Londoño et al 2013; Londoño et al 2014) provided a study of the influence of brace stiffness on the damping action of linear viscous fluid dampers. It is a different approach based on the observation that the effects of brace stiffness can be represented as a first-order filter: in the first phase, the dampers are sized by using an optimization strategy that assumes the braces as infinitely stiff elements; then, the minimum brace stiffnesses are calculated based on desired damper efficiency over a predetermined frequency range. Numerical simulations of systems with added brace-damper assemblies acting under earthquake excitation were used to show the optimality of the solutions delivered using the proposed design procedure.

Castaldo and De Iuliis (Castaldo and De Iuliis 2014) proposed an optimal integrated seismic design procedure of the elastic stiffness resources and viscoelastic properties of a dissipative bracing-damper system, to achieve a seismic design displacement, by explicitly considering the dynamic behavior both of the structural and dissipative bracing systems. The optimal combination of the elastic and viscoelastic design variables is evaluated by minimizing a cost index assumed as an optimized objective function. The obtained results showed that the use of the viscoelastic resources is more convenient for high period systems, in particular, with reference to periods longer than 0.5s and high design performance, optimal solutions present high amount of viscoelastic resources and minimal value for lateral stiffness resources of the structural system. Differently, in the case of low performance as well as for periods lower than 0.5s, the optimal solution is pursued by maximizing the lateral stiffness of the structural system.

Singh and Moreschi (Singh and Moreschi 2001) suggested a gradient based approach that minimizes a performance index to achieve a target level of response reduction with the optimal distribution of viscous and viscoelastic dampers in building structures.

Park et al. (Park et al 2004) applied a gradient-based optimization algorithm to minimize both the size of VED size and supporting brace stiffness to obtain a determined reduction of inter-story drifts below given target values.

Viola and Guidi (Viola and Guidi 2009) (Caughey 1960; Viola and Guidi 2009)suggested a procedure to analyze the supporting brace stiffness influence on the damping optimization of a linear-elastic shear-type model, by minimizing the sum of mean-square inter-story drifts to stationary random excitation.

The procedure proposed in this Chapter is able to highlight the influence of supporting brace stiffness on both the structural dynamic response and the optimization of the devices' damping coefficient in controlled shear-type buildings. A frequency domain approach is adopted for solving the equation of motion of a controlled shear-type multi-story elastic frame, defining the complex stiffness contribution of the brace + viscous damper equipment. The system of complex linear equations of motion provides the effect of both brace elastic stiffness and viscous damper coefficient on dynamic response, thus allowing to define an optimal supplemental damping system. The minimization of the transfer functions' (FRFs) amplitude is set as target level by taking into account the effect of the dissipative braces on the frequencies of the structure. A FRF approach is also adopted in Takewaki (Takewaki 1997), but in that case undamped fundamental frequency of the system and constrained value of damping coefficients are assumed.

The spatial distribution of brace + damper assemblies is assumed to be uniform along height, even if it is well known that damping coefficients should be higher at lower floors, where more significant relative displacements and velocity are expected.

Another issue considered in the proposed work, is that excessive damping brings higher accelerations at higher floors, due to the predominance of the stiffening effect with respect to damping. However, the assumption of an elastic response of the bare frame is pursued, since high level of damping can ensure significant reduction of stresses in the structural elements even for design earthquakes.

5.3 Steady-state response of a dissipative braced multy-story frame subjected to harmonic base motion

The response to a harmonic base motion of a multi-story braced frame, equipped with passive viscous (VD) dampers, is analytically examined using the frequency domain approach (Chopra 2011), in order to determine the influence of the elastic brace's stiffness (normalized parameter κ) and the viscous damper coefficient (normalized parameter ν).

The force–displacement relationship for a Maxwell element (Figure 5.1), composed by the spring k_b and the viscous dashpot C_d arranged in series and subjected to a harmonic displacement with frequency ϖ, can be expressed as

$$F_d\left(x_f\right) = K_d\left(\varpi\right) \cdot x_f$$
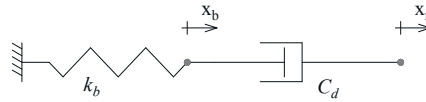
Figure 5.1 Maxwell element with a spring and a dashpot connected in series.

The complex stiffness $K_d\left(\varpi\right)$ is obtained as follows:

$$x_f = x_b + \frac{\dot{x}_f - \dot{x}_b}{i\varpi} = F_d\left(\frac{1}{k_b} + \frac{1}{i\varpi C_d}\right) \quad \Rightarrow \quad F_d = \frac{k_b C_d^2 \varpi^2 + i k_b^2 C_d \varpi}{k_b^2 + \varpi^2 C_d^2} x_f \quad \Rightarrow$$

$$\Rightarrow \quad K_d\left(\varpi\right) = \frac{k_b C_d^2 \varpi^2}{k_b^2 + \varpi^2 C_d^2} + i \frac{k_b^2 C_d \varpi}{k_b^2 + \varpi^2 C_d^2} = K_d'\left(\varpi\right) + i K_d''\left(\varpi\right)$$

(5.1)

where $K_d'\left(\varpi\right)$ and $K_d''\left(\varpi\right)$ are, respectively, the storage and the loss modulus of the Maxwell element.

Neglecting inherent structural damping, the equations of motion for a linear n-story frame provided with viscous dissipative braces, each made of an elastic component (a steel brace) and a viscous dashpot connected in series (Figure 5.2), represent a system of n 2nd order differential equations with constant coefficients, having the following matrix

$$\mathbf{M} \cdot \ddot{\mathbf{x}}_\mathbf{f} + \mathbf{K} \cdot \mathbf{x}_\mathbf{f} + \mathbf{F}_\mathbf{d} = \mathbf{M} \cdot \mathbf{l} \cdot \varpi^2 x_{g,\max} \cdot e^{i\varpi t}, \tag{5.2}$$

where

$$\mathbf{x}_\mathbf{f}^T = \begin{bmatrix} x_{f1} & x_{f2} & x_{f3} & \dots & x_{fi} & \dots & x_{fn-1} & x_{fn} \end{bmatrix} \tag{5.3}$$

is the vector of the unknown floor displacements,

$$\mathbf{M} = \begin{bmatrix} m_{f1} & 0 & 0 & \cdots & 0 & \cdots & 0 & 0 \\ 0 & m_{f2} & 0 & \cdots & 0 & \cdots & 0 & 0 \\ 0 & 0 & m_{f3} & \cdots & 0 & \cdots & 0 & 0 \\ \cdots & \cdots & \cdots & \cdots & \cdots & \cdots & \cdots & \cdots \\ 0 & 0 & 0 & \cdots & m_{fi} & \cdots & 0 & 0 \\ \cdots & \cdots & \cdots & \cdots & \cdots & \cdots & \cdots & \cdots \\ 0 & 0 & 0 & \cdots & 0 & \cdots & m_{fn-1} & 0 \\ 0 & 0 & 0 & \cdots & 0 & \cdots & 0 & m_{fn} \end{bmatrix} \tag{5.4}$$

is the mass matrix,

$$\mathbf{K} = \begin{bmatrix} k_{f1}+k_{f2} & -k_{f2} & 0 & \cdots & 0 & \cdots & 0 & 0 \\ -k_{f2} & k_{f2}+k_{f3} & -k_{f3} & \cdots & 0 & \cdots & 0 & 0 \\ 0 & -k_{f3} & k_{f3}+k_{f4} & \cdots & 0 & \cdots & 0 & 0 \\ \cdots & \cdots & \cdots & \cdots & \cdots & \cdots & \cdots & \cdots \\ 0 & 0 & 0 & \cdots & k_{fi}+k_{fi+1} & \cdots & 0 & 0 \\ \cdots & \cdots & \cdots & \cdots & \cdots & \cdots & \cdots & \cdots \\ 0 & 0 & 0 & \cdots & 0 & \cdots & k_{fn-1}+k_{fn} & -k_{fn} \\ 0 & 0 & 0 & \cdots & 0 & \cdots & -k_{fn} & k_{fn} \end{bmatrix} \tag{5.5}$$

is the stiffness matrix,

$$\mathbf{F_d} = \mathbf{K_b} \cdot \begin{bmatrix} \mathbf{x_f}^T & \mathbf{x_b}^T \end{bmatrix} = \mathbf{C_d} \cdot \begin{bmatrix} \dot{\mathbf{x}}_f^T & \dot{\mathbf{x}}_b^T \end{bmatrix}, \tag{5.6}$$

with

$$\mathbf{x_b}^T = \begin{bmatrix} x_{b1} & x_{b2} & x_{b3} & \cdots & x_{bi} & \cdots & x_{bn-1} & x_{bn} \end{bmatrix}, \tag{5.7}$$

the vector of the unknown brace displacements,

$$\mathbf{K_b} = \begin{bmatrix} k_{b2} & 0 & 0 & \cdots & 0 & \cdots & 0 & 0 & k_{b1} & -k_{b2} & 0 & \cdots & 0 & \cdots & 0 & 0 \\ -k_{b2} & k_{b3} & 0 & \cdots & 0 & \cdots & 0 & 0 & 0 & k_{b2} & -k_{b3} & \cdots & 0 & \cdots & 0 & 0 \\ 0 & -k_{b3} & k_{b4} & \cdots & 0 & \cdots & 0 & 0 & 0 & 0 & k_{b3} & \cdots & 0 & \cdots & 0 & 0 \\ \cdots & \cdots & \cdots & \cdots & \cdots & \cdots & \cdots & \cdots & \cdots & \cdots & \cdots & \cdots & \cdots & \cdots & \cdots & \cdots \\ 0 & 0 & 0 & \cdots & k_{bi+1} & \cdots & 0 & 0 & 0 & 0 & 0 & \cdots & k_{bi} & \cdots & 0 & 0 \\ \cdots & \cdots & \cdots & \cdots & \cdots & \cdots & \cdots & \cdots & \cdots & \cdots & \cdots & \cdots & \cdots & \cdots & \cdots & \cdots \\ 0 & 0 & 0 & \cdots & 0 & \cdots & k_{bn} & 0 & 0 & 0 & 0 & \cdots & 0 & \cdots & k_{bn-1} & -k_{bn} \\ 0 & 0 & 0 & \cdots & 0 & \cdots & -k_{bn} & 0 & 0 & 0 & 0 & \cdots & 0 & \cdots & 0 & k_{bn} \end{bmatrix} \tag{5.8}$$

the dissipative-brace's stiffness matrix, and

$$
\mathbf{C_d} = \begin{bmatrix}
C_{d2} & -C_{d2} & 0 & \dots & 0 & \dots & 0 & 0 & -C_{d1} & C_{d2} & 0 & \dots & 0 & \dots & 0 & 0 \\
0 & C_{d2} & -C_{d3} & \dots & 0 & \dots & 0 & 0 & 0 & -C_{d2} & C_{d3} & \dots & 0 & \dots & 0 & 0 \\
0 & 0 & C_{d3} & \dots & 0 & \dots & 0 & 0 & 0 & 0 & -C_{d3} & \dots & 0 & \dots & 0 & 0 \\
\dots & \dots & \dots & \dots & \dots & \dots & \dots & \dots & \dots & \dots & \dots & \dots & \dots & \dots & \dots & \dots \\
0 & 0 & 0 & \dots & C_{di} & \dots & 0 & 0 & 0 & 0 & 0 & \dots & -C_{di} & \dots & 0 & 0 \\
\dots & \dots & \dots & \dots & \dots & \dots & \dots & \dots & \dots & \dots & \dots & \dots & \dots & \dots & \dots & \dots \\
0 & 0 & 0 & \dots & 0 & \dots & C_{dn-1} & -C_{dn} & 0 & 0 & 0 & \dots & 0 & \dots & -C_{dn-1} & C_{dn} \\
0 & 0 & 0 & \dots & 0 & \dots & 0 & C_{dn} & 0 & 0 & 0 & \dots & 0 & \dots & 0 & -C_{dn}
\end{bmatrix}
\tag{5.9}
$$

the viscous damping matrix, with $\mathbf{l}^T = \begin{bmatrix} 1 & 1 & 1 & \dots & 1 & \dots & 1 & 1 \end{bmatrix}$.
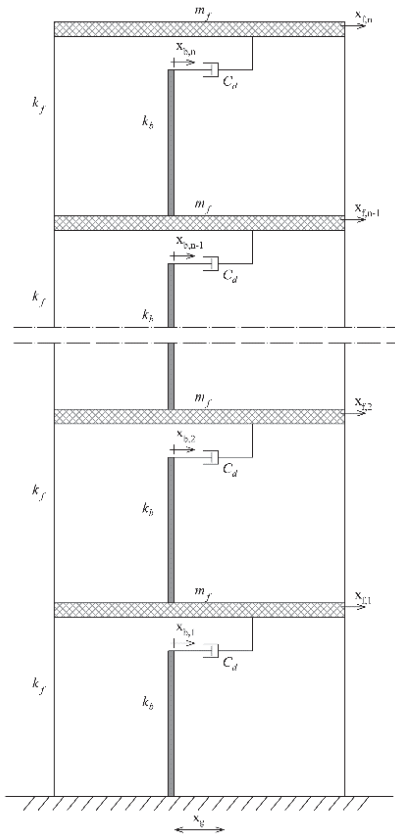
Figure 5.2 Multi-story shear-type frame equipped with dissipative braces.

The slab horizontal displacements x_{f1}, x_{f2}, ..., x_{fn} and the top brace horizontal displacements x_{b1}, x_{b2}, ..., x_{bn} are relative to the base and represent the $2 \cdot n$ kinematic unknowns of the problem.

The following assumptions $m_{f1} = m_{f2} = ... = m_{fn} = m_f$, $k_{f1} = k_{f2} = ... = k_{fn} = k_f$, $k_{b1} = k_{b2} = ... = k_{bn} = k_b$ and $C_{d1} = C_{d2} = ... = C_{dn} = C_d$ are made, denoting by m_{fi}, k_{fi}, k_{bi} and C_{di}, respectively, the floor mass, the floor stiffness, the brace stiffness and the viscous damping coefficient for the i-th story.

152

The force-displacement relationships for the Maxwell elements, each composed by the spring k_{bi} and the viscous dashpot C_{di} connected in series, are given by the expression $\mathbf{F_d(x_f)} = \mathbf{K_d}(\varpi) \cdot \mathbf{x_f}$, where the complex stiffness matrix $\mathbf{K_d}(\varpi)$ is the following:

$$\mathbf{K_d}(\varpi) = \begin{bmatrix} K_{d1}+K_{d2} & -K_{d2} & 0 & \dots & 0 & \dots & 0 & 0 \\ -K_{d2} & K_{d2}+K_{d3} & -K_{d3} & \dots & 0 & \dots & 0 & 0 \\ 0 & -K_{d3} & K_{d3}+K_{d4} & \dots & 0 & \dots & 0 & 0 \\ \dots & \dots & \dots & \dots & \dots & \dots & \dots & \dots \\ 0 & 0 & 0 & \dots & K_{di}+K_{di+1} & \dots & 0 & 0 \\ \dots & \dots & \dots & \dots & \dots & \dots & \dots & \dots \\ 0 & 0 & 0 & \dots & 0 & \dots & K_{dn-1}+K_{dn} & -K_{dn} \\ 0 & 0 & 0 & \dots & 0 & \dots & -K_{dn} & K_{dn} \end{bmatrix} \qquad (5.10)$$

with $K_{di}(\varpi) = \dfrac{k_{bi}C_{di}^2\varpi^2 + ik_{bi}^2 C_{di}\varpi}{k_{bi}^2 + \varpi^2 C_{di}^2} = K'_{di} + iK''_{di}$, being $K'_{di}(\varpi)$ and $K''_{di}(\varpi)$ the storage and the loss modulus of the Maxwell element, respectively.

Therefore, Eq. (5.2) can be written as

$$\mathbf{M} \cdot \ddot{\mathbf{x}}_{\mathbf{f}} + [\mathbf{K} + \mathbf{K_d}(\varpi)] \cdot \mathbf{x_f} = \mathbf{M} \cdot \mathbf{l} \cdot \varpi^2 x_{g,\max} \cdot e^{i\varpi t}, \qquad (5.11)$$

thus reducing kinematic unknowns to only n frame displacements.

The above equation can be written in non-dimensional form, by considering the initial hypothesis (floor mass, floor stiffness, brace stiffness and viscous coefficients equal for all the storys) and by introducing the non-dimensional time $\tau = t \cdot \omega_b$, where $\omega_b = \sqrt{(k_f + k_b)/m_f}$, and the non-dimensional displacement $\zeta_{\mathbf{f}}(\tau) = \mathbf{x_f}(\tau)/x_{g,\max}$:

$$\zeta''_{\mathbf{f}}(\tau) + \mathbf{f}(\zeta_{\mathbf{f}}) = \mathbf{l} \cdot \beta^2 e^{i\beta\tau}, \qquad (5.12)$$

with $\qquad \beta = \varpi/\omega_b \qquad$ and $\qquad \mathbf{f}(\zeta_{\mathbf{f}}) = [\mathbf{K} + \mathbf{K_d}(\varpi)] \cdot \mathbf{x_f}/[(k_f + k_b) \cdot x_{g,\max}] =$

$= [\mathbf{K} \cdot \mathbf{x_f} + \mathbf{F_d(x_f)}]/[(k_f + k_b) \cdot x_{g,\max}] = \mathbf{K_s}(\beta) \cdot \zeta_{\mathbf{f}}(\tau).$

The dynamic response is completely defined once the complex normalized stiffness matrix $\mathbf{K_s}(\beta)$ of the controlled structure is known:

$$K_s(\beta) = \begin{bmatrix} 2\bar{\kappa}+2K_s(\beta) & -\bar{\kappa}-K_s(\beta) & 0 & \dots & 0 & \dots & 0 & 0 \\ -\bar{\kappa}-K_s(\beta) & 2\bar{\kappa}+2K_s(\beta) & -\bar{\kappa}-K_s(\beta) & \dots & 0 & \dots & 0 & 0 \\ 0 & -\bar{\kappa}-K_s(\beta) & 2\bar{\kappa}+2K_s(\beta) & \dots & 0 & \dots & 0 & 0 \\ \dots & \dots & \dots & \dots & \dots & \dots & \dots & \dots \\ 0 & 0 & 0 & \dots & 2\bar{\kappa}+2K_s(\beta) & \dots & 0 & 0 \\ \dots & \dots & \dots & \dots & \dots & \dots & \dots & \dots \\ 0 & 0 & 0 & \dots & 0 & \dots & 2\bar{\kappa}+2K_s(\beta) & -\bar{\kappa}-K_s(\beta) \\ 0 & 0 & 0 & \dots & 0 & \dots & -\bar{\kappa}-K_s(\beta) & \bar{\kappa}+K_s(\beta) \end{bmatrix} \quad (5.13)$$

where $\quad K_s(\beta) = \dfrac{4\beta^2\nu^2\kappa(1+\kappa)}{(1+\kappa)[1+4\beta^2\nu^2\kappa(1+\kappa)]} + i\dfrac{2\beta\nu\sqrt{\kappa(1+\kappa)}}{(1+\kappa)[1+4\beta^2\nu^2\kappa(1+\kappa)]},\quad \bar{\kappa} = \dfrac{\kappa}{1+\kappa}\quad$ (with

$\kappa = k_f / k_b$ representing for the *i*-th floor the frame to brace relative stiffness) and

$\nu = C_d / 2\sqrt{k_f m_f}$.

The equations of motion become

$$\zeta_f''(\tau) + K_s(\beta) \cdot \zeta_f(\tau) = \mathbf{1} \cdot \beta^2 e^{i\beta\tau} \quad (5.14)$$

and the steady-state solution can be written as

$$\zeta_f(\tau) = \zeta_{f,max} e^{i\beta\tau} \quad (5.15)$$

with $\zeta_{f,max}^T(\beta) = \begin{bmatrix} \zeta_{f1,max} & \zeta_{f2,max} & \zeta_{f3,max} & \dots & \zeta_{fn,max} \end{bmatrix}$. By substituting Eq. (5.15) into Eq. (5.14), after simple algebraic manipulations one obtains

$$\left[-\mathbf{I}_{n\times n} \cdot \beta^2 + \mathbf{K}_s(\beta) \right] \cdot \zeta_{f,max} = \mathbf{1} \cdot \beta^2 \quad (5.16)$$

5.3.1 Solution of the equation of motion

Eq. (5.16) represents a system of complex linear equations in the unknowns $\zeta_{f,max}(\beta)$, whose solution provides the structural response as a function of β :

$$\zeta_{f,max}(\beta) = \left[-\mathbf{I}_{n\times n} \cdot \beta^2 + \mathbf{K}_s(\beta) \right]^{-1} \cdot \mathbf{1} \cdot \beta^2 \quad (5.17)$$

The solution of the system in Eq. (5.17) provides the *n* frequency response functions (FRFs) $\zeta^i_{f,max}(\beta)$, in terms of floor displacements relative to the base.

Given a certain value of κ, for $\nu = 0$ and $\nu = \infty$, each transfer function exhibits as many unbounded resonance as the degree of freedom of the frame, corresponding to the *n* natural frequencies of the un-braced and braced systems, respectively. It can be observed that, for $\nu = 0$

and $v = \infty$, the normalized dissipative-brace stiffness contribution $K_d(\beta)$ is equal, respectively,

to 0 and $\dfrac{1}{1+\kappa}$.

For any v between zero and infinite, the generic function $\zeta^i_{f,max}(\beta)$ tends to show n resonance amplitudes for values of β corresponding to the n frequencies of the system. Increasing v, a progressive shift of each frequency from $v = 0$ towards $v = \infty$ limit case is observed. It must be noted that, only for $v = 0$ and $v = \infty$ the system frequencies are natural, i.e. no damping takes place with a mathematical resonance.

For the practical purpose of analyzing the earthquake induced response, it is reasonable just to consider the first vibration mode. Due to both regularity in mass-stiffness distribution and typical strong motion frequency content, higher modes can be deemed not likely to be excited. Under this assumption, the first normalized frequencies of the system, corresponding to $v = 0$ and $v = \infty$, are denoted by β_i and β_s, respectively. Any finite value of v in the range $0\div\infty$, would produce a damped response with an effective resonance in the range $\beta_i\div\beta_s$. It is clear that, with respect to the case $v = 0$, increasing damping above a certain optimal value is not beneficial because extremely large value of v would result in a much stiffened undamped system (limit case $v = \infty$).

This strong influence of the device's damping coefficient on the structural response comes out from Eq. (5.17), i.e. a deep modification in the dynamic behavior of the structure can be produced by a change of the device's viscous constant.

Transfer functions expressed by Eq. (5.17) have been plotted for a 3 DOFs system, for different values of v (0, 0.1, 1, 100) and κ (0.1, 1). The results are shown in Bode plot format (Figure 5.3, Figure 5.4), together with two vertical grey lines representing the normalized frequencies β_i ($v=0$) and β_s ($v=\infty$).

(a)   (b)
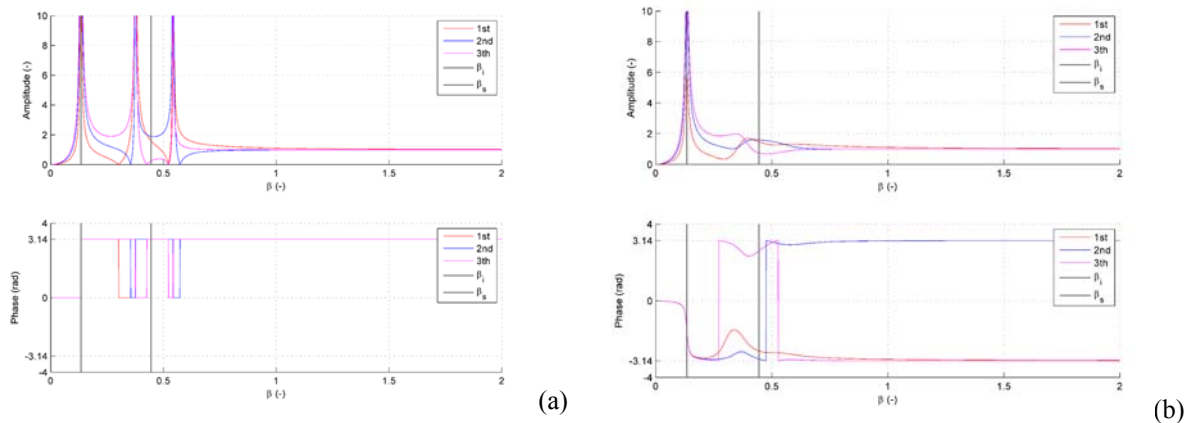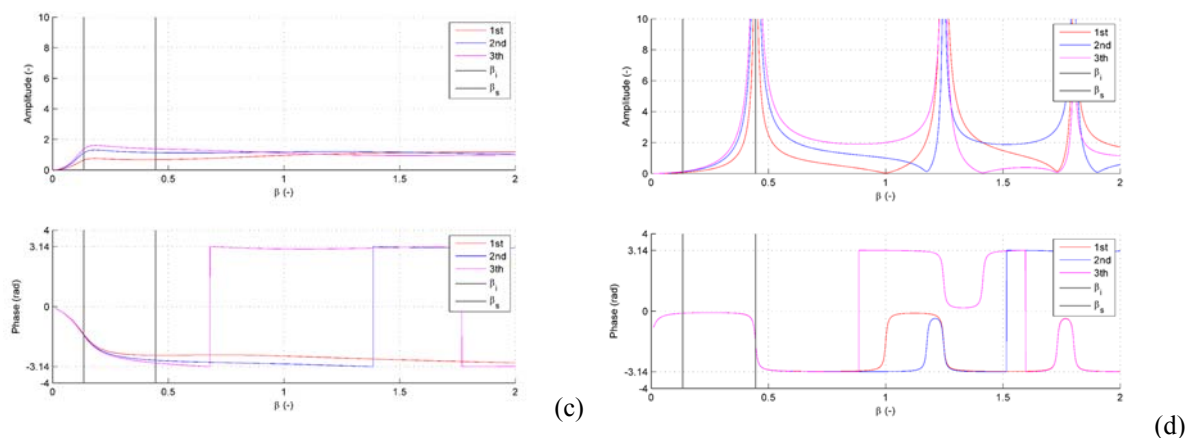
Figure 5.3 Bode plot for a 3-story frame with κ=0.1: (a) $v = 0$**, (b)** $v = 0.1$**, (c)** $v = 1$**, (d)** $v = 100$**.**
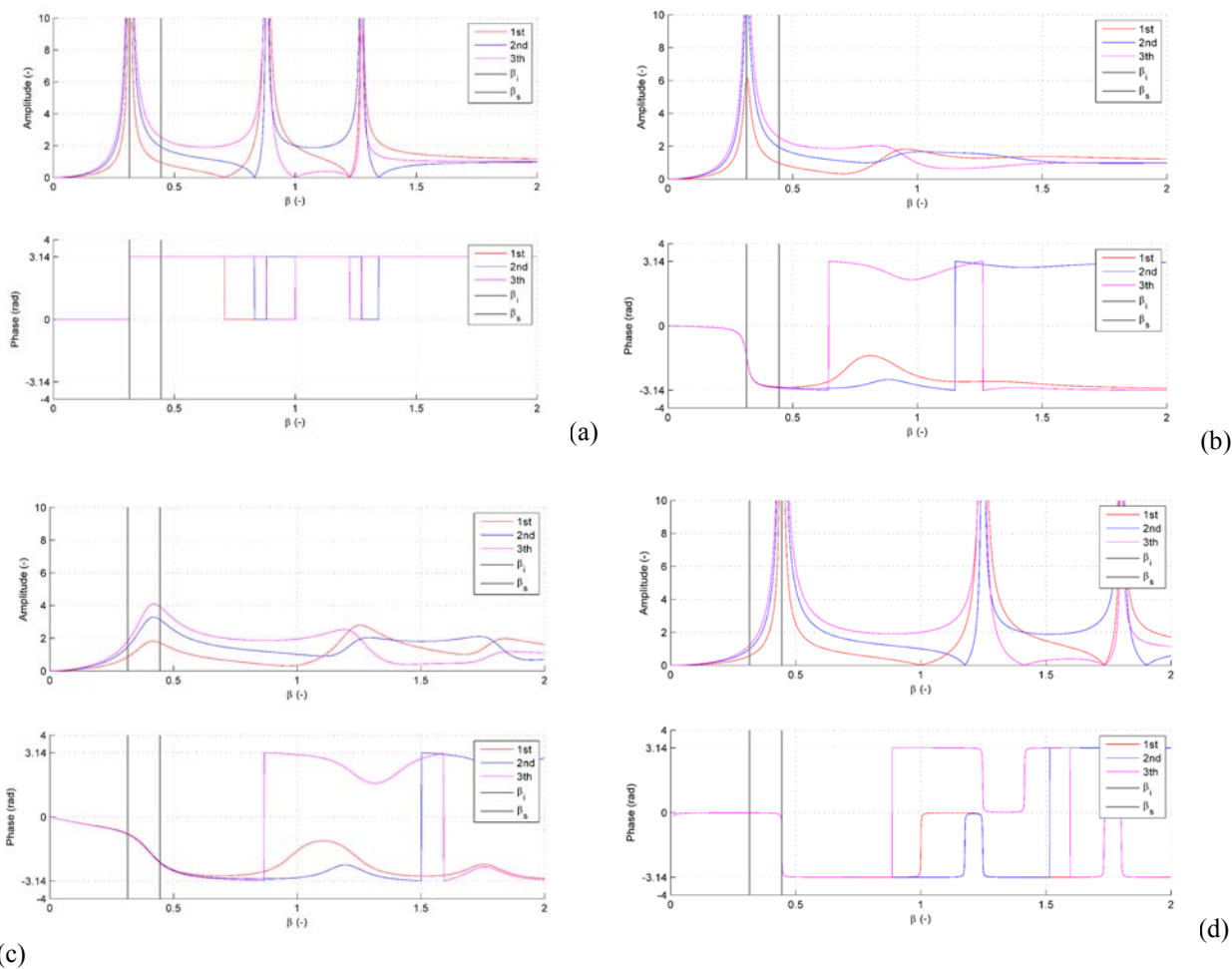
Figure 5.4 Bode plot for a 3-story frame with κ=1: (a) $v = 0$**, (b)** $v = 0.1$**, (c)** $v = 1$**, (d)** $v = 100$**.**

Therefore, fixed κ, the effect of ν is remarkable both in terms of shift in the frequency of the system and peak amplitude at resonance. For ν→0 and ν→∞, Bode plots clearly show that, at resonance, amplitudes are unbounded and phase angles have a sudden change of ±π.

From this perspective, an optimization criterion could be derived: an optimal value ν_{opt} can be searched as the one capable to yield a minimum resonance peak at the first frequency $\bar{\beta}$ (in the range $\beta_i \div \beta_s$). It must be noted that, thanks to structural regularity, a minimum of displacements corresponds to a minimum of interstory drifts. The value $\bar{\beta}$ represents the normalized eigenfrequency of the system for the assigned value of ν ($\bar{\omega} = \bar{\beta} \cdot \omega_b$), and represents the dominant frequency that the system would exhibit if excited by an external force. In other words, an external pulsing force having frequency $\bar{\omega}$ would be responsible for the first resonance. Physical meaning of $\bar{\beta}$ ($\bar{\omega}$) is different from both natural undamped and damped frequencies, for any finite value of ν. Just for $\nu = 0$ and $\nu = \infty$, the frequency $\bar{\beta}$ reduces to β_i and β_s, respectively.

5.4 Analytical evaluation of brace-damper efficiency

A numerical determination of the value ν_{opt} has been made for each value of κ in the range $[0,1\div5]$, for 3 DOFs, 6 DOFs and 10 DOFs systems (Figure 5.5(a)). In addition to this, the value of the normalized peak displacements $\zeta^i_{f,max}$, calculated for the value $\nu_{opt}(\kappa)$ at the frequency $\bar{\beta}$, are plotted in Figure 5.5(b) for both base and top floor levels.

(a)   (b)
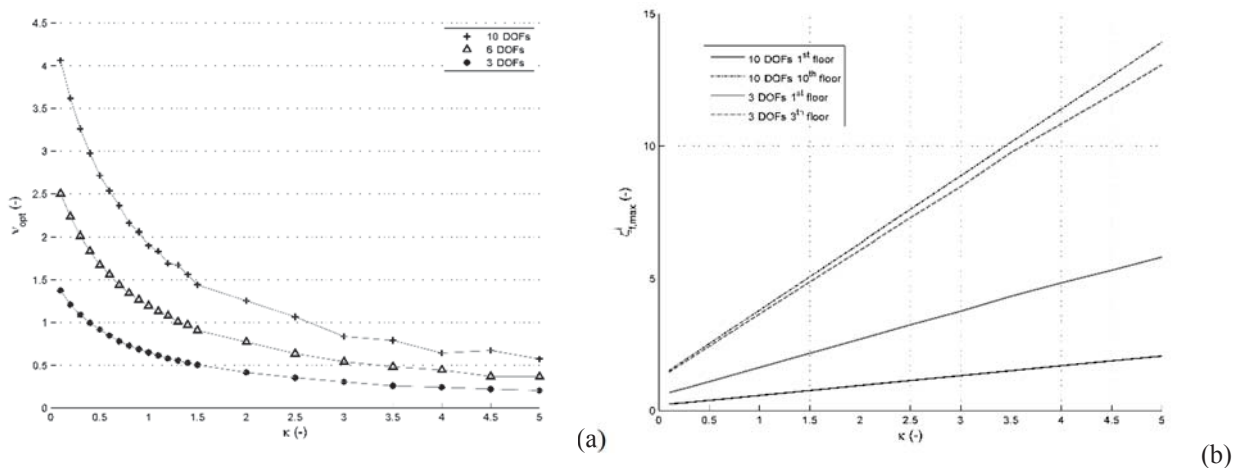
Figure 5.5 (a) Values of ν_{opt} vs κ and (b) $\zeta^i_{f,max}$ vs κ.

For each number of DOFs, a decreasing trend of ν is detected, having a higher slope in the range of κ [0.1÷2]. This means that higher values of κ require lower values of the optimal parameter due to the "loss of efficiency" of the dissipative bracing system in reducing the dynamic response. This outcome is opposite to the idea that, for a high value of κ, a higher

value of ν could be needed. It is worth to note that the finite stiffness of the elastic supporting brace should be properly accounted for, since the choice of the optimum ν is directly related to the parameter κ.

As far as the influence of the number of DOFs is concerned, an increasing of it requires a larger ν_{opt}, for any value of κ. This can be interpreted as due to the larger flexibility and larger mass of a taller frame, and so to the need of higher equivalent optimal damping ν_{opt} to achieve an optimal response.

Peak displacements $\zeta^i_{f,\max}(\nu_{opt})$ increase versus κ, thanks to the larger flexibility. A particular outcome is that, for a given κ, a model with a higher number of DOFs has lower 1st floor displacements than low-rise ones. Despite to this, the difference at the top floor is very narrow, especially for lower κ. This can be explained in relation to the higher optimal values of ν required by the larger DOFs models, with the consequent more significant improvement of the response.

A measure of the brace-damper efficiency ε, can be defined as the ratio between maximum displacement at the base evaluated at resonance for ν_{opt} corresponding to κ, with respect to the reference case $\kappa = 0.1$ (Figure 5.6):

$$\varepsilon = \frac{\zeta^1_{f,\max}(\nu_{opt}, \kappa)}{\zeta^1_{f,\max}(\nu_{opt}, \kappa = 0.1)} \tag{5.18}$$
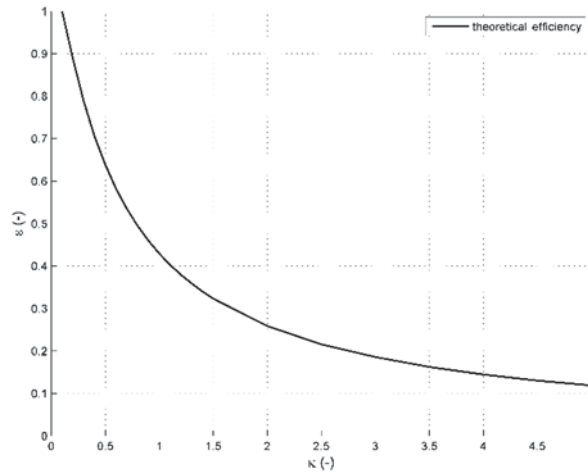
Figure 5.6 Value of the efficiency ε *vs* κ.

An important outcome is that the efficiency does not depend on the number of DOFs. As expected, the effectiveness of the control system tends to vanish for high values of κ.

158

5.5 Numerical analysis

The aim of the paragraph is to investigate the effect of real strong motions on the structural response of a retrofitted 3 storey-one bay concrete frame, equipped with dissipative braces having different stiffness and viscous coefficients. Differently from theoretical procedure, in this case excitation is not a pulsing force but can be decomposed into a series of harmonic components by means of the discrete Fourier Transform algorithm. In addition to this, not only the steady state response, but also the transitory phase plays an important role and is accounted for.

The single bay has 3 m height and 5 m span, with a mass of 20 t, columns cross section 0,40x0,40 m^2 and concrete modulus 30000 MPa. For every bay, an equivalent diagonal brace with horizontal stiffness k_b is considered as supporting the damping device C_d.

The structural model of a n-story frame is defined by a $2 \cdot n$ DOFs system, where the first n dynamic DOFs are associated to the floor displacements. The equation of motion has been formulated as follows:

$$\mathbf{M} \cdot \ddot{\mathbf{x}} + \mathbf{C} \cdot \dot{\mathbf{x}} + \mathbf{K} \cdot \mathbf{x} = -\ddot{x}_g \mathbf{M} \cdot \mathbf{l} \qquad (5.19)$$

where $\mathbf{x}$ is the $2 \cdot n$ displacement vector, $\mathbf{M}$, $\mathbf{K}$ and $\mathbf{C}$ are $2 \cdot n \ x \ 2 \cdot n$ matrix, $\mathbf{I}$ is the identity vector and $\ddot{x}_g$ the base acceleration.

The equation of motion has been solved numerically by implementing the Newton-Raphson integration method (Δt=0.01s, γ=1/2, β=1/4). The input ground motion is represented by four unscaled recorded earthquakes (Seismosoft 2013): Imperial Valley (1979 - USGS STATION 5115), Kobe (1995 - KAKOGAWA STATION), Loma Prieta (1989 - CDMG STATION 47381), Northridge (1994 - CDMG STATION 24278). For these events, the average maximum ground displacement $x_{g,max}$ is estimated equal to 0.10 m.

The dynamic response of the case-study under the above mentioned ground motions, characterized by different frequency content, has been obtained in order to numerically determine the effects of the design parameters (κ, ν) and single out an optimal value of the parameter ν. Three different frames kind have been considered, characterized as below:

a.   shear type frame - κ=0.1

b.   shear type frame - κ=1

c.   finite beam stiffness (30x40 cm^2 cross section) frame - κ=1

In Figure 5.7, the response for three different values of ν (0.05, 0.65, 15) has been calculated for case *a*, under Imperial Valley ground motion. It is evident that both the lowest (ν=0.05) and the highest assumed value (ν=15) are detrimental with respect to ν=0.65 (theoretical optimal value ν_{opt} from Figure 5.7), both in terms of maximum top floor displacements and accelerations. The effect of ν is remarkable also in terms of dominant frequency of the response: systems with higher ν tends to vibrate faster.
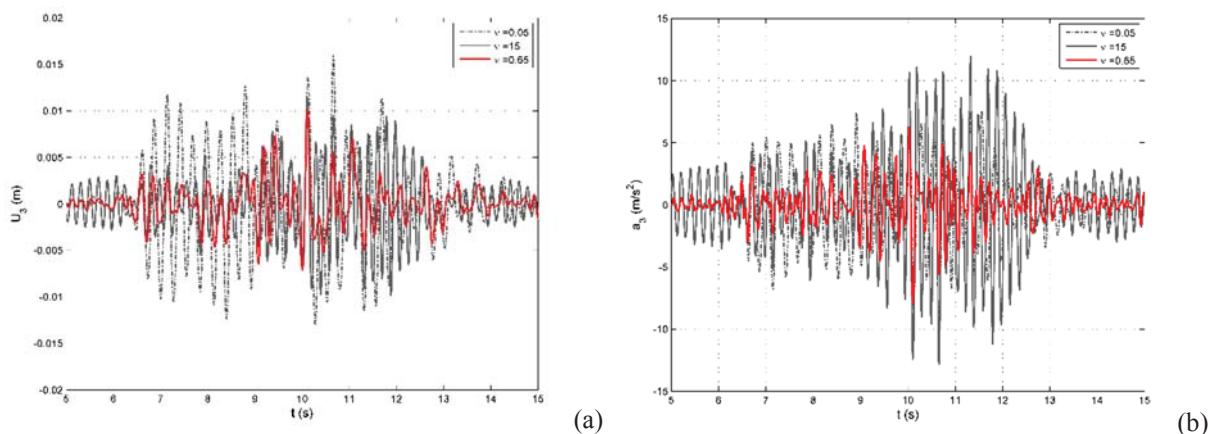
Figure 5.7 (a) Top floor displacements and (b) accelerations for three different values of ν.

A parametric investigation has been performed for each ground motion and for each case, by assigning extremely different values to ν (200 logarithmically spaced values between 10^{-3} and 10^5): the maximum response has been considered as result for each time history case and is plotted in what follows. The effective optimal value $\overline{\nu}_{opt}$, numerically determined, is assumed as the value corresponding to the minimum structural response, under each seismic excitation. The following figures summarize some relevant results of the numerical analyses performed on the case studies: the maximum response is plotted versus the value of the parameter ν in a semi-logarithmic scale. The structural response is shown both in terms of kinematics (maximum floor displacements and accelerations), and static parameters (base shear force V and base axial force N due to the bracing system). Displacements and accelerations are normalized, respectively, with respect to $x_{g,max}$ and g, while forces are normalized with respect to the quantities $x_{g,max} \cdot (k_b + k_f)$ or $m_{tot} \cdot g$, where m_{tot} is the total mass of the frame. It must be noted that a gain of the parameter ν always produces an increase of the axial force in the columns. Drawbacks of bracing systems are mainly related to the detrimental effects on the foundation, both in terms of incremental base shear and additional axial force. This is a main issue for conventional

bracing systems, but it must be taken into account also in case of dissipative braces that provide both damping and stiffness.

Main results are summarized in the following figures (Figure 5.8 to Figure 5.19) where the vertical straight line indicates the optimal value v_{opt} determined from the previous paragraph (Figure 5.5(a)).

(a)

(b)
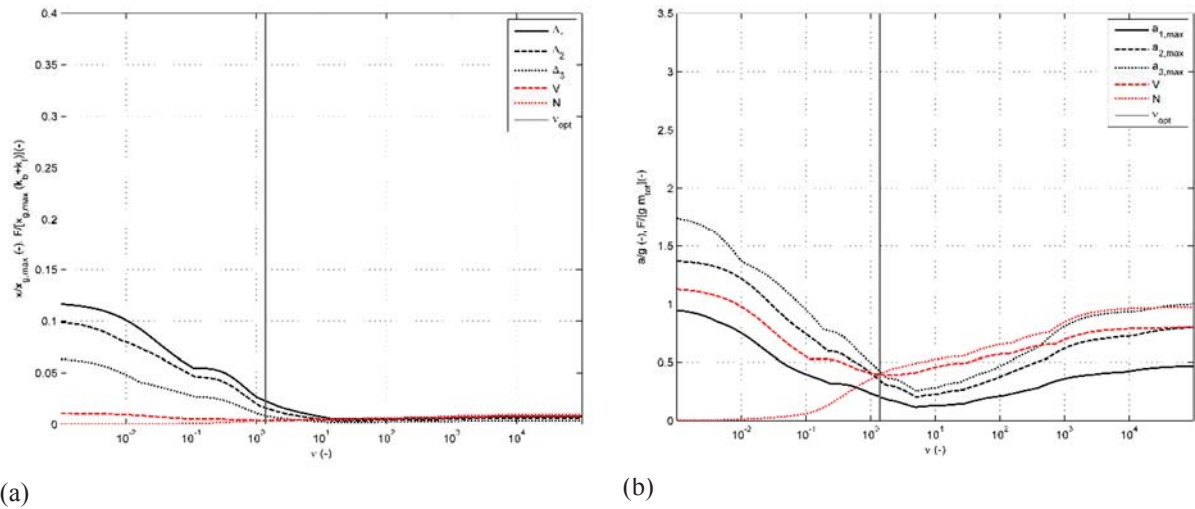
Figure 5.8 Numerical results for case *a* under Imperial Valley ground motion: (a) relative displacements and forces, (b) relative accelerations and forces.

(a)

(b)
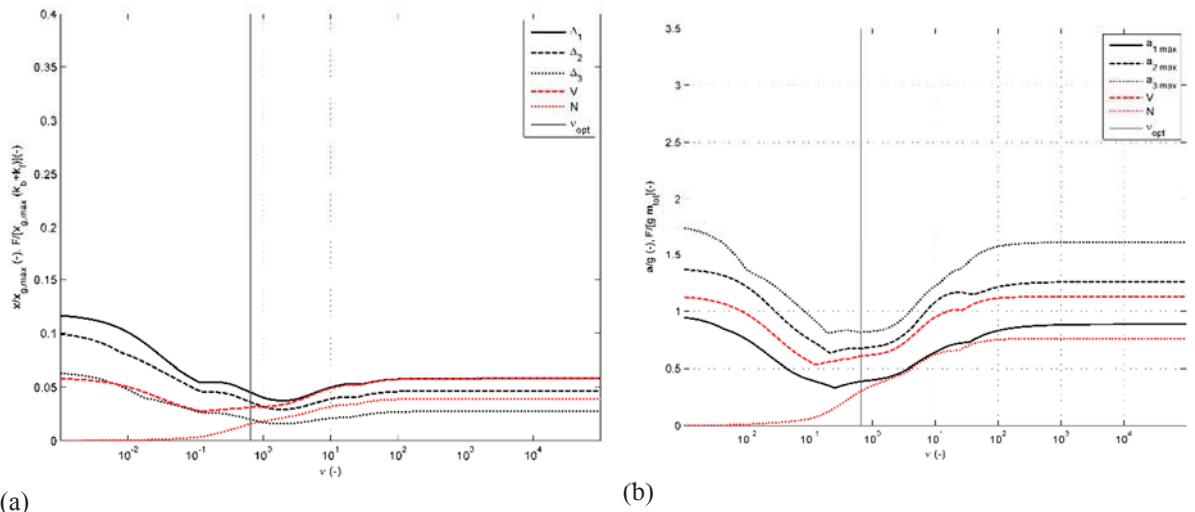
Figure 5.9 Numerical results for case *b* under Imperial Valley ground motion: (a) relative displacements and forces, (b) relative accelerations and forces.

(a)

(b)
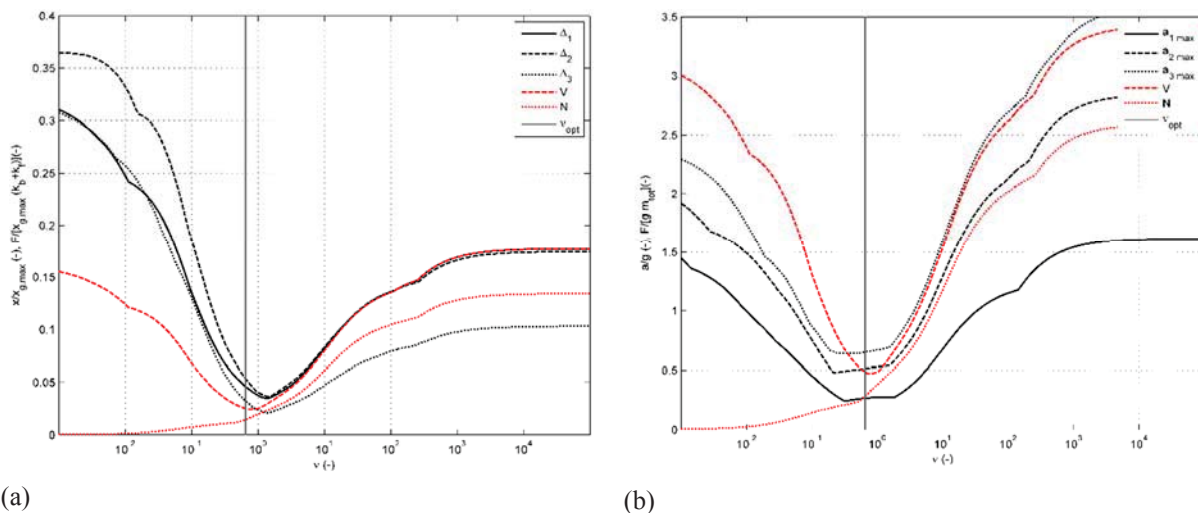
Figure 5.10 Numerical results for case *c* under Imperial Valley ground motion: (a) relative displacements and forces, (b) relative accelerations and forces.

(a)

(b)
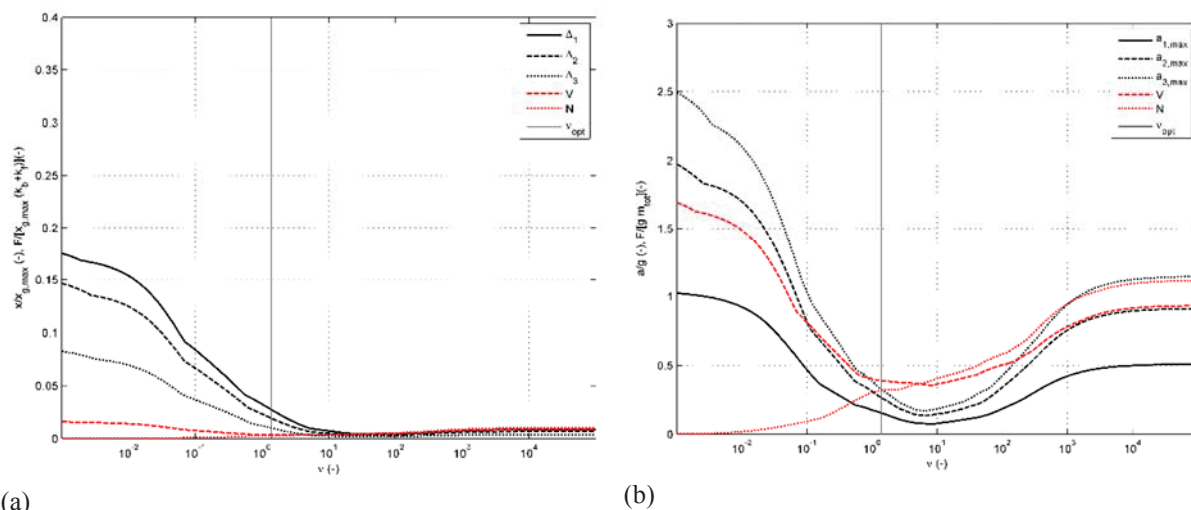
Figure 5.11 Numerical results for case *a* under Kobe ground motion: (a) relative displacements and forces, (b) relative accelerations and forces.

(a)

(b)

162
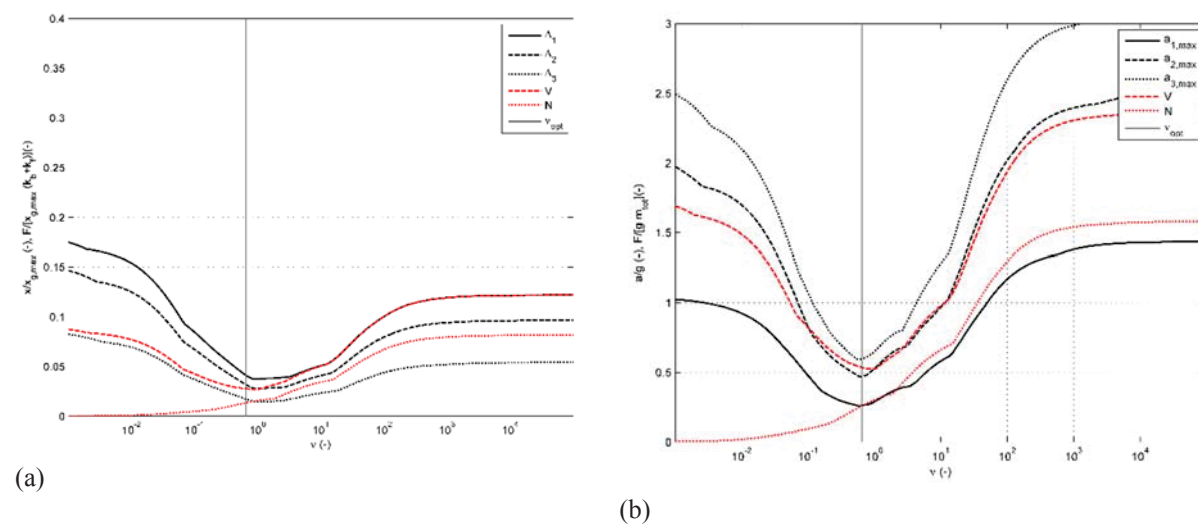
Figure 5.12 Numerical results for case *b* under Kobe ground motion: (a) relative displacements and forces, (b) relative accelerations and forces.

(a)   (b)
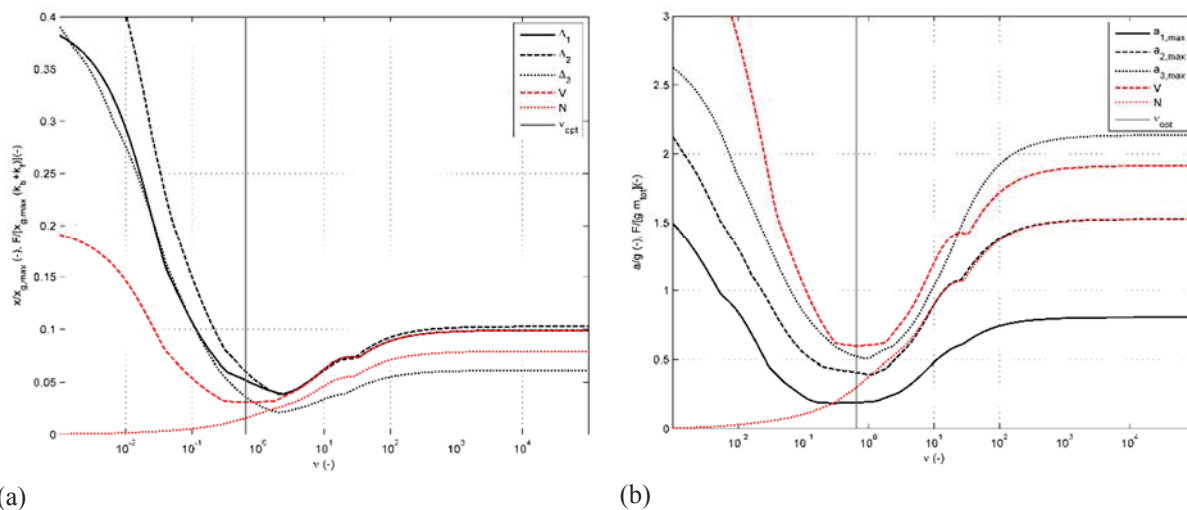
Figure 5.13 Numerical results for case *c* under Kobe ground motion: (a) relative displacements and forces, (b) relative accelerations and forces.

(a)   (b)
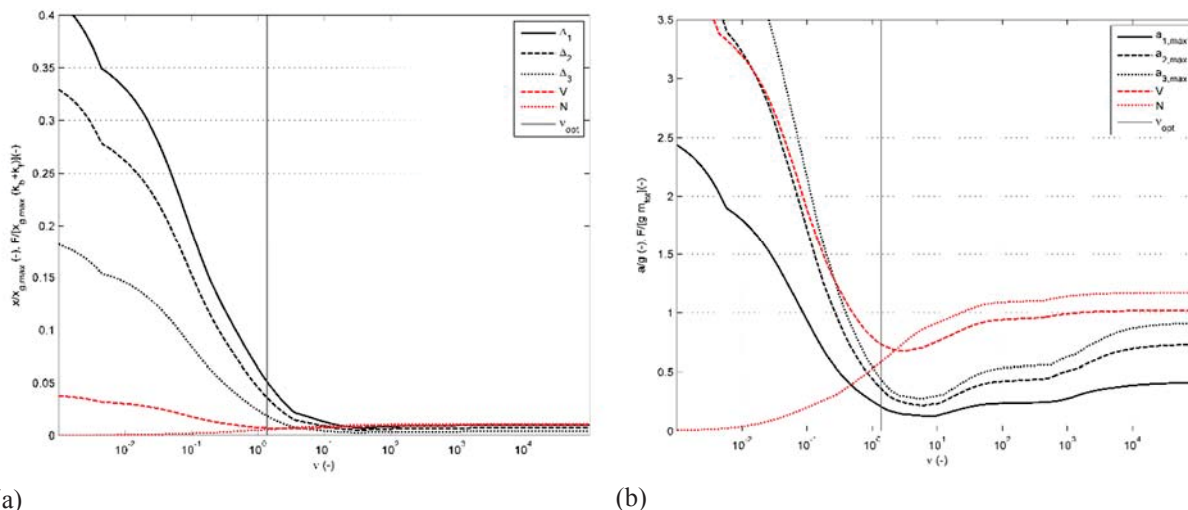
Figure 5.14 Numerical results for case *a* under Northridge ground motion: (a) relative displacements and forces, (b) relative accelerations and forces.

(a)   (b)
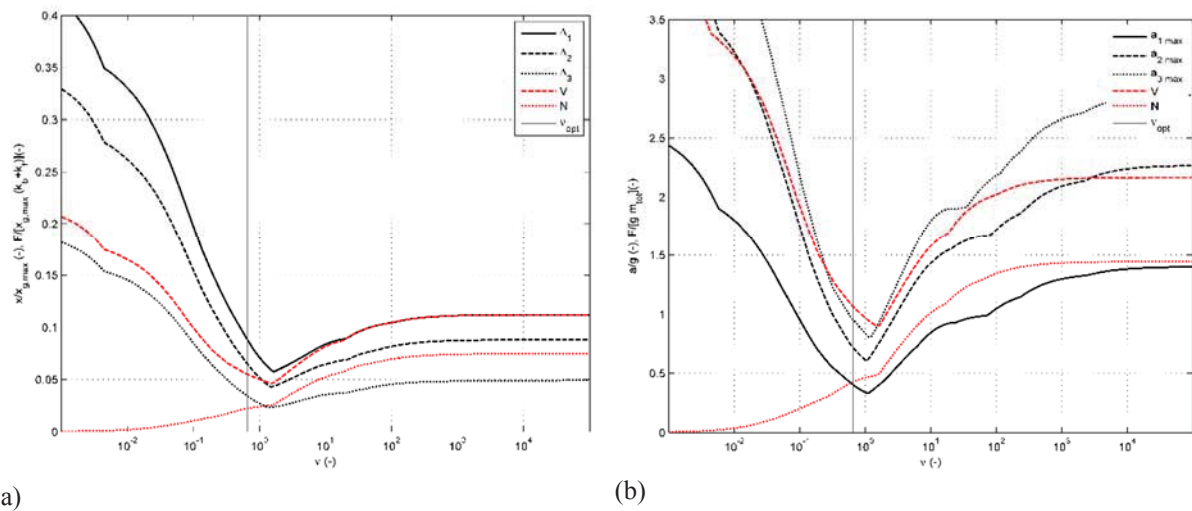
Figure 5.15 Numerical results for case *b* under Northridge ground motion: (a) relative displacements and forces, (b) relative accelerations and forces.

(a)   (b)
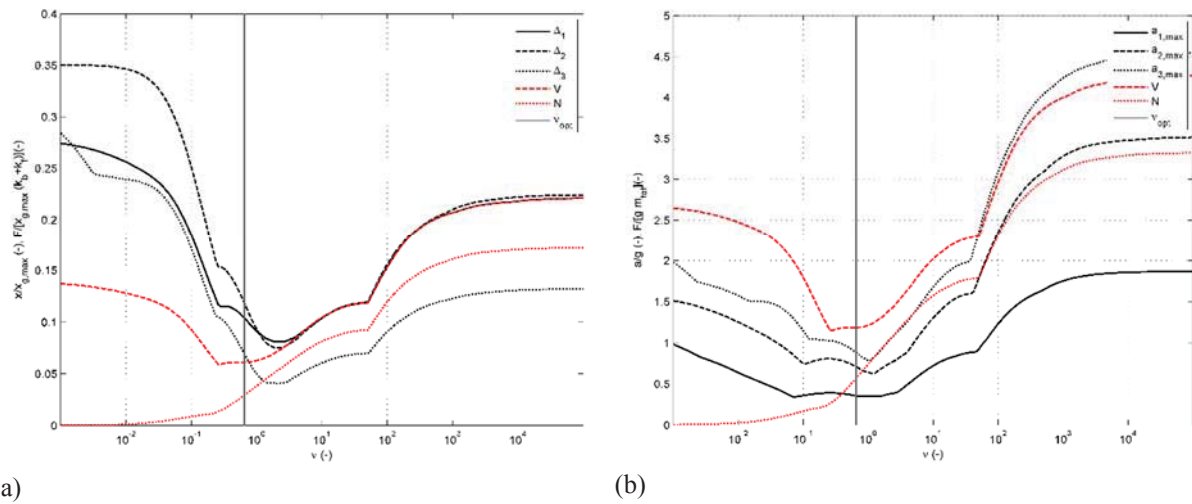
Figure 5.16 Numerical results for case *c* under Northridge ground motion: (a) relative displacements and forces, (b) relative accelerations and forces.

164
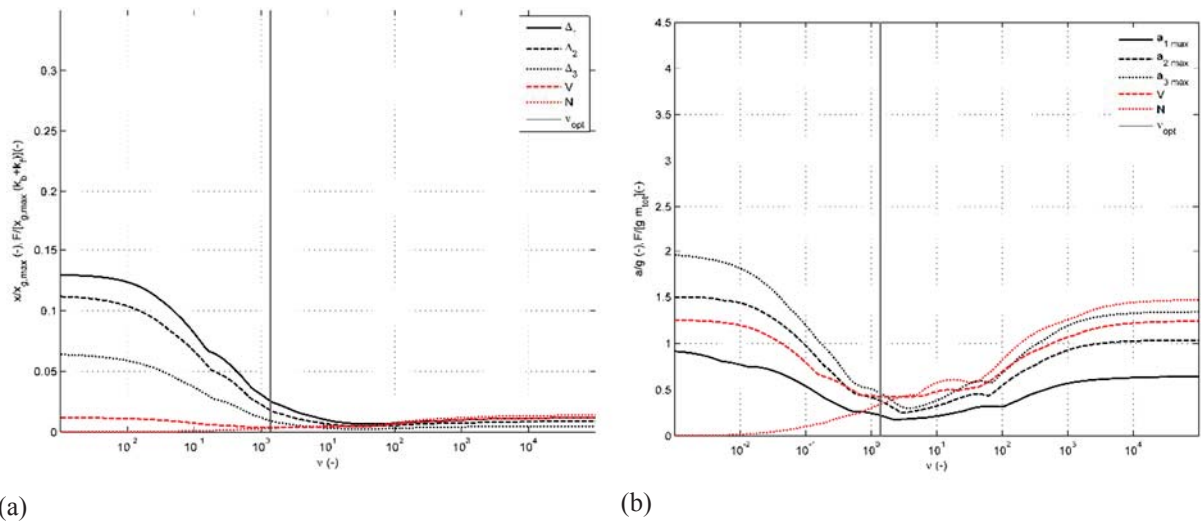
(a)

(b)

Figure 5.17 Numerical results for case *a* under Loma Prieta ground motion: (a) relative displacements and forces, (b) relative accelerations and forces.
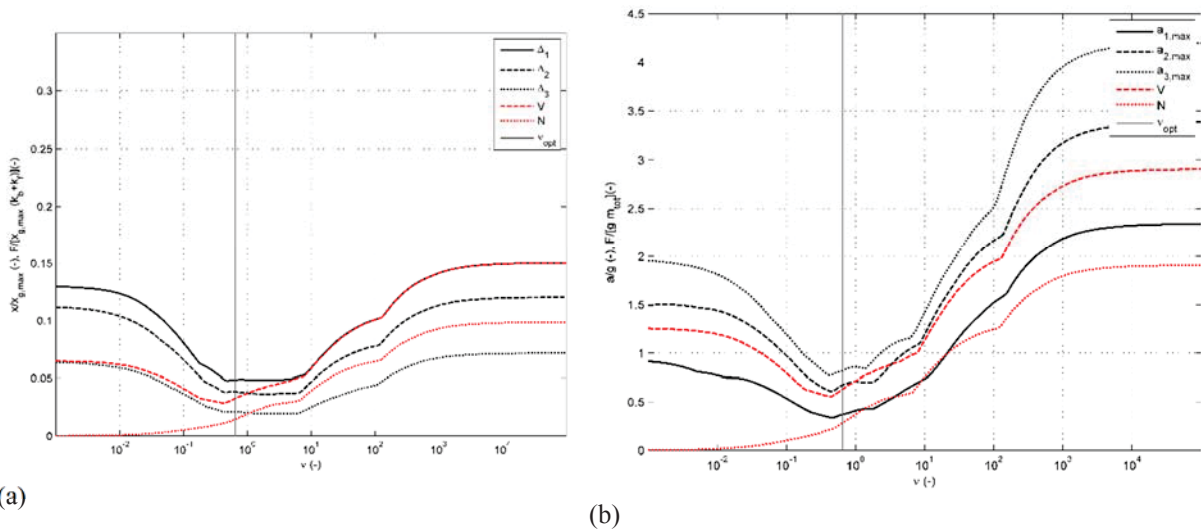
(a)

(b)

Figure 5.18 Numerical results for case *b* under Loma Prieta ground motion: (a) relative displacements and forces, (b) relative accelerations and forces.

(a)   (b)
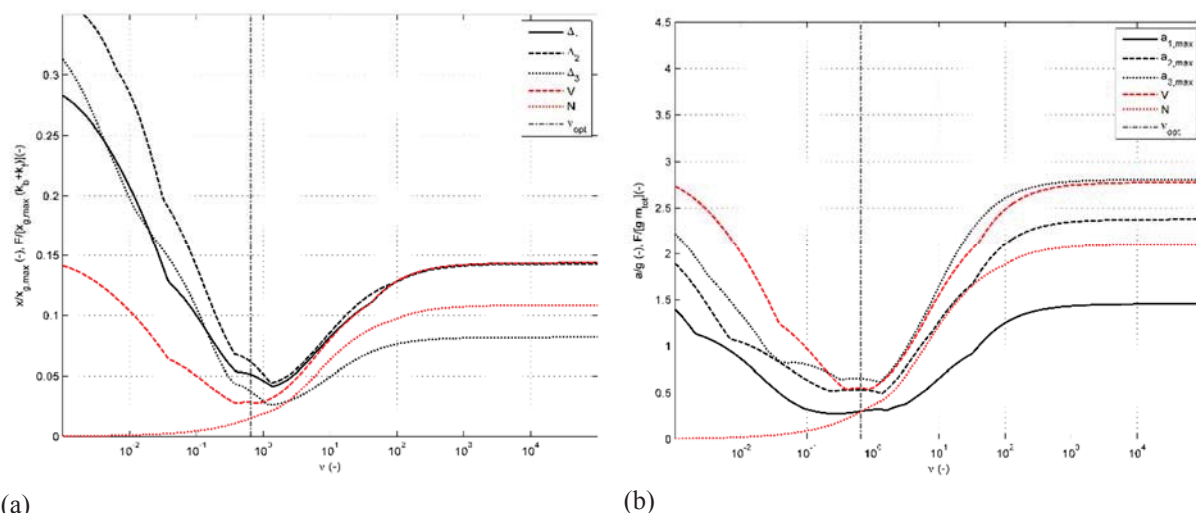
Figure 5.19 Numerical results for case *c* under Loma Prieta ground motion: (a) relative displacements and forces, (b) relative accelerations and forces.

The global behavior of dissipative braced frames is strongly affected by both parameters κ and ν. For a given κ, the variation of ν in the range $10^{-3} \div 10^{5}$ produces a shift of the frame lateral stiffness from the unbraced to the perfectly braced case, that for a shear-type frame means moving from single story stiffness k_f ($\nu \to 0$) to $k_f + k_b$ ($\nu \to \infty$).

In all the analyzed cases, the response in terms of interstory drift, maximum accelerations and base shear, shows a minimum for a value $\bar{\nu}_{opt}$ between the two limit cases. Minimum frame displacements occur for a value of ν larger than that one theoretically proposed, and result, for κ=0.1, almost coincident with those corresponding to the limit case $\nu = \infty$ (rigid frame-to-brace connection). Maximum displacements evaluated for ν_{opt} are strongly reduced with respect to the unbraced case (ν=0).

It is worth to note that minimum accelerations and base shear V_{min} occur for a value $\bar{\nu}_{opt}$ very close to ν_{opt}. In any case the minimum value assumed by the aforementioned quantities is almost equal to the value calculated for ν_{opt}. With respect to this value, higher values of ν would be usually responsible for a worsened condition in terms of maximum accelerations and base shear, due to the predominance of the brace stiffening effect.

Despite this, resultant axial force at the base level due to bracing effect, increases as far as ν increases. The value ν_{opt} resulted a good compromise which allows to optimize at the same time both frame displacements and accelerations, together with the base shear, having a limited effect in terms of additional axial stress in the columns (about $10 \div 40\%$ of the value that would arise in a rigid-braced connection $\nu = \infty$). The assumption of shear-type frame is not limiting,

since even better results are obtained in case of finite beam stiffness, with a full stiffness matrix of the bare frame. For lower values of κ, numerical results confirmed that optimal response is obtained with larger values of ν, also achieving improved efficiency.

5.6 Numerical evaluation of brace-damper efficiency

As in the theoretical case, the efficiency parameter ε has been evaluated as defined in Eq. (5.18), both in terms of base shear and first interstory drift. As expected, this parameter decreases as far as κ increases, even if the numerical curve has lower slope than the theoretical one, the latter representing a lower bound (Figure 5.20Figure 5.19).

(a)

(b)
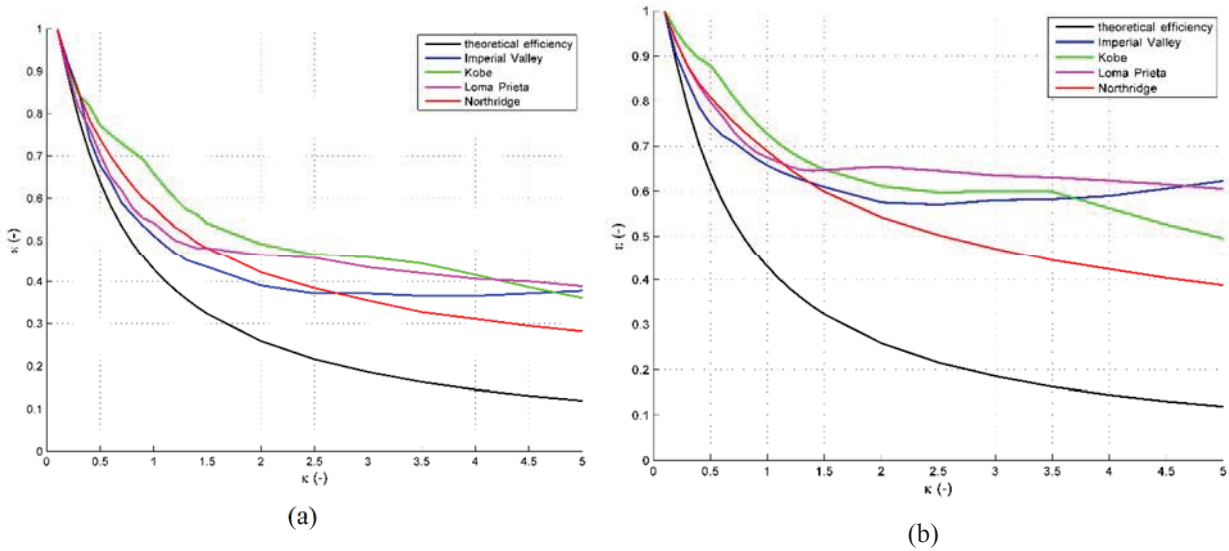
Figure 5.20 Numerical values of the efficiency in terms of (a) first interstory drift and (b) base shear.

With respect to the common practice of neglecting the presence of the supporting brace, some analysis were run assuming the 3 story frame as a 3 DOFs model just having inter-story dampers without any brace, for every value of ν_{opt}. For any κ in the analysis range, the error e is defined as

$$e = 1 - \frac{R(\nu_{opt}, \kappa = \infty)}{R(\nu_{opt}, \kappa)}$$

(5.20)

where:

- $R(\nu_{opt}, \kappa = \infty)$ is the response parameter in the 3 kinematic DOFs model, neglecting the brace;

- $R(\nu_{opt}, \kappa)$ is the response parameter computed in the 6 kinematic DOFs (complete) model, including the brace stiffness κ.

With respect to the real model including the brace effect, this assumption leads almost always

to unsafe evaluations of base shear and interstory drift, with an underestimate of maximum effects about 25÷35% (Figure 5.20). Dependency of error on κ is not immediately clear, due to sensible effect of strong motion parameters.
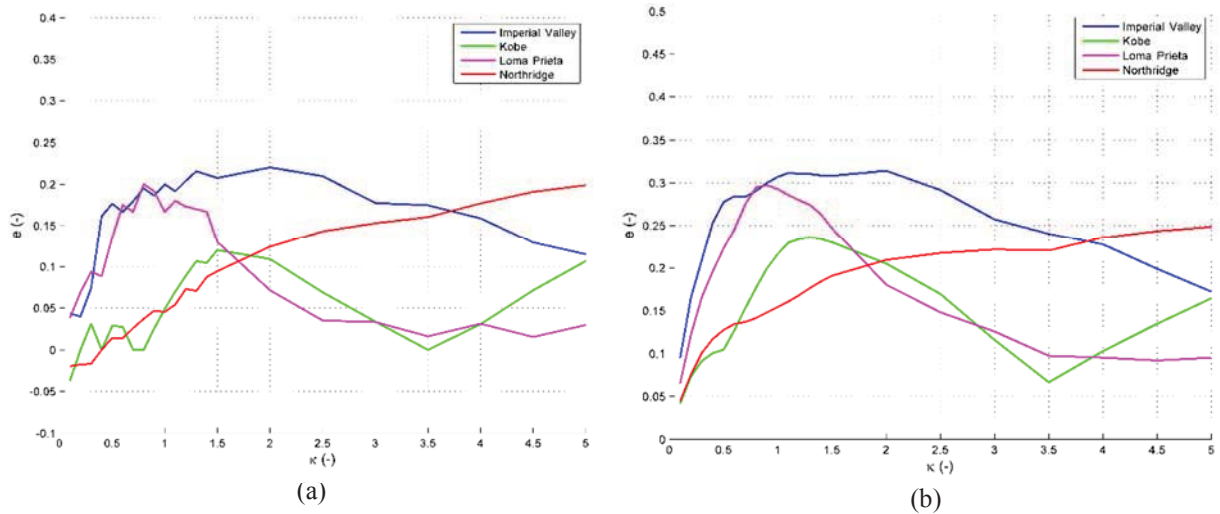
Figure 5.21 Numerical errors for simplified 3 DOFs dynamic model in terms of (a) first interstory drift and (b) base shear.

For interstory drift estimate, just in few cases for $\kappa < 0.5$ a small negative error has been appreciated, meaning that real models provide reduced displacements thanks to the coupling effect generated by the damper between the brace and the frame stiffness, for a high value of v_{opt}. A part from this, base shear estimate is always underestimated.

5.7 Conclusions

The effect of the brace stiffness in energy dissipation mechanism of supplemental viscous dampers is still not fully addressed in design and optimization procedures. Even if it is well known that stiffer braces improve the damping capacity, the exact value of the brace stiffness is usually neglected, while in practice brace dimensions have to be limited for functional or aesthetic requirements. This Chapter properly addresses the effects of the relative frame to brace stiffness parameter on the dynamic behavior and the optimization procedure of a shear type multistory frame.

In the first part of the Chapter, a theoretical study in frequency domain has been developed in order to detect the dynamic behavior of a MDOFs frame equipped with viscous dissipative braces. Each brace mounted in series with a damper was modeled by a Maxwell element having a complex stiffness acting in parallel with the stiffness of the bare frame. The proposed

approach allowed to take into account the effect of the brace stiffness (k_b) on the optimal value of the viscous damping coefficient (C_d), and the effectiveness of the supplemental damping system (ε). It was proved that extremely varying damping coefficients are able to vary the dynamic properties (frequency and mode shapes) of the structure between two limit cases, namely those corresponding to the bare frame ($C_d=0$) and the elastically braced frame ($C_d=\infty$). With the aim to define an optimal damping parameter, defined as the one able to yield the minimum resonance peak in the overall range of frequencies, a numerical solution $\nu_{opt}(\kappa)$ for different MDOFs systems was provided.

The assumptions of elastic frame behavior and negligible inherent structural damping are acceptable, since a strong reduction of demand on structural and non-structural components is expected for an optimally designed supplemental damping system.

In the second part of the Chapter, a wide numerical investigation was carried out on different 3 DOFs concrete frames under different recorded earthquakes, assumed to be subjected to a retrofit intervention by means of viscous dissipative braces. The analysis was devoted to prove the combined effect of the brace-damper stiffness on the dynamic behavior of the frame structures, and to validate the optimization procedure. Time history analyses proved the effectiveness of the theoretically obtained design parameter $\nu_{opt}(\kappa)$.

Both theoretical and numerical results showed the dynamic effect of extremely varying damping coefficients ($0<C_d<\infty$) and the "loss of efficiency" of the dissipative system, due to the finite stiffness of the elastic supporting brace arranged in series with the viscous damper. The common practice to neglect the presence of the supporting brace, just modeling inter-story dampers, may lead to underestimate maximum effects of more than 30%.

An extension of the proposed design method could provide a more effective distribution of the optimal viscous coefficients along the height: the total viscous coefficient $n \cdot \nu_{opt}$ could be assigned according to the inter-story drift distribution. In addition to this, the sum of damper coefficients and their cost were not constrained in the present work, but it is an important issue to be properly considered in practical applications.

REFERENCES

Castaldo P, De Iuliis M (2014) Optimal integrated seismic design of structural and viscoelastic bracing-damper systems. Earthq Eng Struct Dyn 43:1809–1827. doi: 10.1002/eqe.2425

Caughey T (1960) Sinusoidal Excitation of a System with Bilinear Hysteresis. J Appl Mech 32:640–648.

Chen Y-T, Chai YH (2011) Effects of brace stiffness on performance of structures with supplemental Maxwell model-based brace–damper systems. Earthq Eng Struct Dyn 40:75–92. doi: 10.1002/eqe.1023

Chopra AK (2011) Dynamics of Structures: Theory and Applications to Earthquake Engineering. Prentice Hall/Pearson Education

Londoño JM, Neild SA, Wagg DJ (2013) A noniterative design procedure for supplemental brace–damper systems in single-degree-of-freedom systems. Earthq Eng Struct Dyn 42:2361–2367. doi: 10.1002/eqe.2339

Londoño JM, Wagg DJ, Neild SA (2014) Supporting brace sizing in structures with added linear viscous fluid dampers: A filter design solution. Earthq Eng Struct Dyn 43:1999–2013. doi: 10.1002/eqe.2433

Park J-H, Kim J, Min K-W (2004) Optimal design of added viscoelastic dampers and supporting braces. Earthq Eng Struct Dyn 33:465–484. doi: 10.1002/eqe.359

Seismosoft (2013) A computer program for signal processing of strong-motion data. http://www.seismosoft.com.

Singh MP, Moreschi LM (2001) Optimal seismic response control with dampers. Earthq Eng Struct Dyn 30:553–572. doi: 10.1002/eqe.23

Takewaki I (1997) Optimal damper placement for minimum transfer functions. Earthq Eng Struct Dyn 26:1113–1124. doi: 10.1002/(SICI)1096-9845(199711)26:11<1113::AID-EQE696>3.0.CO;2-X

Viola E, Guidi F (2009) Influence of the supporting braces on the dynamic control of buildings with added viscous dampers. Struct Control Heal Monit 16:267–286. doi: 10.1002/stc.234

Chapter 6

6. A PROCEDURE FOR OPTIMAL DESIGN OF THE SEISMIC PROTECTION SYSTEM FOR ISOLATED BRIDGES

6.1 Introduction

Aim of the chapter is the definition of optimal design parameters characterizing the isolation system of a bridge, both in the case of elastomeric (VI) and sliding bearings (SI), having viscoelastic or rigid-plastic behavior, respectively, installed between the piers and the deck (Losanno et al 2014). The problem is treated by means of an analytical approach. Using the frequency response analysis, a simple procedure is proposed to determine the optimal value of the viscous coefficient or the yield displacement of the isolators. The adequacy of the proposed procedure is finally verified through time-history analyses performed on a practical case under natural earthquakes.

6.1 State of the art

The seismic protection of bridge decks by using passive isolation systems represents a widely studied technique since the Eighties (Bhuiyan and Alam 2013), even though different more complex control strategies (e.g., semi-active and active ones) have been investigated and implemented in civil structures in the last twenty years. The design of a passive isolation system

for bridges is often treated as an optimization problem: once the objective of the optimization is defined, together with the constraints imposed by the problem, the design methodology is developed with the aim to determine the optimal mechanical characteristics of the protection devices. In the following, some proposals of different researchers will be summarized, first reporting those adopting optimization concepts in formulating the design criteria.

Ciampi and De Angelis (Ciampi et al 1995) and Ciampi (Ciampi 1998) proposed an energy-based methodology for the optimal design of dissipation devices used as base isolation systems of typical bridges. The approach consisted in the maximization of an appropriate nondimensional energy index defined as the ratio between the energy dissipated by the isolators and the input energy to the controlled bridge. Preliminary numerical results on a single degree of freedom (DOF) system allowed to build manageable design graphs of the optimal mechanical characteristics of the dissipative devices. Further curves were also provided for a check of the relevant structural response quantities and the damage level suffered by the devices.

Hwang & Tseng (Hwang and Tseng 2005) derived some design formulas for both supplemental linear and non-linear viscous dampers to bridge structures. The damping coefficients of the added dampers were determined based on the concept of "composite damping ratio" in which the bridge components such as rubber bearings, piers and abutments may have different stiffnesses, lumped masses and damping ratios. In addition to the validation on a two DOFs simplified bridge model, a three-span bridge model was also used for the seismic response analysis, showing a good agreement with the proposed design formulas.

Paolacci (Paolacci 2013) proposed a criterion to optimize the characteristics of viscoelastic control devices, based on an energy-based index (EDI) as objective function. An optimal design of the control system was obtained by maximizing the EDI index. An interesting outcome was that the multi-objective nature of the index induced a simultaneous reduction of both kinematic and static response quantities. The optimization procedure was applied to a single DOF system, representative of a structure equipped with viscoelastic dampers (VED): the behavior of the latter was modelled using a Maxwell unit. The comparison of the response to simple excitations, like harmonic and white-noise inputs, with the response to synthetic accelerograms, showed that the optimal design of the VED was practically independent of the input. This means that it is possible to obtain preliminary indications on the optimal characteristics of the dampers, even in closed form.

On the other hand, other authors proposed to single out the optimal control system by the results of a wide parametrical investigation on benchmark bridges.

Madhekar and Jangid (Madhekar and Jangid 2009) presented the dynamic behavior of benchmark highway bridges using variable dampers under six bidirectional earthquake ground motions: a viscous damper was used as a passive control device and a variable damper, developed from a magnetorheological (MR) damper, was used as a semi-active control device. The study was based on the simplified lumped-mass finite element model of a highway bridge in Southern California. The prime aim of the study was to investigate the effectiveness of viscous dampers and variable dampers with a friction-type damping force scheme and a two-step viscous damping force scheme, with important parametric variation. Numerical simulations were conducted by installing the devices between the deck and abutments of the bridge: the seismic response of the bridge was compared with the corresponding uncontrolled case, and controlled by alternative sample control strategies.

Ozbulut & Hurlebaus (Ozbulut and Hurlebaus 2011) investigated the seismic response of a multi-span continuous bridge isolated with novel superelastic-friction base isolator (S-FBI), under near-field earthquakes. The isolation system consisted of a flat steel-Teflon sliding bearing and a superelastic NiTi shape memory alloy (SMA) device: while the sliding bearing decouples the superstructure of the bridge from its piers and dissipates energy through friction, the SMA device provides restoring force and additional damping. The key design parameters of an S-FBI system were the natural period of the isolated bridge, the yielding displacement of the SMA device, and the friction coefficient of the sliding bearings. The goal of this study was to obtain optimal values for each design parameter by performing sensitivity analysis of a bridge isolated by an S-FBI system.

In the present chapter, it is adopted the same philosophical approach presented in previous works (Di Marzo et al 2000; Paolacci and Serino 2001), aiming to define the optimal design of an isolation system, in case of elastomeric and sliding bearings. In these two cited works, a simple operative procedure is delivered for singling out the optimal design parameter of a simple 1-DOF system representing an isolated simply supported bridge or a building's isolated floor. The optimal design parameter, in case of both viscoelastic and rigid-plastic isolators, is defined under the action of a harmonic excitation, and then verified for a case study subjected to a seismic input.

The proposed work presents a more complete design methodology for the isolation system, installed between the piers and the bridge deck. This methodology is the result of a detailed analytical treatment of simple dynamic systems incorporating the viscoelastic or rigid-plastic dissipative behaviors. With respect to previous works, the optimization process is developed

also in terms of top pier displacements, besides the deck displacements. Moreover, the proposed procedure includes specific seismic numerical analyses able to immediately confirm the analytical results or, eventually, state the need of a further iteration.

The design procedure proposed in the present chapter is based on a different approach with respect to those adopted by other authors, developing different optimization concepts in formulating the design criteria. In Ciampi and De Angelis (1996), Ciampi (1998) and Paolacci (2013), an energy-based index, related to the energy dissipated by the devices, is formulated as objective function to maximize. Hwang & Tseng (2005) provided design formulas for supplemental linear and non-linear viscous devices for bridge structures, as a function of the desired dissipation level, assumed as given and not correlated to response parameters of the structure.

6.2 Steady-state response of an isolated bridge subjected to a harmonic base motion

The behavior of a simply supported bridge isolated by means of viscoelastic (i.e. laminated rubber bearing *LRB*) or rigid-plastic devices (i.e. friction pendulum system *FPS*), is analyzed (Figure 6.1(a)).

The dynamic model simulating such a simple structure is also illustrated in the same Figure: it is a 2 DOFs model (x, x_c), where the parameters k_c and k_i are the total lateral stiffness of the columns and the bearings, respectively. The procedure is valid in the case of i columns having the same stiffness k_{c1}, being $k_c = i \cdot k_{c1}$, and j isolators of equal stiffness k_{i1}, being $k_i = j \cdot k_{i1}$. The damping behavior is completely defined by the damping coefficient c (in the case of viscoelastic isolators – *VI*) or by the yield strength F_y (in the case of rigid-plastic or sliding isolators – *SI*) of the whole isolation system, thus neglecting damping in the columns. Moreover, m and m_c are the mass of the deck and the participating mass of all piers, respectively. It is worth to note that, in most cases, m_c is small compared to m and therefore can be neglected, so that the model reduces to a single dynamic DOF with two kinematic DOFs (Figure 6.1(b)).

The dynamic problem of the bridge subjected to a harmonic base excitation can be formulated and solved as shown in the following. The equations of motion are derived together with the definition of the relevant design parameters and response quantities, and the optimal damping characteristics are obtained under the hypothesis that the ratio $\kappa = k_c / k_i$ and the deck mass m are known. For both *VI* and *SI* cases, a closed-form solution of the response is obtained.

Even if earthquake motion is usually random, by means of the Discrete Fourier Transform Function (DFT), properly working on non-periodic data, it can be decomposed into a linear combination of harmonic functions. Typical ground motions contain a wide range of frequencies and system displacement response shows a dominant period very close to its natural period. A sweeping frequency of the excitation (i.e., harmonic function with $0 \le \omega \le \infty$) at the base is assumed, since due to extremely different values of the damping parameter, the effective frequency of the system vary significantly. In addition to this, for a damped system, the higher is the damping the shorter will be the transitory condition so that structural response will tend to a single period harmonic function.
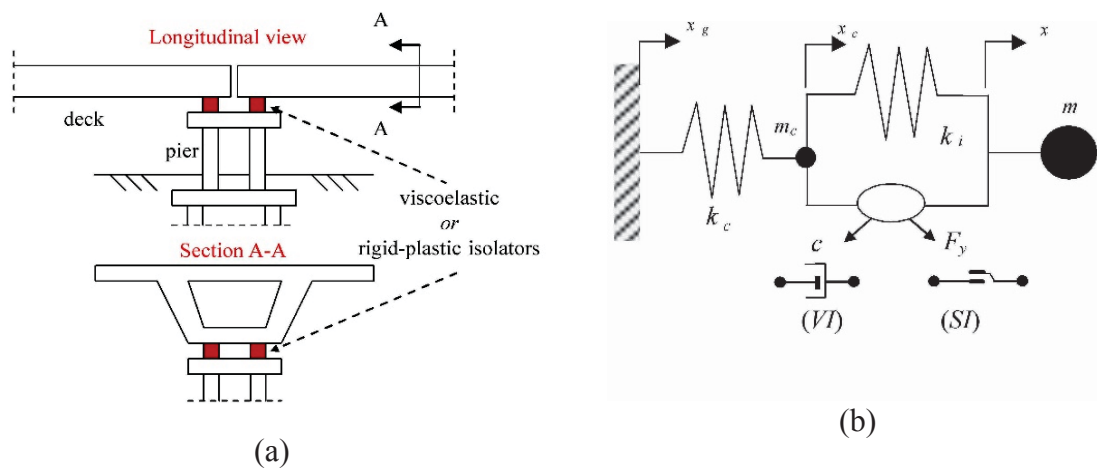
Figure 6.1 (a) Bridge structure and (b) rheological model

The problem is first solved by making reference to the deck displacement x: the optimization procedure is developed with the aim to determine the value of the normalized device's damping parameter ($\nu_{i,opt}$ or δ_{opt}) corresponding to the minimum deck displacement over the whole range of frequency excitation.

On the other hand, different parameters can be also assumed as reference: the displacement of columns x_c in order to control the column base shear, or the relative displacement $x - x_c$ in the isolators in order to check the maximum allowable movement between the deck and the top of columns.

175

6.2.1 Formulation of the equation of motion

Neglecting the participating mass of the piers ($m_c = 0$), the general expression of the equation of motion for the model illustrated in Figure 6.1(b), subjected to a harmonic base displacement $x_g(t) = x_{g,max} \cdot \cos \overline{\omega} t$, is simply the following:

$$m\ddot{x} + F(x, x_c, \dot{x}, \dot{x}_c, ...) = m\overline{\omega}^2 x_{g,max} \cos \overline{\omega} t \tag{6.1}$$

where x is the relative deck displacement, $F(x, x_c, \dot{x}, \dot{x}_c, ...)$ is the linear or non-linear restoring force in the whole system and dot notation represents derivation with respect to time.

In order to single out the relevant design parameters of the control devices and the structural response parameters, it is needed to write Eq. (6.1) in an adimensionalized form. Afterwards, introducing the non-dimensional time $\tau = \Omega t$, a different normalized form of the equation of motion can be found, being Ω a normalization frequency corresponding to the natural frequency of the system in one of the three following cases:

i) infinitely stiff piers ($k_c \to \infty$): $\omega_i = \sqrt{k_i/m}$

ii) undamped system ($c = 0$ or $F_y = 0$): $\omega_b = \sqrt{k_c k_i/(k_c + k_b) \cdot m}$

iii) not isolated bridge ($k_i \to \infty$): $\omega_c = \sqrt{k_c/m}$

Considering the non-dimensional time parameter $\tau = \omega_i t$, Eq. (6.1) can be expressed as:

$$\omega_i^2 x''(\tau) + \frac{F(x, x_c, \dot{x}, \dot{x}_c, ...)}{m} = \overline{\omega}^2 x_{g,max} \cos \beta \tau \tag{6.2}$$

where ($'$) represents derivation with respect to τ. After simple manipulations:

$$x''(\tau) + \frac{F(x, x_c, \dot{x}, \dot{x}_c, ...)}{m\omega_i^2} = \beta^2 x_{g,max} \cos \beta \tau \tag{6.3}$$

$$\zeta''(\tau) + \frac{F(x, x_c, \dot{x}, \dot{x}_c, ...)}{m\omega_i^2 x_{g,max}} = \beta^2 \zeta(\tau) \cos \beta \tau \tag{6.4}$$

$$\zeta''(\tau) + \kappa f(\zeta) = \beta^2 \zeta(\tau) \cos \beta \tau \tag{6.5}$$

where $\zeta = x/x_{g,max}$ is the normalized deck displacement, $f(\zeta) = F(x, x_c, \dot{x}, \dot{x}_c, ...)/k_c x_{g,max}$ is the normalized restoring force, $\beta = \overline{\omega}/\omega_i$ is the normalized frequency. Eq. (6.5) represents the final form of the normalized equation of motion and it is developed in the following paragraphs for the two defined cases.

6.2.2 Solution of the equation of motion for the VI case

In the case of viscoelastic isolators (*VI*) having damping coefficient c, the equivalent damping ratio is defined as:

$$v_i = \frac{c}{2m\omega_i} \tag{6.6}$$

The force in the passive control system, i.e. the base shear of the pier, can be expressed in the frequency domain through the complex response method:

$$F(\overline{\omega}) = (k_i + i\overline{\omega}c) \cdot (x(\overline{\omega}) - x_c(\overline{\omega})) \tag{6.7}$$

Since the top column displacement is given by $x_c(\overline{\omega}) = F(\overline{\omega})/k_c$, Eq. (6.7) can be rewritten as:

$$F(\overline{\omega}) = (k_i + i\overline{\omega}c) \cdot (x(\overline{\omega}) - \frac{F(\overline{\omega})}{k_c}) = K_d(\overline{\omega}) \cdot x(\overline{\omega}) \tag{6.8}$$

where:

$$K_d(\overline{\omega}) = \frac{F(\overline{\omega})}{x(\overline{\omega})} = \frac{k_i + i\overline{\omega}c}{1 + \dfrac{k_i + i\overline{\omega}c}{k_c}} \tag{6.9}$$

represents the complex stiffness of the controlled bridge.

Dividing Eq. (6.9) by k_c, the dimensionless system stiffness is:

$$\overline{K}_d(\overline{\omega}) = \frac{\dfrac{1}{\kappa} + \dfrac{i\overline{\omega}c}{k_c}}{\dfrac{1+\kappa}{\kappa} + \dfrac{i\overline{\omega}c}{k_c}} \tag{6.10}$$

Substituting Eq. (6.6) in Eq. (6.10), the normalized stiffness becomes:

$$\overline{K}_d(\beta) = \frac{\dfrac{1}{\kappa} + \dfrac{i2v_i\beta}{\kappa}}{\dfrac{1+\kappa}{\kappa} - \dfrac{i2v_i\beta}{\kappa}} = \frac{\dfrac{(1+\kappa)}{\kappa^2} + 4v_i^2\dfrac{\beta^2}{\kappa^2}}{(\dfrac{1+\kappa}{\kappa})^2 + 4v_i^2\dfrac{\beta^2}{\kappa^2}} + i\frac{2v_i\dfrac{\beta}{\kappa}}{(\dfrac{1+\kappa}{\kappa})^2 + 4v_i^2\dfrac{\beta^2}{\kappa^2}} = \tag{6.11}$$

$$= \overline{K}_d'(\beta) + i\overline{K}_d''(\beta)$$

where $\overline{K}_d'(\beta)$ and $\overline{K}_d''(\beta)$ are, respectively, the overall normalized storage and loss modulus of the controlled bridge.

The normalized restoring force of Eq. (6.5) becomes:

$$f(\zeta) = \overline{K}_d(\beta) \cdot \zeta \tag{6.12}$$

and is illustrated in Figure 6.2.
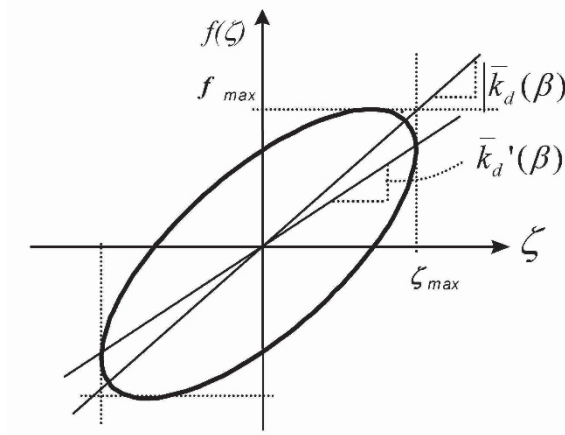
Figure 6.2 Normalized restoring force - displacement relationship for the VI case.

The global dynamic behavior of a rubber isolated bridge is completely defined by three parameters: κ, ν_i and β.

In this case, the system is linear and an exact solution for the steady-state response can be evaluated. The solution of Eq. (6.5) is extremely straightforward using the frequency domain approach.

Assuming that a solution of Eq. (5) can be expressed in the form $\zeta(\tau) = \zeta_{max}(\beta)e^{i(\beta\tau + \phi(\tau))}$, the Fourier transform applied to Eq. (6.5) gets:

$$-\beta^2 \zeta_{max}(\beta) + \kappa(\overline{K}'_d(\beta) + i\overline{K}''_d(\beta))\zeta_{max}(\beta) = \beta^2 \qquad (6.13)$$

where the storage modulus $\overline{K}'_d(\beta)$ and loss modulus $\overline{K}''_d(\beta)$ are those defined in Eq. (6.11). From Eq. (6.13) it is possible to express the complex response of the bridge in terms of maximum deck displacement:

$$\zeta_{max}(\beta) = \frac{\beta^2}{\left[\kappa\overline{K}'_d(\beta) - \beta^2\right] + i\kappa\overline{K}''_d(\beta)} \qquad (6.14)$$

The amplitude of the response and its phase angle can be evaluated respectively as the modulus and the argument of the above complex relationship:

$$\left|\zeta_{max}(\beta)\right| = \frac{\beta^2}{\sqrt{\left[\kappa\overline{K}'_d(\beta) - \beta^2\right]^2 + \kappa^2\overline{K}''_d(\beta)^2}} \qquad (6.15)$$

$$\tan\phi(\beta) = \frac{\kappa\overline{K}''_d(\beta)}{\kappa\overline{K}'_d(\beta) - \beta^2} \qquad (6.16)$$

178

The relations (6.15) and (6.16) are simply an extension of the classical amplitude – frequency and phase angle – frequency relationships for a standard linear elastic oscillator subjected to a harmonic base motion.

Introducing the definitions of storage and loss moduli in (6.15) and (6.16), they become:

$$|\zeta_{max}(\beta)| = \frac{\beta^2}{\sqrt{\left[\frac{\frac{(1+\kappa)}{\kappa} + 4v_i^2 \frac{\beta^2}{\kappa}}{\left(\frac{1+\kappa}{\kappa}\right)^2 + 4v_i^2 \frac{\beta^2}{\kappa^2}} - \beta^2\right]^2 + \kappa^2 \left(\frac{2v_i \frac{\beta}{\kappa}}{\left(\frac{1+\kappa}{\kappa}\right)^2 + 4v_i^2 \frac{\beta^2}{\kappa^2}}\right)^2}} \tag{6.17}$$

$$\tan\phi(\beta) = \frac{2v_i\beta}{\frac{(1+\kappa)}{\kappa} + 4v_i^2 \frac{\beta^2}{\kappa} - \beta^2} \tag{6.18}$$

Eq. (6.17) is plotted in Figure 6.3 for different values of κ and damping ratio v_i.

The two limit cases, for which the behavior reduces to an elastic undamped system, are the following:

$v_i = 0 \quad \Rightarrow \quad c = 0$ (no damping)

$$|\zeta_{max}(\beta)| = \frac{\beta^2}{\frac{\kappa}{1+\kappa} - \beta^2}; $$

$$\beta_{resonance} = \sqrt{\frac{\kappa}{(1+\kappa)}} \tag{6.19}$$

$v_i \rightarrow +\infty \quad \Rightarrow \quad c \rightarrow +\infty$ (infinite damping)

$$|\zeta_{max}(\beta)| = \frac{\beta^2}{\kappa - \beta^2}; $$

$$\beta_{resonance} = \sqrt{\kappa} \tag{6.20}$$

The two limit curves intersect in the point of coordinates $\overline{\beta} = \sqrt{(2\kappa + \kappa^2)/[2(1+\kappa)]}$ and $\zeta_{max}(\overline{\beta}) = (2+\kappa)/\kappa$. A very low value of v_i produces a peak of the curve near to the one of the no damping limit case. This peak decreases as far as v_i increases but a large increase of the damping coefficient induces a shift of the resonance frequency toward the infinite damping limit case, with an increment, at the same time, of the peak amplitude. For $\beta = \overline{\beta}$, Eq. 6.17

gives $\zeta_{max}(\overline{\beta}) = (2+\kappa)/\kappa$ for any other value of υ_i, thus demonstrating that the point of coordinates $(\overline{\beta}, \zeta_{max}(\overline{\beta}))$ is a common point for all curves.

The value of $\nu_{i,opt}$ can be computed by imposing the condition that the above common point ($\overline{\beta}, \zeta_{max}(\overline{\beta})$) corresponds to the maximum of the generic curve, i.e., by imposing that $\zeta'_{max}(\overline{\beta}) = 0$. In this way, we get the following 3rd degree equation in the unknown υ_i^2 :

$$8(2k+k^2)^3 \upsilon_i^6 + 4(2k^2+3k+1)(2k+k^2)^2(1+k)\upsilon_i^4 + ...$$
$$.... + 2(2k+k^2)(1+k)^5(k-1)\upsilon_i^2 - (1+k)^8 = 0$$

(6.21)

whose only real solution (all the other solutions are complex) is:

$$\nu_{i,opt} = \sqrt{\frac{(1+\kappa)^2}{2\kappa(2+\kappa)}}$$

(6.22)

Therefore, the minimum resonance peak within the range $\nu_i = [0, +\infty]$ corresponds to the optimal resonance frequency $\beta_{opt} = \overline{\beta}$.
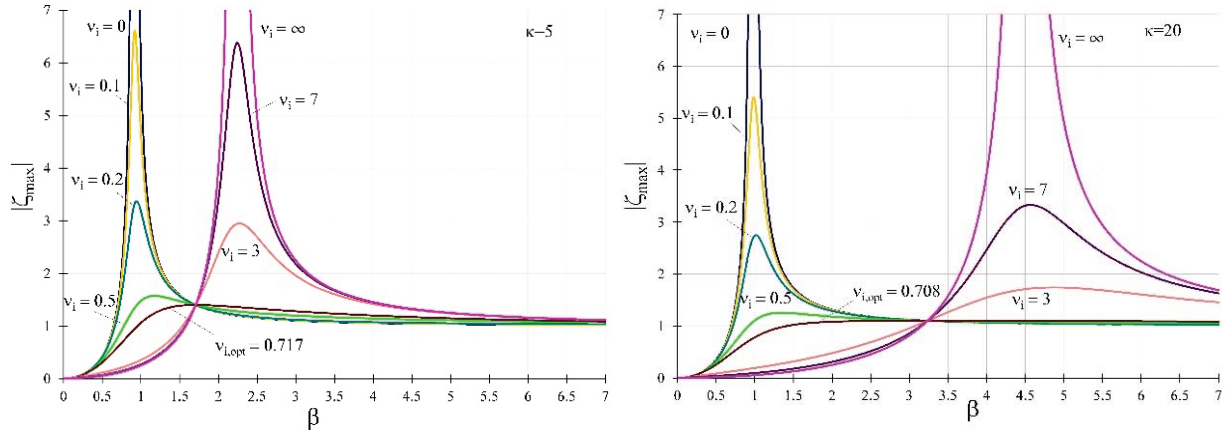
Figure 6.3 Maximum deck displacement versus frequency ratio β (κ = 5, 20).

The complex expression of the maximum force in the pier (equal to its normalized displacement), as well as in the control system, is given by:

$$f_c(\beta) = \zeta_{c,max}(\beta) = \overline{K}_d(\beta) \frac{\beta^2}{[\kappa \overline{K}'_d(\beta) - \beta^2] + i\kappa \overline{K}''_d(\beta)}$$

(6.23)

Figure 6.4 shows the modulus of Eq. (6.23) as function of the frequency ratio β. It can be noted again that all curves have a common point corresponding to the intersection between the limit curves. The intersection point has now coordinates $\overline{\beta}_c = \sqrt{\frac{2\kappa}{2+\kappa}}$ and $\overline{\zeta}_{c,max} = \frac{2}{\kappa}$ but this point

180

does not represent a maximum for all the curves. For $v_i \to \infty$ the column displacement is practically the same as the deck displacement. For all finite values of $v_i \neq 0$, $\zeta_{c,\max}(\beta)$ is always lower than $\zeta_{\max}(\beta)$ even if for $\beta \to \infty$ both $\zeta_{\max}(\beta)$ and $\zeta_{c,\max}(\beta)$ tend to 1.

On the other hand, the quantity $\Delta\zeta = \zeta_{\max} - \zeta_{c,\max}$ (see Figure 6.5) is always decreasing with increasing v_i.
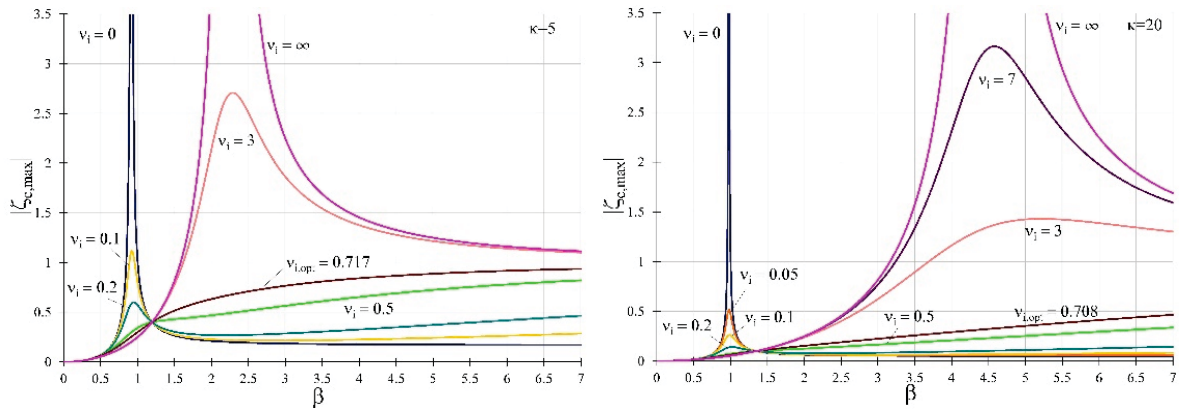
Figure 6.4 Top column displacement versus frequency ratio β ($\kappa = 5, 20$).
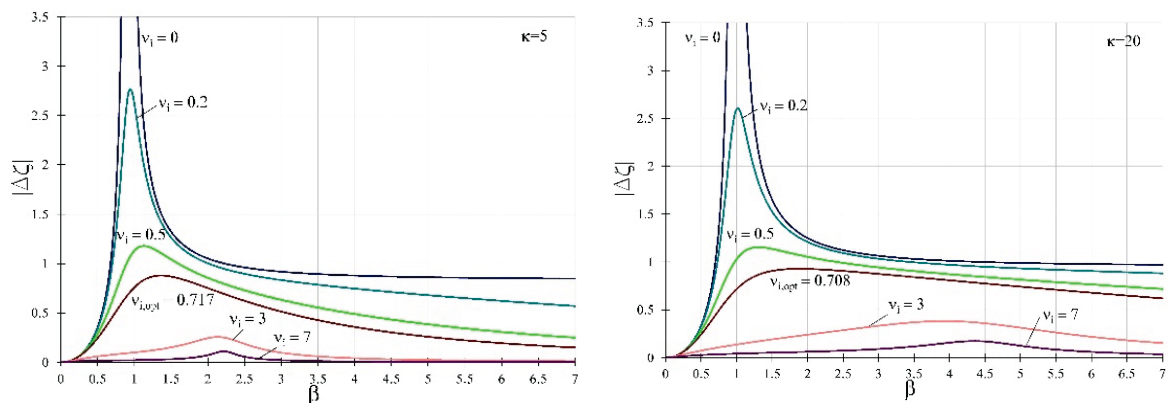
Figure 6.5 Relative deck to pier displacement versus frequency ratio β ($\kappa = 5, 20$).

An optimization criterion for the design of the control system is the minimization of the maximum displacement $\zeta_{\max}(\beta)$ in the whole range of β, and the check a posteriori of the response in terms of base-shear. This means to select as design parameter the value $v_{i,opt}$ given in Eq. 6.22: a design spectrum is showed in Figure 6.6(a), for several values of κ. High values of damping ratio are required for small values of κ, whereas, for $\kappa > 10$ $v_{i,opt}$ remains practically constant around the value 0.7. It is interesting to note in Figure 6.6(b) that the optimum deck displacement, i.e. the minimum resonance peak for any value of κ given by

$v_{i,opt}$, decreases with κ and tends to 1. For values of κ greater than $20 \div 30$, a small decrease in the optimum response is produced.
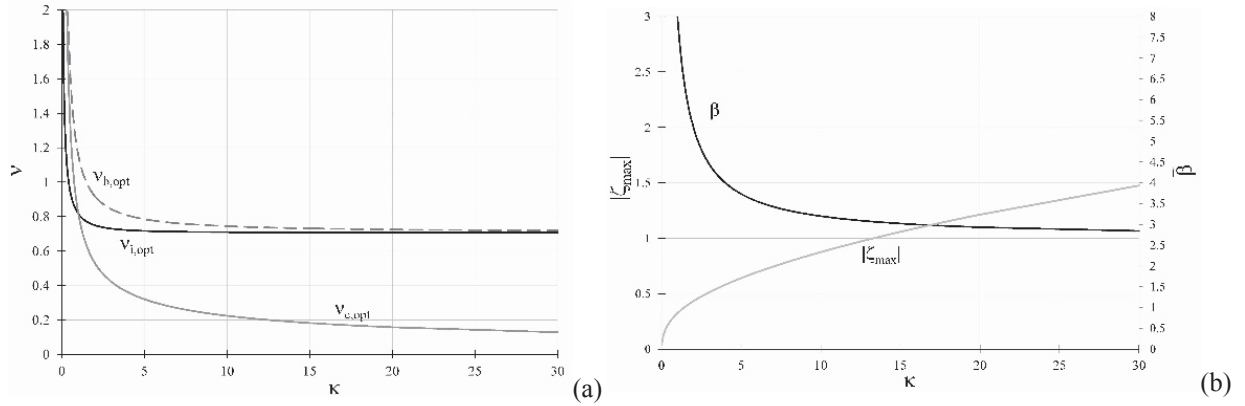
Figure 6.6 (a) *VI* optimal parameters for different normalizations and (b) deck optimal displacement and corresponding frequency ratio versus κ.

If the other two expressions of the normalized frequency Ω are used, the expression of the optimal parameter can be easily evaluated as follows, and is also shown in Figure 6.6(a):

$$v_{b,opt} = \frac{c_{opt}}{2m\omega_b} = \sqrt{\frac{1+\kappa}{\kappa}}\frac{c_{opt}}{2m\omega_i} = \sqrt{\frac{(1+\kappa)^3}{2\kappa^2(2+\kappa)}} \qquad (6.24)$$

$$v_{c,opt} = \frac{c_{opt}}{2m\omega_c} = \frac{1}{\sqrt{\kappa}}\frac{c_{opt}}{2m\omega_i} = \sqrt{\frac{(1+\kappa)^2}{2\kappa^2(2+\kappa)}} \qquad (6.25)$$

6.2.3 Solution of the equation of motion for the SI case

In the case of sliding isolators (*SI*), the restoring force $F(x, x_c, \dot{x}, \dot{x}_c...)$ is a bilinear relationship characterized by an initial stiffness k_c and a post-yielding stiffness $k_c k_i / (k_c + k_i)$. The supplemental device has a rigid-plastic behavior (Figure 6.7(a)) modeled by a spring (k_i) acting in parallel with a friction element (sliding force F_y).

The normalized restoring force is shown in Figure 6.7(b). It depends on two dimensionless parameters $\kappa = k_c/k_i$ and δ. The normalized initial stiffness is equal to unity while the post-elastic stiffness becomes $1/(1+\kappa)$; δ is the normalized deck displacement $x_y/x_{g,max}$ corresponding to the achievement of yielding in the device, and it is equal to the normalized yield strength f_y.
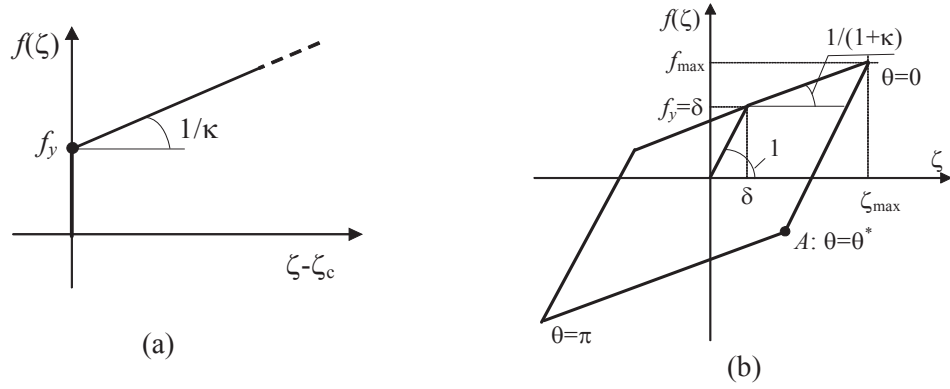
Figure 6.7 Normalized restoring force-displacement relationships (a) in the sliding isolators and (b) in the controlled bridge.

On the basis of the observations above, it is possible to state that the dynamic behavior of the *SI* bridge case is completely defined by the following three dimensionless parameters: κ, δ and β.

The equation of motion is non-linear and a closed form solution cannot be easily derived. In the following, the slowly varying parameters method (Caughey 1960) is adopted. It can be reasonably assumed that, under a harmonic base motion, the steady-state response is periodic with frequency β:

$$\zeta(\tau) = \zeta_{max}(\tau)\cos[\beta\tau + \phi(\tau)] = \zeta_{max}\cos\theta \tag{6.26}$$

where ζ_{max} and ϕ are slowly varying functions of τ, and $\theta = \beta\tau + \phi(\tau)$. Differentiating Eq. (6.26) with respect to τ, one obtains:

$$\zeta'(\tau) = -\beta\zeta_{max}\sin\theta - \zeta_{max}\phi'\sin\theta + \zeta'_{max}\cos\theta \tag{6.27}$$

For the hypothesis of the slowly varying parameters method, it is possible to approximate the values of ζ_{max} and ϕ by their mean values and to assume that the velocity $\zeta'(\tau)$ is harmonic, i.e:

$$\zeta'_{max}\cos\theta - \zeta_{max}\phi'\sin\theta = 0 \tag{6.28}$$

Differentiating again Eq. (6.27) with respect to τ:

$$\zeta''(\tau) = -\beta^2\zeta_{max}\cos\theta - \beta\zeta_{max}\phi'\cos\theta - \beta\zeta'_{max}\sin\theta \tag{6.29}$$

and substituting it in Eq. (6.5), leads to:

$$-\beta^2\zeta_{max}\cos\theta - \beta\zeta_{max}\phi'\cos\theta - \beta\zeta'_{max}\sin\theta + \kappa f(\zeta) = \beta^2\zeta_{max}\cos(\theta-\phi) \tag{6.30}$$

We can multiply Eq. (6.30) by $\sin\theta$ and Eq. (6.28) by $\beta\cos\theta$ and subtract them, thus obtaining:

$$-\beta^2\zeta_{max}\sin\theta\cos\theta - \beta\zeta'_{max}(\sin^2\theta + \cos^2\theta) + \kappa f(\zeta)\sin\theta = \beta^2\cos(\theta-\phi)\sin\theta \tag{6.31}$$

183

The average made over one cycle of θ leads to:

$$-\beta\zeta'_{max} + \frac{1}{2\pi}\int_0^{2\pi}\kappa f(\zeta)\sin\theta d\theta = \frac{\beta^2}{2}\sin\phi \tag{6.32}$$

Now, multiplying Eq. (6.28) by $\beta\sin\theta$, Eq. (6.30) by $\cos\theta$ and adding them:

$$-\beta^2\zeta_{max}\cos^2\theta - \beta\zeta_{max}\phi' + \kappa f(\zeta)\cos\theta = \beta^2\cos(\theta-\phi)\cos\theta \tag{6.33}$$

and averaging over one cycle of θ, one obtains:

$$-\beta\zeta_{max}\phi' - \frac{\beta^2}{2}\zeta_{max} + \frac{1}{2\pi}\int_0^{2\pi}\kappa f(\zeta)\cos\theta d\theta = \frac{\beta^2}{2}\cos\phi \tag{6.34}$$

If $S(\zeta_{max})$ and $C(\zeta_{max})$ are the two quantities:

$$S(\zeta_{max}) = \frac{1}{\pi}\int_0^{2\pi}f(\zeta)\sin\theta d\theta$$
$$C(\zeta_{max}) = \frac{1}{\pi}\int_0^{2\pi}f(\zeta)\cos\theta d\theta \tag{6.35}$$

hence Eqs. (6.32) and (6.34) become:

$$-2\beta\zeta'_{max} + \kappa S(\zeta_{max}) = \beta^2\sin\phi$$
$$-2\beta\zeta_{max}\phi' - \beta^2\zeta_{max} + \kappa C(\zeta_{max}) = \beta^2\cos\phi \tag{6.36}$$

Using Figure 6.7(b), if $\theta* = \cos^{-1}\left(1-\dfrac{2\delta}{\zeta_{max}}\right)$ the quantities $S(\zeta_{max})$ and $C(\zeta_{max})$ are readily

evaluated:

$$\begin{cases} S(\zeta_{max}) = -\dfrac{\kappa}{1+\kappa}\dfrac{\zeta_{max}}{\pi}\sin^2\theta* & \text{if} \quad \zeta_{max} > \delta \\ S(\zeta_{max}) = 0 & \text{if} \quad \zeta_{max} \leq \delta \end{cases} \tag{6.37}$$

$$\begin{cases} C(\zeta_{max}) = \dfrac{\zeta_{max}}{\pi}\left[\dfrac{\kappa}{1+\kappa}\theta* + \dfrac{\pi}{1+\kappa} - \dfrac{\kappa}{2(1+\kappa)}\sin 2\theta*\right] & \text{if} \quad \zeta_{max} > \delta \\ C(\zeta_{max}) = \zeta_{max} & \text{if} \quad \zeta_{max} \leq \delta \end{cases} \tag{6.38}$$

The steady state response is obtained by setting $\zeta'_{max}(\tau)$ and $\phi'(\tau)$ equal to zero in Eq. (6.36),

which becomes:

$$\kappa S(\zeta_{max}) = \beta^2\sin\phi$$
$$\kappa C(\zeta_{max}) - \beta^2\zeta_{max} = \beta^2\cos\phi \tag{6.39}$$

Eliminating ϕ and β^2 from Eq. (39), we get the following displacement – frequency and phase

angle – frequency relationships in the unknowns ζ_{max} and ϕ:

$$\left[C(\zeta_{max}) - \frac{\beta^2}{\kappa}\zeta_{max}\right]^2 + \left[S(\zeta_{max})\right]^2 = \frac{\beta^4}{\kappa^2} \tag{6.40}$$

$$\tan\phi = \frac{S(\zeta_{max})}{C(\zeta_{max}) - \frac{\beta^2}{\kappa}\zeta_{max}} \tag{6.41}$$

Differently from the *VI* case, now it is convenient to express the quantity ζ_{max} implicitly as a function of β from Eq. (40):

$$\frac{\beta^2}{\kappa} = \left[\zeta_{max}C(\zeta_{max}) \pm \sqrt{\zeta_{max}^2 C^2(\zeta_{max}) - (\zeta_{max}^2 - 1)(C^2(\zeta_{max}) + S^2(\zeta_{max}))}\right] \Big/ (\zeta_{max}^2 - 1) \tag{6.42}$$

The maximum deck displacement ζ_{max} is attained at the point where β^2 has a double root, i.e. for the value $\tilde{\zeta}_{max}$ which makes void the radical quantity in Eq. (6.42), i.e. satisfies the equation:

$$\tilde{\zeta}_{max}^2 = C^2(\tilde{\zeta}_{max})/S^2(\tilde{\zeta}_{max}) + 1$$

$$\tilde{\zeta}_{max}^2 - \frac{\left\{\kappa\arccos\left(1 - \frac{2\delta}{\tilde{\zeta}_{max}}\right) + \pi - \frac{\kappa}{2}sen\left[2\arccos\left(1 - \frac{2\delta}{\tilde{\zeta}_{max}}\right)\right]\right\}^2}{\kappa^2 sen^4\left[\arccos\left(1 - \frac{2\delta}{\tilde{\zeta}_{max}}\right)\right]} - 1 = 0 \tag{6.43}$$

and the corresponding frequency is:

$$\tilde{\beta} = \sqrt{\kappa S(\tilde{\zeta}_{max})\sqrt{S^2(\tilde{\zeta}_{max}) + C^2(\tilde{\zeta}_{max})}\Big/C(\tilde{\zeta}_{max})} \tag{6.44}$$

The limit cases ($\delta = 0$ and $\delta \to +\infty$) again correspond, respectively, to the case of two springs (k_c and k_i) connected in series or a single spring (k_c), and are expressed as $\beta(\zeta_{max})$:

$$\delta = 0 \quad \Rightarrow \quad F_{dy} = 0$$

$$\beta^2 = \frac{\kappa\zeta_{max}}{(1+\kappa)(1+\zeta_{max})};$$

$$\beta_{resonance} = \sqrt{\frac{\kappa}{(1+\kappa)}} \tag{6.45}$$

$$\delta \to +\infty \quad \Rightarrow \quad F_{dy} \to +\infty$$

$$\beta^2 = \frac{k\zeta_{max}}{(1+\zeta_{max})};$$

$$\beta_{resonance} = \sqrt{\kappa} \tag{6.46}$$

185

The function $\beta^2(\zeta_{max})$ in Eq. (6.42) is a continuous function whose derivative is discontinuous when $\zeta_{max} = \delta$. This is because the response is linear for any value of $\zeta_{max} < \delta$, being the flexibility of the system due to the only spring k_c.

By analyzing the frequency response function $\zeta_{max}(\beta)$, it is possible to figure out the role of the parameter δ and propose a design methodology for determining its optimal value.

The quantity ζ_{max} as a function of β is plotted in Figure 6.8 for $\kappa = 5, 20$ and for several values of δ. The point of coordinates $\overline{\beta} = \sqrt{(2\kappa + \kappa^2)/[2(1+\kappa)]}$ and $\zeta_{max}(\overline{\beta}) = (2+\kappa)/\kappa$ still represents the intersection of the two limit cases (Eqs. (6.45) and (6.46)) but does not belong to all other curves. One notes that a very low value of δ produces a peak of the curve near to the one relative to $\delta = 0$, and its value decreases as far as the previous parameter increases; however, a further increase of the yield displacement induces a shift of the resonance frequency toward the value $\beta = \sqrt{\kappa}$ with an increment of the peak amplitude. Therefore, the resonance peak within the range $\delta = [0, +\infty]$ has a minimum value in correspondence of the frequency β_{opt}, quite close to the one ($\overline{\beta}$) of the intersection point between the limit curves. Therefore, settled a certain κ, the value δ_{opt} is defined as the one which satisfies the condition that its corresponding curve $\zeta_{max}(\beta)$ has the minimum resonance peak.
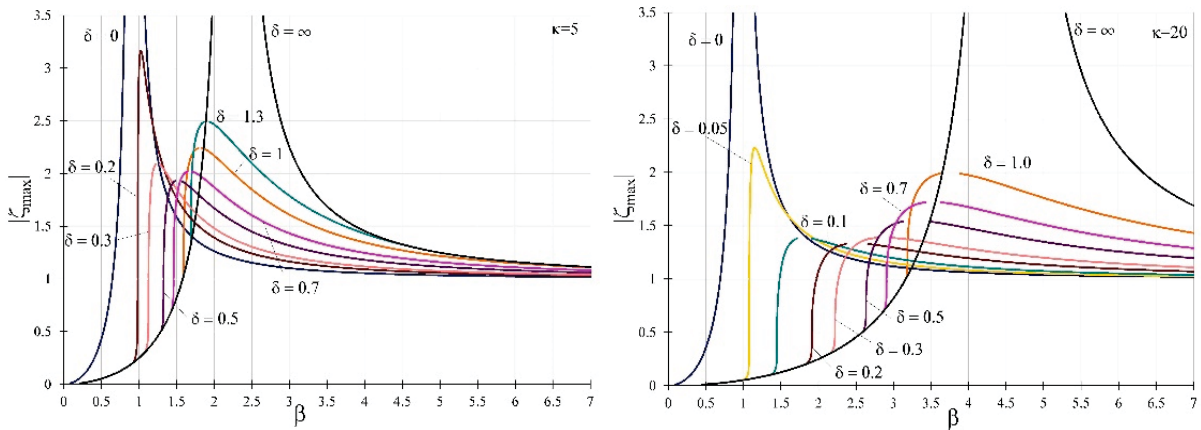
Figure 6.8 Maximum deck displacement versus frequency ratio β ($\kappa = 5, 20$).

In order to get the derived response quantities, simple expressions, involving the normalized displacement ζ_{max} and stiffness κ, are introduced. When $\zeta_{max} > \delta$, the top column displacement $\zeta_{c,max}$ (equal to the base shear) and the relative displacement $\Delta\zeta = \zeta - \zeta_{c,max}$ assume the expressions (Figure 6.9 and Figure 6.10):

$$\zeta_{c,max} = \frac{\kappa\delta + \zeta_{max}}{1+\kappa} \tag{6.47}$$

$$\Delta\zeta = \frac{\kappa(\zeta_{max} - \delta)}{1+\kappa} \tag{6.48}$$

while, $\zeta_{c,max} = \zeta_{max}$ and $\Delta\zeta = 0$ when $\zeta_{max} < \delta$.

One notes that once the device yields, the top column displacement $\zeta_{c,max}$ is always lower than ζ_{max} and that the relative displacement $\Delta\zeta$ is always decreasing for increasing values of δ. In addition to this, $\zeta_{c,max}$ has a maximum value after the yielding of the control device, which is approximately equal to δ for high values of κ, because of the limited force transmitted by the isolator after yielding. This behavior indicates a great advantage of the *SI* system with respect to the *VI* case: rigid-plastic devices apply a strong control on the maximum base-shear force, practically a known value ($\cong F_y$) for high values of κ. Differently from the *VI* case, it is now possible to derive a different optimal value $\delta_{c,opt}$ giving the minimum resonance peak $\zeta_{c,max}$ in the columns.
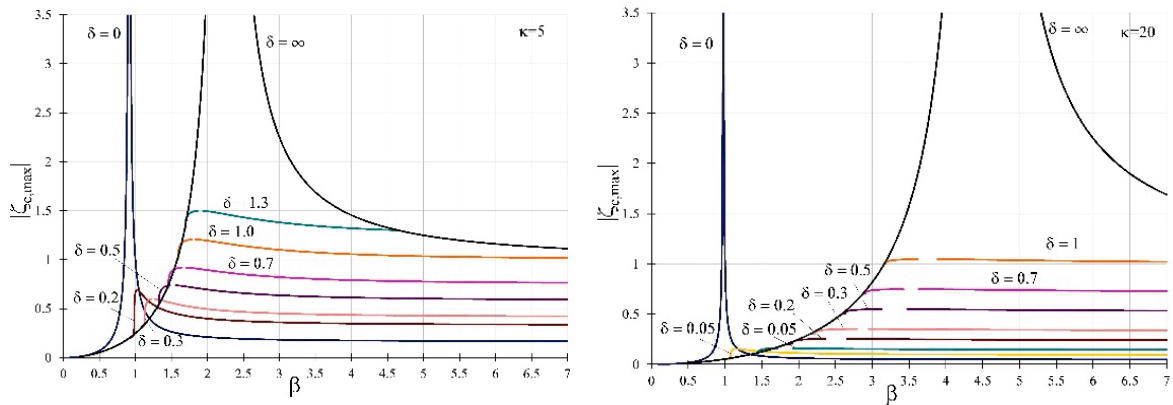

**Figure 6.9 Top column displacement versus frequency ratio β (κ = 5, 20).**
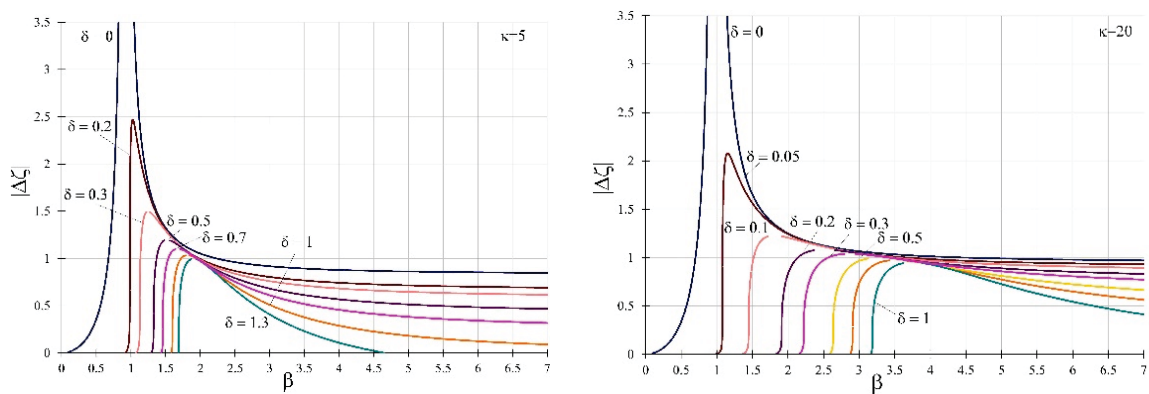
Figure 6.10 Relative deck to pier displacement versus frequency ratio β (κ = 5, 20).

187

A design spectrum has been numerically derived and is plotted in Figure 6.11(a), where both the optimal values δ_{opt} and $\delta_{c,opt}$ are shown as a function of the relative stiffness κ. In Figure 6.11(b) are also plotted both the quantity $\zeta_{max}(\delta_{opt})$ and $\zeta_{c,max}(\delta_{c,opt})$, and also the values β_{opt} and $\overline{\beta}$, all versus κ.
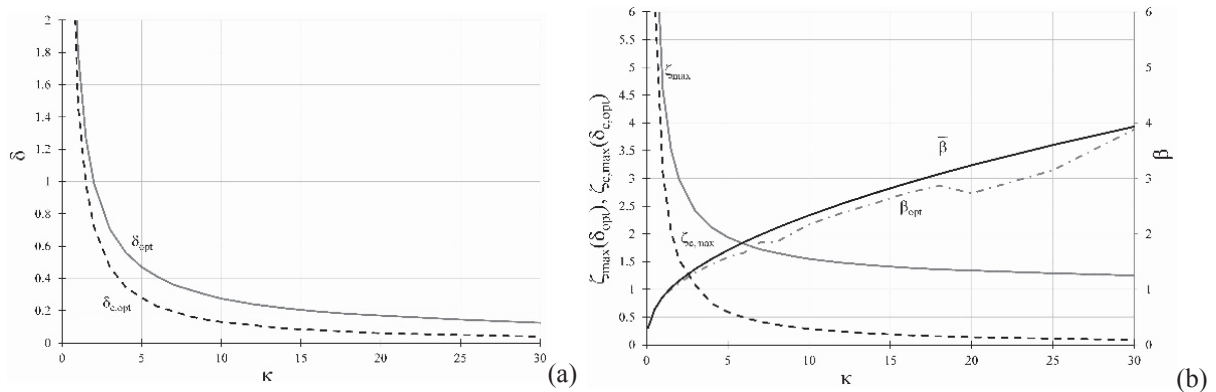
Figure 6.11 (a) *SI* optimal parameters for both deck and pier displacement and (b) deck optimal displacement, column optimal displacement, optimal frequency ratio and limit curves intersection point versus κ.

From Figure 6.11 it is clear that, as far as κ increases, both the optimal parameters and the maximum displacements decrease. Besides, the value of β_{opt} is close to $\overline{\beta}$ and both parameters show a growing trend with κ.

6.3 Numerical validation of proposed design procedure

The design procedure proposed in the previous paragraphs has been verified through a numerical investigation performed on a typical isolated bridge having a target period $T_i = 2 \cdot \pi/\omega = 2.5$ *s*. The equation of motion has been solved by implementing the Newton-Raphson integration method (Chopra 2011) in Matlab® environment (Mathworks 2010).

According to the Italian building code (NTC 2008), the design spectra (Figure 6.12) with 5% of critical damping have been defined for the near collapse limit state of a bridge (functional class III) located in Grottaminarda, Italy (15.03° longitude, 41.06° latitude) on soil type B ($360 \leq V_{s,30} \leq 800$ m/s) with a nominal life of 50 years, corresponding to a return period of 1462 years. A set of seven unscaled spectrum matching accelerograms (Figure 6.12, Table 6.1) was found in the European ground motion database using Rexel v3.4 beta (Iervolino et al 2010). The average spectrum has 10% lower and 30% upper tolerance in the period range 0.15-2 s.
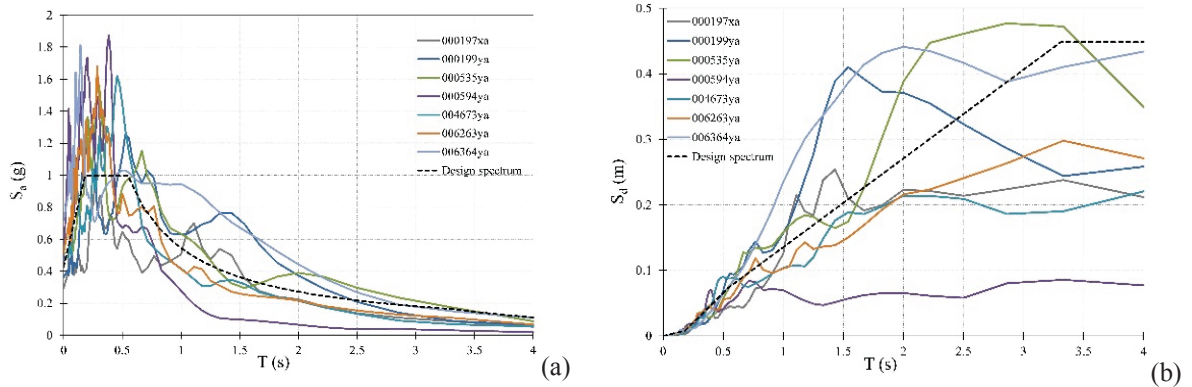
Figure 6.12 (a) Acceleration and (b) displacement design spectra (ν =5%) and selected ground motion spectra.

Table 6.1 Selected spectrum-compatible accelerograms for site class B.

Waveform ID	Earthquake ID	Station ID	Earthquake Name	M_w	Epicentral Distance [km]	PGA [m/s²]	PGV [m/s]
4673	1635	ST2482	South Iceland	6.5	15	4.68	0.48
535	250	ST205	Erzincan	6.6	13	5.03	1.02
6263	1635	ST2484	South Iceland	6.5	7	6.14	0.50
199	93	ST67	Montenegro	6.9	16	3.68	0.52
197	93	ST63	Montenegro	6.9	24	2.88	0.47
6334	2142	ST2488	South Iceland (as)	6.4	11	7.07	0.97
594	286	ST60	Umbria Marche	6	11	5.14	0.32
mean:				6.54	13.86	4.94	0.61

In order to estimate the maximum expected ground displacement $x_{g,max}$ corresponding to the aforementioned spectra, it is necessary to compute the spectral displacement S_d in the long-period range up to 10 s. Several authors (Faccioli et al 2004; Smerzini et al 2013) and also the NTC suggest to assume the following relationship:

$$x_{g,\max} = 0.025 \cdot a_g \cdot S \cdot T_C \cdot T_D \tag{6.49}$$

where a_g = 0.428 g is the peak ground acceleration on bedrock, S = 1.003 is the soil amplification factor and T_C = 0.547 s is the control period corresponding to the beginning of the constant velocity branch of the design spectrum and T_D = 3.310 s is the corner period denoting the beginning of the maximum displacement plateau. Eq. 6.49 provides $x_{g,max}$ = 0.19 m and this has been taken as reference for the *SI* case.

The response of the *VI* and *SI* bridge has been evaluated under seven ground motions characterized by different frequency content, to numerically determine the optimal values of

189

the parameters v_i and δ, and to compare them with those obtained from the analytical approach presented in the previous paragraph.

Structural response is showed in the following both in terms of deck and top pier absolute displacement, and also of deck-pier relative displacement. The numerical investigation has been repeated for 2 different values of κ (5 and 20), which correspond to the following dynamic structural properties in case of rigid deck-to-pier connection (limit case $v_i \to \infty$ or $\delta \to \infty$ - Table 6.2):

Table 6.2 Bridge dynamic properties for rigid deck-to-pier connection.

κ [-]	T_{fb} [s]	ω_{fb} [rad/s]	f_{fb} [hz]
5	1.12	5.59	0.89
20	0.56	11.17	1.78

where $\omega_{fb} = \omega_i \sqrt{\kappa}$ and the corresponding normalized frequency β at resonance is $\sqrt{\kappa}$.

If no supplemental damping is provided (limit case $v_i = 0$ or $\delta = 0$), the dynamic properties of the system reduce to those in Table 6.3:

Table 6.3 Bridge dynamic properties with $v_i = 0$ or $\delta = 0$.

κ [-]	T_0 [s]	ω_0[rad/s]	f_0 [hz]
5	2.75	2.28	0.36
20	2.58	2.44	0.39

where the frequency $\omega_0 = \omega_i \sqrt{\dfrac{\kappa}{1+\kappa}}$ of the undamped structure corresponds to the normalized

frequency ratio $\beta = \sqrt{\dfrac{\kappa}{1+\kappa}}$ at resonance.

A parametric investigation has been performed for each ground motion and for each value of κ, by assigning extremely different values to both v_i (100 logarithmically spaced value between 10^{-3} and 10^5) and δ (100 logarithmically spaced value between 10^{-4} and 10): the pier and deck maximum displacements have been considered as result for each time history case and are plotted in what follows. The optimal parameter is the value corresponding to the minimum structural response in terms of pier or deck displacement, under each seismic excitation for a given κ.

The following Figures summarize some relevant results of the numerical analyses performed on the case study for both control systems. In particular, the maximum normalized displacement is plotted versus the value of the parameter v_i and δ in a semi-logarithmic scale, so to make clear how different the response could be, ranging from one extreme to the other.

6.3.1 VI case

In the *VI* case, the structural model is defined as a two DOFs system (deck displacement x and pier displacement x_c - see § 6.2.2), where the only dynamic DOF is associated to the deck displacement. The equation of motion has been formulated as follows:

$$\mathbf{M} \cdot \ddot{\mathbf{x}} + \mathbf{C} \cdot \dot{\mathbf{x}} + \mathbf{K} \cdot \mathbf{x} = -\ddot{x}_g \mathbf{M} \cdot \mathbf{l}$$

where $\mathbf{x}^T = \begin{bmatrix} x & x_c \end{bmatrix}$, $\dot{\mathbf{x}}^T = \begin{bmatrix} \dot{x} & \dot{x}_c \end{bmatrix}$, $\ddot{\mathbf{x}}^T = \begin{bmatrix} \ddot{x} & \ddot{x}_c \end{bmatrix}$, $\mathbf{M} = \begin{bmatrix} m & 0 \\ 0 & 0 \end{bmatrix}$, $\mathbf{K} = \begin{bmatrix} k_i & -k_i \\ -k_i & k_c + k_i \end{bmatrix}$,

$\mathbf{C} = \begin{bmatrix} c_i & -c_i \\ -c_i & c_i \end{bmatrix}$, $\mathbf{I} = \begin{bmatrix} 1 \\ 1 \end{bmatrix}$ and $\ddot{x}_g$ is the base acceleration.

In this case, the time step has been assumed equal to 0.01s while the parameters γ and β have been set to 1/2 and 1/4, respectively. Figure 6.13 to Figure 6.19 show the peak value of x, x_c and x-x_c under different applied earthquake records for the different values of v_i. In the same Figures, the vertical straight line indicates the optimal value determined from the proposed design procedure ($v_{i,opt} = 0.7171$ for $\kappa = 5$, $v_{i,opt} = 0.7079$ for $\kappa = 20$).
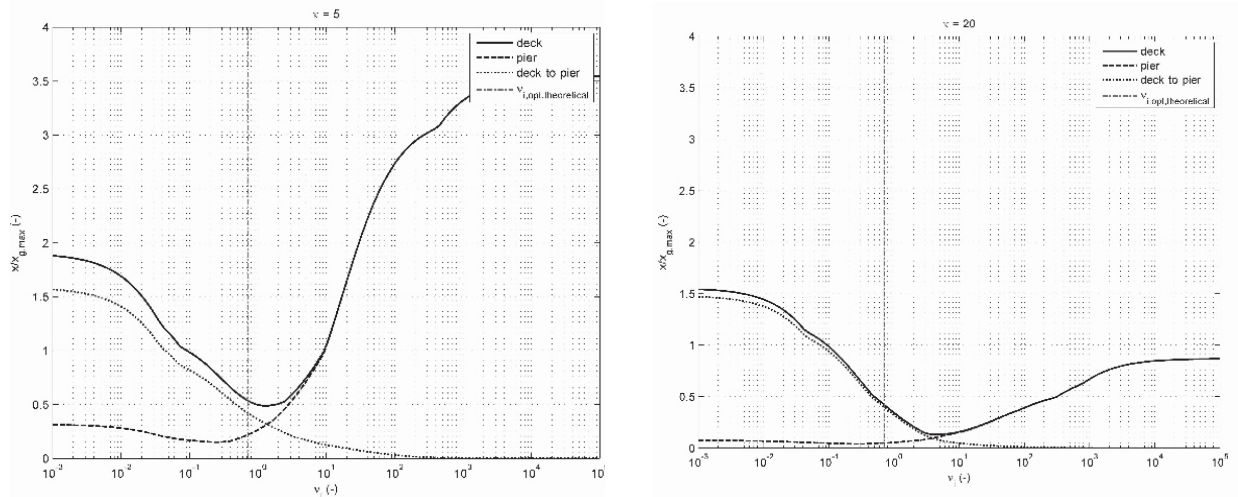
Figure 6.13 VI case: numerical results for ground motion #197.
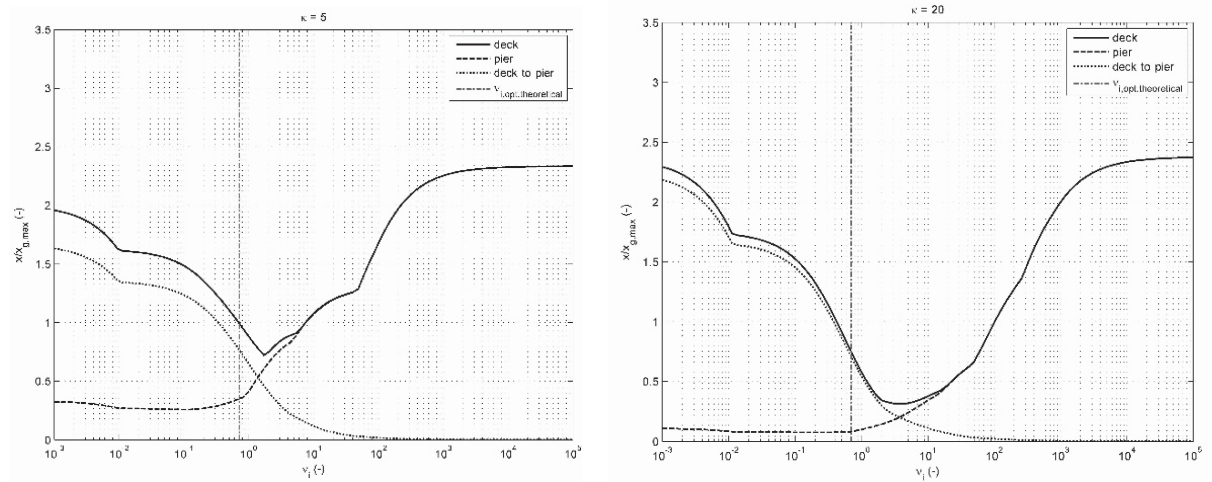
Figure 6.14 VI case: numerical results for ground motion #199.
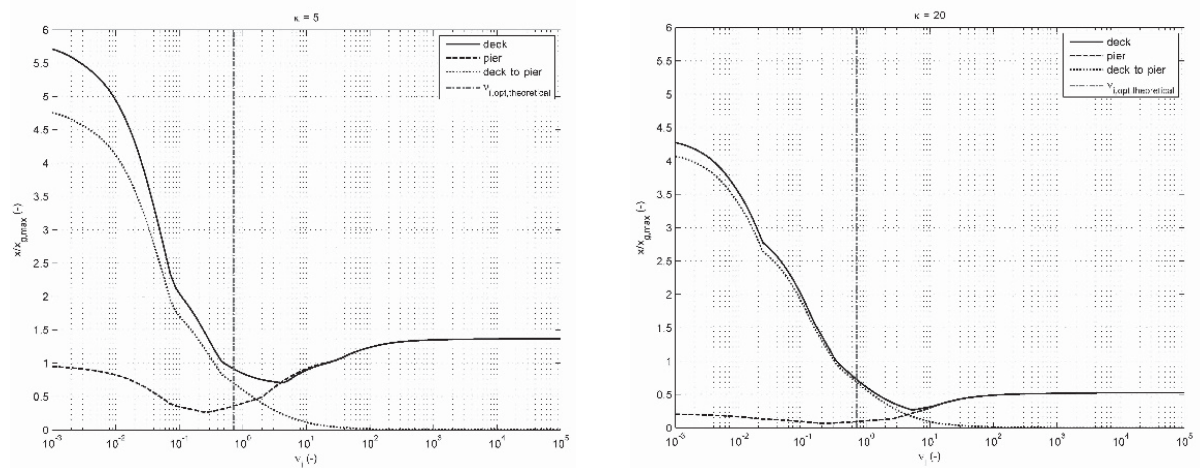
Figure 6.15 VI case: numerical results for ground motion #535
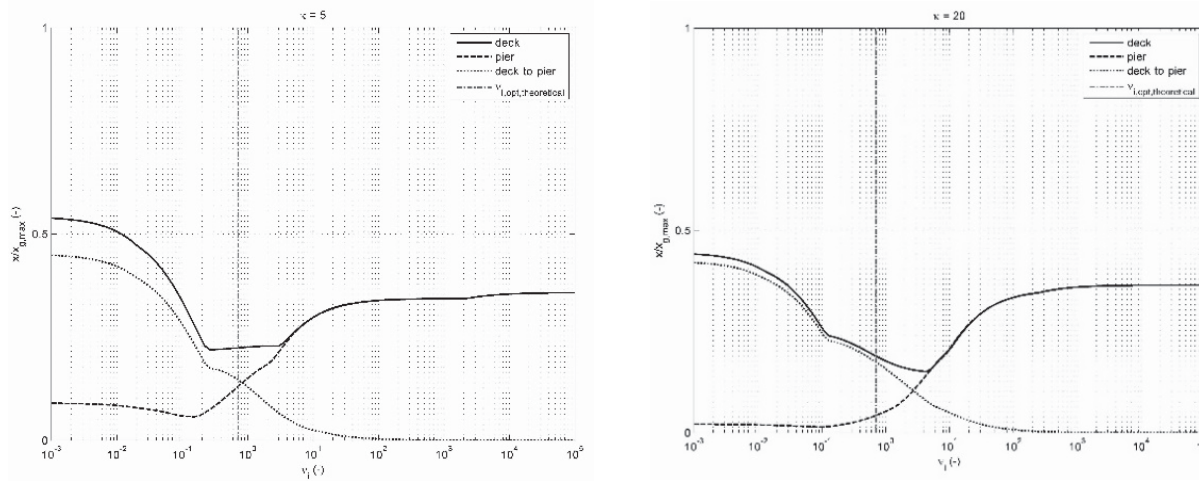
Figure 6.16 VI case: numerical results for ground motion #594
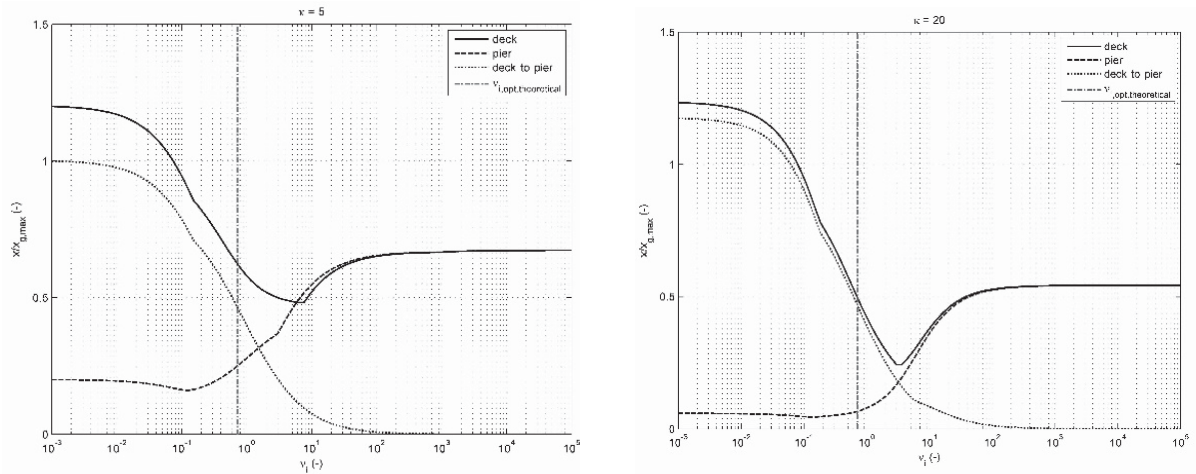
Figure 6.17 VI case: numerical results for ground motion #4673.
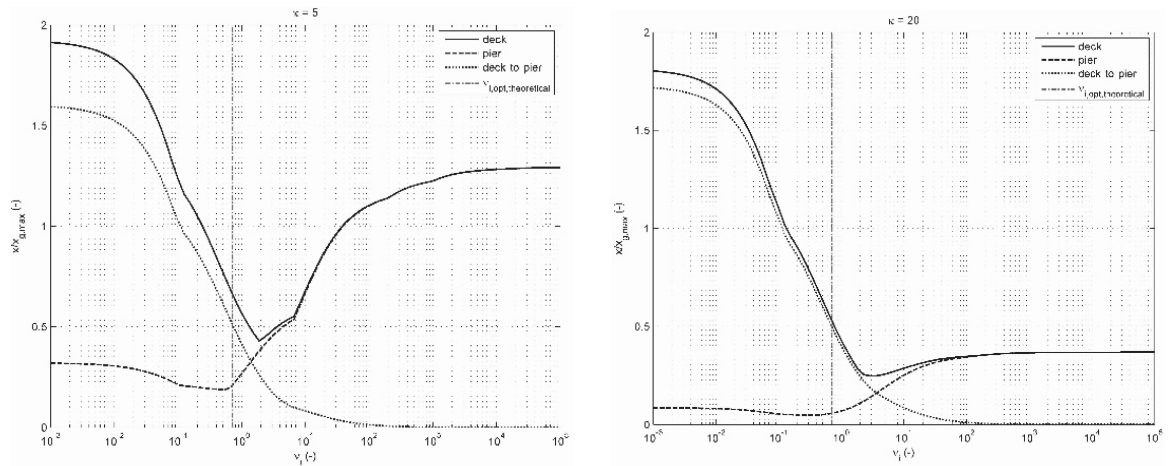
Figure 6.18 VI case: numerical results for ground motion #6263.
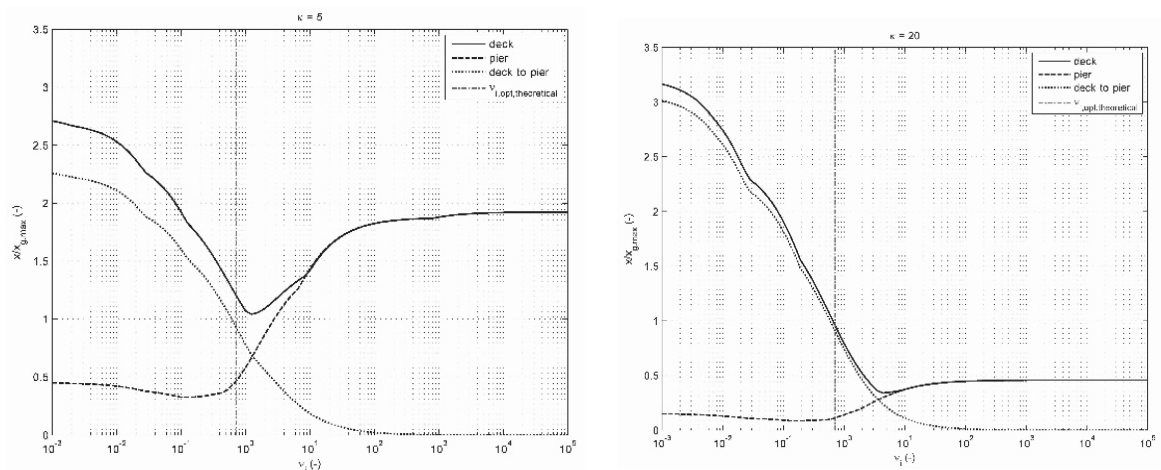
Figure 6.19 VI case: numerical results for ground motion #6334.

As expected, in all the analyzed cases, the response in terms of deck displacement shows a minimum value but this occurs for a value of v_i almost always larger than the theoretically

proposed one. With respect to the undamped case ($\nu_i=0$), the deck response is strongly reduced. Main results are reported in Table 6.4:

Table 6.4 Numerical optimum values of ν_i for the deck displacement

κ	#197	#199	#535	#594	#4673	#6263	#6334	$\nu_{i,opt}$
5	1.18	1.71	4.33	0.26	7.56	1.87	1.23	0.7171
20	4.33	3.59	5.21	4.32	2.98	3.51	4.32	0.7079

Regarding top pier displacement, it is worth to note that an increase in the value ν_i is almost always responsible for a larger response of the column, due to the additional force transmitted by damping. However, it is clear from the above Figures that top pier peak response slightly reduces for ν_i increasing between 0 and a value very close or slightly lower than $\nu_{i,opt}$. In other words, $\nu_{i,opt}$ represents a good compromise value which allows to optimize at the same time both the deck and top pier maximum displacement. Table 6.5. summarizes the numerical optimal values ν_i, always lower than $\nu_{i,opt}$:

Table 6.5 Numerical optimum values of ν_i for the pier displacement.

κ	#197	#199	#535	#594	#4673	#6263	#6334	$\nu_{i,opt}$
5	0.27	0.1	0.27	0.15	0.13	0.53	0.12	0.7171
20	0.32	0.22	0.22	0.09	0.15	0.35	0.15	0.7079

6.3.2 SI case

In the *SI* case, the structural model is defined as a bilinear single DOF system (see § 6.2.3). A time step of 0.0001s has been adopted to improve the accuracy of the integration with $\gamma=1/2$ and $\beta=1/6$. The damping ratio ν has been set equal to zero, due to the lack of supplemental viscous damping.

Figure 6.20 to Figure 6.26 show the peak value of x, x_c and x-x_c under different applied earthquake records for the different values of δ. In the same Figures, the vertical straight lines indicates the theoretically determined optimal δ for the deck ($\delta_{opt} = 0.47$ for $\kappa = 5$, $\delta_{opt} = 0.17$ for $\kappa = 20$) and for the column ($\delta_{c,opt} = 0.28$ for $\kappa = 5$, $\delta_{c,opt} = 0.06$ for $\kappa = 20$).
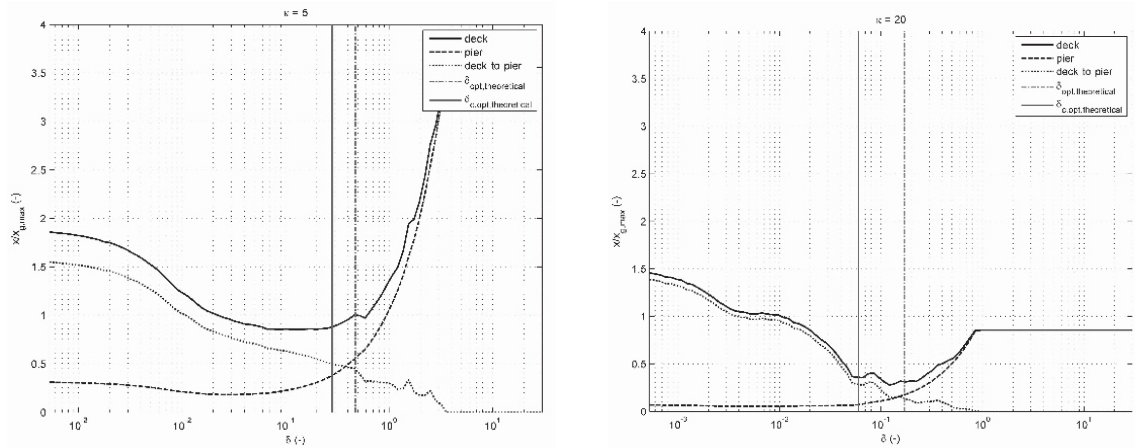
Figure 6.20 SI case: numerical results for ground motion #197.
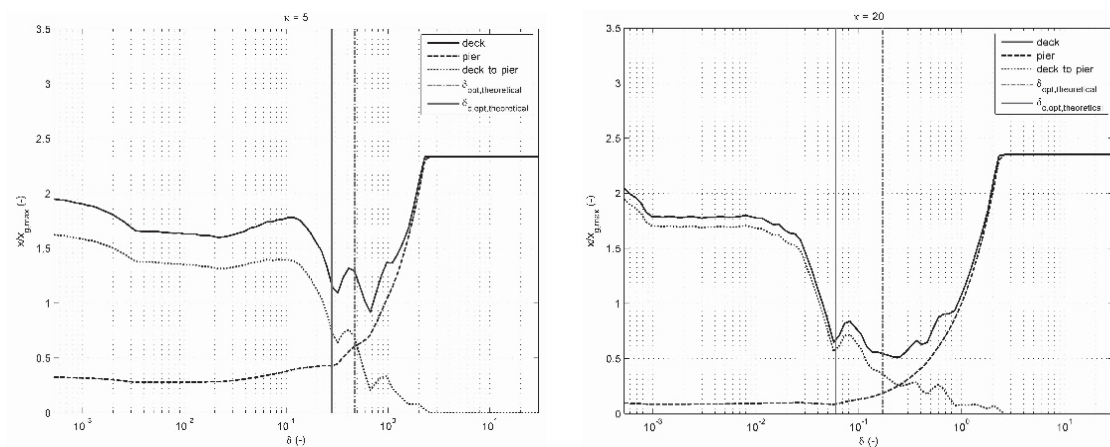
**Figure 6.21 SI case: numerical results for ground motion #199.**
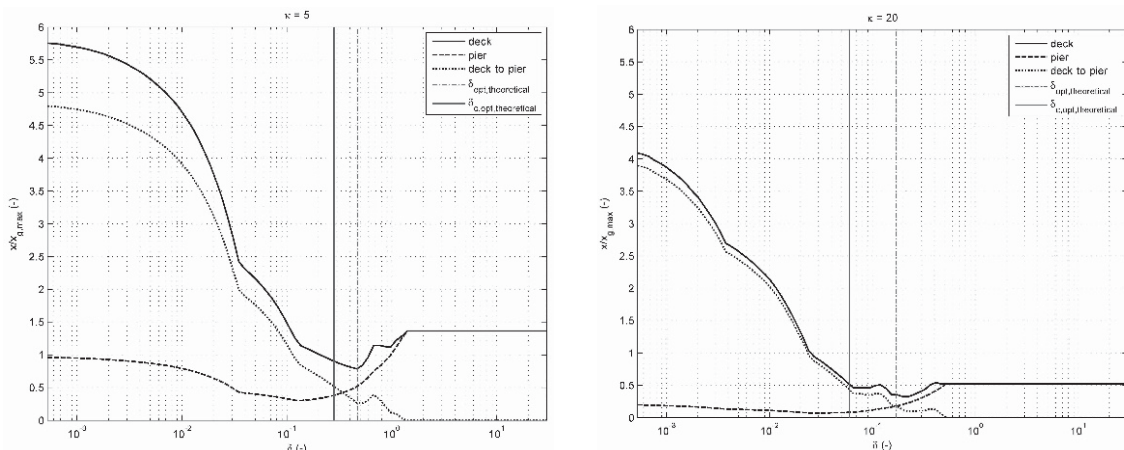

**Figure 6.22 SI case: numerical results for ground motion #535.**
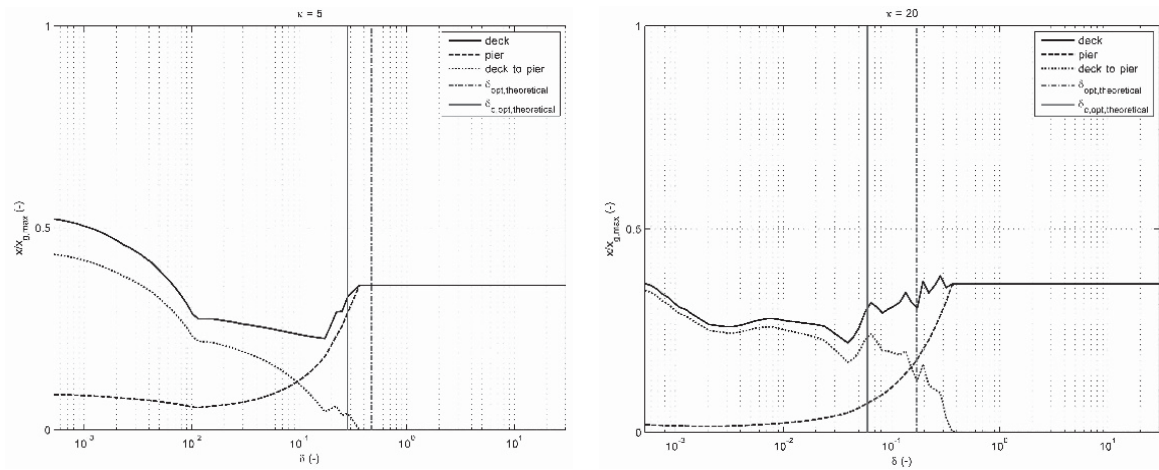
**Figure 6.23 SI case: numerical results for ground motion #594.**
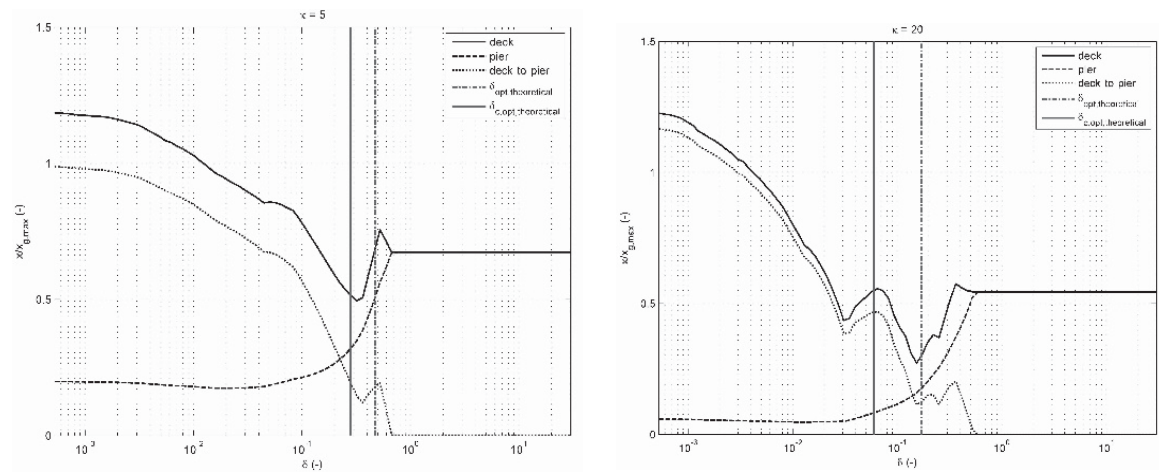
Figure 6.24 SI case: numerical results for ground motion #4673
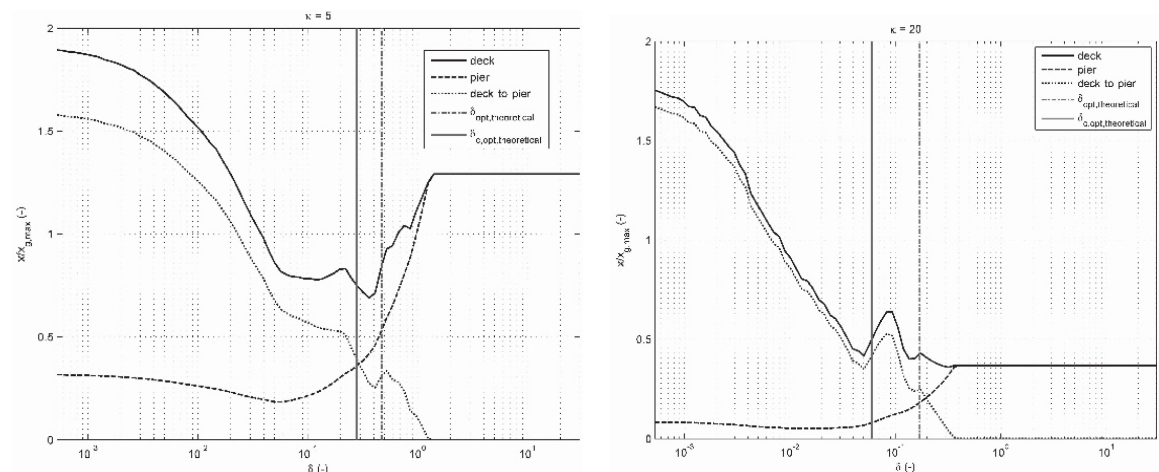
Figure 6.25 SI case: numerical results for ground motion #6263.
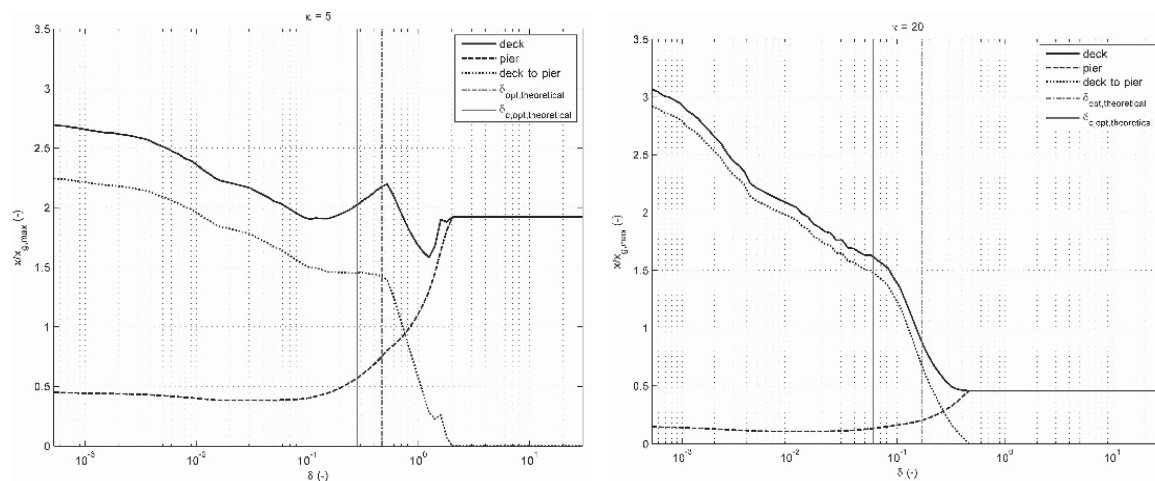
Figure 6.26 SI case: numerical results for ground motion #6334.

Differently from the *VI* case, the minimum of the deck response is not always between the two limit cases but sometimes reduces to the rigid deck-to-pier connection case, so implying the worst condition for the pier. For the value δ_{opt} the deck response is always reduced with respect to the undamped case ($\delta = 0$). It must be noted that that the average of the actual numerical values in Table 6.6 is very close to the theoretically derived δ_{opt} :

Table 6.6 Numerical optimum values of δ for the deck displacement.

κ	#197	#199	#535	#594	#4673	#6263	#6334	δ_{opt}
5	0.13	0.67	0.46	0.17	0.32	0.36	1.24	0.47
20	0.12	0.22	0.22	0.03	0.15	0.32	0.46	0.17

Similarly to the *VI* case, due to the coupling effect with the deck, the pier displacement significantly increases with δ, except for a very low value of the ratio varying from 0 to a value lower than $\delta_{c,opt}$ (Table 6.7).

Table 6.7 Numerical optimum values of δ for the pier displacement

κ	#197	#199	#535	#594	#4673	#6263	#6334	$\delta_{c,opt}$
5	0.032	0.006	0.13	0.011	0.02	0.057	0.05	0.28
20	0.005	0.057	0.027	0.002	0.013	0.013	0.017	0.06

The outcome is that $\delta_{c,opt}$, instead of δ_{opt}, may be taken as design value able to strongly reduce the deck response while lightly affecting the pier response.

In a *SI* system, it has also been verified what is the effect of damping in the piers on the structural response: a value of $\nu=2\%$ strongly reduces the response in case of elastic behaviour ($\delta = 0$ or

197

$\delta \rightarrow \infty$) while, in case of significant sliding in the isolation system, maximum displacements are mainly dependent on hysteretic dissipation (Figure 6.27).
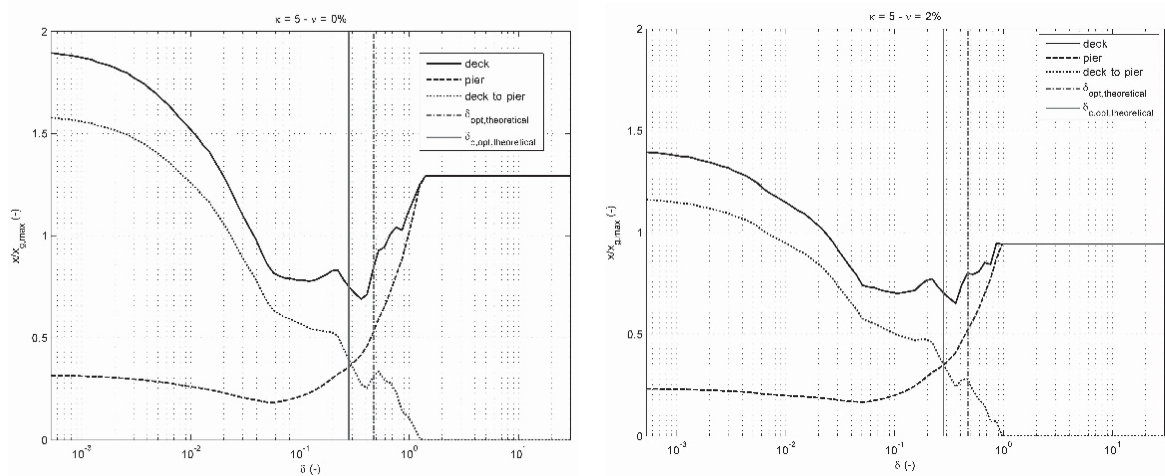
Figure 6.27 Numerical results with additional viscous damping ν=2% for ground motion #6263

6.4   Effective design procedure

This paragraph summarizes the useful proposed design method. It has been developed taking into account the results of both theoretical treatment and numerical validation and is explained in the flowchart of Figure 6.28. Given the fixed-base bridge properties, the stiffness of the isolation system k_i is defined to get a target period T_i. A starting value of the damping parameter is assumed equal to $\nu_{i,opt}$ or $\delta_{c,opt}$, from Figure 6.6(a) or Figure 6.11(a) respectively, since they were proved to be very close to the effective numerical optimum. Time history analysis are then performed under the code provided seismic action and the performance is checked a posteriori (i.e., average or maxima of results depending on the number of assumed accelerograms). If not satisfactory, a modification of the damping parameter can be made in order to get an improvement in the achievement of the desired target performance level (e.g. in terms of absolute minimum deck displacement). Some iterations could be needed to define the effective optimal values (ν_{opt} or δ_{opt}).
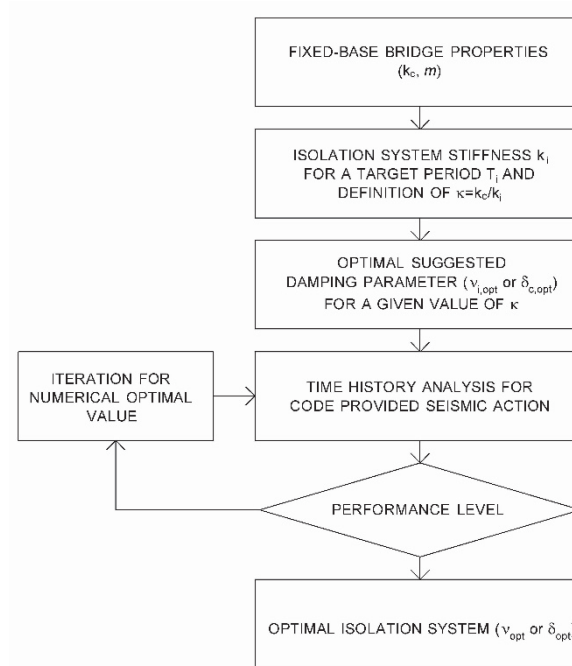
Figure 6.28 Flowchart of the suggested design procedure.

Near fault ground motion was not properly addressed in this work even if it is of great concern for structures with long natural periods (Jònsson et al 2010). Near fault effects are mainly characterized by low frequency pulses, short duration and higher horizontal accelerations with a significant component in the vertical direction too. Due to their natural period, base isolated structures are more vulnerable when subjected to near fault motion: for single pulse excitation, the maximum response mainly depends on the ratio of the impulse duration to the natural period of the structure while the influence of damping is expected to be negligible (Chopra 2011), so isolators' displacement may significantly increase. In this case, at the stage of numerical validation, some accelerograms were selected with low epicentral distance (R<15 km) and no significant difference emerged from response.

Effects of different soil conditions and non-synchronous motion were neglected. The isolated bridge was designed as if subjected to a standard input motion, i.e., synchronous excitation and uniform soil condition. Its response under spatially varying ground motion can be evaluated by numerical simulations at the design stage. Design codes normally require consideration of ground motion spatial variability only for bridges several hundreds meters long, or in case of drastic variations of soil profiles. Eurocode 8 (1998-1 EN 2004) requires spatial variability to be considered in case of more than one ground type at the supports in case of continuous deck's length exceeding 200 m over soil type D (higher values are suggested in case of better soil conditions). In the formulation of the equation of motion with input spatial variability, the

model must include the degrees of freedom at the supports so that kinematic vectors are splitted in n- unconstrained and m-support degrees of freedom. The n-vector x of the total displacements is the combination of a pseudo-static component x^s and a dynamic component x^d . The component x^s is computed from an m- vector u of prescribed support displacements while the term x^d is the effect of base accelerations. The spatial variation of the seismic action could be estimated using a simple approximate model based on pseudo-static effects of appropriate displacement sets imposed at the foundation of the supports, and then combined with the main inertial response. When a time-history analysis is performed, a sample acceleration motion, obtained by means of a vector of zero-mean random process having a power spectrum consistent with the elastic response spectrum, can be applied at each support, thus reflecting the probable spatial variability of the seismic action. Irrespective of bridge configuration, the displacement demand of most of the isolators increases in the presence of spatial variability (Lupoi 2009). Especially in the case of non uniform soil conditions underneath the bridge foundations (the source of the greater negative influence on the bridge response), specific studies are necessary and a safety factor approach cannot be pursued.

Pounding effects must be properly considered in a seismically isolated bridge, since lateral displacements are expected to increase significantly. Available clearances at deck movement joints and abutment back-walls must be checked in order to avoid collision, according to code requirements. A design criterion for the optimal isolation system was defined to obtain the minimum deck displacement, so implying minimum required clearances. It was proved that deck displacement is strongly reduced thanks to a value of damping very close to the optimal one, thus giving an optimal deck displacement not so different or sometimes lower than the fixed-base one. Taking benefits from damping, the question of pounding can be properly mitigated in seismically isolated bridges.

The proposed procedure was explained with reference to the Italian Code, where the collapse prevention limit state (SLC) has to be taken into account for the design of the isolation system: seismic action is defined for a 5% over 50 years probability of occurrence during the reference life V_R, whose value strongly affects the definition of the return period T_R (in this case about 1500 years). In the Eurocode 8 non-collapse requirement must be fulfilled for bridge design at Ultimate limit state (ULS): an importance factor γ_I depending on the importance class of the bridge is provided to scale seismic action (for class II-average importance, T_R=475 years). In the US code, the maximum considered earthquake (MCE) must be taken into account in

designing the isolation unit (International Code Council 2000), with a 2% probability of exceedance in 50 years.

In conclusion, the following recommendations are given: at the first-step of the design procedure, the suggested values of the reference parameters ($\nu_{i,opt}$ or $\delta_{c,opt}$) have to be assumed; then, after acceleration input motion has been defined according to code provisions, time history analysis need to be performed. Seismic input has to take into account, if necessary, near fault effects and ground motion spatial variability. Numerical results are then compared with the design performance level, that may concern minimum deck displacement or pier base shear. Even if initial suggested values were numerically validated for real ground motions, optimum definition is case-dependent and the achievement of the desired performance level may require some iterations due to randomness of earthquake. Actually, real strong motion properties (magnitude, duration, frequency content, etc.) may play an important role in the determination of the effective design optimal value.

6.5 Conclusions

In an isolated bridge deck, the increase in the horizontal period of vibration implies the need for supplemental damping in order to reduce the deck displacement. In this chapter, a theoretical approach was suggested for determining the optimal value of the inherent viscous damping in case of viscoelastic isolators (*VI*) or the yielding force in case of sliding isolators (*SI*). The proposed method is based on the analytical determination of the response to a harmonic base motion, with the aim of obtaining the optimal values of the adimensionalized viscous damping parameter (ν_i) or yielding displacement (δ) able to minimize the structural response, for each value of the piers to isolators relative stiffness κ. The method can be applied to a single or multispan bridge, supported by two or more columns all having the same stiffness, isolated by means of elastomeric or sliding bearings.

It was demonstrated that, given a certain target period of isolation T_i, for different values of the design parameters (ν_i or δ), the behavior would span between two extreme cases both corresponding to an undamped response with an unbounded resonance. The process of adding damping is not beneficial to any extent but just up to a certain level, depending on the objective of the optimization process. Within this field, the optimal values of ν_i and δ have been assumed as the ones corresponding to a minimum of the response curve in the overall frequency range,

for the deck or the pier displacement. Design spectra are provided where theoretical optimal values are given as a function of κ.

In the second part of the work, numerical analysis have been carried out to validate the proposed design method in case of two typical isolated bridges subjected to seven spectrum-compatible earthquake records for a near collapse limit state, according to the NTC. This was devoted to determine the change in the structural response produced by varying the parameters ν_i and δ. The numerical analysis demonstrated that the value $\nu_{i,opt}$ minimizing the peak amplitude of the deck frequency response curve is usually of the same order of magnitude but slightly lower than that corresponding to the actual numerical optimum for the deck. This can be explained taking into account that the frequency content of a ground motion can vary significantly and does not correspond to a white noise exciting the overall range of frequencies of the system. Despite that, the theoretical value $\nu_{i,opt}$ is very close to the numerical optimum for the pier, being also able at the same time to significantly reduce the deck response.

As regard the *SI* case, it has been proved that δ_{opt} is in the average in good agreement with the numerical optimum values minimizing the deck response, the latter sometimes related to the rigid deck-pier connection behavior. On the other hand, the pier displacement increases with δ, a part for a small range of δ from 0 to a value lower than $\delta_{c,opt}$. In the *SI* case, numerical results are not only depending on the frequency content of the ground motion but also on the assumption regarding the definition of the maximum ground displacement $x_{g,max}$ that in the suggested analytical procedure represents the amplitude of the harmonic base motion and has been estimated by means of seismic hazard parameters. A part from the approximations and hypothesis of the method, $\delta_{c,opt}$ seems to be an acceptable value capable to strongly reduce the deck response without significantly affecting the pier displacement.

When designing an isolated bridge with elastomeric or sliding bearings, the optimal inherent viscous damping coefficient or the optimal sliding force, respectively, can be first adopted as $\nu_{i,opt}$ or $\delta_{c,opt}$. In this case the expected structural response is characterized by significantly reduced deck displacements with not affected or just lightly worsened pier response respect to the case $\nu_i = 0$ or $\delta = 0$. Both parameters can be assumed as a starting point in a case-dependent optimization process, therefore being necessary to perform iterative analysis for the code provided seismic action in order to check and find out the effective optimum value for the minimization of the desired response.

From numerical results it has also been observed that, for a given κ and ground motion, the absolute minimum deck displacement is obtained by means of viscous damping rather than hysteretic damping while for the minimum pier displacement there is no significant difference.

REFERENCES

1998-1 EN (2004) EN 1998-1. Eurocode 8: Design of structures for earthquake resistance – Part 1: General rules, seismic actions and rules for buildings

Bhuiyan AR, Alam MS (2013) Seismic performance assessment of highway bridges equipped with superelastic shape memory alloy-based laminated rubber isolation bearing. Eng Struct 49:396–407.

Caughey T (1960) Sinusoidal Excitation of a System with Bilinear Hysteresis. J Appl Mech 32:640–648.

Chopra AK (2011) Dynamics of Structures: Theory and Applications to Earthquake Engineering. Prentice Hall/Pearson Education

Ciampi V (1998) On the optimal design of energy dissipation devices for existing bridges. Proc. US-Italy Work. Prot. Syst. Bridg

Ciampi V, De Angelis M, Paolacci F (1995) Design of yielding or friction-based dissipative bracings for seismic protection of buildings. Eng Struct 17:377–396.

Di Marzo D, Mandara A, Serino G (2000) Earthquake Protection of Buildings and Bridges with Viscous Energy Dissipation Devices. Behav. Steel Struct. Seism. Areas

Faccioli E, Paolucci R, Rey J (2004) Displacement Spectra for Long Periods. Earthq Spectra 20:347–376.

Hwang J-S, Tseng Y-S (2005) Design formulations for supplemental viscous dampers to highway bridges. Earthq Eng Struct Dyn 34:1627–1642. doi: 10.1002/eqe.508

Iervolino I, Galasso C, Cosenza E (2010) REXEL: computer aided record selection for code-based seismic structural analysis. Bull Earthq Eng 8:339–362. doi: 10.1007/s10518-009-9146-1

International Code Council (2000) International Building Code.

Jònsson MH, Bessason B, Haflidason E (2010) Earthquake response of a base-isolated bridge subjected to strong near-fault ground motion. Soil Dyn Earthq Eng 30:447–455.

Losanno D, Spizzuoco M, Serino G (2014) Optimal design of the seismic protection system for isolated bridges. Earthquakes Struct 7:969–999.

Lupoi A (2009) The response of isolated bridges accounting for Spatial Variability of Ground Motion. J Earthq Eng 13:814–834.

Madhekar SN, Jangid RS (2009) Variable dampers for earthquake protection of benchmark highway bridges. Smart Mater Struct 18:1–18.

Mathworks T (2010) Matlab.

NTC (2008) Ministero delle Infrastrutture. D.M. 14 gennaio 2008: Nuove norme tecniche per le costruzioni

Ozbulut OE, Hurlebaus S (2011) Optimal design of superelastic-friction base isolators for seismic protection of highway bridges against near-field earthquakes. Earthq Eng Struct Dyn 40:273–291. doi: 10.1002/eqe.1022

Paolacci F (2013) An energy-based design for seismic resistant structures with viscoelastic dampers. Earthq Struct 4:219–239.

Paolacci F, Serino G (2001) Optimal design of passive energy dissipation systems for seismic protection of concrete bridges. Fifth World Conf. Joints, Bear. Seism. Syst. Concr. Struct.

Smerzini C, Galasso C, Iervolino I, Paolucci R (2013) Ground motion record selection based on broadband spectral compatibility. Earthq Spectra 30:1427–1448.

Chapter 7

7. CONCLUSIONS AND FINAL REMARKS

Aim of the thesis is the investigation of the effects of supplemental damping on the definition of its optimal value in typical passively controlled civil engineering structures, such as damper-braced frames or isolated bridges.

The design of a passive control system, i.e. a supplemental damping system or a seismic isolation one, usually involves a trial and error process for the achievement of a satisfactory performance of the structural system. To improve competitiveness and effectiveness of passive control systems, their design should be tuned to an optimal value corresponding to a target performance.

Design of such control systems is an open issue and is often quite far from common engineering practise.

After introduction to most acknowledged supplemental damping and seismic isolation systems (Chapter 1) and their modeling (Chapter 2), Chapter 3 depicted the state of art of applicable seismic regulations, mainly represented by America codes and FEMA provisions. A deficiency has been recognized in European framework. Different analysis methods have been analysed, with particular focus on the operational definition of effective damping, essential parameter for adoption of simplified non liner analysis methods (linear static and modal analysis). Attention

must be paid to proper modeling of the passive control system: in case of supplemental damping system, other than the damper behavior (hysteretic, viscous or viscoelastic), also the supporting brace stiffness needs to be properly accounted.

Chapter 4 proposed a procedure for the optimal design of linear-elastic SDOF frame equipped with dissipative hysteretic or viscous braces. In Chapter 5 the same procedure is extended to the case of linear-elastic MDOF frame, just in case of viscous dampers.

Each dissipative brace is assumed made by a steel diagonal brace in series with a dissipative viscous or friction device. The assumptions of elastic frame behavior and negligible inherent structural damping are acceptable, since a strong reduction of demand on structural and non-structural components is expected for an optimally designed supplemental damping system. Objective of the procedure is the definition of the optimal value of the viscous damping coefficient and the yielding force of a supplemental damping brace, in function of the brace to frame relative stiffness.

In Chapter 6, a procedure for the optimal design of the damping of the isolation system of a bridge deck has been proposed. Objective of the procedure was the determination of the optimal value of the inherent viscous damping in case of viscoelastic isolators or the yielding force in case of sliding isolators, in function of the pier to isolation system relative stiffness. The method can be applied to a single or multispan bridge, supported by two or more columns all having the same stiffness, isolated by means of elastomeric or sliding bearings.

A similar dissertation was developed in all the aforementioned optimization cases. A theoretical approach based on frequency response functions was suggested for determining an analytical optimal value of the viscous damping coefficient and the yielding force of a supplemental damping brace or bridge isolation system. It was demonstrated that, given a certain relative stiffness, for different values of the design parameters, the behavior would span between two extreme cases both corresponding to an undamped response with an unbounded resonance.

In a passive control system, the process of adding damping would not be beneficial to any extent but just up to a certain level, depending on the objective of the optimization process. Within this field, the optimal values of the damping parameters have been assumed as the ones corresponding to a minimum of the response curve in the overall frequency range for the frame/pier displacement and the base shear. Design spectra have been provided, where theoretical optimal values are given as a function of a relative stiffness parameter.

Numerical analysis were performed to validate the proposed design methods.

In case of viscous behavior, it was found that the analytically determined values are the same order of magnitude than that corresponding to actual numerical optimum. This can be explained taking into account that the frequency content of a ground motion can vary significantly and does not correspond to a white noise exciting the overall range of frequencies of the system. Despite that, theoretical values tend to well approximate numerical ones.

As regard the hysteretic case, it has been proved that theoretically suggested values are usually higher than effective optimum. In this case, numerical results are not only depending on the frequency content of the ground motion but also on the assumption regarding the definition of the maximum ground displacement, that in the suggested analytical procedure represents the amplitude of the harmonic base motion and has been estimated by means of seismic hazard parameters. For this reason, the numerical validation process may provide a tuning factor with the aim of considering as design parameter a reduced equivalent displacement with respect to the harmonic excitation.

Both theoretical and numerical results demonstrated that:

1. In a brace-damper system, brace stiffness is an additional design parameter that has to be properly selected taking into account that the higher is the brace stiffness the more effective is the control system in reducing inter-story drifts, but it may be detrimental in terms of base reaction;

2. Both theoretically and numerically, it comes out that the optimal damping parameter corresponding to minimum base shear is lower than the one giving the minimum displacements;

3. For a given relative stiffness, the absolute minimum displacement and base shear are obtained by means of viscous rather than hysteretic damping.

Based on both theoretical and numerical results, design procedures are defined providing effective optimum values. The suggested reference values can be assumed as a starting point in a case-dependent optimization process, then being necessary to perform iterative analysis under code provided seismic action, in order to check and find out the effective optimum value for the minimization of the desired response. The optimum properties of the passive control system depend on both the properties of the ground motion and of the structural system.

As a perspective into future developments, the case of MDOF system with hysteretic dampers need to be developed, with the aim of obtaining a closed form solution for the design of optimal yielding force, according to a given brace stiffness distribution. State of art design procedures are mainly based on capacity curve definition and iterations for setting damping parameters. An extension of the proposed design method could provide a more effective distribution of the optimal viscous coefficients along the height: the story viscous coefficient could be arranged according to inter-story drift distribution. In addition to this, the sum of damper coefficients and their cost were not constrained in the present work, but it is an important issue to be properly considered in practical applications.